EFFECTS OF THE PHOSPHATASE SHP2 IN BREAST CANCER AND METASTASIS

Inauguraldissertation

zur
Erlangung der Würde eines Doktors der Philosophie
vorgelegt der
Philosophisch-Naturwissenschaftlichen Fakultät
der Universität Basel

von

NINA SAUSGRUBER
aus Friedrichshafen, Deutschland

Basel, Juni 2013

Genehmigt von der Philosophisch-Naturwissenschaftlichen Fakultät

auf Antrag von

Prof. Dr. Nancy Hynes

Dr. Mohamed Bentires-Alj

Prof. Dr. Gerhard Christofori

Basel, den 21. Mai 2013

<div align="right">

Prof. Dr. Jörg Schibler

Dekan

</div>

creative commons

Namensnennung-Keine kommerzielle Nutzung-Keine Bearbeitung 2.5 Schweiz

---

Sie dürfen:

das Werk vervielfältigen, verbreiten und öffentlich zugänglich machen

Zu den folgenden Bedingungen:

Namensnennung. Sie müssen den Namen des Autors/Rechteinhabers in der von ihm festgelegten Weise nennen (wodurch aber nicht der Eindruck entstehen darf, Sie oder die Nutzung des Werkes durch Sie würden entlohnt).

Keine kommerzielle Nutzung. Dieses Werk darf nicht für kommerzielle Zwecke verwendet werden.

Keine Bearbeitung. Dieses Werk darf nicht bearbeitet oder in anderer Weise verändert werden.

- Im Falle einer Verbreitung müssen Sie anderen die Lizenzbedingungen, unter welche dieses Werk fällt, mitteilen. Am Einfachsten ist es, einen Link auf diese Seite einzubinden.

- Jede der vorgenannten Bedingungen kann aufgehoben werden, sofern Sie die Einwilligung des Rechteinhabers dazu erhalten.

- Diese Lizenz lässt die Urheberpersönlichkeitsrechte unberührt.

Quelle: http://creativecommons.org/licenses/by-nc-nd/2.5/ch/   Datum: 3.4.2009

"It always seems impossible until it's done." - Nelson Mandela

1   SUMMARY

Breast cancer is the most frequent cancer in women and the most common cause of cancer related deaths in females. 90% of all cancer related deaths are due to metastatic spread to distant organs. In cancer, signaling pathways controlling proliferation, survival and migration are frequently deregulated. Tyrosine phosphorylation, controlled by protein tyrosine kinases (PTKs) and protein tyrosine phosphatases (PTPs), plays an important role in cell signaling. While the role of PTKs in cancer pathogenesis has been extensively studied over the past 30 years, the role of specific PTPs is less defined. We therefore studied the effects of the Src homology 2 domain containing phosphatase 2 (SHP2) in breast cancer. SHP2, encoded by PTPN11, is the first identified bona fide PTP proto-oncogene. It is a ubiquitously expressed phosphatase that acts as a signal enhancer downstream of growth factor, cytokine, and extracellular matrix receptors.

In the present study, we found an SHP2-dependent positive feedback loop that enhances the propagation of tumor initiating cells and the maintenance of breast tumors. We show that SHP2 is important for proliferation, loss of cell polarity, and invasion in a 3D culture model of invasive breast cancer. SHP2 promotes the progression from in situ to invasive carcinoma in vivo and is required for the maintenance and tumor-seeding ability of tumor initiating cells. We further demonstrate that knockdown of SHP2 in different breast cancer cell lines blocks tumor growth in vivo. Mechanistically, SHP2 promoted ERK1/2 activation leading to the upregulation of the transcription factors c-Myc and ZEB1. Increased expression of c-Myc led to upregulation of LIN28B which in turn repressed let-7 miRNA leading to overexpression of let-7 targets, including RAS and c-Myc. SHP2 also increased the expression of ZEB1, a transcription factor important in Epithelial-Mesenchymal Transition (EMT). Knockdown of SHP2 decreased the expression

of the EMT markers fibronectin, vimentin and N-cadherin and reduced the metastatic load in a HER2-positive cell line.

We then assessed the effects of SHP2 on tumor cell motility, invasion and dissemination; all of which are characteristics crucial for metastasis formation. We found SHP2 to be important for cell migration, chemotaxis, and invasion in vitro and also for tumor cell motility and dissemination in vivo, suggesting a role for SHP2 in the early steps of metastasis. In an unbiased proteomics screen, we found that SHP2 activates several Src family kinases to induce migration and invasion. Depletion of SHP2 led to inactivation of c-Src and several Src substrates and blocked cell migration and invasion in vitro and in vivo.

SHP2 was recently suggested to have nuclear functions. We explored the mechanism of its nuclear import and its nuclear roles in different breast cancer models. We confirmed nuclear localization of SHP2 in several breast cancer cell lines and identified a nuclear localization signal facilitating the nuclear import of SHP2. Future studies will be necessary to fully understand the nuclear functions of SHP2 in breast cancer.

In summary, we identified and validated SHP2 as a target in breast cancer. We identified its downstream effectors, which mediate its pro-migratory invasive effects and started the exploration of its nuclear functions. Future studies should address the effects of pharmacological inhibition of SHP2 in breast cancer, provided the availability of selective SHP2 inhibitors. In addition, assessment of the effects of nuclear SHP2 in breast cancer is warranted.

CONTENTS

2   INTRODUCTION

2.1   Breast cancer

Breast cancer is the most frequent cancer in females and the second most common cause of cancer related mortality in women worldwide (Ferlay, Shin et al. 2010). 1.64 Million new cases of breast cancer were diagnosed in women worldwide in 2010 and 425,000 died from the disease (Ferlay, Forman et al. 2012). Using cancer death and population data from the World Health Organization (WHO) database, researchers from Italy and Switzerland estimated 88,101 deaths from breast cancer in Europe alone in 2012 (Malvezzi, Bertuccio et al. 2012). This number corresponds to almost 16% of all cancer deaths in European woman, making breast cancer mortality the most frequent cause of death due to cancer in European females in 2012.

The first documented case of breast cancer dates back more than 5,000 years and was described in ancient Egypt (Farrow 1971). For a long time breast cancer was believed to be a 'systemic' disease caused by black bile as initially suggested by Hippocrates (460– 377 BC) and later elaborated by Galen (AD 131–203) (Sakorafas and Safioleas 2009). Over the centuries the knowledge increased and during the Renaissance the human anatomy was studied challenging Galen's theory. An increasing number of surgeons developed techniques to excise breast tumors. However before the 19th century brought the development of anesthesia and antiseptic surgery conditions, operations had to be rapid and often ended fatal due to infections (Sakorafas and Safioleas 2009). In the middle of the 18th century the French surgeon Le Dran (1685–1773) suggested the lymphatic spread of breast cancer during the progression of the disease and described tumor cell dissemination as "cancer is a local disease in early stages, and it is spread by lymphatics to regional nodes and then to the general circulation" (Naruke, Tsuchiya et al. 1999). A milestone in

the breast cancer treatment was the radical mastectomy, which is a surgical removal of the breast, the axillary lymph nodes and both underlying chest muscles in one block, introduced by the surgeon William Halsted (1852–1922) in 1894 (Halsted 1894). Additional landmarks altering the history of breast cancer treatment included the discovery of x-rays by Röntgen (1845–1923) in 1895, providing the basis for mammography and radiotherapy, the latter first applied to a breast cancer patient shortly after (Grubbe 1947, Ekmektzoglou, Xanthos et al. 2009). The Halsted mastectomy remained the most performed treatment for the next decade, until increasing criticism was voiced concerning the highly invasive procedure (Sakorafas and Safioleas 2010). Retrospective studies showed no increased survival benefit for surgeries done using Halsted`s technique when compared to less invasive procedures. This insight led to a gradual replacement of the radical mastectomy by the modified radical mastectomy (Williams, Murley et al. 1953, Handley and Thackray 1969). Breast conservation became an alternative to mastectomy and methods like quadrantectomy (a partial mastectomy removing about one quarter of the breast) and lumpectomy (local removal of the tumor mass) were developed, achieving the same relapse-free and overall survival rates as mastectomy (Fisher, Bauer et al. 1985). This was partly possible due to earlier detection allowing surgical removal at a smaller tumor size. The broad application of radiotherapy and systemic therapy, such as chemotherapy and hormonal therapy, before (neoadjuvant) and after (adjuvant) surgery further improved the success of breast cancer treatment in the 20th century (Sakorafas and Safioleas 2010).

However, despite these advances in breast cancer management over the last decades, metastatic breast cancer remains a serious issue costing the lives of many women each year. Due to the heterogeneity of the disease, finding the right treatment regime for each patient remains a challenge. Therefore, great effort is put into finding targeted

therapies pinpointing the molecular alterations discriminating different subtypes of breast cancer.

2.2 Classification of breast tumors

Breast cancer is a heterogeneous disease, which can be classified based on the expression of the hormone receptors (HR) estrogen receptor (ER) and progesterone receptor (PR), the expression of the epidermal growth factor receptor 2 (ERBB2 or HER2), response to therapy, and outcome (Perou, Sorlie et al. 2000, Sorlie, Perou et al. 2001, Cancer Genome Atlas 2012). Genome wide gene-expression based profiling revealed the existence of six subtypes of breast cancer (Perou, Sorlie et al. 2000, Sorlie, Perou et al. 2001, Carey, Perou et al. 2006, Prat, Parker et al. 2010). Based on aggressiveness, invasive potential and available therapies, each of these subtypes is associated with a different prognosis. Generally women with hormone receptor positive breast cancer have a better prognosis than those with hormone receptor negative disease (Cordera and Jordan 2006). Basal-like, claudin-low and HER2-positive (before the introduction of trastuzumab) breast cancers are associated with the worst outcome (Perou, Sorlie et al. 2000, Sorlie, Perou et al. 2001, Carey, Perou et al. 2006, Prat, Parker et al. 2010).

2.2.1 Luminal A and Luminal B breast cancers

Luminal tumors are the largest group comprising ~60% of all breast cancer cases. These tumors are characterized by the expression of ER and a subpopulation expresses PR in addition. While luminal A tumors generally co-express ER and PR, only a subset of luminal B tumors have been shown to express PR (Sims, Howell et al. 2007). This means that luminal tumors are hormone dependent and their growth can be inhibited by endocrine therapy blocking the effects of estrogen. Patients with luminal A breast cancer are more responsive to hormone therapy and have a better overall survival than patients suffering

from luminal B breast cancer (Vargo-Gogola and Rosen 2007). For over 35 years, the ER antagonist tamoxifen that blocks the binding of estrogen to its receptor has been the standard treatment for HR-positive breast cancers. (Johnston and Dowsett 2003). Tamoxifen is a prodrug that is metabolized to 4-hydroxytamoxifen in the liver, which acts as an ER antagonist outcompeting estrogen to bind to the ER, therefore inhibiting the transcription of estrogen-dependent genes (Desta, Ward et al. 2004). More recently, the use of inhibitors that block estrogen synthesis, such as aromatase inhibitors, has been promoted. Aromatase inhibitors are recommended for post-menopausal women with ER-positive disease, either as initial therapy or as sequential therapy following 2-3 years of tamoxifen treatment. Both treatment regimes are equally effective and superior to tamoxifen alone (Johnston 2010). For pre-menopausal women tamoxifen remains the first line of treatment (Rao and Cobleigh 2012). Unfortunately, de novo or acquired endocrine resistance is a common problem encountered during the treatment. Resistance mechanisms are mediated by changes in ER signaling such as loss or decreased expression and crosstalk between ER and receptor tyrosine kinases (RTKs). Examples include the upregulation of the HER2, epidermal growth factor receptor (EGFR) or insulin-like growth factor I (IGF-I) receptor and pathways downstream of these RTKs such as the phosphoinositol-3-kinase (PI3K) pathway (Arpino, Wiechmann et al. 2008, Musgrove and Sutherland 2009, Aguilar, Sole et al. 2010). Downstream effectors of these pathways can trigger the transcription of ER-dependent genes in absence of the ligand, thus interfering with estrogen (by aromatase inhibitors and trastuzumab) is no longer effective (Fedele, Calvani et al. 2012). A second-line treatment for postmenopausal women who have progressed after initial endocrine therapy is fulvestrant, which works by degrading the ER (Croxtall and McKeage 2011).

2.2.2   HER2-positive breast cancer

In 20% of breast cancers, the epidermal growth factor receptor 2 (ERBB2 or HER2) is amplified (Hynes and MacDonald 2009). HER2-amplified breast cancer is one of the more aggressive subtypes, however the development of targeted therapies improved the prognosis for this group of patients tremendously (Slamon, Clark et al. 1987, Slamon, Leyland-Jones et al. 2001). The current first-line treatment of HER2-positive breast cancer is the humanized monoclonal antibody trastuzumab (Herceptin) that is directed against the extracellular domain of HER2, in combination with chemotherapy (Baselga, Perez et al. 2006). This combination prolongs disease free survival and shows improved outcome for many patients with early HER2-positive breast cancer (Romond, Perez et al. 2005). However, because 70% of HER2-positive breast cancers show intrinsic or acquired resistance to trastuzumab treatment, alternative therapies either as monotherapies or in combination with trastuzumab are being explored (Arribas, Baselga et al. 2011, Wong and Lee 2012). These include but are not limited to the tyrosine kinase inhibitors (TKIs) lapatinib, neratinib, and afatinib, trastuzumab-DM1 (trastuzumab emtansine), heat shock protein 90 (HSP90) inhibitors, and the dimerization inhibitor pertuzumab (Capelan, Pugliano et al. 2013). Currently trastuzumab, lapatinib, trastuzumab-DM1, and pertuzumab are approved for metastatic HER2-positive breast cancer.

Lapatinib is a small molecule reversible TKI targeting EGFR and HER2. Unlike lapatinib, neratinib and afatinib are irreversible TKIs. Afatinib targets the same receptors as lapatinib, whereas neratinib is a pan-HER inhibitor used in patients with advanced breast cancer (Burstein, Sun et al. 2010, Wong and Lee 2012). Trastuzumab-DM1 is a recently FDA approved antibody–drug conjugate, consisting of the antibody trastuzumab and the microtubule inhibitor DM1. Being linked to the anti-HER2 antibody targets the cytotoxic drug to HER2-overexpressing cells and thus reduces side effects (Peddi and

Hurvitz 2013). The chaperone protein HSP90 assists in stabilizing and folding of many oncoproteins including HER2. Several HSP90 inhibitors are currently in clinical trials in combination with trastuzumab (Wong and Lee 2012). Another treatment option, which has been recently approved by the FDA, is the humanized monoclonal antibody pertuzumab. This antibody targets the extracellular dimerization domain of HER2, thereby blocking the heterodimerization of HER2 and HER3, which is a critical step in HER2 activation (Arpino, Gutierrez et al. 2007, Capelan, Pugliano et al. 2013).

2.2.3   Triple-negative breast cancer

The third group, representing 10-20% of all breast cancer cases, is triple-negative breast cancer (TNBC) (Morris, Naidu et al. 2007, Cancer Genome Atlas 2012). TBNCs do not express ER, PR or HER2 and include the basal-like and the claudin-low subtypes (Perou 2011). Basal-like breast cancers got their name as they have a genetic profile similar to basal/myoepithelial cells in the normal breast (Perou, Sorlie et al. 2000). Molecular hallmarks of this tumor subtype include the expression of the basal cytokeratins 5/6, 14, and 17 (Elsawaf and Sinn 2011). Claudin-low tumors on the other hand, frequently show immune cell infiltration, stem cell and Epithelial-Mesenchymal Transition (EMT) characteristics. The EMT features include a low expression of cell-cell junction proteins such as E-cadherin and claudin 3, 4, and 7 (Perou 2010). The majority of TNBCs do not respond to endocrine or anti-HER2 therapies, leaving chemotherapy as the only treatment option besides surgery. To date, no targeted therapies are available for this subtype (Crown, O'Shaughnessy et al. 2012). Less than 30% of women diagnosed with metastatic TNBC will survive 5 years and the majority of the patients finally succumb to their disease (Dent, Trudeau et al. 2007). Generally initial response rates to chemotherapy are good and patients achieving a complete response to therapy have survival rates similar to other breast cancer subtypes (Carey, Dees et al. 2007). Unfortunately, complete response is

seldom achieved due to the high metastatic potential, leading to poorer overall survival prognoses of TNBC patients compared to patients with other breast cancer subtypes (Crown, O'Shaughnessy et al. 2012).

There is an urgent need for new therapies to treat TBNC and numerous clinical studies are ongoing. Targets under investigation include proteins overexpressed in TNBC such as EGFR, c-kit or cytokeratins 5/6, 14, and 17. Anti-angiogenic therapies, such as the anti-vascular endothelial growth factor (VEGF) monoclonal antibody bevacizumab and the anti-VEGFR tyrosine kinase inhibitors sunitinib and sorafenib are being investigated (Crown, O'Shaughnessy et al. 2012). Other possibilities currently tested include poly (ADP-ribose) polymerase (PARP) inhibitors such as olaparib (Tutt, Robson et al. 2010) and agents targeting mTOR and Src (Finn, Dering et al. 2007). Claudin-low breast tumors were shown to have stem cell characteristics (Creighton, Li et al. 2009). Therefore, agents targeting breast cancer stem cells are under investigation in connection with claudin-low breast cancers (Perou 2011).

2.3   The breast cancer stem cell model

According to the cancer stem cell (CSC) hypothesis, tumors are composed of hierarchically organized malignant cells (Sottoriva, Vermeulen et al. 2011). At the top of this hierarchy are the CSCs, also called cancer stem-like cells or tumor initiating cells (TICs), which drive and sustain the proliferation of the tumor. CSC are operationally defined as cells that form tumors after transplantation into immunodeficient mice giving rise to CSCs and non-stem cancer cells (NSCC) and thus recapitulating the heterogeneity of the tumor (Clarke, Dick et al. 2006). Others have suggested additional properties for these cells such as: metastatic potential, prolonged periods of dormancy, and resistance to radiotherapy and chemotherapy (Clevers 2011).

The hierarchical organization of tumors was noticed several decades ago, when the presence of TICs was assessed by a series of transplantation experiments (Clevers 2011). In 1937, Furth and Kahn showed that a single leukemic cell was sufficient to initiate leukemia when transplanted into a recipient mouse and subsequent studies estimated CSC frequencies in leukemia and solid tumors in the range of 1:1,000 to 1:10,000,000 (Clevers 2011). Pierce and colleagues showed that single teratocarcinoma cells were capable to differentiate into multiple non tumorigenic cell types (Kleinsmith and Pierce 1964, Pierce and Wallace 1971). Based on his observations, Pierce described the CSCs concept in 1988 as "a concept of neoplasms, based upon developmental and oncological principles, states that carcinomas are caricatures of tissue renewal, in that they are composed of a mixture of malignant stem cells, which have a marked capacity for proliferation and a limited capacity for differentiation under normal homeostatic conditions, and of the differentiated, possibly benign, progeny of these malignant cells" (Pierce and Speers 1988, Clevers 2011). In the 1990s the CSC theory received new attention and grew into a field of intensive research. In 1995, Dick and colleagues identified CSCs in acute myeloid leukemia (AML) using newly developed Fluorescent-activated cell sorting (FACS) techniques based on the expression of specific surface markers in different cell compartments (Bonnet and Dick 1997). In 2003, Al-Hajj and colleagues validated the CSC hypothesis in some breast cancers. In a xenografts assay they showed that 100 CD44^{high}/CD24^{low} cells were sufficient to form a tumor, containing both, CSCs and NSCCs, when transplanted into immunodeficient recipient mice. Other subpopulations failed to engraft even at much higher numbers (Al-Hajj, Wicha et al. 2003). Similar studies confirmed the CSC hypothesis in samples from other solid cancers such as brain (Singh, Hawkins et al. 2004), pancreas (Li, Heidt et al. 2007), colon (O'Brien, Pollett et al. 2007,

Ricci-Vitiani, Lombardi et al. 2007), liver (Yang, Ho et al. 2008), and melanoma (Schatton, Murphy et al. 2008).

CSCs are believed to play a crucial role in relapse after initial successful treatment (Lawson, Blatch et al. 2009). Conventional chemotherapy and radiotherapy are tailored to target the bulk of the tumor cells but are not effective in depleting quiescent CSCs. While the overall tumor size decreases, a small amount of CSCs may remain or disseminate to distant organs resulting in local relapse or distant metastases later on (Aguirre-Ghiso 2007). This was demonstrated in patients receiving neoadjuvant chemotherapy. Paired samples were evaluated for their percentage of $CD44^{high}/CD24^{low}$ cells, before and after the treatment, and chemotherapy was found to increase the fraction of $CD44^{high}/CD24^{low}$ cells (Li, Lewis et al. 2008). Therefore their intrinsic properties enable CSCs to escape current treatments and seed metastases (Li, Tiede et al. 2007, Li, Lewis et al. 2008, Charafe-Jauffret, Ginestier et al. 2009, Morrison, Schleicher et al. 2011). Ongoing research seeks to identify targets to develop therapies to deplete CSCs, rather than the bulk of the tumor cells. However, a more profound knowledge about the characteristics of CSCs is required. The development of more specific CSC markers is essential, and the stability of the CSC phenotype needs to be addressed, as studies have shown plasticity between the CSC and NSCC state suggesting a dynamic equilibrium (Clevers 2011, Vermeulen, de Sousa e Melo et al. 2012). Meyer and colleagues showed that the breast CSC markers $CD44^{high}/CD24^{low}$ are under dynamic regulation by demonstrating that non-invasive, epithelial-like $CD44^{high}/CD24^{high}$ cells gave rise to invasive, mesenchymal $CD44^{high}/CD24^{low}$ progeny in vitro and in vivo (Meyer, Fleming et al. 2009). Iliopoulos and colleagues proposed a dynamic equilibrium between the CSC and the NSCC state mediated by interleukin 6 (Iliopoulos, Hirsch et al. 2011). Considering this plasticity of the

CSC state, it seems that the combination of therapies targeting CSCs and NSCCs will most likely be needed to cure cancer.

2.4   Breast cancer progression

Breast cancer arises from the epithelial cells of the mammary gland. The classical linear progression model suggests that breast cancer initiates as flat epithelial atypia (FEA) or hyperplasia, progresses to atypical ductal hyperplasia (ADH), evolves into ductal carcinoma in situ (DCIS), and culminates in the potentially lethal stage of invasive ductal carcinoma (IDC) (**Figure 1**). The final, and usually fatal step of breast cancer progression is metastatic spread to distant organs such as lung, bone, liver, and brain (Eckhardt, Francis et al. 2012).

In contrast, Klein and colleagues have proposed a parallel progression model. According to this model, metastatic cells can quit the primary tumor site as early as DCIS. Tumor cells leave the tumor before acquiring a fully malignant phenotype to then undergo rounds of selection and mutation at the distant sites (Klein 2009). Klein`s laboratory has found disseminated breast cancer cells which were detected in the bone marrow of patients, to be in a much less progressed genetic state than predicted by the linear progression model, which states that only fully transformed cells quit the primary tumor. These findings suggested, that early disseminated tumor cells might acquire the mutations needed for metastatic behavior at a later stage (Schmidt-Kittler, Ragg et al. 2003). They further showed in mouse models and in samples from breast cancer patients with DCIS, that disseminated tumor cells in bone and micrometastases could originate from the time of first epithelial alterations at the primary tumor site (Husemann, Geigl et al. 2008). Due to this progression at the distant metastatic site, the parallel progression model suggests a greater difference between the primary tumor and the distant metastases (Klein 2009).

Because early disseminated tumor cells are not fully transformed, they often only grow out

years, or even decades, after dissemination (Aguirre-Ghiso 2007).
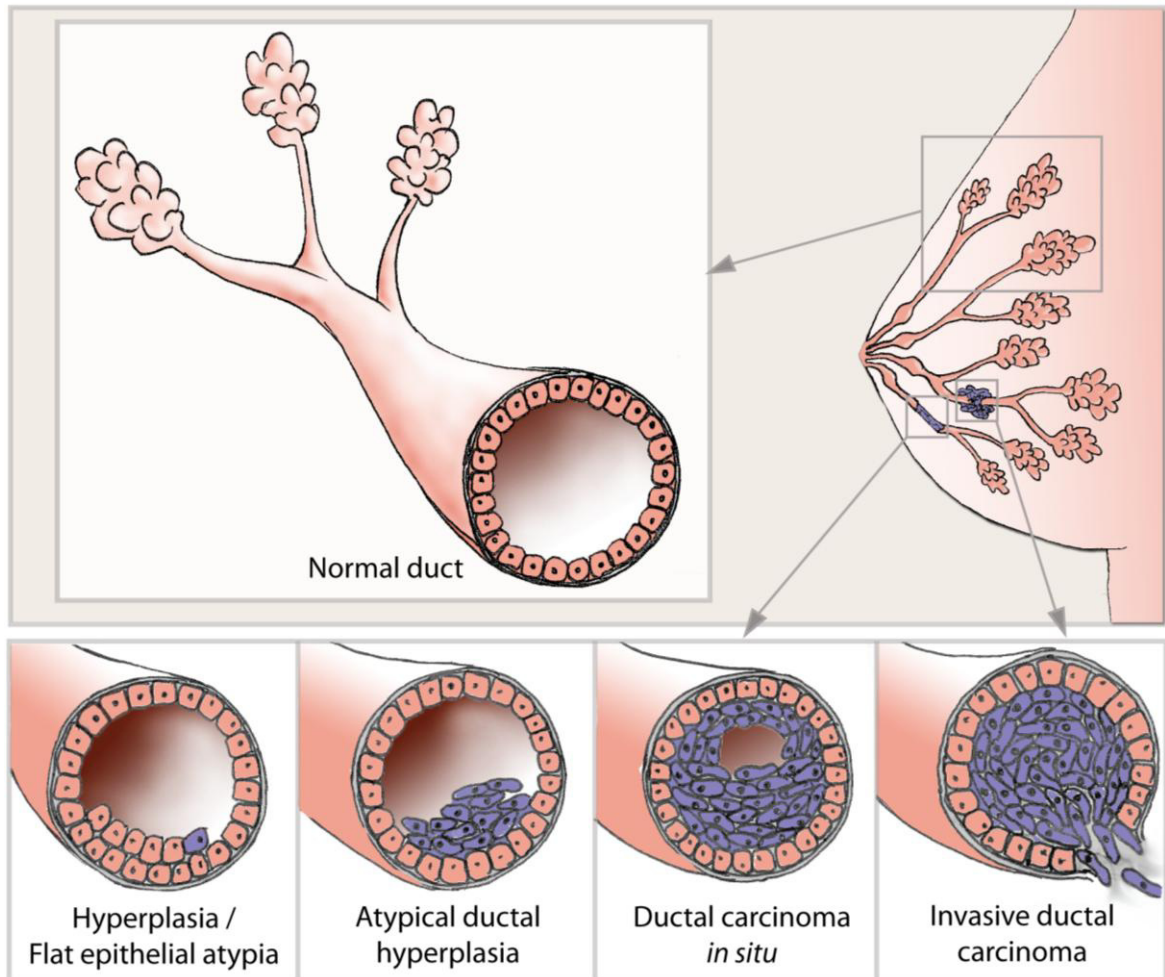
Figure 1. Breast cancer linear progression model
Schematic of the breast cancer progression steps according to the linear progression model. Breast cancer arises from the epithelial cells of the mammary gland as flat epithelial atypia or hyperplasia, which is a benign proliferative breast condition. It can progress into atypical ductal hyperplasia, where the proliferating cells look abnormal, and evolve into ductal carcinoma in situ, a non-invasive stage, in which the duct is filled with cancerous cells remaining inside the duct. The last and potentially lethal step of the metastatic cascade is the progression into invasive ductal carcinoma, in which the cancer cells spread from the duct to surrounding tissue, to seed and colonize at distant sites.

2.5   EMT during cancer progression and metastasis

As described above, the final and often fatal step in the progression of breast cancer is the formation of distant metastases. Approximately 90% of all cancer related deaths are caused by metastatic dissemination to distant organs (Christofori 2006). Metastases formation is a multistep progress. First, metastatic tumor cells have to acquire the ability to emigrate from the primary tumor. To detach from the tumor mass, metastatic cells must lose their cell-cell junctions and become motile. To leave the primary tumor site, the cells must not only be motile, but also have to acquire invasive potential to degrade the surrounding extracellular matrix (ECM), basement membrane, and endothelial barrier to intravasate into the lymphatic vessels or bloodstream. This population of cells further needs to be capable to survive in the bloodstream. After traveling through the lymphatic or vascular system to a distant site, the cells require adhesion potential to attach to the endothelium. Finally, metastatic cells need the potential to extravasate through the vessel basement membrane to form micrometastases at the distant site (Friedl and Gilmour 2009) (**Figure 2**).
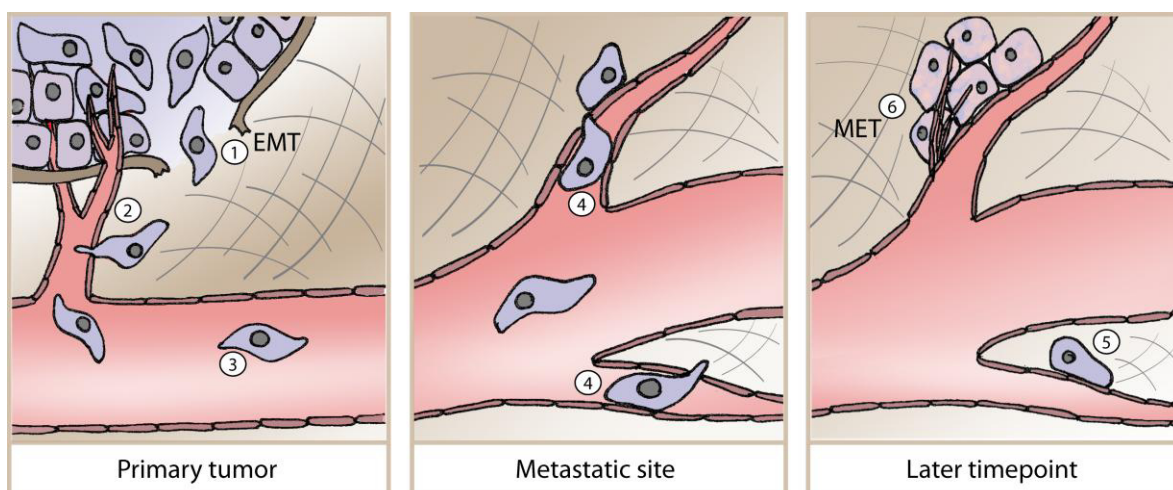
Figure 2. Schematic of the metastatic cascade
Metastasis is a multistep progress. 1) Cells in the primary tumor undergo Epithelial-Mesenchymal Transition (EMT), acquire invasive potential, and degrade the basement membrane. 2) Invasive tumor cells intravasate into the bloodstream either via the

lymphatic system or directly. 3) Metastatic cells are transported through the circulation to distant sites. 4) Circulating tumor cells attach to the endothelial membrane or are arrested in small capillaries and extravasate. 5) Extravasated tumor cells can stay dormant for years or 6) undergo Mesenchymal-Epithelial Transition (MET) and micrometastases can progress into macrometastases at the distant site.

The currently accepted theory of how initially quiescent tumor cells acquire motility and metastatic potential is Epithelial-Mesenchymal Transition (EMT). First described in 1982 in three-dimensional cultures of corneal epithelial cells by Hay and colleagues (Hay 1982), EMT has gradually become better characterized. EMT can be grouped into 3 classes, depending on the context in which it appears (Kalluri 2009). Type 1 EMT and its reverse process Mesenchymal-Epithelial Transition (MET), have been well described in mammalian embryogenesis where the development of many organs depends on the switch between epithelial and mesenchymal cell fates (Micalizzi, Farabaugh et al. 2010). Type 2 EMT have been shown to play a role in tissue regeneration, wound healing, and fibrosis and are associated with inflammation (Kalluri 2009). More recently, the same cellular program, termed type 3 EMT, was implicated in cancer progression and metastasis formation (Lopez-Novoa and Nieto 2009). The exact molecular mechanism underlying the switch of epithelial tumor cells to an invasive phenotype, has been and still is subject of many studies. Type 3 EMT has emerged as the primary theory of how tumor cells acquire the attributes necessary to metastasize (Thiery 2002).

The progression from polarized epithelial tumor cells to invasive carcinoma requires several steps (Kalluri 2009, Yilmaz and Christofori 2009). The first step of the EMT process in cancer progression is the loss of apico-basal polarity and tight junctions. Next, cell-cell junctions including adherens and gap junctions begin to disassemble and the underlying basement membrane is degraded (Peinado, Portillo et al. 2004). A molecular hallmark of EMT is the downregulation of cell-cell adhesion molecules and epithelial

markers such as E-cadherin, claudins and cytokeratins (Kalluri 2009). A downregulation of E-cadherin expression followed by an upregulation of N-cadherin has been proposed to be responsible for breast cancer cell invasion (Sommers, Thompson et al. 1991, Sommers, Gelmann et al. 1994). However, not all breast cancer cell lines express E-cadherin and/or N-cadherin and it has been shown that N-cadherin leads to cell motility and an invasive phenotype regardless of the E-cadherin expression level (Nieman, Kim et al. 1999, Nieman, Prudoff et al. 1999). Besides changes in the cadherin expression levels, cytoskeletal elements are reorganized during EMT. The peripheral actin cytoskeleton is replaced by stress fibers and the intermediate filaments are replaced by vimentin. Phenotypically, these changes alter the cell morphology from cuboidal cobblestone appearance to spindle shaped. The cells become invasive, motile, and resistant to anoikis and begin to respond to extracellular stimuli, directing the migrating cells (Micalizzi, Farabaugh et al. 2010) (**Figure 3**).
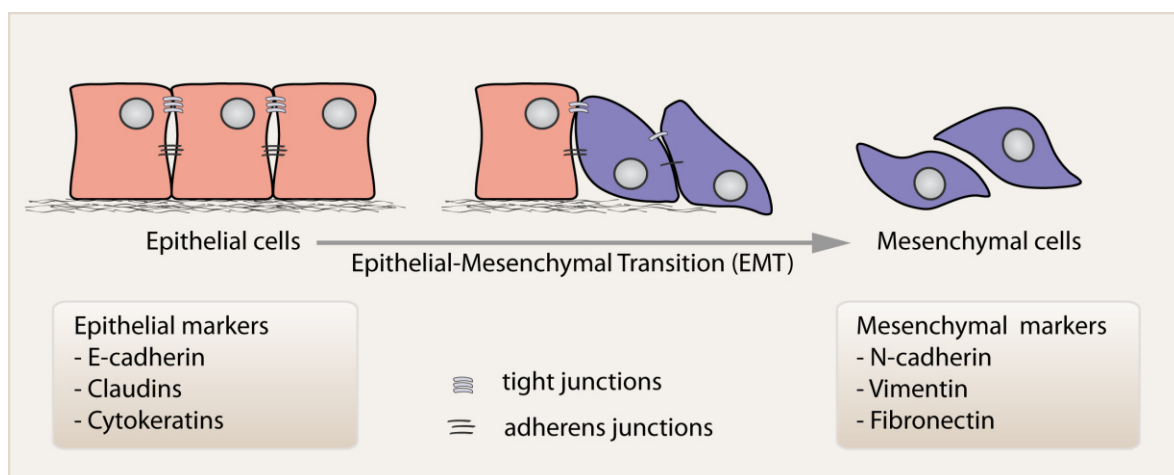
Figure 3. Diagram of molecular and phenotypic transitions of cells undergoing EMT
During the process of EMT, epithelial cells lose their cell-cell junctions and polarity which is accompanied by a change of morphology from cobblestone like to the elongated, motile, and invasive phenotype of mesenchymal cells (Chaffer, Thompson et al. 2007).

2.6   Cell migration

The understanding of the mechanisms underlying the regulation of cell migration multiplied over the last two decades (Huttenlocher and Horwitz 2011). Significant advances have been made in the involvement of the actin cytoskeleton and its fine regulation in the maintenance of cellular integrity and the dynamic responses that drive cell migration (Vicente-Manzanares, Webb et al. 2005).

Cell migration over a substrate has been described as the succession of protrusion at the leading edge and stabilization by the formation of new adhesions, followed by the release of adhesions at the rear of the cell, detachment and translocation (Abercrombie, Heaysman et al. 1971, Huttenlocher and Horwitz 2011) (**Figure 4**). The first step in the sequence, protrusion, is driven by actin polymerization at the leading edge of the cell (Pollard and Borisy 2003). Two morphological structures, lamellipodia and filopodia, which are comprised of different F-actin networks and dynamics are the basic units of cell migration (Svitkina, Verkhovsky et al. 1996). Protrusion is followed by retraction of the trailing edge and finally the cell translocates to a new position.

1. Protrusion at the leading edge

actin network

substrate

2. Adhesion at the leading edge

new actin
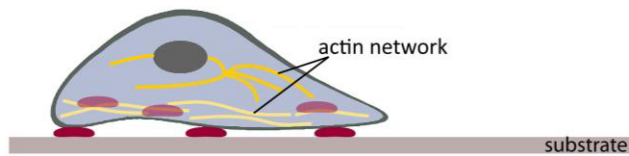
new adhesion

substrate
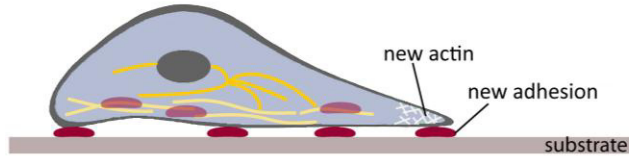
3. Retraction of the trailing edge

substrate
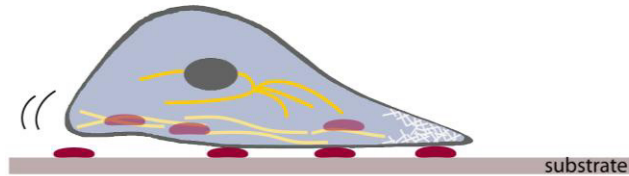
4. Translocation of the cell body

substrate

actin network   stress fibers

focal adhesion   microtubules
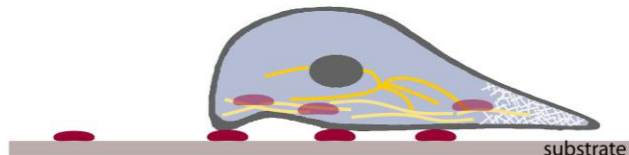
Figure 4. Model of cell migration
Cell migration consists of the following successive steps:

1. Protrusion
Extracellular stimuli induce de novo actin polymerization at the leading edge resulting in the formation of F-actin based membrane protrusions such as lamellipodia and filopodia.

2. Adhesion
Stabilization of protrusions at the leading edge by formation of new adhesions.

3. Retraction
Stress fibers and adhesive structures at the trailing edge are broken down.

4. Translocation
As a result, the cell moves to a new position.

Integrins are the best described transmembrane receptors mediating interactions between the ECM and the actin cytoskeleton during cell motility (Hynes 2002, Huttenlocher and Horwitz 2011). Integrins are non-covalently linked heterodimers, composed of one of 18 different α chains and one of 8 different β subunits in humans. Both subunits have a large extracellular domain binding to the ECM and a short cytoplasmic tail linking the cytoskeleton (Hynes 2002). The binding specificity is determined by the extracellular domain, which specifically recognizes matrix ligands. The α1β1 and α2β1 integrins bind collagen, while α4β1, α5β1, and αvβ3 integrins are major fibronectin receptors and integrins α3β1 and α6β1 are receptors for laminins (Hood and Cheresh 2002, Hynes 2002). Changes in integrin subtype expression have been correlated

with changes in migration and invasion (Huttenlocher and Horwitz 2011). Integrin expression has further been shown to be predictive for the outcome of breast cancer (dos Santos, Zanetti et al. 2012). Specifically, the integrins α6β4 and αvβ3 have been linked to increased tumor metastases formation and decreased survival in breast cancer (Desgrosellier and Cheresh 2010). Highly migratory and invasive cells form specialized types of integrin-mediated adhesions, called podosomes or invadopodia (in invasive cells) (Weaver 2006). Both, podosomes and invadopodia are actin rich protrusions capable of matrix degradation and invadopodia are a hallmark of metastatic cancer cells (Weaver 2006, Huttenlocher and Horwitz 2011). In breast cancer cell lines, the presence of invadopodia has been linked to their metastatic potential (Yamaguchi, Lorenz et al. 2005, Yamaguchi, Takeo et al. 2009). In addition, invadopodia-like structures have been observed in vivo by intravital imaging (Yamaguchi, Wyckoff et al. 2005, Sidani, Wyckoff et al. 2006). For cell migration, the dynamic formation and turnover of integrin-mediated adhesions, and the polarized assembly and disassembly of focal adhesions are crucial for optimum cell speed and directional persistence (Huttenlocher and Horwitz 2011).

Focal adhesions, connecting the cytoskeleton to the ECM, are the best described cell-matrix adhesions. They consist of clusters of integrin receptors associated with large complexes of signaling and structural proteins linked to the actin cytoskeleton (Burridge and Chrzanowska-Wodnicka 1996, Yamada and Geiger 1997). The turnover of focal adhesions is regulated by focal adhesion kinase (FAK) and Src family kinases (SFKs). FAK deficient fibroblasts or cancer cells exhibit reduced migration rates and form increased numbers of large adhesions with an impaired turnover (Ilic, Furuta et al. 1995, Sieg, Hauck et al. 2000, Hsia, Mitra et al. 2003). Likewise, fibroblasts from mice lacking c-Src, Fyn, and Yes, or expressed a kinase-dead c-Src mutant, also showed impaired migration and large peripheral adhesions with reduced turnover (Fincham and Frame 1998,

Klinghoffer, Sachsenmaier et al. 1999). In addition to SFKs and FAK, the phosphatase SHP2 has also been implicated in cell migration. SHP2-deficient fibroblasts showed impaired migration and large peripheral adhesions, resembling the phenotype of FAK and Src deficient cells (Yu, Qu et al. 1998).

In conclusion, these studies show that dynamic cycles of phosphorylation and dephosphorylation at adhesion sites are fundamental for adhesion turnover and migration (Huttenlocher and Horwitz 2011). Both, tyrosine kinases and phosphatases play important roles in the regulation of cell migration. Cancer cell migration is the first step in the progression of the primary tumor towards metastatic spread (Etienne-Manneville 2008). It is therefore crucial to better understand the roles of kinases and phosphatases in this early step, to interfere with the cancer progression to the potentially lethal metastatic state.

2.7   Cell signaling in cancer: Kinases & Phosphatases

Many important signaling pathways in eukaryotic cells rely on reversible phosphorylation of tyrosine residues on proteins. Abnormal tyrosine phosphorylation is linked to the pathogenesis of a multitude of human diseases including cancer (Hunter 2009, Pawson and Kofler 2009). Although phosphotyrosines account only for 0.05-1.5% of a cells total phosphoamino acid content depending on the cell type, tyrosine phosphorylation plays an important role in cell signaling (Cooper and Hunter 1981, Frank and Sartorelli 1986, Conrads and Veenstra 2005). Phosphorylation at this residue can alter target proteins by inducing conformational changes that influence protein activity, by creating docking sites for other proteins therefore enabling protein complex formation, or by influencing the subcellular localization (Stoker 2005). This enzymatic reaction is controlled by protein tyrosine kinases (PTKs) that add phosphate groups to their substrates and protein tyrosine phosphatases (PTPs) that remove them (Tonks 2006). While the role of protein tyrosine

kinases in cancer pathogenesis has been thoroughly studied over the past 30 years providing a wealth of knowledge (Hunter 2009), the role of PTPs in the development of cancer is less well defined (Ostman, Hellberg et al. 2006). Initially, PTPs were thought to only play a signal attenuating role, but further research provided evidence that PTPs can act as positive signal transducers (signal enhancing) (Alonso, Sasin et al. 2004, Tonks 2006). They can, for example, activate PTKs by dephosphorylation of inhibitory sites or prolong activation signals (Scott, Lawrence et al. 2010).

2.8   Protein tyrosine phosphatases

PTPs are a large family of related enzymes. They are divided into two families: Classical PTPs that dephosphorylate only tyrosine (Tyr) residues, whereas dual-specificity phosphatases can dephosphorylate serine (Ser), threonine (Thr) or Tyr residues (Tonks 2006). The classical PTP family contains 37 different PTPs in the human genome, which are grouped into receptor-like PTPs and non-transmembrane or intracellular PTPs (Andersen, Mortensen et al. 2001) (**Figure 5**).
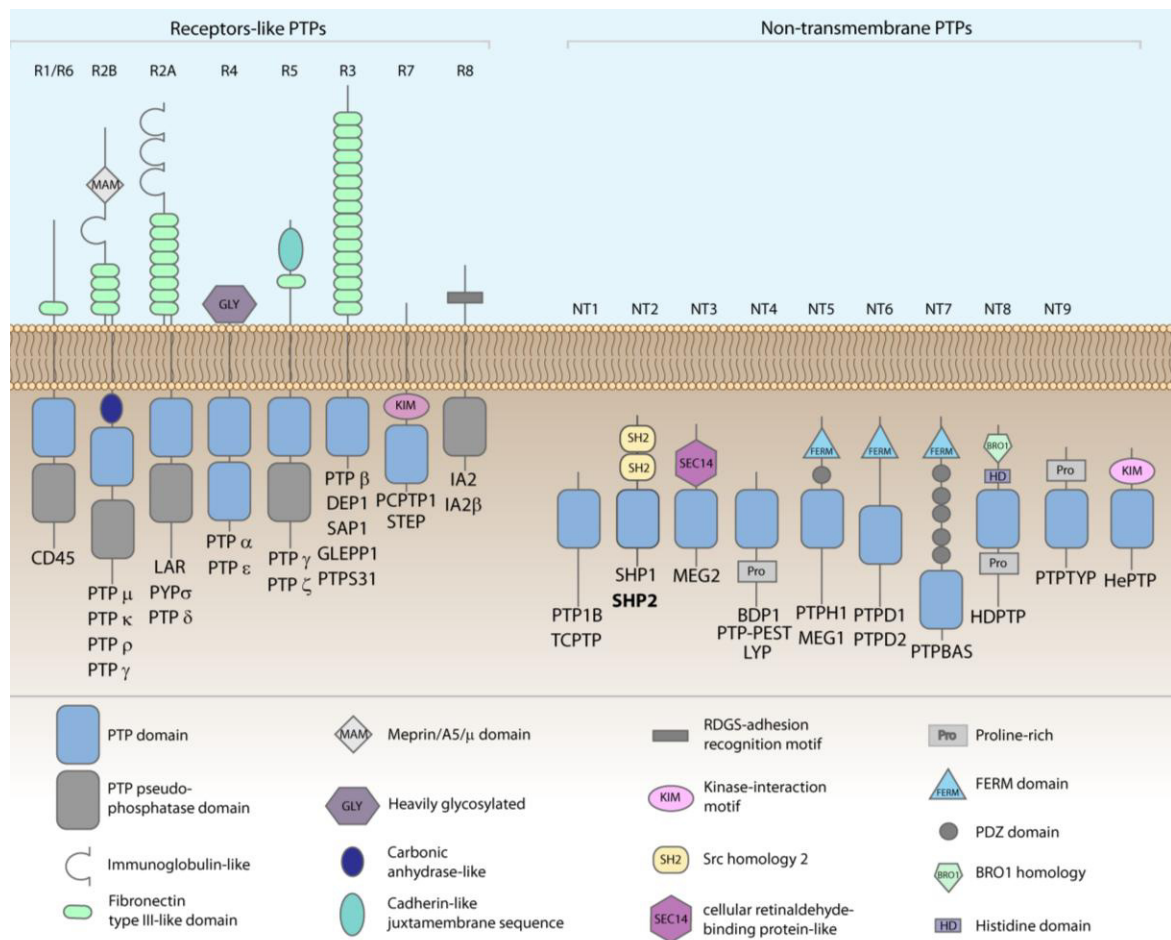
Figure 5. Schematic overview of the classical PTP family

The family consists of 37 human members divided into receptor-like PTPs and non-transmembrane PTPs. The receptor-like PTPs contain an intracellular PTP domain, consisting of the catalytic-site motif $HC(X)_5R$, a transmembrane domain and different types of extracellular domains responsible for cell-cell, cell-matrix or cell-ligand interactions (Freiss and Vignon 2004). The intracellular PTPs are more diverse in their structure. They contain a PTP domain with the catalytic-site motif and several other types of domains including SH2, FERM, and PEST like domains that target them to specific cellular locations or enable binding to specific adapter proteins (Tonks 2006).

All members of the PTP family follow the same catalytic mechanism to dephosphorylate their respective substrates. They catalyze the hydrolysis of a phosphoester bond via a phosphate-cysteine intermediate requiring the catalytic cysteine (Cys) residue. Therefore, the phosphatase activity depends on the catalytic cysteine (Cys459 in SHP2) located in the PTP signature motif, which sits at the base of the catalytic cleft and is crucial

for the substrate recognition (Andersen, Mortensen et al. 2001, Tiganis and Bennett 2007).

In SHP2, the catalytic cleft is located at the base of the phosphate-binding loop (P-loop) that extends to a depth of up to 9 Å from the molecular surface (Hof, Pluskey et al. 1998). This depth determines the specificity for pTyr-containing peptides and prevents binding of shorter pSer and pThr side chains (Jia, Barford et al. 1995). The P-loop is composed of mainchain amide groups and the sidechain of an arginine (Arg) residue (Arg465 in SHP2) (Hof, Pluskey et al. 1998). During the two step catalysis, the catalytic Cys459 acts as a nucleophile to attack the phosphate of the phosphotyrosyl substrate (Barford, Flint et al. 1994, Jia, Barford et al. 1995). First, the sulfur atom of the thiolate ion of Cys459 attacks the phosphorous atom of the phosphate group of the substrate. The P-O linking the phosphate group to the Tyr is protonated by a conserved aspartic acid residue (Asp425 in SHP2). This Asp425 resides in the WPD-loop and is brought in close proximity by a conformational change of the protein upon substrate binding. In the second step, the phosphate-cysteine intermediate is hydrolyzed by a water molecule and Asp425 (now functioning as a general base) resulting in the release of the phosphate (Hof, Pluskey et al. 1998, Tonks 2006, Tautz and Mustelin 2007) (**Figure 6**).
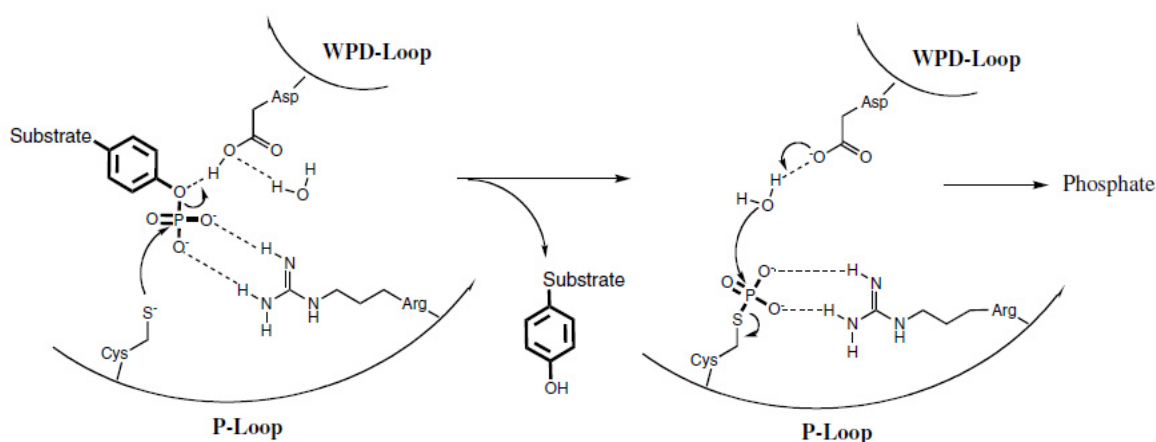
Figure 6. Catalytic mechanism of cysteine-based protein tyrosine phosphatases
The catalytic cysteine (Cys) is part of the PTP signature motif $HC(X)_5R$ located in the phosphate-binding loop (P-loop). The catalytic cysteine (Cys459 in SHP2) acts as a nucleophile to attack the phosphate on the substrate and is needed to catalyze the hydrolysis of the phosphoester bond via a phosphate-cysteine intermediate. A conserved invariant aspartic acid (Asp425 in SHP2), located in the WPD-loop, functions as the general acid/base during hydrolysis (Tautz and Mustelin 2007).

Flint and colleagues demonstrated that the mutation of amino acids playing a crucial role in the catalytic process (Cys and Asp) can generate PTP substrate-trapping mutants. These substrate-trapping mutant PTPs allow isolation of a PTP in complex with their trapped substrates (Flint, Tiganis et al. 1997). It was shown by several groups that PTP trapping-mutants can be obtained by exchanging the Asp residue in the conserved WPD-loop by alanine (Ala) in PTP1B, TC-PTP, and PTP-PEST (Garton, Flint et al. 1996, Flint, Tiganis et al. 1997, Tiganis, Bennett et al. 1998). It was further shown that alteration of the nucleophilic Cys at the catalytic site to Ser or Ala, results in a trapping mutant for some PTPs with varying efficiency (Zhang, Wang et al. 1994, Zhou, Denu et al. 1994, Jia, Barford et al. 1995). This demonstrates that not all mutations work equally well in different PTPs. The Agazie lab developed a SHP2 double trapping mutant by changing Cys459 to Ser and Asp425 to Ala. The trapping efficiency of this double mutant was found to be higher than the trapping efficiency of a single Cys459 to Ser mutant. They observed no trapping effect in the Asp425 to Ala single mutant in SHP2 (Agazie and Hayman 2003).

2.9   The proto-oncogenic phosphatase SHP2

Mammalian Src homology 2 domain containing phosphatase 2 (SHP2) is also known as Syp, SH-PTP2, SH-PTP3, PTP1D or PTP2C and was identified by several groups in the early 1990s (Adachi, Sekiya et al. 1992, Freeman, Plutzky et al. 1992, Ahmad, Banville et

al. 1993, Feng, Hui et al. 1993, Vogel, Lammers et al. 1993). SHP2 is a member of the Src homology 2 (SH2) domain containing phosphatase family consisting of two human members: Src homology 2 domain containing phosphatase 1 (SHP1) encoded by the PTPN6 gene and SHP2 encoded by PTPN11 (Chan, Kalaitzidis et al. 2008). As indicated by their name, these PTPs contain two SH2 domains at their N-terminus and a phosphatase domain at the C-terminus. SHP2 is ubiquitously expressed, whereas the expression of SHP1 is primarily restricted to hematopoietic cells (Feng and Pawson 1994). Upon growth factor or cytokine stimulation, SHP2 was shown to bind a variety of receptor tyrosine kinases (Feng, Hui et al. 1993, Lechleider, Freeman et al. 1993, Vogel, Lammers et al. 1993). SHP2 transduces mitogenic, pro-survival, cell fate and/or pro-migratory signals downstream of many cytokine, growth factor, and extracellular matrix receptors. Further, SHP2 is involved in positive regulation of the mitogen-activated protein kinase (MAPK)/extracellular signal-related kinase (ERK) pathway in response to most growth factors and cytokines (Bennett, Hausdorff et al. 1996, O'Reilly and Neel 1998). The regulation of other pathways is cell specific, receptor specific or both. Examples are the Janus kinase (Jak)-signal transducer and activator of transcription protein (STAT) and the PI3K pathways (Shi, Yu et al. 2000, Ostman, Hellberg et al. 2006, Chan, Kalaitzidis et al. 2008). Another role of SHP2 was found in cell spreading and cell migration (Yu, Qu et al. 1998, Manes, Mira et al. 1999, Oh, Gu et al. 1999).

Depending on the cellular localization, additional functions of SHP2 have been reported. At first, SHP2 was identified as an only cytoplasmic phosphatase. This finding was not questioned for several years, presumably because all functions discovered were linked with tyrosine dephosphorylation of membrane-associated proteins. In 2001, Craggs and Kellie showed that SHP1 was localized in the nucleus of non-hematopoietic cells, which was until then also believed to be solely cytoplasmic. They investigated the

subcellular localization of GFP-tagged SHP1 and SHP2 in human embryonic kidney (HEK) 293 cells and found SHP1 localized in the nucleus whereas SHP2 was predominantly seen in the cytoplasm. They found a cluster of the three basic amino acids Lysine (Lys)-Arg-Lys at the far end of the C-terminal domain of SHP1 which resembled half of a bipartite nuclear localization signal (NLS). This motif was not conserved in the SHP2 sequence (Craggs and Kellie 2001).

Proteins above 40 kDa generally require a NLS to be translocated into the nucleus. To date, no mechanism of nuclear import of the 72 kDa SHP2 protein has been reported. However, over the last years evidence has mounted, that SHP2 is found in other cellular locations than the cytoplasm. It has been found in the nucleus (Chughtai, Schimchowitsch et al. 2002, Wu, Hong et al. 2002, Jakob, Schroeder et al. 2008) and in the mitochondria (Salvi, Stringaro et al. 2004).

2.9.1   Structure and activation of SHP2

SHP2 contains two Src homology 2 (SH2) domains (N-SH2 and C-SH2), a PTP domain, and a C-terminal region which consists of a proline-rich motif and two tyrosyl phosphorylation sites (Tyr542 and Tyr580) (Chan, Kalaitzidis et al. 2008) (**Figure 7**).

Figure 7. Schematic structure of SHP2
The phosphatase SHP2 consists of two N-terminal tandem SH2 domains, a catalytic phosphatase (PTP) domain, and a proline-rich motif at the C-terminus containing the two tyrosine residues Tyr542 (Y542) and Tyr580 (Y580).

SHP2 activity is controlled by its structural conformation (**Figure 8**). In the absence of upstream stimulation, the N-SH2 domain interacts with the PTP domain keeping SHP2 in an inactive state by autoinhibition (Hof, Pluskey et al. 1998). Upon stimulation by growth factors or cytokines, SHP2 is recruited to the membrane and binds to specific tyrosine phosphorylated sites on adapter binding proteins such as Growth factor receptor-bound protein 2 (GRB2)-associated-binding protein 1 (GAB1) and GRB2-associated-binding protein 2 (GAB2) via its SH2 domains. This binding induces a conformational change and releases the inhibitory effect between the N-SH2 domain and the PTP domain resulting in SHP2 activation (Cunnick, Mei et al. 2001). The PTP domain is now exposed and can remove phosphate groups from SHP2 substrates (Chan, Kalaitzidis et al. 2008).
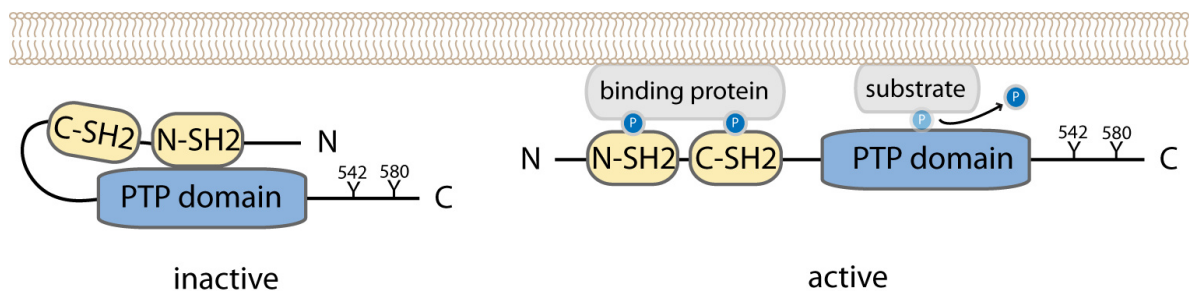
Figure 8. Mechanism of SHP2 activation

Schematic showing the mechanism of SHP2 activation. Left: in the basal, inactive state, SHP2 is autoinhibited by binding of the N-SH2 domain to the PTP domain. Right: Upon stimulation, SHP2 is recruited to the membrane. Binding of the SH2 domains to phosphorylated adapter binding proteins induces a conformational change and releases the autoinhibition and leading to an increase in enzyme activity. SHP2 is now in the open, active conformation and can dephosphorylate its substrates.

2.9.2   SHP2 in normal development and disease

SHP2 is widely expressed in both, embryonic and adult tissues (Neel 1993, Feng and Pawson 1994). SHP2 has been shown to be required for early mouse development and gastrulation as mice with a homozygous deletion of exon 2 (Arrandale, Gore-Willse et al. 1996) or exon 3 (Saxton, Henkemeyer et al. 1997, Saxton and Pawson 1999) resulting in a truncated SHP2 died in utero at mid-gestation. SHP2 null mice died even earlier at peri-implantation (Yang, Klaman et al. 2006). Studies have shown that mutations of SHP2 can lead to pathological conditions including cancer (Zheng, Alter et al. 2009) (**Figure 9**).

Germline missense gain-of-function (GOF) mutations in the PTPN11 gene have been identified in ~50% of patients suffering from a developmental disorder called Noonan syndrome (NS) (Tartaglia, Mehler et al. 2001). With an estimated incidence rate of 1 in 1,000-2,500 live births, NS is a relatively common autosomal dominant developmental disorder (van der Burgt 2007). Symptoms include facial anomalies, short stature, congenital heart defects, and an increased risk of leukemia (Noonan and O'Connor 1996). The missense mutations causing NS are mainly found in exon 3 and 8. These mutations were found to interrupt the autoinhibition between the N-SH2 and the PTP domain and render the enzyme constitutively active (Zheng, Alter et al. 2009).

Another disease caused by mutations in the PTPN11 gene is LEOPARD syndrome (LS) (Digilio, Conti et al. 2002, Legius, Schrander-Stumpel et al. 2002). In 90% of LS cases, PTPN11 mutations in exons 7 and 12 corresponding to the PTP domain, have been identified (Zheng, Alter et al. 2009). LS shares similar clinical characteristics with NS. However, in contrast to NS, it is caused by loss-of-function (LOF) mutations in the PTP domain resulting in a dominant negative SHP2 protein that interferes with SHP2 mediated signaling. The catalytically defective LS-SHP2 adapts an open conformation and interferes with growth factor-induced activation of the ERK pathway (Kontaridis, Swanson et al.

2006). The question, how the catalytically impaired LS-SHP2 can result in LS, is still under investigation. Recently, Yu and colleagues have shown that LS-SHP2 mutants are hypersensitive to growth factors and are able to compensate decreased phosphatase activity by longer binding to scaffold proteins and upstream activators to therefore increasing substrate turnover (Yu, Wu et al. 2013).
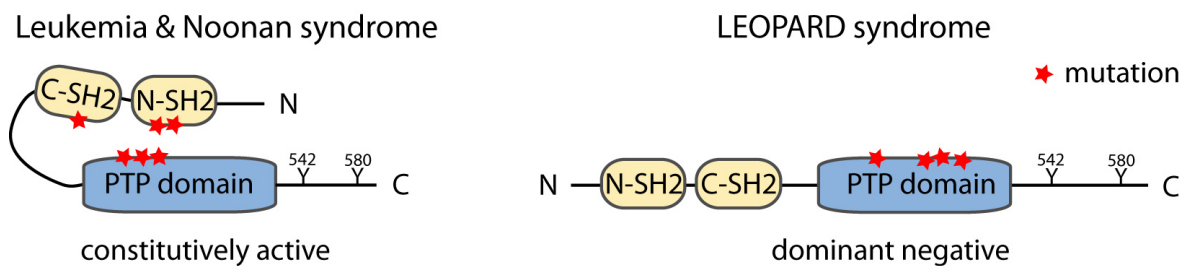
Figure 9. SHP2 mutations associated with disease
Overview of frequent SHP2 mutations leading to disease. Left: In leukemia and Noonan syndrome, gain-of-function mutations are located mainly in the N-SH2 domain or in the PTP domain. These mutations interfere with the autoinhibition, rendering the phosphatase constitutively active, causing increased and sustained activation of downstream pathways. Right: LEOPARD syndrome loss-of-function mutations are found only in the PTP domain resulting in a catalytically defect SHP2 enzyme. The mutated SHP2 acts as a dominant negative and locks the ERK pathway inactive.

2.9.3 SHP2 in cancer

SHP2 is the first identified bona fide PTP proto-oncogene (Tonks 2006). GOF mutations in PTPN11 have been reported in various types of human cancers. These mutations disrupt the auto inhibitory binding between the N-SH2 and the PTP domain and render the SHP2 constitutively active. Somatic missense mutations in PTPN11 have been identified in ~35% of juvenile myelomonocytic leukemia (JMML) patients. Additional mutations have been found in other pediatric leukemias, namely in 10% of childhood myelodysplastic syndromes, in ~7% of B-cell precursor acute lymphoblastic leukemia, and in ~4% of cases of pediatric and adult acute myelogenous leukemia (AML) (Tartaglia, Niemeyer et al.

2003, Loh, Reynolds et al. 2004, Tartaglia, Martinelli et al. 2004). PTPN11 mutations in solid tumors have also been reported, however these mutations occur at lower frequency than in hematological diseases. Bentires-Alj and colleagues identified mutations in the N-SH2 domain in cases of lung cancer, colon cancer, and neuroblastoma and mutations in the C-SH2 domain of SHP2 were found in melanoma, but no mutations of SHP2 have been found in breast cancer to date (Bentires-Alj, Paez et al. 2004).

However, there are other mechanisms that result in elevated SHP2 signaling besides SHP2 GOF mutations. In solid tumors, the oncogenic potential of SHP2 arises mainly from aberrant activation of the phosphatase, which can also be caused by over and/or inappropriate expression of SHP2 binding proteins or cytotoxin-associated gene A (CagA) in gastric cancer with H. pylori infections. In breast cancer the gene encoding the SHP2-activating protein GAB2 was found to be amplified or overexpressed in 10–15% of tumors (Bentires-Alj, Gil et al. 2006, Bocanegra, Bergamaschi et al. 2010). SHP2 is also implicated in CagA mediated gastric cancer (Hatakeyama 2002, Higashi, Tsutsumi et al. 2002). CagA is secreted by virulent Helicobacter pylori (H. pylori) strains. SHP2 forms a complex with CagA in gastric epithelial cells which leads to oncogenic transformation of these cells resulting in the hummingbird phenotype. Disruption of the CagA-SHP2 complex reverses the CagA dependent morphological changes (Hatakeyama 2002). Further, aberrant SHP2 activation can occur downstream of constitutive active forms of EGFR and fibroblast growth factor receptor 3 (FGFR3), upon BCR-ABL activation, and downstream of active RTKs such as RET and HER2 (Sattler, Mohi et al. 2002, Agazie, Movilla et al. 2003, D'Alessio, Califano et al. 2003, Zhan and O'Rourke 2004, Bentires-Alj, Gil et al. 2006). Zhou and colleagues reported SHP2 to be overexpressed in 72% of infiltrating ductal carcinoma (Zhou, Coad et al. 2008). More recently, the Condeelis group

reported overexpression of SHP2 in invasive migratory tumor cells (Patsialou, Wang et al. 2012).

In contrast to this positive signal enhancing oncogenic role, SHP2 has been suggested to have a tumor-suppressive function in hepatocellular carcinoma (HCC). Bard-Chapeau and colleagues showed that hepatocyte-specific deletion of SHP2 led to increased inflammatory signaling, regenerative hyperplasia, and tumor formation in aged mice. They further showed that SHP2 expression was decreased in a subset of human HCC patient samples (Bard-Chapeau, Li et al. 2011).

2.10   The Src family kinase c-Src

Src is the best characterized member of the largest family of non-receptor protein tyrosine kinases, the Src family kinases (SFKs) (Frame 2002). Other SFK members are Fyn, Yes, Blk, Yrk, Frk (also known as Rak), Fgr, Hck, Lck, Srm, and Lyn (Summy and Gallick 2003, Yeatman 2004, Sen and Johnson 2011).

Src was first discovered in 1911 by Peyton Rous, who described a transmissible noncellular transforming agent in chicken sarcomas that could give rise to new sarcomas (Rous 1910, Rous 1911). 60 years later, the agent responsible for this transformation process was identified as the viral SRC gene (v-SRC) (Martin 1970). Subsequently, it was found that normal avian DNA contained a gene that was closely related to v-SRC, termed cellular SRC (c-SRC), which was the first human proto-oncogene to be identified (Stehelin, Guntaka et al. 1976). In contrast to v-Src, which lacks the C-terminal negative regulatory domain and contains 12 substituted C-terminal amino acids along with numerous point mutations throughout the molecule allowing for higher levels of activity and greater transforming ability, c-Src is poorly transforming (Jove and Hanafusa 1987, Parsons and Weber 1989).

2.10.1 Structure and activation of c-Src

The protein c-Src is a 60 kDa nonreceptor kinase consisting of an N-terminal myristoylation sequence (M), a unique region, a Src homology 3 (SH3) and a Src homology 2 (SH2) protein interaction domain, a kinase domain that contains a conserved autophosphorylation site (Tyr419 in humans, Tyr418 in mice, and Tyr416 in chicken), and a C-terminal regulatory domain that contains a negative-regulatory tyrosine residue (Tyr530 in humans, TyrY529 in mouse, and Tyr527 in chicken) (**Figure 10**).
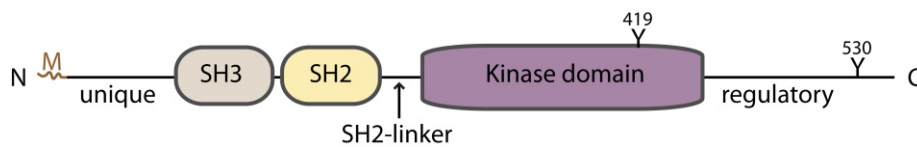
Figure 10. Schematic structure of c-Src
The kinase c-Src consists of a myristoylation sequence (M) at the N-terminus, a unique region, a SH3 and a SH2 protein interaction domain, a kinase domain containing the autophosphorylation site Tyr419 (Y419) and a C-terminal regulatory domain containing the inhibitory phosphorylation site Tyr530 (Y530). The SH2-linker between the SH2 domain and the kinase domain contains a proline-rich region that is bound by the SH3 domain in the closed conformation.

The N-terminal myristoylation site is important for membrane localization (Pawson 1995) and is crucial for the transformation of oncogenic Src mutants (Frame 2002). The unique domain varies between Src kinase family members. The SH3 domain binds to proline-rich regions and the SH2 domain recognizes and binds to tyrosine-phosphorylated peptide sequences which determine the substrate specificity of the protein (Songyang, Shoelson et al. 1993). The interaction of these SH domains and therefore the activity of the Src kinase is dependent on phosphorylation of the autophosphorylation site in the kinase domain Tyr419 and the negative regulatory site in the C-terminal regulatory domain Tyr530 (Brown and Cooper 1996).

In the inactive state, Src kinase is phosphorylated at Tyr530, which is conserved among the SFK members. Upon phosphorylation, Tyr530 binds to the SH2 domain leading to a closed conformation. In addition, the SH3 domain interacts with a proline-rich region in the SH2-linker forming an intramolecular bond further stabilizing the closed conformation (Shoji, Kurosawa et al. 1990) (**Figure 11**). Src is inactive in this closed conformation as the substrate binding sites in both, SH2 and SH3 domains are blocked. Dephosphorylation of Tyr530 by phosphatases including SHP1, SHP2, protein tyrosine phosphatase α (PTP α), and protein tyrosine phosphatase 1B (PTP1B) breaks the intramolecular bonds, leading to an open and active conformation (Zheng, Wang et al. 1992, Bjorge, Pang et al. 2000, Jung and Kim 2002). Full Src activation further requires autophosphorylation at the activating site Tyr419 (Roskoski 2005).
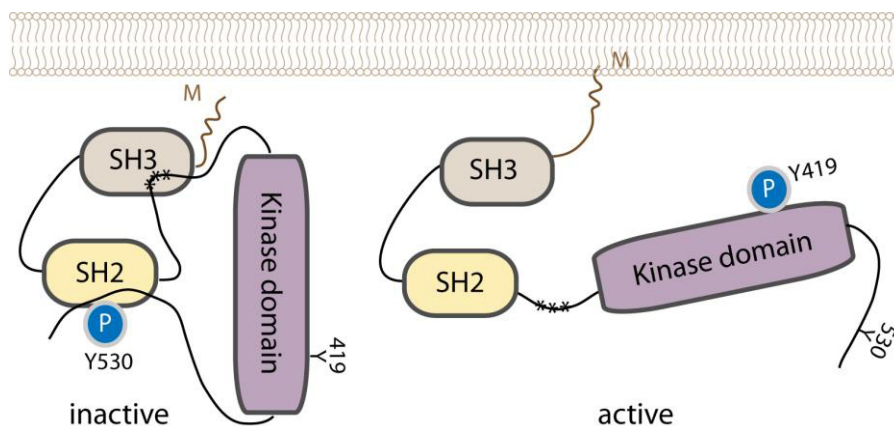
Figure 11. Mechanism of c-Src activation
Schematic of the mechanism of c-Src activation. Left: Inactive Src is kept in a closed conformation by two intramolecular interactions. The inhibitory tyrosine Tyr530 (Y530) is phosphorylated and binds the SH2 domain and the SH3 domain interacts with a proline-rich region in the SH2-linker (***). Right: Src is activated either by dephosphorylation of Y530 or by interaction of the SH2 and SH3 domains with Src binding partners. This results in an open conformation of the kinase, allowing autophosphorylation of Tyr419 (Y419) leading to full Src kinase activity. Inactive Src is usually located in the cytoplasm, whereas activated Src is translocated to the membrane for full activation. The N-terminal myristoylation (M) sequence is important for binding to the membrane.

Besides phosphorylation, subcellular localization is an important mechanism to regulate c-Src activity (Bjorge, Jakymiw et al. 2000). SFKs are present at different subcellular locations, but are most abundant in the cytoplasm. For example, Fincham and colleagues studied the role of the SH3 domain in the assembly of focal adhesions and found inactive Src to be localized in the perinuclear region of the cell. Upon activation, Src was transported to the plasma membrane where it is recruited to focal adhesions (Fincham, Brunton et al. 2000). Generally, inactive Src phosphorylated at Tyr530, resides in the cytoplasm and is translocated to the membrane upon activation, where it is autophosphorylated at the activating site Tyr419 further enhancing catalytic activity (Cooper and Howell 1993). Localization at the membrane was found to be essential for the transforming potential of Src as it brings Src in close proximity of its upstream and downstream effectors (Nigg, Sefton et al. 1982, Cowan-Jacob, Fendrich et al. 2005).

Elevated c-Src activity can result from activating mutations or gene amplification, but generally it results from structural alternations mediated by upstream kinases and phosphatases (Sen and Johnson 2011). Src interacting cytoplasmic proteins include focal adhesion kinase (FAK) or its molecular partner Crk-associated substrate (CAS), which are important for integrin signaling (Burnham, Bruce-Staskal et al. 2000, Xing, Ge et al. 2000). Growth factor receptors regulating c-Src activity include EGFR, HER2, platelet-derived growth factor receptor (PDGFR), fibroblast growth factor receptor (FGFR), and vascular endothelial growth factor receptor (VEGFR) (Landgren, Blume-Jensen et al. 1995, Thomas and Brugge 1997, Tice, Biscardi et al. 1999, Bowman, Broome et al. 2001, Chou, Wang et al. 2002).

Alternatively, Src activation was found to be elevated in some human tumors due to a reduced expression of c-Src kinase (Csk), a negative regulator of Src (Sen and Johnson 2011). In hepatocellular carcinoma, levels of Csk were found to be reduced in

comparison with normal liver correlating with high Src activity in these tumors (Masaki, Okada et al. 1999).

2.10.2 c-Src in normal development

Each SFK member has a different distribution in normal tissues. c-Src is expressed ubiquitously in many adult tissues with greater levels of expression in platelets, neurons and osteoclasts (Thomas and Brugge 1997, Roskoski 2004). Blk, Hck, and Fgr are found solely within blood cells, while Lck and Lyn are found mainly in blood cells and in the brain and Srm is expressed in keratinocytes. Yes and Fyn are ubiquitously expressed. Frk is expressed in bladder, breast, brain, colon, and lymphoid cells. (Thomas and Brugge 1997, Sen and Johnson 2011).

The kinase c-Src is involved in numerous cellular processes such as cell cycle progression, adhesion, angiogenesis, migration, apoptosis, and differentiation (Tatosyan and Mizenina 2000, Frame 2002). Soriano and colleagues reported mice with a null mutation of the c-SRC gene to be viable, possibly due to the functional overlap between members of the SFKs (Soriano, Montgomery et al. 1991). A direct role of c-Src in osteoblast/osteoclast regulation was suggested, as c-Src knockout mice develop osteopetrosis, a disease caused by failure of osteoclastic bone resorption (Soriano, Montgomery et al. 1991, Lowe, Yoneda et al. 1993, Yoneda, Niewolna et al. 1993). Mice with double knockouts of Src/Fyn or Src/Yes were found to die perinatally (Stein, Vogel et al. 1994). Mouse embryos with homozygous triple null mutations in c-SRC, YES and FYN genes, died in utero by day 9.5 and displayed severe developmental defects (Klinghoffer, Sachsenmaier et al. 1999). Germline deletion of c-Src was shown to cause defects in the initial stages of mammary ductal outgrowth as well as in uterine and ovarian development (Kim, Laing et al. 2005). Fibroblasts isolated from these Src null embryos showed reduced cell spreading and migration potential when plated on extracellular matrix (ECM) proteins

(Klinghoffer, Sachsenmaier et al. 1999). Similarly, Src-deficient mammary epithelial cells were unresponsive to estrogen stimulation and displayed reduced cell spreading and migration capacities when plated on ECM proteins (Kim, Laing et al. 2005).

2.10.3 c-Src in cancer

The kinase c-Src was the first proto-oncogene discovered (Stehelin, Varmus et al. 1976). Overexpression and/or activation of c-Src have been shown to play an important role in cell survival, growth, adhesion, and invasion and lead to an overall aggressive and metastatic phenotype of many human cancers (Frame 2002). Studies indicate that c-Src expression and/or activity is elevated in several types of human cancers, including melanoma (Barnekow, Paul et al. 1987), colon (Irby, Mao et al. 1999), pancreatic (Lutz, Esser et al. 1998), esophageal, gastric, ovarian (Wiener, Nakano et al. 1999) as well as head and neck cancer (van Oijen, Rijksen et al. 1998), and breast cancer (Jacobs and Rubsamen 1983, Ottenhoff-Kalff, Rijksen et al. 1992, Verbeek, Vroom et al. 1996, Egan, Pang et al. 1999). In some cancers including breast cancer, a positive correlation between elevated c-Src expression and cancer aggressiveness has been found (Egan, Pang et al. 1999). Consistent with this, c-Src inhibition was reported to suppress the transformed phenotype of breast cancer cell lines (Ishizawar, Tice et al. 2004) and resulted in the reduction of cancer progression in several cancer types including breast cancer (Gonzalez, Agullo-Ortuno et al. 2006). These observations and the positive correlation between increased Src activity and cancer progression, suggested Src as a promising target for anticancer therapy.

There are several small molecule Src inhibitors currently undergoing clinical trials after promising preclinical studies, such as the ATP-binding competitive inhibitors dasatinib, bosutinib, and saracatinib or the substrate binding-site inhibitor KX2–391 (Sen and Johnson 2011). Despite promising preclinical data, Src inhibitors have shown little

activity in monotherapy trials in unselected solid tumor patient populations. With the development of suitable biomarkers, the effects in selected patients, who are more likely to benefit from treatment, will be evaluated. Further, several combination strategies are currently tested in clinical trials (Puls, Eadens et al. 2011).

3   RATIONALE OF THE WORK

Breast cancer is the most frequent cancer and cause of death in women worldwide. Signaling pathways controlling critical cellular functions become frequently deregulated during the progression of cancer. An in-depth understanding of signaling events influencing tumor onset, progression and metastatic spread is crucial for identifying new therapeutic targets. Many cellular functions in eukaryotic cells rely on the reversible phosphorylation of tyrosine residues governed by PTKs and PTPs. Previous work from our lab had implicated the phosphatase SHP2 in breast tumor growth and proliferation. We asked whether SHP2 is important for breast tumor maintenance and progression and assessed its cellular and molecular mechanism of action in these processes.

Specifically I wanted to elucidate the following aspects of SHP2 effects in breast cancer:

  i.   What is the molecular mechanism of action of SHP2 in breast cancer progression?

 ii.   What are the effects of SHP2 on cell motility, invasion and in metastatic spread?

iii.   What are the physiological substrates of SHP2?

 iv.   How is SHP2 translocated into the nucleus and what is its nuclear function?

4   RESULTS PART1 – Effects of SHP2 on breast cancer progression

Manuscript published in Nature Medicine.

Tyrosine phosphatase SHP2 promotes breast cancer progression and maintains tumor-initiating cells via activation of key transcription factors and a positive feedback signaling loop

Nicola Aceto[1], Nina Sausgruber[1], Heike Brinkhaus[1], Dimos Gaidatzis[1], Georg Martiny-Baron[2], Giovanni Mazzarol[3], Stefano Confalonieri[3], Micaela Quarto[3], Guang Hu[4,6], Piotr J Balwierz[5], Mikhail Pachkov[5], Stephen J Elledge[4], Erik van Nimwegen[5], Michael B Stadler[1] & Mohamed Bentires-Alj[1]

[1]Friedrich Miescher Institute for Biomedical Research (FMI), Basel, Switzerland. [2]Novartis Institutes for Biomedical Research, Basel, Switzerland. [3]Fondazione Istituto FIRC di Oncologia Molecolare (IFOM) and Istituto Europeo di Oncologia (IEO), Milan, Italy. [4]Howard Hughes Medical Institute and Department of Genetics, Harvard Medical School, Division of Genetics, Brigham and Women's Hospital, Boston, Massachusetts, USA. [5]Biozentrum, University of Basel and Swiss Institute of Bioinformatics, Basel, Switzerland. [6]Present address: Laboratory of Molecular Carcinogenesis, National Institute of Environmental Health and Sciences, Research Triangle Park, North Carolina, USA.

This work was done in collaboration and only data to which I contributed is shown.

4.1 INTRODUCTION

Breast cancer is a heterogeneous disease that progresses to the fatal hallmark of metastasis (Nguyen, Bos et al. 2009). Breast tumors, like normal breast, are hierarchically organized at the cellular level (Al-Hajj, Wicha et al. 2003, Dontu, Al-Hajj et al. 2003, Visvader 2009). Tumor-initiating cells (TICs) are operationally defined as cells that form tumors after transplantation into immunodeficient mice (Clarke, Dick et al. 2006). Although identification of the 'Achilles' heel' of tumorigenic cells is of paramount clinical importance in the search for therapeutic targets, signaling networks influencing TICs remain poorly defined.

In cancer, many signaling networks are subverted at the biochemical level (Vogelstein and Kinzler 2004, Pawson and Kofler 2009). Abnormal tyrosine phosphorylation underlies various diseases of deregulated growth and differentiation, including cancer (Hunter 2009, Pawson and Kofler 2009). The first identified bona fide protein-tyrosine phosphatase (PTP) proto-oncogene was the Src-homology 2 domain-containing phosphatase SHP2 (encoded by PTPN11), a ubiquitously expressed PTP that transduces mitogenic, pro-survival, cell-fate and/or pro-migratory signals from numerous growth-factor, cytokine and extracellular-matrix receptors. SHP2 is required for the full activation of the mitogen-activated protein kinase (MAPK)/extracellular signal-related kinase (ERK) pathway downstream of most receptors; however, its regulation of other pathways (for example, the Janus kinase (Jak)-signal-transducer and activator of transcription protein (STAT) and phosphoinositide-3-kinase (PI3K) pathways) is cell specific, receptor specific or both (Shi, Yu et al. 2000, Ostman, Hellberg et al. 2006, Chan, Kalaitzidis et al. 2008). Notably, gain-of-function germline mutations of SHP2 cause ~50% of the instances of Noonan syndrome developmental disorder (Tartaglia, Mehler et al. 2001). Moreover, mouse genetics, gene silencing and sequencing studies have shown a

broad role for SHP2 in development, cell fate and tumorigenesis (Tartaglia, Mehler et al. 2001, Feng 2007, Chan, Kalaitzidis et al. 2008, Grossmann, Rosario et al. 2010).

In malignancies, SHP2 is hyperactivated either downstream of oncoproteins or by mutations. Gain-of-function somatic mutations are found in ~35% of juvenile myelomonocytic leukemias and at various incidences in other myeloid malignancies but are rarely present in solid cancers (Tartaglia, Niemeyer et al. 2003, Bentires-Alj, Paez et al. 2004, Chan, Kalaitzidis et al. 2008). SHP2 is also activated downstream of oncogenes in gastric carcinoma, anaplastic large-cell lymphoma and glioblastoma (Higashi, Tsutsumi et al. 2002, Voena, Conte et al. 2007, Chan, Kalaitzidis et al. 2008, Zhan, Counelis et al. 2009). Although we did not find SHP2 mutations in breast cancer in our previous studies, we and others have found that the gene encoding the SHP2-activating protein growth factor receptor bound protein 2-associated protein 2 (GAB2) is amplified and overexpressed in 10-15% of human breast tumors (Bentires-Alj, Paez et al. 2004, Bentires-Alj, Gil et al. 2006, Bocanegra, Bergamaschi et al. 2010).

Summary of previous results

Using inducible small hairpin RNAmiRs (miRs) to deplete SHP2 in a 3D culture model of invasive breast cancer, we showed that SHP2 is necessary for invasion, proliferation and loss of polarity. Overexpression of HER2 and HER3 caused the immortalized but non-transformed human breast epithelial cells MCF10A to form invasive, unpolarized and hyperproliferative 3D structures with a filled lumen and SHP2 knockdown blocked HER2/3-evoked invasion by 85%. Expression of a non-targetable SHP2 cDNA in cells expressing SHP2 miR2 rescued the MCF10A-HER2/3 cell-invasiveness. To test the effect of SHP2 knockdown on in vivo invasiveness of breast cancer cells, a human-in-mouse intraductal transplantation model was used (Behbod, Kittrell et al. 2009) and we found that

knockdown of SHP2 markedly decreased the ability of BT474 cells to progress from DCIS to IDC.

To shed light on the role of SHP2 in breast tumor growth and progression in vivo, xenografts of three HER2-positive (BT474, SKBR3 and MCF10A-NeuNT) and two triple-negative (SUM159 and SUM1315) breast cancer cell lines expressing dox-inducible CTRL or SHP2 miRs were used. Depletion of SHP2 significantly decreased tumor growth and studies using the HER2-positive BT474 cells subsequently showed a decrease in the number of lung metastases as a consequence of decreased tumor burden.

Next, the influence of SHP2 on self-renewal of spherogenic breast cancer cells was examined. Assessing the tumorsphere-formation efficiency of HER2-positive and triple-negative breast cancer cell lines in the presence or absence of SHP2, we found that SHP2 knockdown reduced self-renewal of breast tumorsphere-forming cells of both HER2-positive and triple-negative tumors. SHP2 depletion was found to decrease the proportion of cells with the CSC phenotype as shown by a decrease of the CD44^{high}/CD24^{low} population in MCF10A HER2/3 cells and a decrease in ALDH activity upon SHP2 knockdown in SUM159 cells. This observation suggested a role of SHP2 in cancer stem cell regulation.

To characterize this effect of SHP2 on the tumor-seeding capacity of breast tumor initiating cells (TICs), single cells from SHP2 knockdown xenografts were isolated and serially transplanted in limiting dilutions into recipient mice in the absence of dox and used for tumorsphere forming assays. While CTRL cells efficiently seeded new tumors, depletion of SHP2 in vivo strongly impaired both tumorsphere formation and tumor seeding capacity. The fact that neither the mice transplanted with cells nor the cells grown as tumorspheres were treated with dox indicated that depletion of TICs or tumorsphere-forming cells upon knockdown of SHP2 occurred in vivo during dox treatment of the

primary tumors. These data indicated that SHP2 is active in the maintenance and propagation of breast TICs.

In summary, this previous work from our lab showed that SHP2 is necessary for invasion, proliferation and loss of polarity in a 3D culture model of invasive breast cancer. SHP2 promotes the transition from in situ to invasive carcinoma in vivo and is required for the maintenance and tumor-seeding ability of tumor initiating cells. Knockdown of SHP2 in different breast cancer cell lines blocked the tumor growth in vivo. However, the mechanism of action remained undefined.

4.2 RESULTS

SHP2 acts via activation of the ERK pathway in vivo and in vitro.

We sought to define the biochemical pathways in breast cancers in vivo that rely upon SHP2 action. A screen for changes in phosphorylation upon SHP2 knockdown in tumors using a reverse-phase protein array (RPA) revealed a decrease in phosphorylation of several signaling molecules. Immunoblotting of tumor lysates confirmed decreases in the phosphorylation of ERK5, ERK1/2, AKT, PLCγ, EGFR and HER2 Analysis of protein phosphorylation in lysates from BT474 tumorspheres showed a phosphorylation of ERK5 and ERK1/2 and to a lesser extent of PLCγ, AKT, EGFR and HER2. Consistently, we also observed reduced phosphorylation of ERK5 and ERK1/2 in MCF10A-HER2/3 tumorspheres upon knockdown of SHP2.

We then used shRNAs to knockdown ERK5 and measured the tumorsphere-formation efficiency of BT474 and MCF10A-HER2/3 cells in the presence (CTRL vector) or absence of ERK5. Knockdown of ERK5 reduced tumorsphere formation (~30% fewer primary and secondary tumorspheres in ERK5 shRNA cells than in CTRL cells) but did not affect self-renewal (**Figure 12A**).
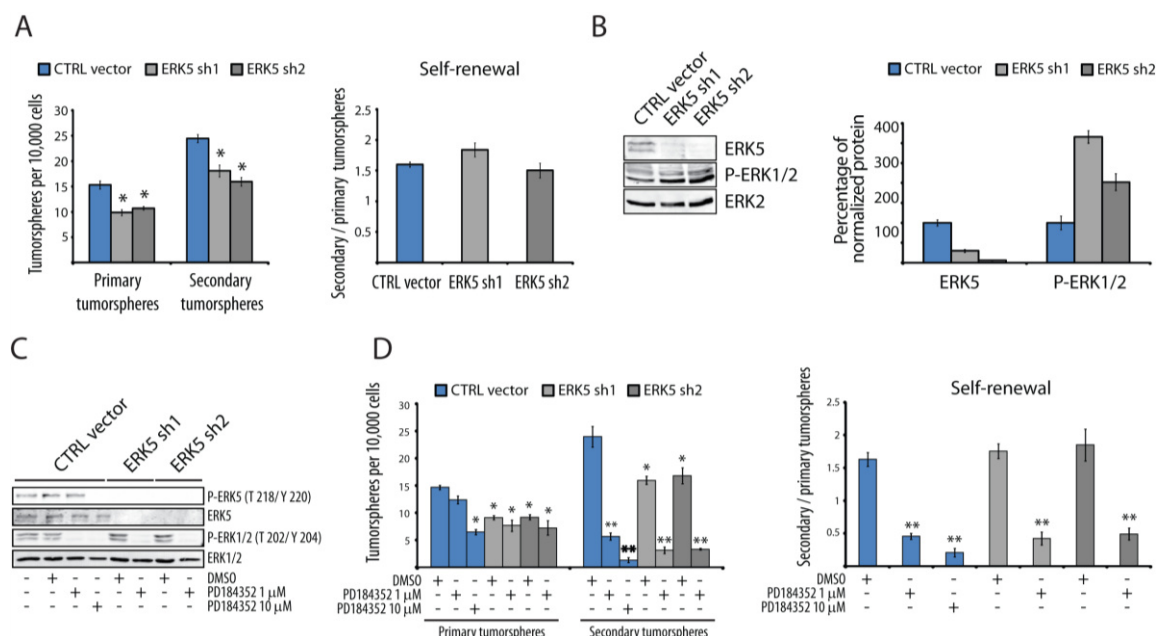
Figure 12. SHP2 acts via activation of the ERK pathway

(A) ERK5 knockdown partially reduces the tumorsphere-forming capacity but does not affect self-renewal of BT474 cells. Bar graphs showing self-renewal capacities and the mean number of BT474 tumorspheres/10^4 cells ± SEM (n=3). **P < 0.004.

(B) Left: Immunoblot of lysates from BT474 primary tumorspheres in the presence or absence of ERK5 (n=3). Right: The bar graph shows the percentage of normalized protein ± SEM (n=3).

(C) Immunoblot of lysates from BT474 primary tumorspheres expressing ERK5 shRNA alone or in combination with PD184352 treatment.

(D) Inhibition of ERK1 and ERK2 phosphorylation alone or in combination with ERK5 inactivation decreased BT474 tumorsphere-formation efficiency and the self renewal of tumorsphere-forming cells. The bar graph shows the self renewal capacities and the mean number of BT474 tumorspheres ± SEM (n=3). *P < 0.001, **P < 0.0008 by Student's t test.

These results showed that ERK5 depletion is not sufficient to phenocopy the effect of SHP2 loss on tumorsphere-forming cells. Interestingly, BT474 and MCF10A-HER2/3 tumorspheres expressed higher levels of active ERK1/2 upon ERK5 knockdown, suggesting that phosphorylation of ERK1/2 compensated for ERK5 loss (**Figure 12B**). We next combined ERK5 depletion with the MEK inhibitor PD184352. Consistent with previous observations (Mody, Leitch et al. 2001), PD184352 blocked ERK1/2 phosphorylation at 1 μM and both ERK1/2 and ERK5 phosphorylation at 10 μM (**Figure 12C**). Knockdown of ERK5 and treatment of BT474 and MCF10A-HER2/3 tumorspheres with PD184352 at 1 μM, or a treatment with 10 μM PD184352 that abrogates phosphorylation of both ERK5 and ERK1/2, reduced tumorsphere-formation efficiency and self renewal similar to SHP2 knockdown (**Figure 12D**). To assess whether inhibition of both ERK1/2 and ERK5 is required for mimicking the effect of SHP2 knockdown on tumorsphere-forming cells, we treated BT474 tumorspheres with PD184352 at 1 μM, which inhibits ERK1/2 but not ERK5. This dramatically reduced tumorsphere formation and self-renewal, thus recapitulating the effect of SHP2 knockdown (**Figure 12D**). These results suggested that SHP2 action on tumorsphere forming cells is predominantly dependent on ERK1/2 activation.

To dissect the effects of SHP2-evoked activation of ERK5 and ERK1/2 on the number of cells with the CSC phenotype, we examined MCF10A-HER2/3 cells lacking ERK5 and/or treated with PD184352 by measuring the proportion of CD44^{high}/CD24^{low} cells. A complete depletion of the CD44^{high}/CD24^{low} population was only seen upon simultaneous inhibition of ERK5 and ERK1/2, or ERK1/2 inhibition alone while ERK5 depletion led to a decrease of ~35% suggesting that SHP2 signals primarily through ERK1/2. Further, inhibition of ERK1/2 alone or in combination with ERK5 inactivation completely blocked HER2/3-evoked invasion. Rescue experiments using a wt SHP2 construct or phosphatase dead SHP2 C459S (SHP2 C/S) in MCF10A-HER2/3 cells lacking endogenous SHP2, showed that catalytic activity of SHP2 was required for ERK1/2 phosphorylation, self-renewal of spherogenic cells and invasion.

Altogether, these results showed that although ERK5 is hyperactivated in the presence of SHP2, it contributes only partially to the multiple effects of SHP2 in breast cancer. Thus, SHP2 acts predominantly by activating ERK1/2.

SHP2 activates stemness-associated transcription factors that repress let-7 miRNA and increases self-renewal of spherogenic cells, invasion and breast tumor growth.

The effects of SHP2 on gene expression in cancer have not been examined. To address this, we analyzed gene expression profiles of BT474 CTRL and SHP2 miRs tumors after 30 days of dox-induced knockdown of SHP2. The 180 downregulated genes identified are referred to as the "SHP2 signature" (**Figure 13A**). Gene ontology analysis of the signature revealed enrichment in development-associated genes, mainly of the HOX gene family (**Figure 13B and C**).
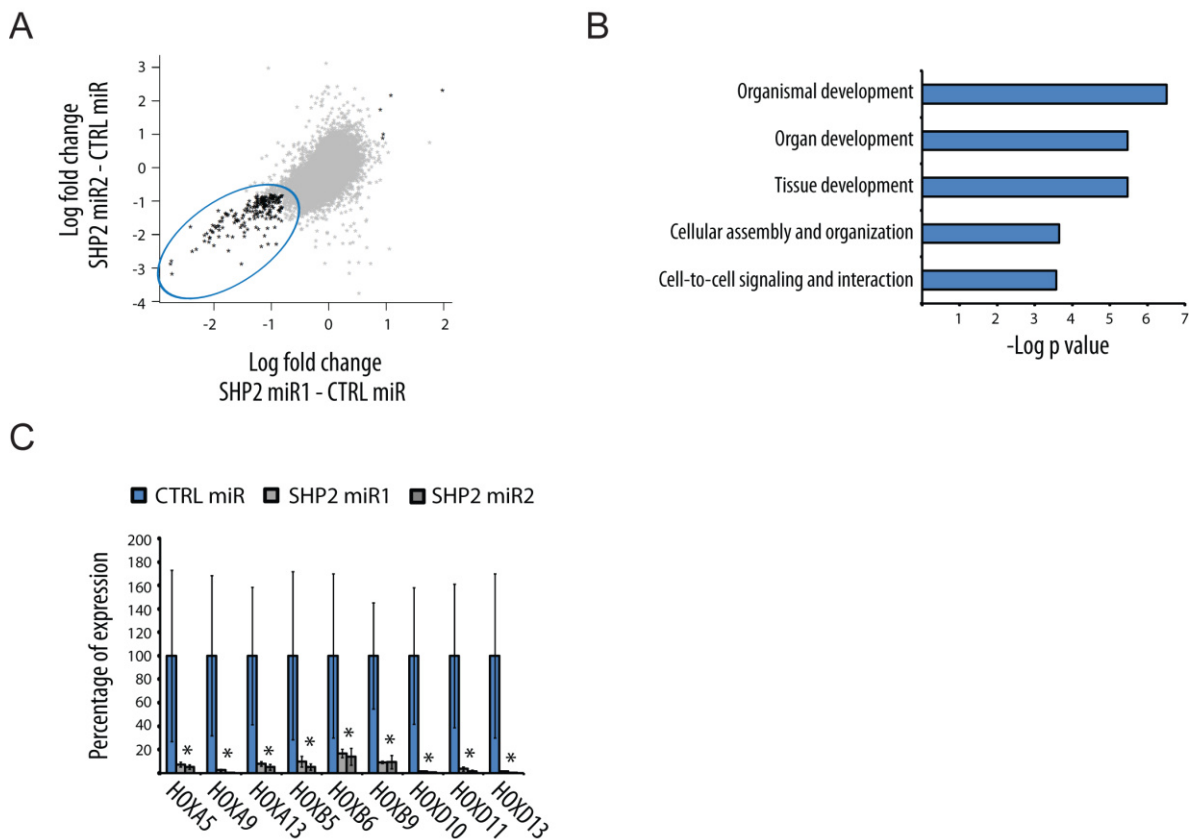
Figure 13. SHP2 induces the expression of a set of development-associated genes

(A) Plot of the gene expression contrast in BT474 SHP2 miR1 minus control miR tumors compared to SHP2 miR2 minus control miR tumors. The blue line circles the genes in the SHP2 signature.

(B) Gene ontology analysis (Ingenuity) of the "SHP2 signature" revealed a remarkable enrichment in development-associated genes. This enrichment was mainly determined by the presence of 9 HOX genes in the SHP2 signature.

(C) Quantitative real-time PCR confirmed the decrease in the expression of HOX genes upon depletion of SHP2. RNA was isolated from BT474 tumors expressing CTRL or SHP2 miRs treated for 30 days with dox. Quantitative real-time PCR was performed using primers against HOXA5, HOXA9, HOXA13, HOXB5, HOXB6, HOXB9, HOXD10, HOXD11 and HOXD13. Results represent means ± SEM (n=3). *P < 0.05.

To identify the transcription factors whose activity is responsible for the observed changes, we used a computational method (Suzuki, Forrest et al. 2009) to model global gene expression patterns in terms of genome-wide predictions of transcription factor binding sites. This analysis identified 10 transcription regulators that are inferred to cause significant downregulation of their targets upon SHP2 inactivation (**Figure 14A**). Among these transcription factors is ZEB1, a zinc finger E-box-binding homeobox 1 that has been

shown to induce EMT (Wellner, Schubert et al. 2009). Consistently, ZEB1 was downregulated in microarrays of BT474 tumors lacking SHP2. Analysis of RNA from BT474 and SUM159 tumors by real-time PCR confirmed that ZEB1 expression was repressed upon SHP2 knockdown (**Figure 14B**). The repression of ZEB1 was accompanied by downregulation of the EMT markers fibronectin1, vimentin and N-cadherin (**Figure 14C**), indicating the influence of SHP2 on EMT in vivo.
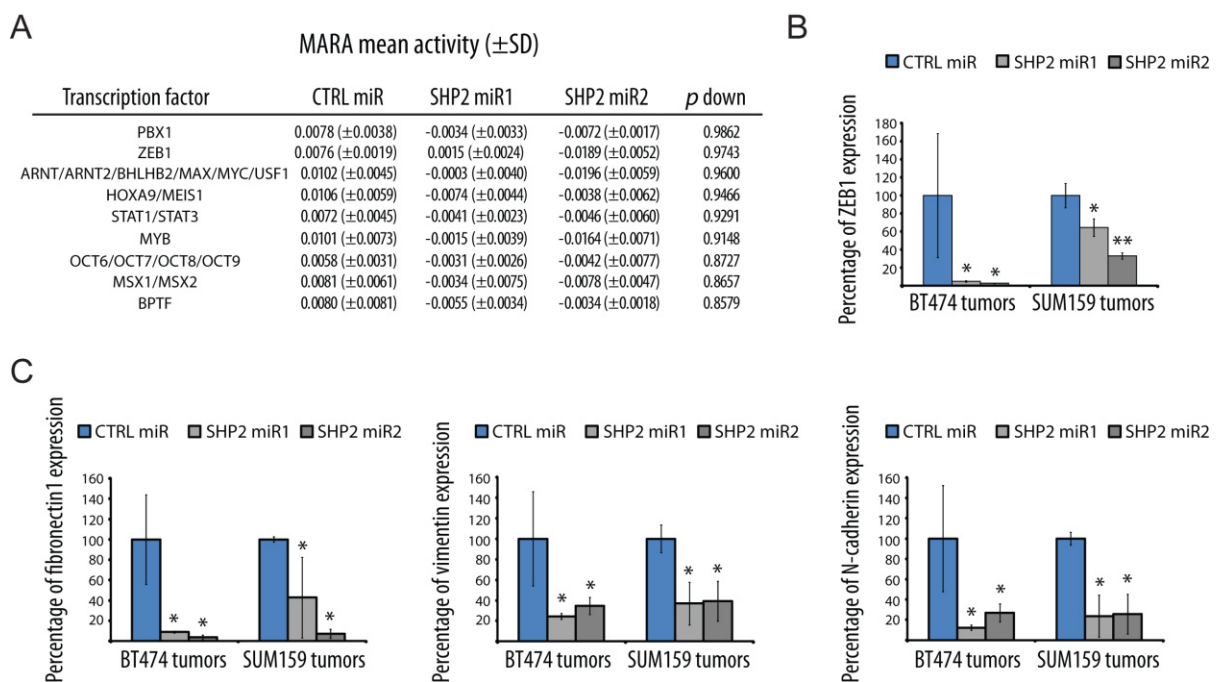
Figure 14. SHP2 activates stemness-associated transcription factors and induces EMT in vivo

(A) Table showing the MARA mean activity scores (± SD) of 10 transcription factors whose activity was reduced upon SHP2 knockdown. "P down" values show for each factor the probability of a decreased activity in SHP2 miRs compared with CTRL miR samples.

(B) Quantitative real-time PCR of ZEB1. Bar graph showing the percentage of ZEB1 expression in BT474 and SUM159 tumors in the presence or absence of SHP2. Results are means ± SEM (n=3). $*P < 0.029$, $**P < 0.018$ by Student's t test.

(C) Quantitative real-time PCR of the EMT markers fibronectin1, vimentin, and N-cadherin. The bar graphs show the percentage of EMT marker expression in BT474 and SUM159 tumors in the presence or absence of SHP2. Results represent means ± SEM (n=3). $*P < 0.05$.

To assess the functional role of ZEB1 downstream of SHP2, we generated pools of MCF10A-HER2/3 cells expressing inducible ZEB1 miR (**Figure 15A**). Knockdown of ZEB1 dramatically reduced invasion in MCF10A-HER2/3 cells grown in 3D cultures (**Figure 15B**). Moreover, ZEB1 depletion reduced the self-renewal of MCF10A-HER2/3 tumorsphere-forming cells (**Figure 15C**), although to a lesser extent than depletion of SHP2. These data indicate that ZEB1 acts downstream of SHP2 to enhance invasion and self-renewal, but also suggest that additional mediators are involved in the effect of SHP2 on the self-renewal capacity of tumorsphere-forming cells/TICs.
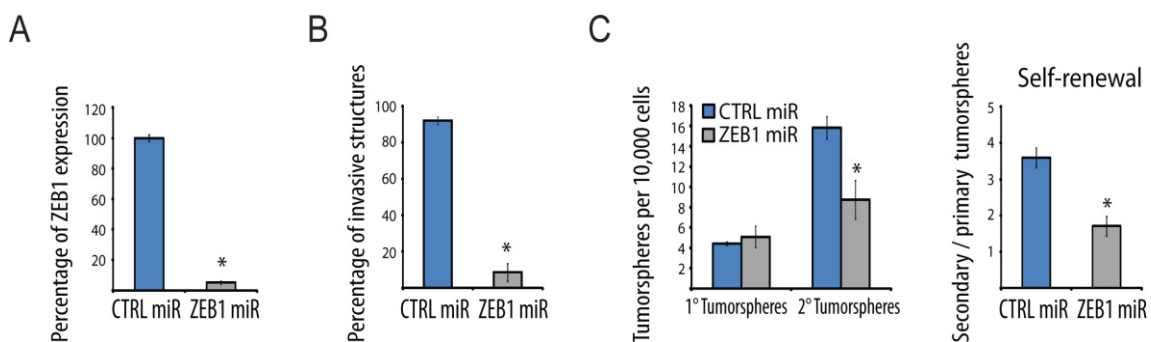
Figure 15. ZEB1 enhances invasion and self-renewal downstream of SHP2
(A) Quantitative real-time PCR of the transcription factor ZEB1. The bar graph shows the mean percentage of ZEB1 expression in MCF10A-HER2/3 cells expressing an inducible ZEB1 miR ± SEM (n=3). *P < 0.00054.
(B) Bar graph showing the mean percentage of invasive structures of MCF10A-HER2/3 cells grown in three-dimensional cultures in the presence or absence of ZEB1 ± SEM (n=3). *P< 0.01 by Student's t test.
(C) Bar graphs showing the self-renewal capacity of tumorsphere-forming cells and the mean number of MCF10A-HER2/3 tumorspheres/10^4 cells in the presence or absence of ZEB1 ± SEM (n=3). *P < 0.05.

To address this further, we analyzed transcriptome changes upon SHP2 knockdown in vivo with the Ingenuity resource. This analysis revealed that SHP2 knockdown strongly affected genes belonging to the c-Myc network (**Figure 16A)**, confirming that c-Myc transcriptional activity is reduced upon SHP2 knockdown in vivo (**Figure 14A**).
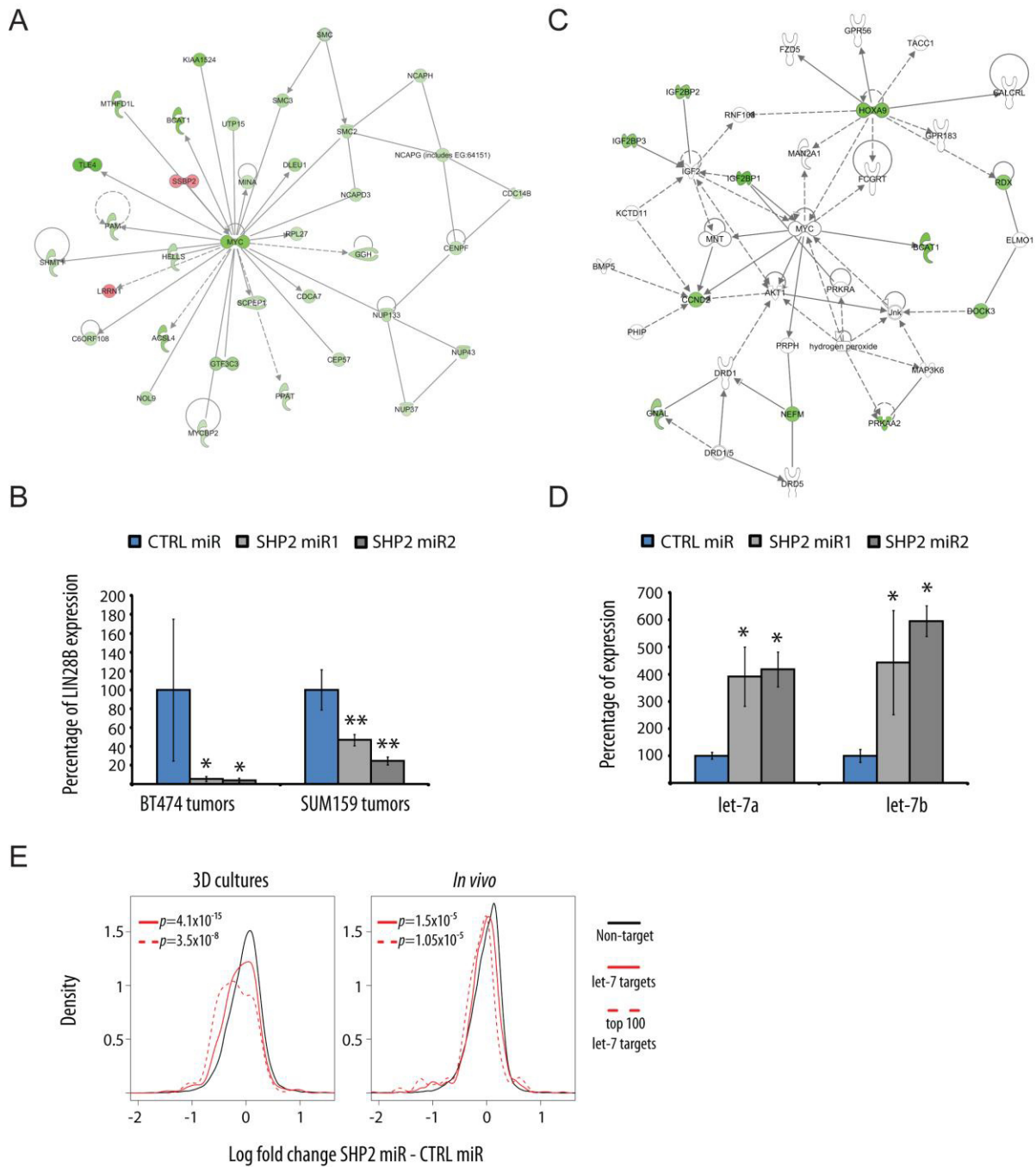
Figure 16. SHP2 acts via ERK1/2-mediated activation of ZEB1 and c-Myc transcription factors

(A) Network analysis (Ingenuity) of downregulated and upregulated genes (greater than ± 0.5 logarithmic fold change) upon SHP2 knockdown in BT474 tumors. The top-ranked network is shown, displaying c-Myc as a key factor. Downregulated genes are shown in green, upregulated genes in red. Ingenuity network score = 47.

(B) Quantitative real-time PCR of LIN28B. Bar graph showing the percentage of LIN28B expression in BT474 and SUM159 tumors in the presence or absence of SHP2. Results are means ± SEM (n=3). *P < 0.03, **P < 0.02 by Student's t test.

(C) Network analysis (Ingenuity) of predicted let-7 targets within the SHP2 signature. The top-ranked network is shown, indicating that let-7 target genes within the SHP2 signature strongly associate with the c-Myc network. Ingenuity network score = 28.
(D) Quantitative real-time PCR of mature let-7a and let-7b miRNAs. The bar graph shows the mean percentage of let-7a and let-7b expression in MCF10A-HER2/3 cells grown in three-dimensional cultures in the presence or absence of SHP2 ± SEM (n=3). *P < 0.04 by Student's t test.
(E) Downregulation of let-7 target genes in the absence of SHP2. Curves showing the relative frequency (density) of genes that are not targeted by let-7 (non-target), genes that are predicted let-7 targets (let-7 targets) and the 100 genes most likely to be let-7 targets (top 100 let-7 targets) after SHP2 knockdown in MCF10A-HER2/3 cells grown in three-dimensional cultures or BT474 tumors (in vivo).

Moreover, expression of the known c-Myc target LIN28B (Chang, Zeitels et al. 2009), a suppressor of miRNA biogenesis, was decreased in microarrays from tumors lacking SHP2. These observations prompted us to dissect the role of c-Myc and LIN28B downstream of SHP2. First, we quantified the expression of LIN28B by real-time PCR in BT474 and SUM159 tumors and confirmed that it was transcriptionally repressed upon SHP2 knockdown in both models (**Figure 16B**). LIN28B was shown previously to suppress biogenesis of let-7 miRNA (Viswanathan, Daley et al. 2008, Chang, Zeitels et al. 2009, Iliopoulos, Hirsch et al. 2009). Consistently, we observed that 20 genes of the "SHP2 signature" are predicted let-7 targets, the majority of which are tightly associated with the c-Myc pathway (**Figure 16C**). To avoid cross-detection of stromal mouse let-7 miRNA present in the tumors, we analyzed its expression in MCF10A-HER2/3 cells grown in 3D cultures in the presence or absence of SHP2. Remarkably, biogenesis of mature let-7a and let-7b increased in these cells in the absence of SHP2 (**Figure 16D**). Consistently, whole gene expression analysis of MCF10AHER2/3 cells grown in 3D cultures or xenografts of BT474 cells showed a greater decrease in the expression of RNAs encoding predicted let-7 target genes than other genes in the absence of SHP2 (**Figure 16E**). We further confirmed the downregulation, at the protein level, of the let-7 targets RAS and c-Myc (Roush and Slack 2008) in tumors lacking SHP2 (**Figure 17A**). Next, we

assessed whether the expression levels of ZEB1 and LIN28B are dependent on activation of ERK1/2. Treatment with PD184352 showed that MEK1/2 inhibition reduced the expression of ZEB1 and LIN28B in both SUM159 and MCF10A-HER2/3 cells (**Figure 17B**). These data suggested that the effects of SHP2 on ZEB1 and LIN28B expression are mediated by ERK1/2.

Our findings suggested that SHP2-evoked activation of ERK1/2 increases the expression of c-Myc and LIN28B in breast cancer. To test this model directly, we asked whether restoring the expression of c-Myc or LIN28B rescues the effects of SHP2 knockdown. Notably, expression of c-Myc restored expression of LIN28B in MCF10A-HER2/3 cells lacking SHP2 (**Figure 17C**). Consistently, expression of either c-Myc or LIN28B restored invasion and self renewal of tumorsphere-forming cells in MCF10A-HER2/3 cells lacking SHP2. Moreover, c-Myc restoration abolished the effects of SHP2 knockdown in BT474 and SUM159 tumor growth (**Figure 17D**).

Finally, to assess the generality of our mechanistic findings, we analyzed the expression of the let-7 targets c-Myc and RAS (Roush and Slack 2008) upon SHP2 knockdown in all the models tested in vivo. c-Myc expression was decreased in all models and RAS expression in 3 of 5 models (**Figure 17A, E**).
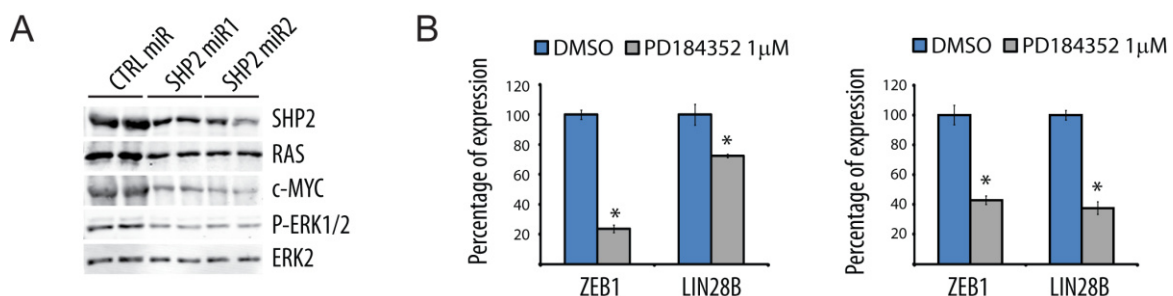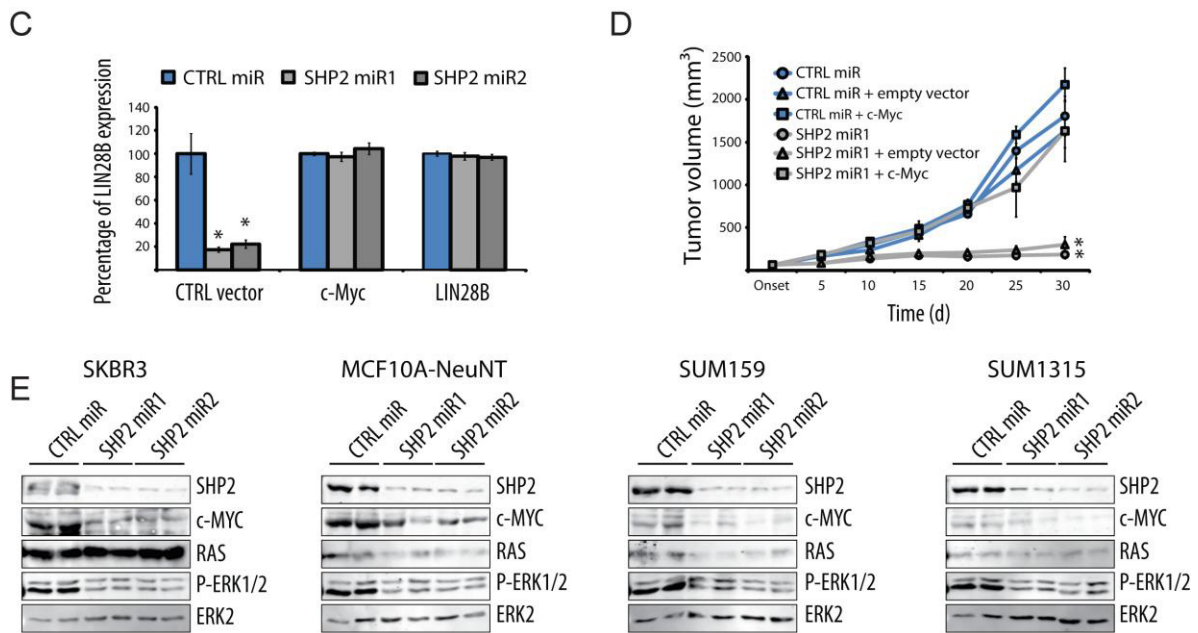
Figure 17. SHP2 increases the activity of key transcription factors and represses let-7 miRNA

(A) Immunoblot showing the expression of SHP2, pERK1/2, ERK2 and the let-7 targets c-Myc and RAS in lysates from BT474 tumors treated with dox.

(B) Quantitative real-time PCR of ZEB1 and LIN28B. Bar graph showing the mean percentage of ZEB1 and LIN28B expression in MCF10A HER2/3 (left) and SUM159 (right) cells after treatment with PD184352 ± SEM (n=3). *P < 0.05 by Student's t test.

(C) Quantitative real-time PCR of LIN28B. The bar graph shows the percentage of LIN28B expression in MCF10A-HER2/3 cells in the presence or absence of SHP2 and expressing a c-Myc or LIN28B rescue. Results represent means ± SEM (n=3). *P < 0.05.

(D) c-Myc rescues the effects of SHP2 knockdown on breast tumor growth. BT474 tumor growth curves in the presence or absence of SHP2 and c-Myc. Curves showing the mean tumor volume (mm^3) ± SEM (n=4). *P < 0.012 by Student's t test.

(E) Immunoblot showing the expression of SHP2, P-ERK, ERK and the let-7 targets c-Myc and RAS in lysates from SKBR3, MCF10A-NeuNT, SUM159 or SUM1315 tumors grown in the presence or absence of SHP2.

In summary, our data demonstrate that SHP2 promotes ERKs activation, causing upregulation of ZEB1 and c-Myc-dependent expression of LIN28B, which leads to repression of let-7 miRNA and overexpression of let-7 target genes including RAS and c-Myc (Roush and Slack 2008) (**Figure 18**). These data identify a key positive feedback signaling loop that is involved in the maintenance of breast TICs and in breast cancer progression.
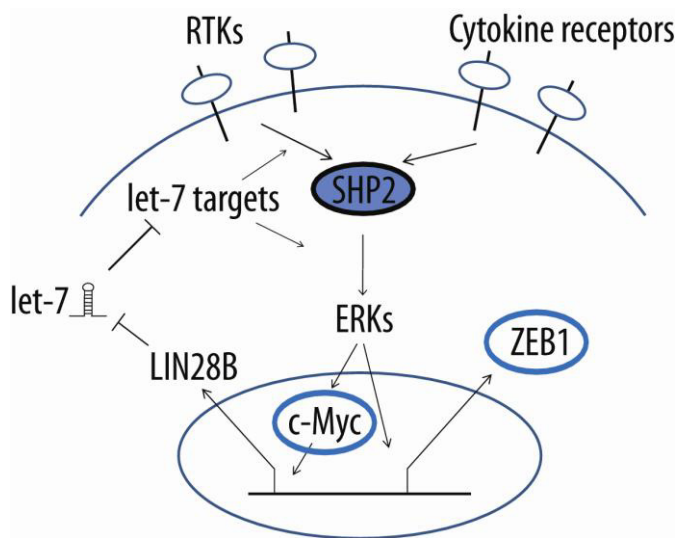
Figure 18. Model of the mechanism of action of SHP2
SHP2 activates the ERK pathway, which in turn promotes ZEB1 transcription and c-Myc dependent LIN28B expression. The expression of LIN28B blocks the processing of let-7, maintaining high expression levels of let-7 targets, including RAS and c-Myc. RTK, receptor tyrosine kinase.

SHP2 is active in a large subset of primary breast tumors associated with poor prognosis.

It has been proposed that SHP2 is overexpressed both, in breast cancer cell lines and infiltrating ductal carcinoma of the breast (Zhou, Coad et al. 2008). To assess whether expression of the "SHP2 signature" could be used to stratify patients with breast cancer, we examined whether the genes from this signature are co-overexpressed in human breast tumors. In four independent publicly available datasets, the "SHP2 signature" genes were found to be co-regulated and cluster the patients into two groups: one with downregulation (group 1) and the other with overexpression (group 2) of the "SHP2 signature" genes. Notably, the clear split into "SHP2 signature" low- and high-expression groups was hardly ever observed in 10,000 randomly-selected gene groups of the same size. In contrast, we

observed no co-overexpression of the "SHP2 signature" genes in unsorted normal breast cells, highlighting the importance of SHP2 predominantly in malignant breast tissue (**Figure 19A**). We grouped the data from the four breast cancer datasets and found that ~55% of all primary breast cancers overexpress the "SHP2 signature" (**Figure 19B**). Strikingly, analysis of two of these datasets for which the molecular subtypes were reported showed that the "SHP2 signature" was high most frequently in triple-negative breast cancers (**Figure 19C**), a subtype characterized by poor outcome and lack of efficient therapy. In addition, we used two-independent datasets to analyze the expression of "SHP2 signature" genes in ductal carcinoma in situ (DCIS) and invasive ductal carcinoma (IDC) (including matched biopsies). We found co-overexpression of the "SHP2 signature" in IDCs (**Figure 19D**). Moreover, we tested the expression of "SHP2 signature" genes in two-independent datasets containing information about patients' prognosis and found them to be highly expressed in patients characterized by bad prognosis in both datasets (**Figure 19E**). Finally, we depleted SHP2 in a primary human triple-negative breast tumor grown as a xenograft to further address its clinical relevance. We found that SHP2 knockdown in vivo reduced tumor growth and abolished tumorsphere formation. Microarray data analysis of the primary tumors revealed that, while "SHP2 signature" genes were highly expressed in CTRL tumors, knockdown of SHP2 decreased their expression.
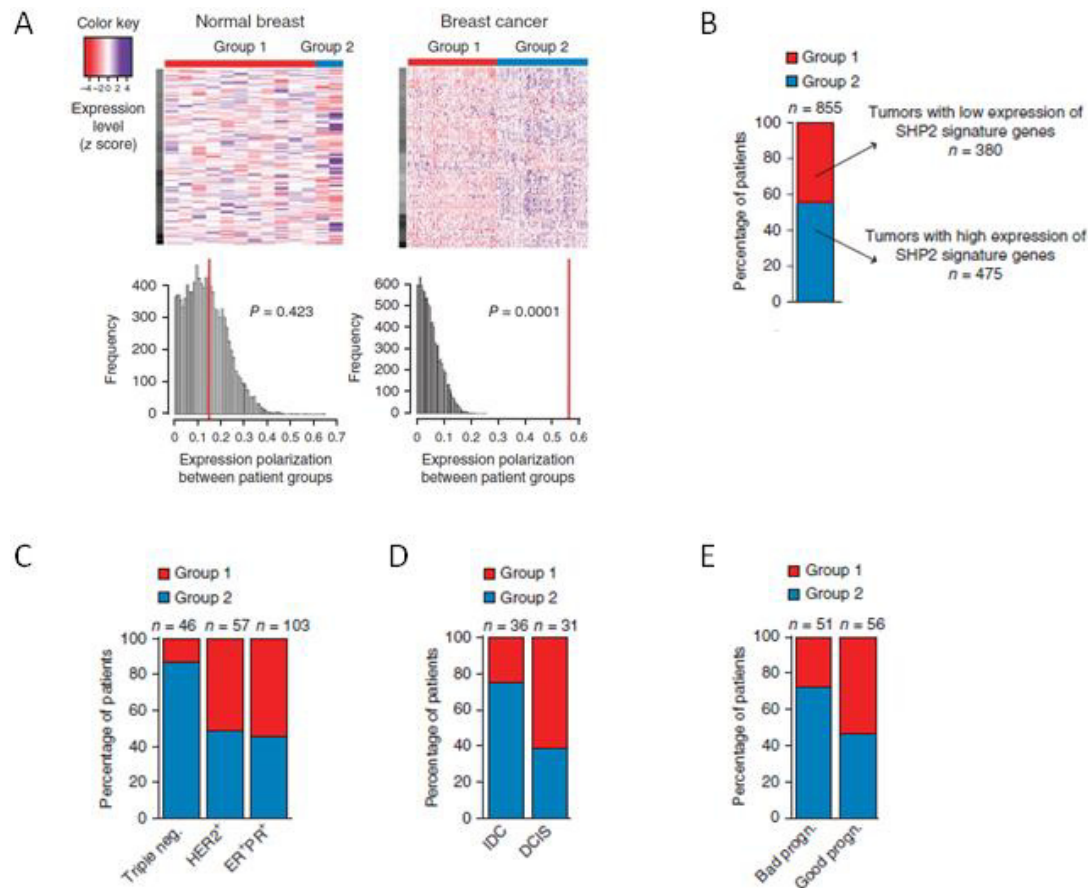
Figure 19. SHP2 is active in a large subset of breast tumors associated with poor prognosis

(A) SHP2 signature genes are simultaneously overexpressed in breast cancers but not normal breast cells. Expression heatmap for SHP2 signature genes in normal human breast and primary breast cancer. Mean expression of each gene is indicated in gray, and expression level z scores are mapped to colors from red (z = -5.0, below the mean) to blue (z = 5.0, above the mean). Genes (rows) and patients (columns) are clustered by expression of these genes, resulting in the patient groups 1 and 2. Expression polarization between the groups of patients is shown as a red line for the SHP2 signature against 10,000 randomly selected gene signatures of the same size (bottom); P = 0.423 for the normal breast data, P = 0.0001 for the breast cancer data.

(B) Bar graph showing the percentage of all patients with breast cancer belonging to group 1 (low SHP2 signature genes) or group 2 (high SHP2 signature genes).

(C) Bar graph showing the percentage of patients from groups 1 and 2 in each breast cancer molecular subtype. Genes of the SHP2 signature are upregulated in all the molecular subtypes but are most frequently upregulated in the triple-negative tumors. P = 6.24 x 10^{-7} by Fisher's exact test. ER, estrogen receptor; PR, progesterone receptor.

(D) Bar graph showing the percentage of patients from groups 1 and 2 with IDC or DCIS. Genes of the SHP2 signature are upregulated more frequently in IDC than DCIS. P = 0.0033 by Fisher's exact test.

(E) Bar graph showing the percentage of patients from groups 1 and 2 with bad or good prognosis (progn.). Genes of the SHP2 signature are upregulated more frequently in tumors characterized by a bad prognosis. P = 0.01 by Fisher's exact test.

4.3   DISCUSSION

The signaling networks influencing TICs are not well defined, although their delineation could lead to the development of targeted, potentially curative cancer therapies. In this study, we provide new insights into the multiple effects of SHP2 in breast cancer. We discovered that SHP2 action increases the propagation of breast TICs and promotes breast tumor maintenance and progression, showing that SHP2 is a high-quality target in human breast cancer.

One line of evidence for an effect of SHP2 on the propagation of TICs is that serial transplantation of limiting dilutions of several breast cancer cell lines after SHP2 knockdown reduced the number of TICs. We gathered evidence that SHP2 enhances breast tumor maintenance and progression from our in vivo and three-dimensional culture experiments. First, SHP2 knockdown reduced the growth of established breast tumors and decreased the number of lung metastases. SHP2 depletion in invasive three-dimensional cultures also reduced proliferation and prevented a loss of polarity, two crucial steps in the oncogenic process (Bissell, Radisky et al. 2002, Zhan, Rosenberg et al. 2008). Third, knockdown of SHP2 prevented invasion in three-dimensional cultures and in a human-in-mouse intraductal transplantation model.

The finding that SHP2 knockdown reduces tumor growth and TIC frequency raised the possibility that SHP2 influences CSCs. The CSC model posits a hierarchical organization of malignant tumors composed of phenotypically and functionally distinct subpopulations of cancer cells (Al-Hajj, Wicha et al. 2003, Dontu, Al-Hajj et al. 2003, Stingl and Caldas 2007, Rosen and Jordan 2009). In this model, tumorigenic cells self renew and produce phenotypically distinct non-tumorigenic cells, recapitulating the heterogeneity of the original tumor. Four of the cell lines we used to assess the effects of SHP2 on tumor initiation, self renewal and regulation of the CD44^{high}/CD24^{low} phenotype

were previously reported to propagate according to a CSC model (Fillmore and Kuperwasser 2008, Charafe-Jauffret, Ginestier et al. 2009, Deng, Yang et al. 2010), which suggests that SHP2 is a key factor affecting breast CSCs.

Mechanistically, we found that the effects of SHP2 on TICs, the self renewal of spherogenic cells and the invasion of breast cancer cells require activation of the ERK pathway. Further, we found that SHP2 activation of ERK1 and ERK2 induces expression of the transcription factors ZEB1 and c-Myc, the latter of which mediates an increase in LIN28B expression. In our studies, c-Myc–induced LIN28B expression repressed let-7 miRNA and led to overexpression of let-7 targets, including RAS and c-Myc (Roush and Slack 2008). These findings uncover a previously unknown mechanism of ERK regulation by SHP2 and identify an SHP2-dependent positive feedback loop that enhances the propagation of TICs and the maintenance and invasiveness of breast tumors.

Our work has led to the discovery of a SHP2 signature, comprised of a set of genes that are overexpressed in ~55% of human primary breast tumors and also correlated with invasive ductal carcinoma and poor prognosis. The results suggest that inhibiting SHP2 might be effective in patients with high expression of SHP2 signature genes, particularly those patients with the triple-negative subtype of breast cancer recently found to be dependent on active receptor tyrosine kinases (Sun, Aceto et al. 2011) that require SHP2 for full activation of ERK (Chan, Kalaitzidis et al. 2008). As SHP2 has been shown to act downstream of most growth-factor and cytokine receptors, targeting SHP2 may be therapeutic in other cancers in which SHP2 is hyperactivated (Higashi, Tsutsumi et al. 2002, Voena, Conte et al. 2007, Chan, Kalaitzidis et al. 2008, Zhan, Counelis et al. 2009). Our findings suggest further experiments to address whether SHP2 also influences TICs, tumor maintenance and progression in these malignancies.

In summary, we have shown that knockdown of SHP2 markedly reduces the propagation of breast TICs and inhibits breast cancer maintenance and progression. These findings reveal a fundamental SHP2-dependent positive feedback loop acting on several features of breast cancer and reinforce the concept of developing selective inhibitors of SHP2 to treat aggressive malignancies.

5   RESULTS PART2 –   Effects of SHP2 on migration and metastasis

5.1   INTRODUCTION

Despite continuous advances in the understanding of breast cancer and increasing therapeutic options, metastasis, the spread of tumor cells to distant sites, remains one of the most life-threatening pathological events (Yilmaz and Christofori 2009). Tumor cells undergo molecular and morphological changes to gain motility, become able to intravasate, survive in the bloodstream, extravasate, and colonize to form a secondary tumor (Bonnomet, Brysse et al. 2010). According to the currently accepted theory, tumor cells undergo Epithelial-Mesenchymal Transition (EMT) before they enter the bloodstream either directly or via the lymphatic system to be transported to distant sites (Yang and Weinberg 2008). The EMT program is characterized by a loss of cell-cell adhesions and cell polarity, in combination with the downregulation of epithelial and the upregulation of mesenchymal markers (May, Sphyris et al. 2011). Tumor cell adhesion, spreading and migration play a fundamental role during early steps of invasion and metastasis of carcinoma cells. These cell motility-related functions are tightly controlled by intracellular signaling mechanisms. Therefore, a thorough understanding of the molecular mechanisms and signals promoting invasive cell behavior might lead to novel approaches for treatment of breast cancer metastases.

We have previously shown that the proto-oncogenic phosphatase SHP2 is necessary for the loss of polarity, proliferation, and invasion in a 3D culture model of invasive breast cancer. We found that SHP2 was required for the maintenance and tumor-seeding ability of tumor initiating cells and the knockdown of SHP2 in HER2-positive and

triple-negative breast cancer cell lines and primary derived xenografts after overt tumor development decreased tumor growth (Aceto, Sausgruber et al. 2012).

SHP2 has been shown to play a role in multiple signaling processes mediating cell adhesion and migration. Fibroblasts lacking functional SHP2 showed impaired cell spreading, migration and showed an increased number of focal adhesions (Yu, Qu et al. 1998). Manes and colleagues found that MCF7 cells expressing a dominant-negative SHP2 mutant had a reduced migratory capacity and an increased number of focal adhesions.

Consistent with its role in cell migration, SHP2 is involved in the onset and/or progression of metastases. SHP2 overexpression in MCF7 cells resulted in decreased E-cadherin expression, secretion of MMP-9 and dephosphorylation of FAK leading to increased migration and metastatic potential (Wang, Liu et al. 2005). In line with this finding, we previously observed a role of SHP2 in EMT and metastasis in a HER2-positive cell line. The knockdown of SHP2 in BT474 tumors decreased not only tumor size, but also metastatic burden. ZEB1, a transcription factor involved in EMT, was downregulated upon knockdown of SHP2. We also found the EMT markers fibronectin, vimentin and N-cadherin downregulated in absence of SHP2 by quantitative real-time PCR (Aceto, Sausgruber et al. 2012).

Triple-negative breast cancers (TNBCs) are highly migratory and metastatic (Perou 2010). However, little is known about the role of SHP2 in tumor cell migration, dissemination, seeding, and metastatic colonization in this subtype. Recently, Hartman and colleagues showed that SHP2 mediated lamellipodia persistence and cell polarity to promote directional cell migration in MDA-MB-231 and MDA-MB-468 cells in vitro. They further showed that SHP2 exerts these effects through dephosphorylation of FAK at Tyr397 (Hartman, Schaller et al. 2013). Moreover, using a micro needle assay to capture motile tumor cells, SHP2 was found 80 x upregulated in migratory cells isolated from

MDA-MB-231 primary tumors in response to epidermal growth factor (Patsialou, Wang et al. 2012).

Given the roles of SHP2 in cell migration in TNBC cell lines in vitro and in MCF7 and BT474 metastases formation in vivo, we hypothesized that SHP2 also may play a role in the metastatic cascade in triple-negative disease. Therefore, we investigated the significance of SHP2 in breast cancer progression to metastasis in TNBC using in vitro and in vivo models. In addition, we attempted to identify downstream targets or substrates of SHP2 in these models.

5.2   RESULTS

Knockdown of SHP2 decreases cell motility and chemotaxis in TNBC in vitro.

To investigate the role of SHP2 in cell motility, we first analyzed patterns of random migration of the TNBC cells SUM159 and MDA-MB-231 in presence or absence of SHP2. We used a dox-inducible system with two different shRNAs SHP2 miR1 and SHP2 miR2 efficiently targeting endogenous SHP2 (**Figure 20A** and **B**).
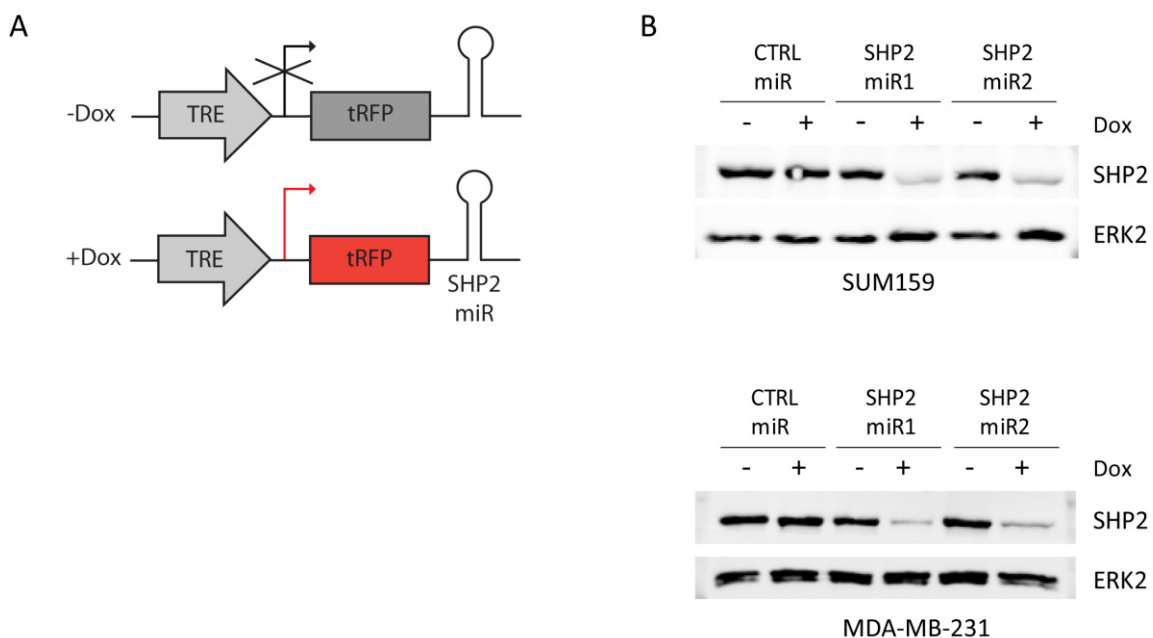
Figure 20. Dox-inducible knockdown of endogenous SHP2

(A) Schematic of the doxycycline (dox)-inducible construct used to knockdown endogenous SHP2 using a small hairpin shRNA (miR). Addition of dox led to the expression of the miR and turbo RFP (tRFP).
(B) Dox-inducible knockdown of SHP2 in cells expressing SHP2 miR1 or SHP2 miR2 but not in cells expressing the CTRL miR. Representative immunoblots showing the expression of SHP2 and the loading control ERK2 in presence (+) or absence (-) of dox in SUM159 (top) and MDA-MB-231 cells (bottom). Cells were lysed after 5 days of dox treatment.

We monitored the trajectories of random migrating cells in presence and absence of SHP2 and found cells lacking SHP2 to move significantly less, as shown by the colored trajectories in the phase contrast pictures (**Figure 21A**) and by overlaying 100 trajectories of SUM159 and MDA-MB-231 cells expressing either CTRL miR or SHP2 miR2 for better visual representation (**Figure 21B**). Whereas SHP2 expressing cells migrated in random directions on the dish, the majority of knockdown cells moved significantly less or circled around the starting point. By analyzing the trajectories of over 100 cells per cell line and condition, we found that knockdown of SHP2 significantly decreased random cell motility. The average velocity as well as the total path travelled in 12 h was significantly decreased in SUM159 and MDA-MB-231 cells lacking SHP2 (**Figure 21C**). SHP2 knockdown cells showed increased ruffling, but less movement. We further found a significant decrease of the distance to start (D2S), which is a measure of directionality (**Figure 21D**). In contrast to the total path length, D2S represents the distance from the starting point of the cell to the location 12 h later.
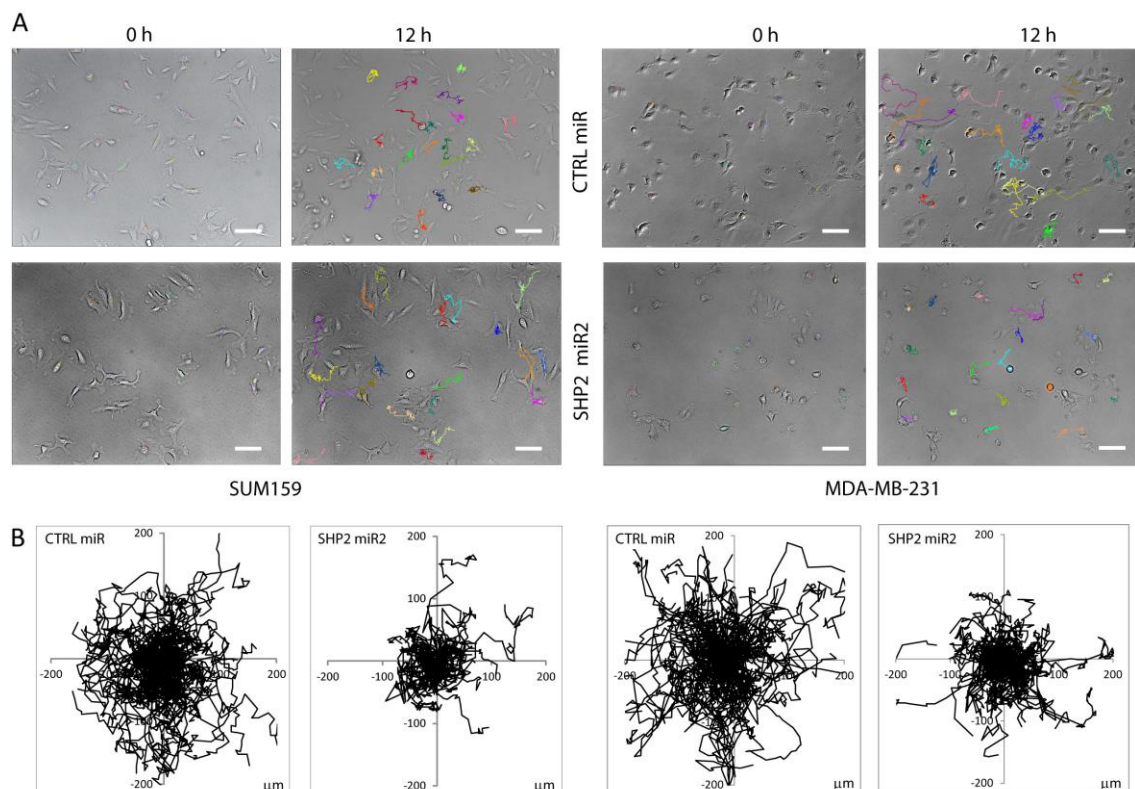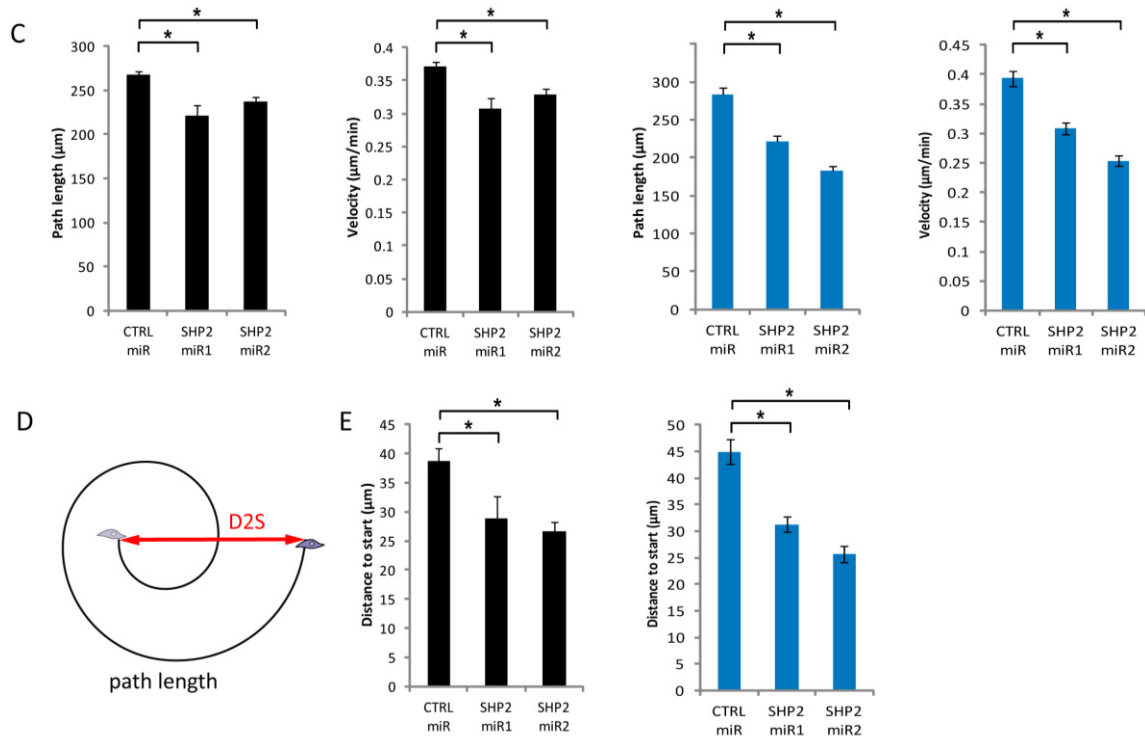
Figure 21. Depletion of SHP2 reduces random migration

(A) Representative images of the time-lapse microscopy. Shown are randomly migrating cells in phase contrast and cell tracks created using the ImageJ/Fiji plugin MTrackJ. Colored trajectories for SUM159 cells (left) and MDA-MB-231 (right) expressing CTRL miR or miR2 targeting SHP2 at time 0 h and after 12 h are shown. Time-lapse microscopy was performed using a Zeiss Axiovert 200M microscope equipped with a heated stage and a CCD camera. 3-4 positions per well were imaged using a 10 x phase objective every 10 min for a total duration of 12 h using MetaMorph software. Scale bars represent 100 µm.

(B) Cell migration trajectories showing the paths in µm travelled by 100 cells per condition in 12 h. The start of all tracks was calculated to be at the origin. Shown are exemplary graphs from SHP2 wt and knockdown SUM159 (left) and MDA-MB-231 cells (right).

(C) Bar graphs representing the average path length covered by SHP2 wt or knockdown cells in 12 h and the average velocity in µm/min for SUM159 (left, black) and MDA-MB-231 (right, blue). 100-140 cells per condition from 2-3 experiments were analyzed using the ImageJ/Fiji plugin MTrackJ and the mean values ± SEM are plotted. *P < 0.001 by Student`s t test.

(D) Schematic illustrating the difference between path length and distance to start (D2S). The path length is defined as the total distance covered in a given time and increases even if the cell moves in circles, while the D2S is the distance between the starting point and the end point.

(E) Bar graphs showing the distance to start measured in SUM159 (left, black) and MDA-MB-231 (right, blue) SHP2 wt or knockdown cells in 12 h. Plotted are mean values ± SEM. *P < 0.001 by Student`s t test.

Next, we tested the effects of SHP2 depletion on chemotaxis, i.e. the migration towards a gradient, using transwell Boyden chambers. Depletion of SHP2 in SUM159 and MDA-MB-231 cells resulted in a significant decrease of chemotaxis in both cell lines. In SUM159 cells, knockdown of SHP2 led to a significant reduction of migration of 83% and 75% in cells expressing SHP2 miR1 and miR2, respectively, when compared to the SHP2 expressing control cells (**Figure 22A**). Similar changes were observed in MDA-MB-231 cells, in which the knockdown of SHP2 reduced chemotaxis by 70% or 85% in cells expressing miR1 or miR2 respectively (**Figure 22B**)
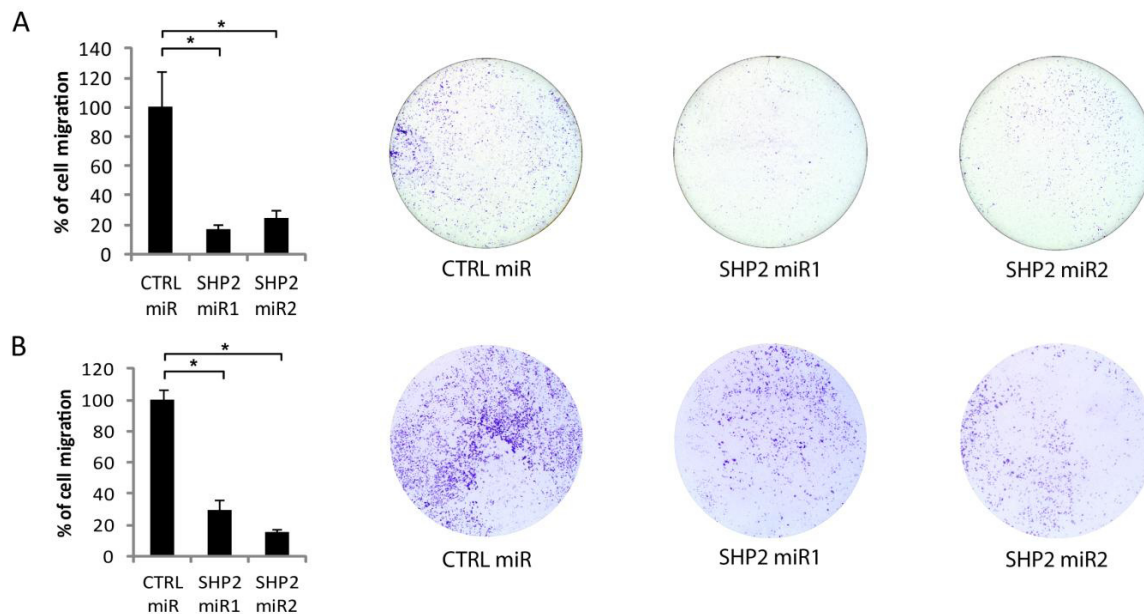
Figure 22. Depletion of SHP2 reduces chemotaxis

15,000 starved cells were plated in Boyden chambers in medium containing 0.25% FBS (SUM159) or 0.5% FBS (MDA-MB-231) and allowed to migrate through the 8 μm pores towards a gradient of FBS. Migrated cells were stained with Crystal violet and imaged using a Leica MacroFluo microscope with a 2 x objective. The number counted for cells expressing CTRL miR was set to 100%.

(A) Left: Bar graphs showing the relative percentages of SUM159 cells migrated in 24 h. Shown are mean values ± SEM (n=3). *P < 0.05 by Student`s t test. Right: Representative pictures of the bottom of the membranes showing the migrated cells after staining with Crystal violet.

(B) Left: Bar graphs showing the relative percentages of MDA-MB-231 cells migrated in 24 h. Shown are mean values ± SEM (n=3). *P < 0.002 by Student`s t test. Right: Representative pictures of the bottom of the membranes showing the migrated cells after staining with Crystal violet.

Knockdown of SHP2 decreases invasion in vitro.

A crucial step in metastasis is the ability of a tumor cell to attach to and penetrate the basement membrane in order to enter the bloodstream (Yamaguchi, Wyckoff et al. 2005). To test the role of SHP2 in this process, we used an in vitro matrigel invasion assay (**Figure 23A**). Using 2 different miRs targeting SHP2, we found that the invasive potential of cells lacking SHP2 towards a gradient of FBS was greatly diminished. In SUM159 cells, the number of invasive cells was reduced by 94% and 81% for SHP2 miR1 and miR2, respectively (**Figure 23B**). In MDA-MB-231 cells, the number of invasive cells was reduced by 86% and 96% for SHP2 miR1 and miR2, respectively (**Figure 23C**).
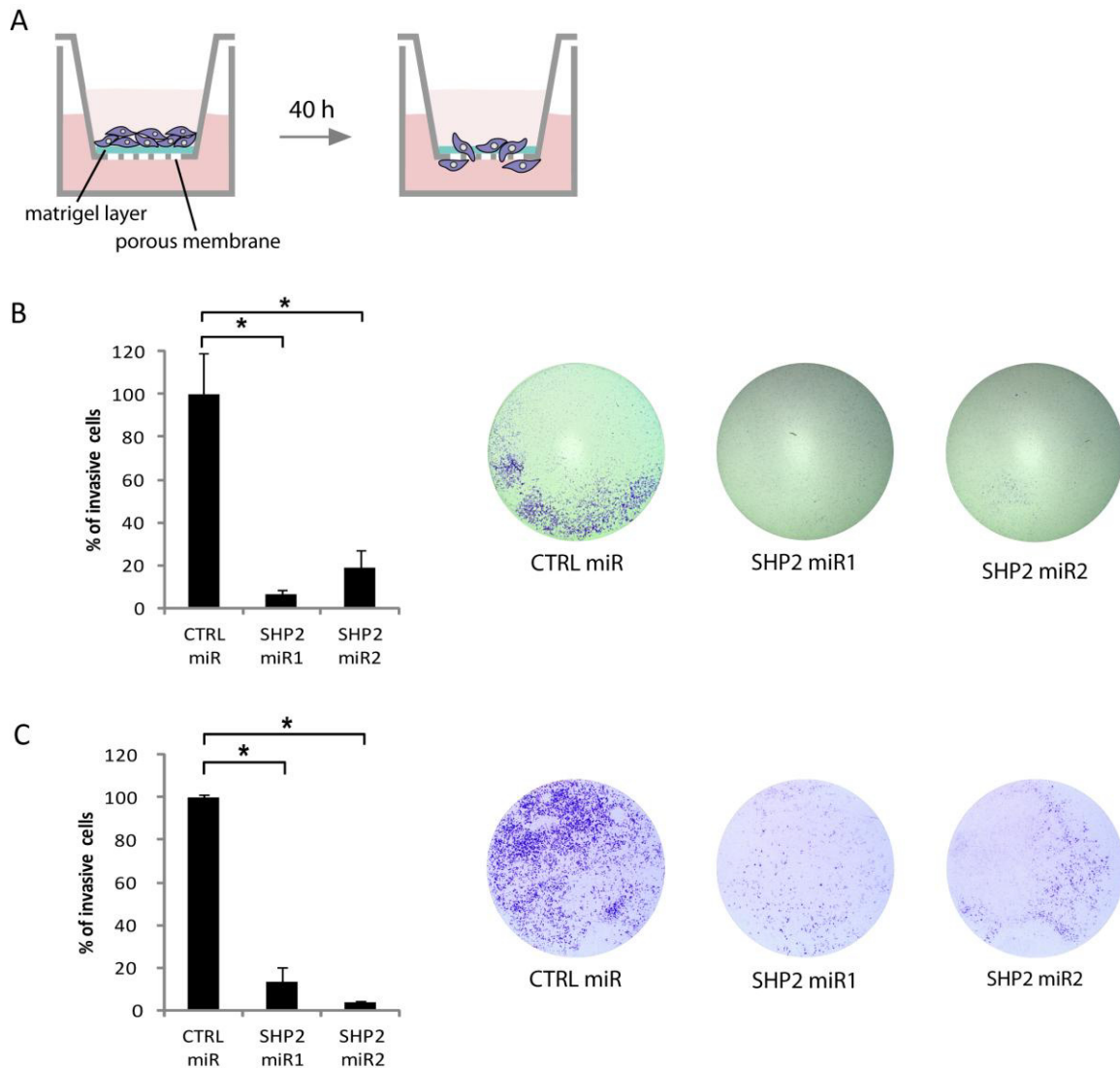
Figure 23. SHP2 knockdown blocks invasion in vitro

(A) Schematic of the matrigel invasion assay. 15,000 starved cells were plated in medium containing 0.25% FBS (SUM159) or 0.5% FBS (MDA-MB-231) in the upper chamber and allowed to invade through a layer of matrigel covering the 8 μm pores towards a gradient of FBS. After 40 h of incubation, invasive cells were counted after removal of non-invasive cells, fixation, and staining with Crystal violet. The whole membranes were imaged using a Leica MacroFluo microscope with a 2 x objective and 0.9 x motor zoom and invasive cells were counted. The average number of invasive cells expressing the control construct was set to 100%.

(B) Left: Bar graph showing the relative percentages of invasive SUM159 cells. Shown are mean values from 3 independent experiments ± SEM. Right: Representative pictures of the bottom of the membranes showing the invasive cells after staining with Crystal violet. *P < 0.001 by Student`s t test.

(C) Left: Bar graph showing the relative percentages of invasive MDA-MB-231 cells. Shown are mean values from 3 independent experiments ± SEM. Right: Representative pictures of the bottom of the membranes showing the invasive cells after staining with Crystal violet. *P < 0.01 by Student`s t test.

Knockdown of SHP2 inhibits tumor cell motility in vivo.

To investigate the effects of SHP2 on cell motility, invasion, and dissemination under physiological conditions, we used intravital multiphoton (IVM) microscopy. Intravital imaging is a powerful technique to study motile tumor cells in the bulk of the tumor at single cell resolution. SHP2 knockdown was induced once tumors had reached 6-8 mm diameter and 10 days later, single cell movement in tumors was imaged by IVM using a custom built two-photon microscope (Bonapace, Wyckoff et al. 2012) (**Figure 24A**). Since we had obtained comparable effects on random migration and chemotaxis towards FBS and invasion in vitro for both miRs targeting SHP2, we chose one knockdown construct for the in vivo experiments.

We used SUM159 and MDA-MB-231 cells expressing the dox-inducible miR2 targeting SHP2 or CTRL miR and stably infected these cells with a constitutively active GFP-Luciferase construct, to allow fluorescent and bioluminescent monitoring of the cells by GFP and Luciferase expression (**Figure 24B**).

We observed that the knockdown of SHP2 significantly decreased tumor cell motility in SUM159 xenografts. The motile cells per field were analyzed in each movie (**Figure 24C**) and depletion of SHP2 resulted in a 74% decrease of cell motility, corresponding to an average of 8.4 moving cells per field in the control group versus only 3.2 moving cells per field in the SHP2 depleted tumors. **Figure 24D** shows a representative picture series of a moving GFP-expressing tumor cell in the control group after 10, 20, and 30 min.

We assessed overall tumor morphology examining tumor cell and blood vessel density and quantified the collagen matrix density imaged by the 2nd harmonic generation. Further, paraffin embedded tumors were cut and stained with H&E to assess overall morphology and stained with anti-mouse CD31 to visualize the vascularization (**Figure**

24E). We found no differences between the control and the SHP2 knockdown tumors after this short term knockdown in already established tumors.

A

Cell injection → 2 weeks → Tumor onset → Tumor ⌀ 6-8 mm → + DOX 10 days → Intravital Imaging

CTRL miR   SHP2 miR2

B

CTRL miR   SHP2 miR2
  +   +   Dox
SHP2
ERK2
GFP
Luciferase
SUM159

C

Motile tumor cells per field

CTRL miR   SHP2 miR2
*

D

Time 0   10 min   20 min   30 min

Tumor cells   Blood vessels

E

CTRL miR

SHP2 miR2

Tumor cells   Blood vessels   collagen   H&E   CD31

68
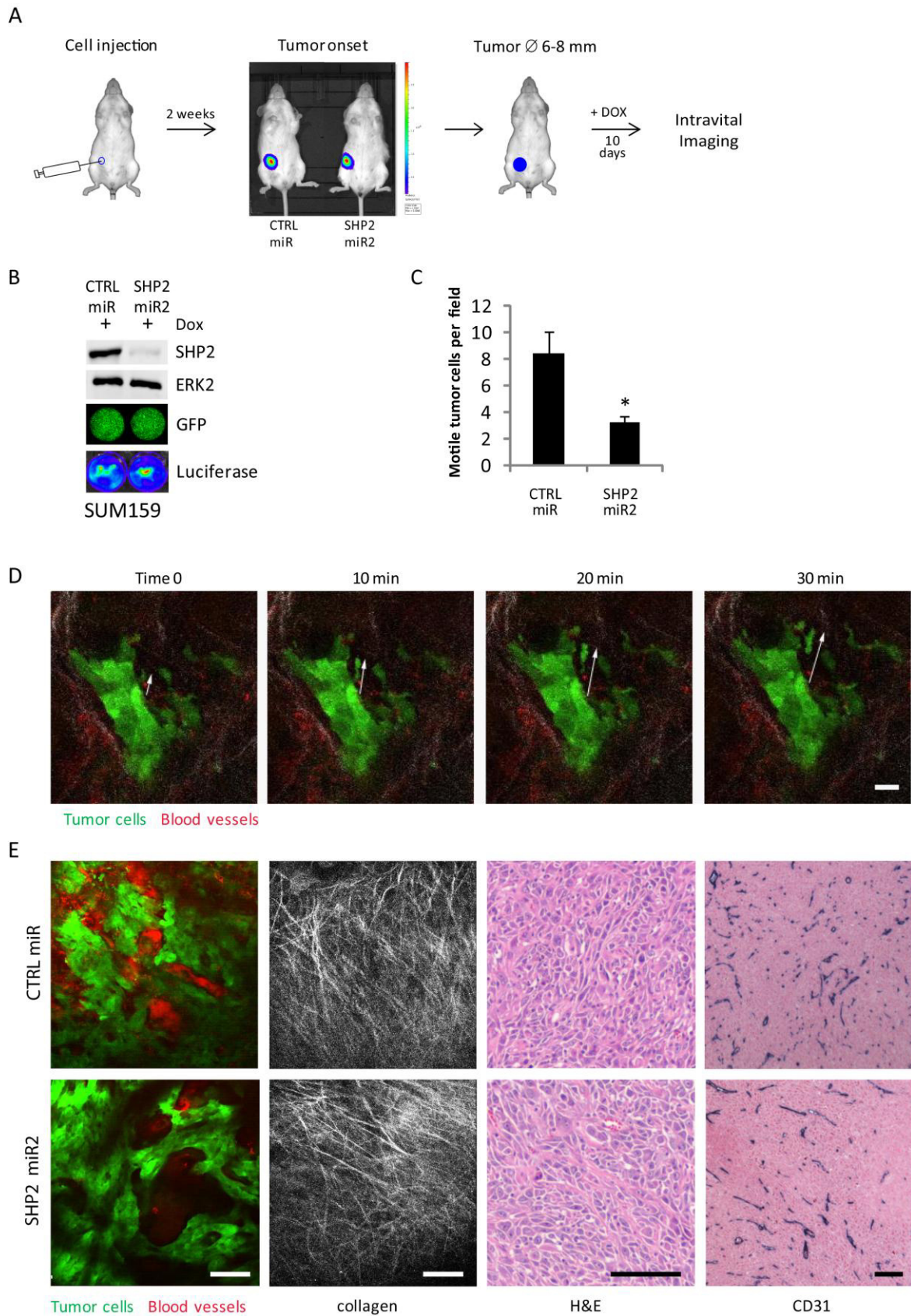
Figure 24. SHP2 knockdown decreases tumor cell migration in SUM159 xenografts

(A) Drawings of the intravital imaging experimental setup. GFP-Luciferase positive cells were injected into gland 4 and tumor onset was controlled by Luciferase bioluminescent signal two weeks after injection. Tumors were allowed to reach 6-8 mm diameter before the knockdown of SHP2 was induced by feeding the mice with dox for 10 days. Then, motile cells were analyzed by intravital microscopy (IVM).

(B) For the in vivo experiments, cells expressing dox-inducible SHP2 miR2 or CTRL miR and tRFP were superinfected with a constitutive active GFP-Luciferase construct. Immunoblot demonstrating the knockdown of endogenous SHP2 in SUM159 cells expressing miR2 targeting SHP2. Representative fluorescence microscopy pictures showing the GFP expression. Upon addition of 150 µg/ml Luciferin to the cell culture medium, Luciferase expression was visualized with an IVIS Lumina XL imaging system.

(C) Bar graph showing the number of motile tumor cells per field. Knockdown of SHP2 led to a 74% decrease in tumor cell motility. For both groups, n=4 mice from 2 independent experiments were used. Per mouse, 5-7 movies were acquired and analyzed. Shown are means of motile tumor cells per field ± SEM. *P < 0.005 by Student`s t test.

(D) Representative time-lapse image series of a migratory tumor cell in a SUM159 control tumor. The white arrow indicates the distance traveled by the motile cell at the beginning of the movie (time 0) and after 10, 20, and 30 min (green: GFP-expressing tumor cells; red: dextran-red labeled blood vessels). Scale bar represents 25 µm.

(E) Representative images of tumor morphology in SHP2 wt and knockdown tumors. Overall tumor morphology was compared by fluorescence images (green: GFP-expressing tumor cells; red: dextran-red labeled blood vessels) and collagen density imaged with the two-photon microscope. Paraffin sections were stained for H&E and mouse CD31 to visualize the tumor vascularization. No differences in tumor morphology were observed after 10 days of SHP2 knockdown. Scale bars represent 100 µm.

To exclude cell line specific effects of SHP2 depletion on in vivo tumor cell migration, we repeated the experiment with the same set-up using a second triple-negative cell line MDA-MB-231 (**Figure 25A**). Consistent with the result from SUM159 cells, knockdown of SHP2 in MDA-MB-231 cells resulted in a dramatic decrease of tumor cell motility. We observed 79% less motility in cells lacking SHP2 corresponding to a mean of only 7.7 moving cells per field compared to a mean of 36.4 motile cells in the control group (**Figure 25B**). **Figure 25C** shows an example of a migratory tumor cell in a mouse from the MDA-MB-231 control group expressing the non-targeting CTRL miR.

We compared the overall morphology on fluorescence images and collagen density was visualized using the 2nd harmonic generation. There was no difference between H&E and CD31 staining when comparing control and SHP2 knockdown tumors (**Figure 25D**).

We therefore concluded that SHP2 is not only important for cell migration in vitro, but also in vivo in xenografts of human triple-negative breast cancer cells.
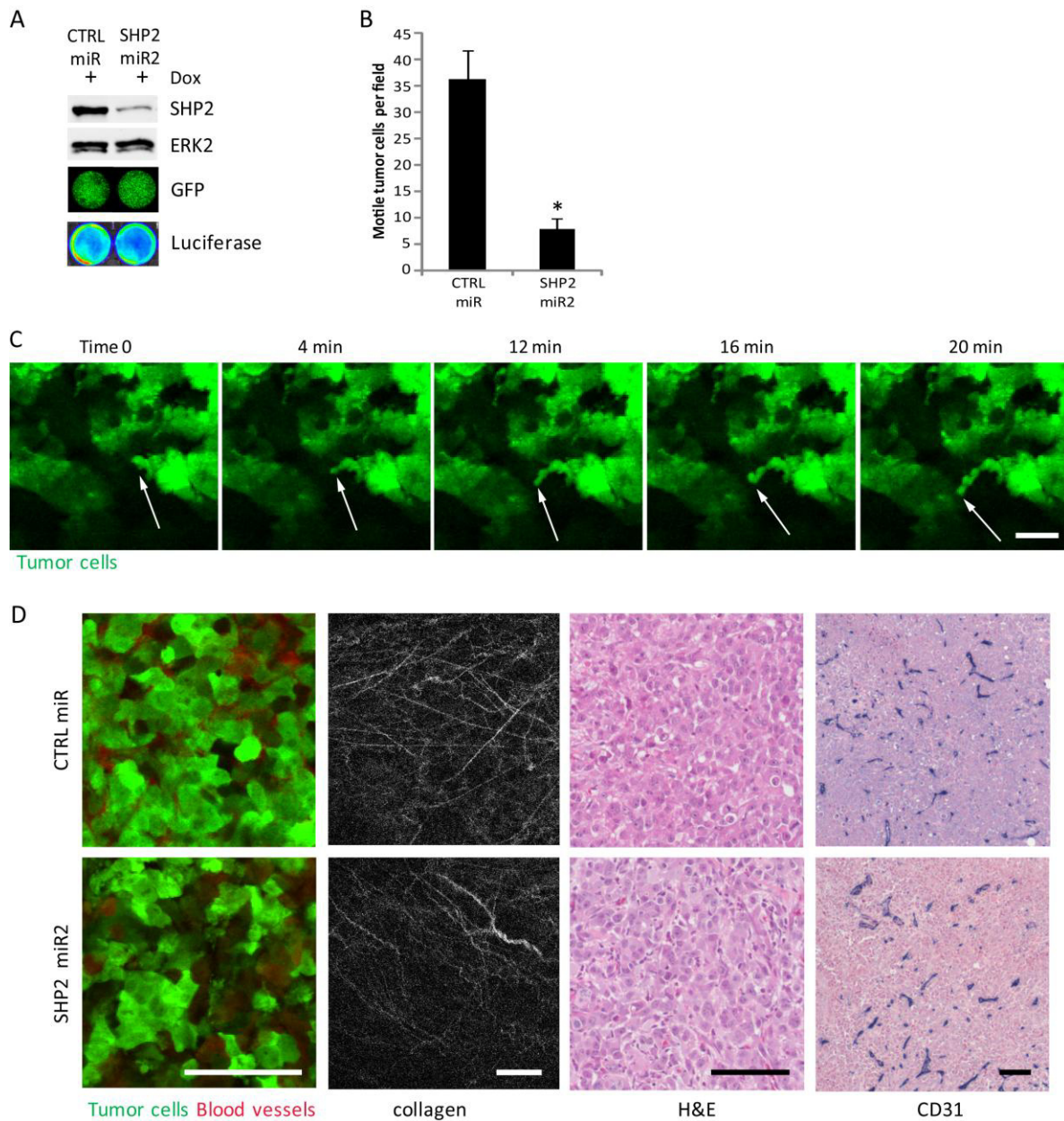
Figure 25. SHP2 knockdown decreases tumor cell migration in MDA-MB-231 xenografts

(A) For in vivo experiments, cells expressing dox-inducible SHP2 miR2 or CTRL miR and tRFP were superinfected with a constitutive active GFP-Luciferase construct. Immunoblot demonstrating the knockdown of endogenous SHP2 in MDA-MB-231 cells expressing miR2 targeting SHP2. Representative fluorescence microscopy pictures showing the GFP-expression in both cell lines. Upon addition of 150 µg/ml Luciferin to the cell culture medium, Luciferase expression was visualized with an IVIS Lumina XL imaging system.

(B) Bar graph showing the motile tumor cells per field. Knockdown of SHP2 led to a 79% decrease in tumor cell motility. Both groups n=3 mice and 5-7 30 min movies were acquired and analyzed per mouse. Shown are means of motile tumor cells per field ± SEM. *P < 0.001 by Student`s t test.

(C) Representative time-lapse image series of a migratory tumor cell in a MDA-MB-231 control tumor. The white arrow indicates the motile cell at the beginning (time 0) and after 4, 8, 12, 16, and 20 min (green: GFP-expressing tumor cells). Scale bar represents 25 μm.

(D) Representative images of tumor morphology in SHP2 wt and knockdown tumors. Overall tumor morphology between SHP2 wt and KD tumors was compared by fluorescence images (green: GFP-expressing tumor cells; red: dextran-red labeled blood vessels) and collagen density. Paraffin sections were stained for H&E and mouse CD31 to visualize the tumor vascularization. No difference in tumor morphology was observed after 10 days of SHP2 knockdown. Scale bars represent 100 μm.

SHP2 depletion results in a decrease of circulating tumor cells.

Tumor cell motility is the first step in the metastatic cascade, before invasive tumor cells intravasate into the circulation. To address the role of SHP2 at this stage of metastases formation, we investigated the effect of SHP2 knockdown on the number of circulating tumor cells. As previously shown (Aceto, Sausgruber et al. 2012), SHP2 knockdown resulted in a significant decrease of tumor growth of SUM159 xenografts correlating with a significant reduction of tumor weight (**Figure 26A-C**).

Blood was drawn from animals bearing SHP2 wt or knockdown tumors and assessed for circulating tumor cells (CTCs) by Fluorescence-activated cell sorting (FACS). We detected CTCs expressing RFP and GFP in all blood samples from the control group and in only two blood samples from the SHP2 knockdown group, but at significantly lower levels than in the SHP2 expressing animals (**Figure 26D**). An average of 5.8 CTCs / 100 μl was detected in the blood of mice with CTRL miR SUM159 xenografts having an average tumor volume of 193 mm³, whereas only an average of 1.7 CTCs / 100 μl blood were detected in SHP2 knockdown animals, resulting in a 3.5 fold decrease (**Figure 26E**).
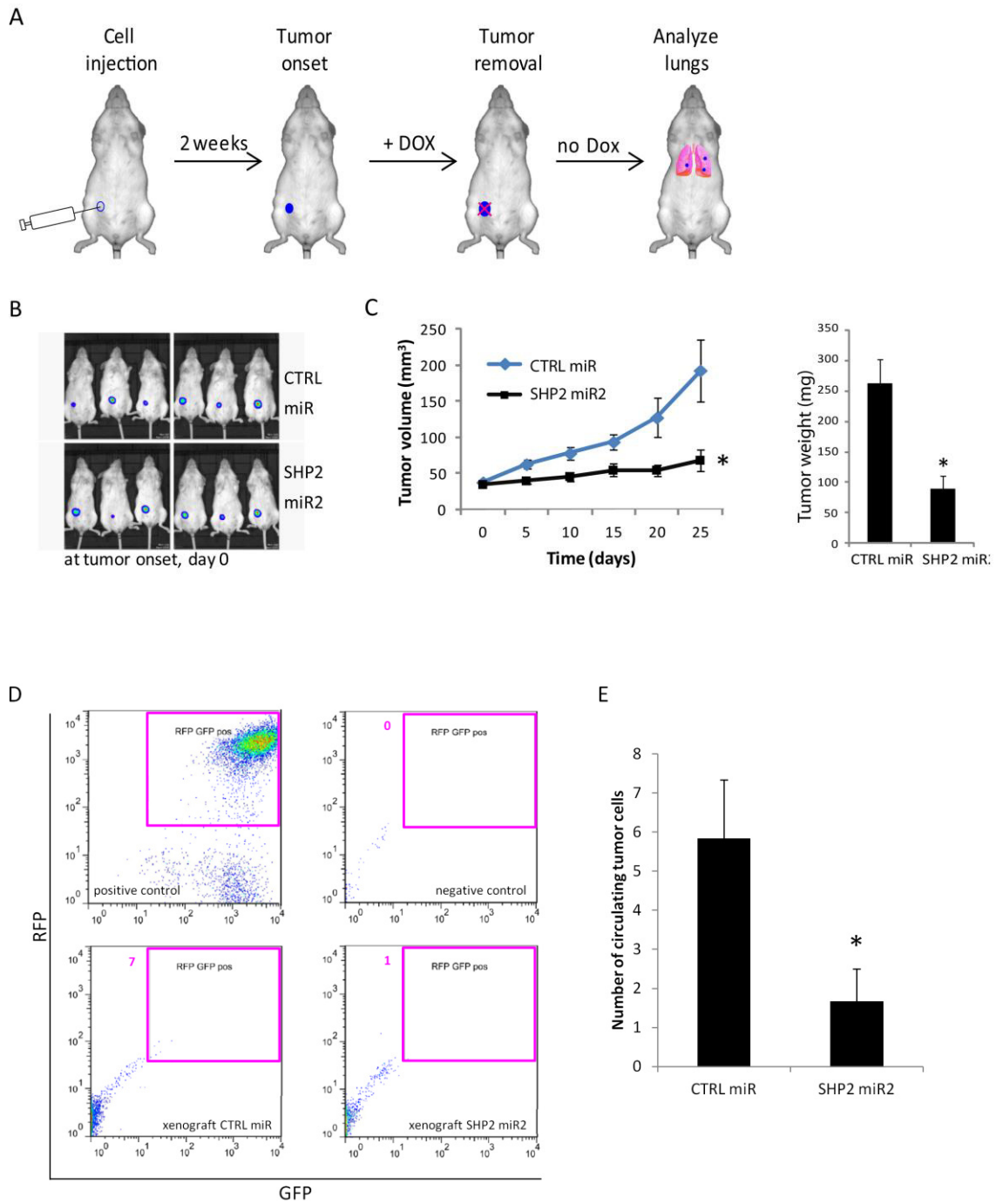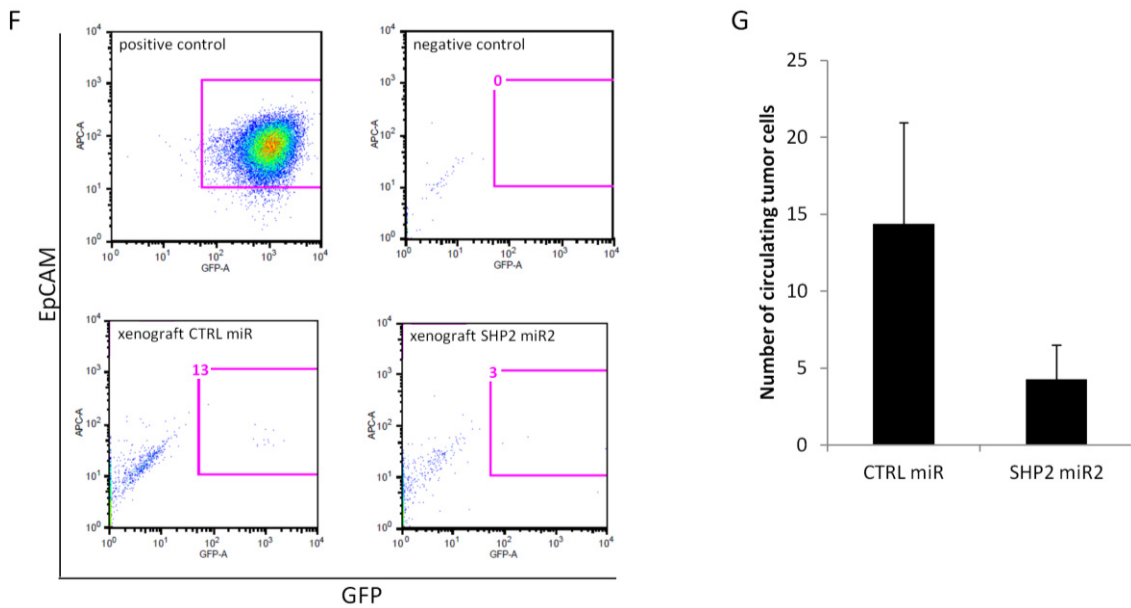
Figure 26. Effects of SHP2 depletion on circulating tumor cells

(A) Schematic of the experimental setup. Mice were injected orthotopically into gland 4 with 1×10^6 SUM159 cells expressing CTRL or SHP2 miR2 and treated with dox for 25 days once tumors became palpable (tumor onset). At day 23, blood was drawn to measure the number of circulating tumor cells (CTCs) before the tumors were surgically removed at day 25 and the mice were kept alive without dox. Metastasis formation was monitored weekly by bioluminescence imaging.

(B) Luciferase bioluminescence images showing the tumors at onset in both groups. Tumors were allowed to develop before dox was added to induce the knockdown of SHP2 in one group.

(C) Left: Tumor growth curve of SUM159 xenografts in presence (CTRL miR) or absence of SHP2 (SHP2 miR2) showing mean tumor volumes ± SEM (n=6). *P < 0.05 by Student`s t test. Right: Tumor weight 25 days after tumor onset. Shown are means ± SEM (n=6). *P < 0.05 by Student`s t test.

(D) FACS analysis of circulating SUM159 tumor cells. Representative dot blots showing the number of circulating tumor cells (CTCs) in the control group (CTRL miR) and in the SHP2 knockdown group (SHP2 miR2). GFP is plotted against RFP expression and CTCs are double positive.

(E) Bar graph showing the mean number of CTCs per 100 µl blood ± SEM (n=6). *P < 0.05 by Mann Whitney test.

(F) FACS analysis of circulating MDA-MB-231 tumor cells. Representative dot blots showing the number of CTCs in the control group (CTRL miR) and in the SHP2 knockdown group (SHP2 miR2). EpCAM was used to gate for epithelial cells and plotted against GFP expression.

(G) Bar graph showing the mean number of CTCs per 100 µl blood from n=5 per group measured at two timepoints ± SEM.

To investigate the effect of SHP2 on SUM159 CTC survival in the blood stream, extravasation, seeding, and proliferation at the metastatic site, we surgically removed the primary tumors. We then monitored metastasis formation by bioluminescence on a weekly basis. Three months after the tumor dissection, the mice had not developed any detectable metastases yet.

We then repeated the experiment with the more aggressive MDA-MB-231 cells. We detected CTCs in the blood of all animals in the control group (5 animals) and only in 2 out of 5 animals in the SHP2 knockdown group (**Figure 26 F and G**).

Phosphotyrosyl proteomic analysis reveals Src family kinases as SHP2 substrates.

To identify the mechanism of action of SHP2 on cell motility and invasion, we set out to find substrates responsible for this phenotype. The physiological substrates of PTPs remain poorly defined, but they are important to understand the molecular mechanism of action of PTPs (Ostman, Hellberg et al. 2006). We used label-free phosphoproteomics on SUM159 cells in presence or absence of SHP2 as an unbiased approach to identify putative substrates.

Randomly growing cells were lysed and the proteins were quantified followed by in-solution tryptic digest of the proteins into peptides. To enrich for phosphopeptides, immunoprecipitation with anti-phosphotyrosine antibodies was performed. After another phospho enrichment step using Titanium dioxide and desalting, the peptides were analyzed by mass spectrometry (**Figure 27A**). Notably, we found 5 out of 11 Src family kinases (SFK), including Src as top hit, to be highly phosphorylated at their inhibitory site Tyr530 in absence of SHP2 (**Figure 27B**). Four of the 5, namely Src, Yes, Fyn and Lyn were among the top 10 highest phosphorylated proteins indentified (**Figure 27C**). We further

found decreased phosphorylation of the Src substrates Paxillin (PXN) at Tyr118, p190RhoGAP (ARHGAP35) at Tyr1105 and Protein zero-related (PZR, MPLZ1) at Tyr263 (**Figure 27B**). Network analysis using the Ingenuity Knowledge Base with the list of identified phosphopeptides confirmed cell migration as a significantly associated network function (**Figure 27D**). When uploading the set of 239 differentially phosphorylated proteins (appendix 9.3), the top networks identified were cellular morphology, cellular movement and cellular assembly and organization. The top five canonical pathways identified were integrin signaling, leukocyte extravasation signaling, actin cytoskeleton signaling, FAK signaling, and ephrin receptor signaling. Concordantly the top bio functions were cellular movement, cellular assembly and organization, cellular function and maintenance, cell morphology and cellular growth and differentiation.
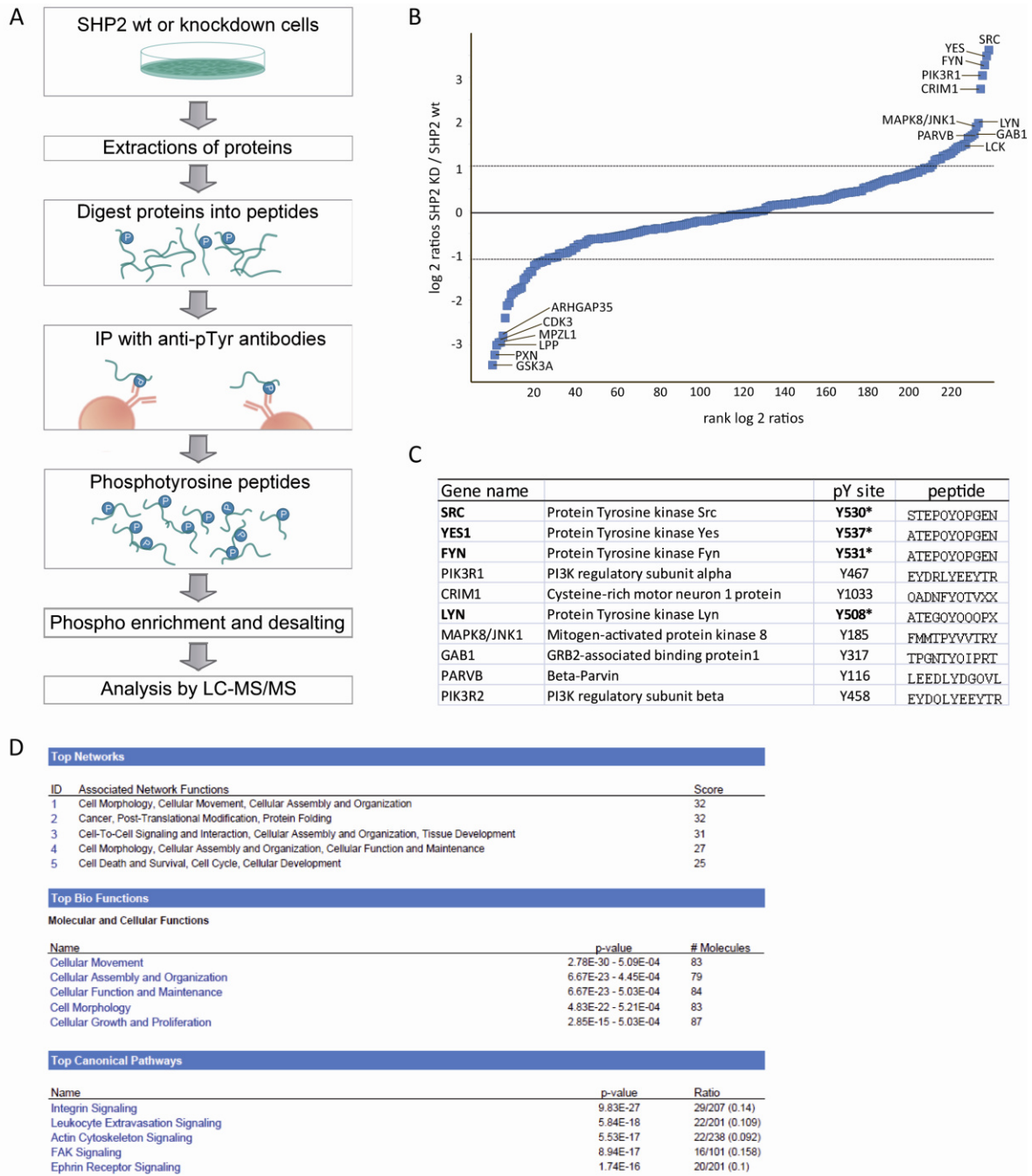
Figure 27. Quantitative phosphoproteomics identified SFKs as SHP2 substrates

(A) Schematic overview of the proteomics workflow. Briefly, SUM159 SHP2 wt or knockdown cells were harvested, lysed and the proteins were digested into peptides. After two steps of phosphopeptide enrichment (IP with anti-phosphotyrosine antibodies and TiO_2 phospho enrichment), the phosphopeptides were analyzed by mass spectrometry.

(B) Scatter plot depicting proteins differentially phosphorylated in presence or absence of SHP2 identified in a quantitative phosphoproteomics experiment. The results are shown as log2 ratios of SHP2 KD/SHP2 wt plotted against the rank of the log2 ratios. Proteins significantly higher phosphorylated in absence of SHP2 (=putative substrates) are shown on top.

(C) List of the top 10 proteins highest phosphorylated in absence of SHP2. Gene names, phospho tyrosine (pY) sites and identified peptide fragments are shown.
(D) Ingenuity pathway analysis of 239 proteins differentially phosphorylated in absence of SHP2. Shown are the top networks (top), top bio functions (middle) and top canonical pathways (bottom).

Validation of the interaction between SHP2 and c-Src.

First, we tested the effect of SHP2 knockdown on Src phosphorylation at Tyr530 by immunoblotting. As for the phosphoproteomics experiment, we used SUM159 cells expressing the dox-inducible miR2 targeting SHP2 and checked for levels of pSrc Tyr530 in presence or absence of SHP2. We confirmed the increased phosphorylation of pSrc at Tyr530 in absence of SHP2 (**Figure 28A**). We then used fluorescence resonance electron transfer (FRET) acceptor photobleaching (**Figure 28B**) to confirm the direct interaction between SHP2 and Src or pSrc Tyr530 in fixed SUM159 and MDA-MB-231 cells. FRET efficiencies were measured between SHP2 and Src and SHP2 and pSrc Tyr530. Significant FRET was found between both pairs in both cell lines. An average FRET efficiency of 23.3% was measured between SHP2 and Src and 28.1% between SHP2 and pSrc Tyr530 in SUM159 cells showing that they interact. In MDA-MB-231 cells, FRET efficiencies of 5.3% were detected between SHP2 and Src and 15.4% between SHP2 and pSrc Tyr530. No FRET was detected in the negative control (**Figure 28C-E**).
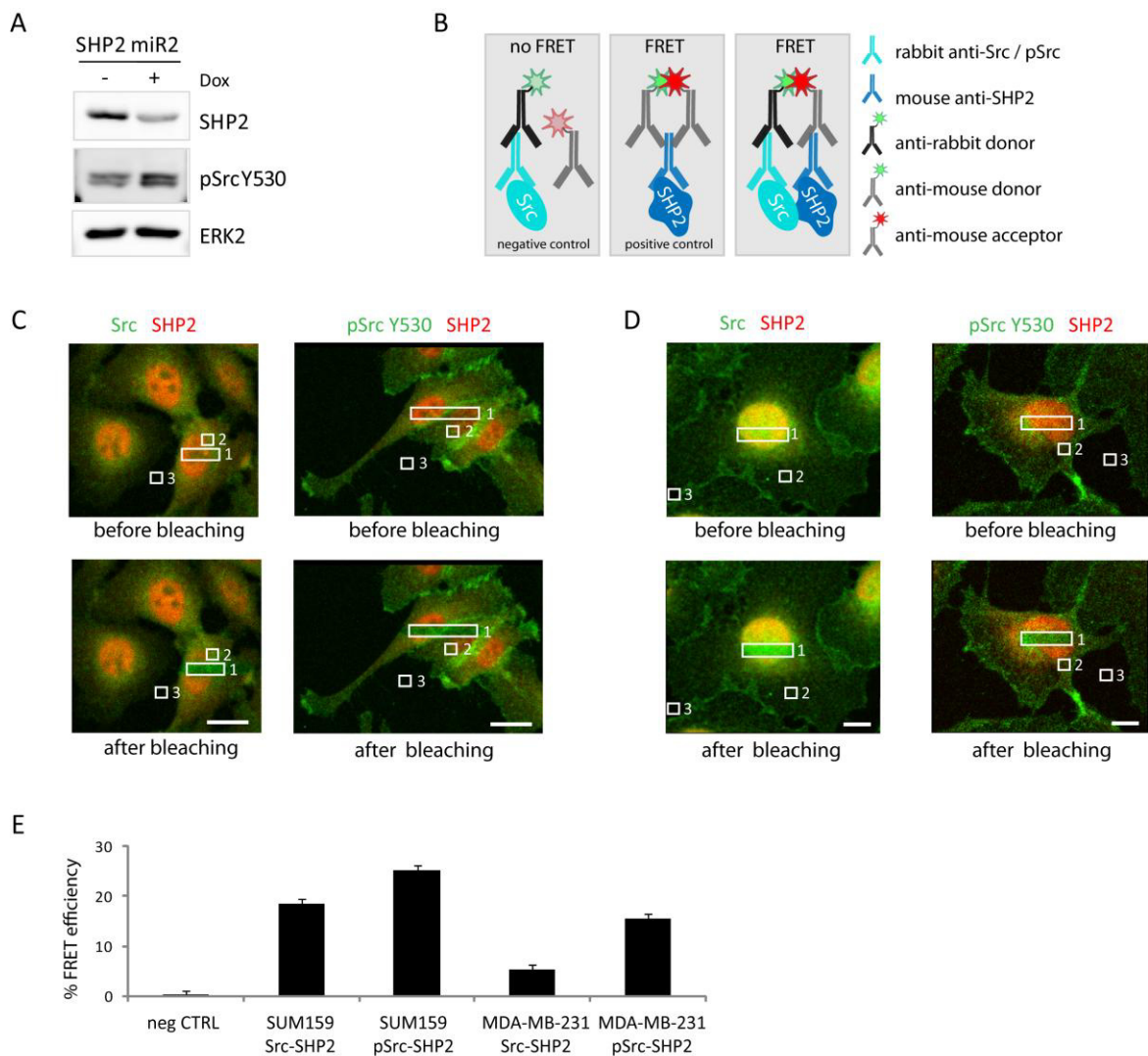
Figure 28. FRET revealed interaction between SHP2 and Src / pSrc Tyr530

(A) Immunoblot showing the phosphorylation of Src in SUM159 cells expressing the dox-inducible miR2 targeting SHP2 in presence (+) or absence (-) of dox. Blotting with anti-SHP2 confirms the knockdown of endogenous SHP2 upon addition of dox and pSrc Tyr530 levels are increased in these cells. ERK2 was used as a loading control.

(B) Schematic overview of FRET interactions and controls. FRET acceptor photobleaching on fixed cells is based on labeling two endogenous proteins with primary antibodies raised in different species, for example rabbit and mouse (protein 1 mouse, protein 2 rabbit), and secondary donor and acceptor fluorophore-conjugated antibodies e.g. protein 1 anti-mouse donor and protein 2 anti-rabbit acceptor. As a negative control only 1 primary antibody is used and labeled with the secondary donor antibody. The secondary acceptor antibody specific for the other species cannot bind and is therefore not close enough to the donor antibody for FRET to occur. In the positive control, 2 secondary antibodies raised against the same species are used both binding to the same protein ensuring FRET signal.

(C) Representative pictures of fixed SUM159 cells immunostained for SHP2 and Src (left), or SHP2 and pSrc Tyr530 (right) before and after FRET acceptor photobleaching. Src and pSrc were labeled with rabbit primary antibodies and anti-rabbit Alexa 568 donor fluorophore (pseudocolor green) and SHP2 was labeled with mouse anti-SHP2 antibody and anti-mouse Alexa 633 acceptor secondary antibody (red). ROI 1 indicates the region bleached, ROI 2 is a control region to check for unspecific bleaching of the donor and ROI 3 is a region to measure the background fluorescence. Scale bars represent 25 μm.

(D) Representative pictures of fixed MDA-MB-231 cells immunostained for SHP2 and Src (left) or SHP2 and pSrc Tyr530 (right) before and after FRET acceptor photobleaching. Src and pSrc were labeled with rabbit primary antibodies and anti-rabbit Alexa 568 donor fluorophore and SHP2 was labeled with mouse anti-SHP2 antibody and anti-mouse Alexa 633 acceptor secondary antibody. Scale bars represent 25 μm.

(E) Bar graph showing the quantification of the FRET efficiencies between SHP2 and Src and SHP2 and pSrc Tyr530 in SUM159 and MDA-MB-231 cells. In each experiment 4-10 individual cells were measured. As a negative control, Src (rabbit) was labeled with anti-rabbit Alexa 568 and measured in presence of anti-mouse Alexa 633. For each measure Alexa 633 bleaching had to be over 95% and FRET efficiency (%E) was calculated after background subtraction and Alexa 568 bleaching correction as follows: $\%E = (D_{post} - D_{pre})/D_{post}$, where D_{pre} and D_{post} are the donor (Alexa 568) intensities in the bleached region before (D_{pre}) and after (D_{post}) bleaching. Shown are means ± SEM.

5.3 DISCUSSION

SHP2 is required for cell migration, chemotaxis and invasion in vitro.

The main cause of death in cancer patients are metastases (Christofori 2006). We investigated the influence of SHP2 on random cell migration by analyzing the migration patterns of SHP2 wt or knockdown cells and found that cells lacking SHP2 moved significantly less than their SHP2-expressing counterparts. We detected significant decreases in the path length, velocity and distance to start. Our findings were in line with previous observations showing a decreased migratory and spreading potential of fibroblasts lacking SHP2 (Yu, Qu et al. 1998). We further found that SHP2 is required for chemotaxis towards an FBS gradient, as depletion of SHP2 resulted in a significant decrease of cell migration. To disseminate from the primary tumor, cells need to acquire not only motility but also invasive potential. Indeed, we further showed that knockdown of SHP2 also strongly inhibited invasion in vitro using a matrigel invasion assay. As the majority of previous studies were done either in fibroblasts or HER2-positive breast cancer cells (Yu, Qu et al. 1998, Wang, Liu et al. 2005) we tested the effects of SHP2 inhibition in metastatic triple-negative breast cancer models. In summary, we found that SHP2 is important for invasion in triple-negative breast cancer, suggesting a broader role for this phosphatase in cell migration and invasion.

SHP2 is required for tumor cell migration and dissemination in vivo.

To validate the role of SHP2 in early metastatic steps under physiological conditions, we used intravital microscopy (IVM). We found that SHP2 depletion led to a massive decrease in tumor cell motility in TNBC cell lines. Similar to the cells on plastic, increased membrane ruffling paired with decreased motility was observed in the xenografts lacking SHP2. We had previously shown that knockdown of SHP2 inhibits tumor cell proliferation

in xenografts (Aceto, Sausgruber et al. 2012). To exclude any artifacts resulting from different tumor volumes at the time of imaging, we let the tumors develop before inducing the knockdown of endogenous SHP2. As expected, histological analysis of the tumors did not reveal morphological differences after this short-term depletion of SHP2. Previous reports mainly showed functions of SHP2 in cell migration in vitro and its function in vivo is less understood. While classical endpoint methods, such as tumor size measurements, only allow a snapshot at the end of the experiment and average the whole tumor cell population, IVM allows the study of the minority of cells having the capacity to leave the primary tumor and metastasize to distant organs (Condeelis and Weissleder 2010, Beerling, Ritsma et al. 2011, Zomer, Beerling et al. 2011). In accordance with our results, SHP2 was recently found to be highly upregulated in motile tumor cells (Patsialou, Wang et al. 2012). These findings suggest that depletion of SHP2 not only inhibits primary tumor growth, but also blocks metastatic spread by impairing tumor cell motility and invasion.

We then tested the requirement of SHP2 in tumor cell dissemination and assessed the number of circulating tumor cells in the blood of tumor bearing mice. Corresponding to the decreased number of motile tumor cells, the number of CTCs was decreased upon depletion of SHP2. These findings were in line with the results of Patsialou and colleagues, which assessed the number of circulating tumor cells using the small molecule SHP1/SHP2 inhibitor NSC87877 (Chen, Sung et al. 2006). These observations demonstrate a crucial role of SHP2 in tumor cell motility, intravasation, and dissemination.

Studies to assess effects of SHP2 on later steps in the metastatic cascade, such as cell survival in the blood stream, extravasation, and colonization potential at the distant site are ongoing and will elucidate the importance of SHP2 in metastatic progression. Several experimental approaches were applied, such as surgical removal of the xenografts or tail vein injections, and the mice are being monitored for lung metastasis formation by

bioluminescence. Another interesting aspect worth testing would be if SHP2 inhibition will be effective after overt onset of metastases.

In summary, we observed strong effects of SHP2 inhibition on the early steps of metastases formation in vivo and in vitro, namely migration, chemotaxis, matrigel invasion, tumor cell migration, and dissemination. These findings validate SHP2 as a valuable target in the treatment of breast cancer.

SHP2 regulates cell migration and invasion via c-Src.

To explain the effects of SHP2 on migration and invasion mechanistically, we aimed to identify the physiological substrates of SHP2. Unbiased quantitative proteomics revealed 5 of the 11 Src family kinases (SFKs) to be highly phosphorylated in absence of SHP2 at Tyr530. Four of them were among the ten highest phosphorylated proteins and Src was found to be the top hit, followed by Yes and Fyn. SFKs are inhibited by phosphorylation of the C-terminal inhibitory site Tyr530 and positively regulated by phosphorylation of the activating site Tyr419 (Zhang, Yang et al. 2004). The hyperphosphorylation of the inhibitory site Tyr530 in several SFKs including c-Src upon knockdown of SHP2 could explain the SHP2 meditated effects on cell migration and metastatic spread. Increased SFK activity strongly correlates with breast cancer invasion and metastasis, and these kinases are frequently activated in human cancers (Ishizawar and Parsons 2004).

In line with these findings, the phosphorylation of two Src substrates implicated in cell migration, paxillin and p190RhoGAP, was found to be strongly decreased in the absence of SHP2. Paxillin is a phosphotyrosine containing adapter protein localized in focal adhesions. It mediates signaling between integrin receptors and the cytoskeleton (Turner, Glenney et al. 1990, Burridge, Turner et al. 1992). Phosphorylated paxillin was found to be involved in controlling actin cytoskeleton rearrangements and thereby changes

of cell morphology and motility (Nakamura, Yano et al. 2000, Iwasaki, Nakata et al. 2002). Paxillin was initially identified as a tyrosine phosphorylated substrate in SRC-transformed fibroblasts (Glenney and Zokas 1989, Schaller 2001). Klinghoffer and colleagues showed that Src-, Fyn- and Yes-deficient fibroblasts exhibited strongly reduced adhesion potential which was dependent on the tyrosine phosphorylation of paxillin (Klinghoffer, Sachsenmaier et al. 1999). Furthermore, c-Src was shown to phosphorylate paxillin at Tyr118 alone or concomitantly with FAK to transduce pro-migratory signals (Sachdev, Bu et al. 2009).

The Rho regulatory protein, p190RhoGAP regulates actin dynamics and cell spreading (Arthur and Burridge 2001) and is phosphorylated by c-Src at Tyr1105 (Roof, Haskell et al. 1998). Overexpression of c-Src was shown to increase p190RhoGAP phosphorylation whereas expression of a dominant-negative c-Src construct decreased the phosphorylation (Chang, Wilson et al. 1993, Chang, Gill et al. 1995).

PZR is another Src substrate we found to be hypophosphorylated at Tyr263 in the absence of SHP2 and active Src. Conceivably, it might serve as a scaffold protein targeting SHP2 and Src to the membrane in the context of integrin signaling. PZR belongs to the immunoglobulin superfamily and was found to recruit and bind SHP2 through its intracellular immunoreceptor tyrosine-based inhibitory motifs (ITIMs) (Zhao and Zhao 1998, Zhao and Zhao 2000). Phosphorylation of PZR at Tyr241 and Tyr263 was found to recruit and activate the phosphatase by inducing a conformational change, thereby altering downstream signaling (Zhao and Zhao 2003, Eminaga and Bennett 2008). This adapter protein has been shown to be phosphorylated by c-Src and other SFK such as Fyn and Lyn and the Src inhibitor PP1 was found to inhibit PZR phosphorylation (Zhao, Guerrah et al. 2002, Zhao and Zhao 2003, Kusano, Thomas et al. 2008).

Src has previously been shown to be important in the regulation of focal adhesion turnover (Huttenlocher and Horwitz 2011). This process is tightly controlled by Rho GTPases (Parri and Chiarugi 2010), which mediate the formation of protrusions at the leading edge of the cell, followed by adhesion, deadhesion, and retraction at the rear (Ridley, Schwartz et al. 2003, Jaffe and Hall 2005). The GTPase-activating protein p190RhoGAP is a functional regulator of RhoA (Arthur and Burridge 2001). Src signaling is transduced through its substrates that regulate GTPase activity and therefore ultimately cell migration (Huttenlocher and Horwitz 2011). Src was found to activate p190RhoGAP which in turn decreases Rho activity and leads to the recruitment of Rac, resulting in an increased focal adhesion turnover (Schober, Raghavan et al. 2007). Conversely, increased Rho activity was shown to stabilize focal adhesion and decrease cell motility in Src deficient fibroblasts (Fincham and Frame 1998, Klinghoffer, Sachsenmaier et al. 1999). Interestingly, SHP2-deficient fibroblasts were also shown to have impaired cell migration and large peripheral focal adhesions (Yu, Qu et al. 1998).

In conclusion, we found SHP2 to play a role in the early steps of metastasis, as depletion of SHP2 impaired tumor cell migration and dissemination into the blood stream. Mechanistically, we found that SHP2 exerts its effect on cell migration and invasion in vitro and in vivo through the regulation of Src activity. Notably, Src has previously been implicated in the early steps of metastatic dissemination in studies using the Src inhibitor saracatinib (Siemann, Dong et al. 2012). Similar results were obtained using other Src inhibitors (Jallal, Valentino et al. 2007). Mechanistically, we suggest that SHP2 activates c-Src by dephosphorylating the inhibitory site Tyr530 in the C-terminal domain of Src, which then in turn activates several downstream effectors including Paxillin and p190RhoGAP by phosphorylation. Paxillin and p190RhoGAP, both important for the regulated turnover of focal adhesions, transduce the positive migratory signal to RhoA

resulting in increased cell migration (**Figure 29**). The Src substrate PZR might act as an adaptor protein in this SHP2-Src mediated signaling downstream of integrin receptors.
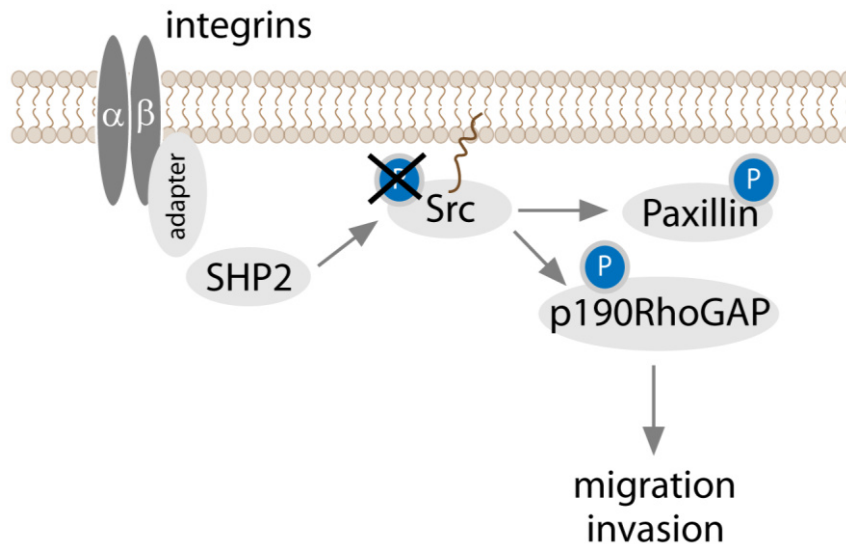
Figure 29. Hypothetical working model of SHP2 signaling in cell migration
We propose that downstream of integrin receptors, SHP2 exerts pro-migratory and pro-invasive signaling through activation of Src by dephosphorylating the inhibitory site Tyr530 and therefore Src substrates implicated in focal adhesion turnover and cell migration. The scaffold protein PZR might serve as an adapter in this setting.

In previous studies, SHP2 has been proposed to regulate the activity of c-Src and SFKs. However, it remains controversial whether this regulation is direct or indirect. Zhang and co-workers reported inhibition of SFKs and downregulation of their substrates in SHP2-deficient cells. In contrast to our observation of a direct interaction of SHP2 and c-Src, they found SHP2 to regulate phosphorylation of the Csk regulator PAG/Cbp, thereby controlling Csk access to SFKs (Zhang, Yang et al. 2004). Ren and colleagues proposed yet another mechanism. According to their model, SHP2 dephosphorylates Paxillin leading to the dissociation of Csk from paxillin. Csk is a negative regulator of c-Src phosphorylating Src at the inhibitory C-terminal tyrosine. The dissociation of Csk

from the Src-Paxillin complex resulted in a decreased phosphorylation of the inhibitory site Tyr530 and hence increased Src activity (Ren, Meng et al. 2004). Other reports suggested SHP2 to regulate Src activity by a non-enzymatic mechanism (Walter, Peng et al. 1999). The same group previously published that SHP2 can dephosphorylate Src at Tyr527 in vitro (Peng and Cartwright 1995). Although different mechanisms of action are proposed, all studies have in common that SHP2 leads to the activation of Src/SFK which in turn leads to downstream signaling important in the context of cell migration. Our studies demonstrate that SHP2 directly activates c-Src and SFKs by dephosphorylation of the inhibitory site Tyr530.

6 RESULTS PART3 – The role of nuclear SHP2 in breast cancer

6.1 INTRODUCTION

When SHP2 was identified more than 20 years ago, it was described as a solely cytoplasmic phosphatase (Adachi, Sekiya et al. 1992, Freeman, Plutzky et al. 1992, Ahmad, Banville et al. 1993, Feng, Hui et al. 1993, Vogel, Lammers et al. 1993). Later, functions of SHP2 in the nucleus have been proposed (Chughtai, Schimchowitsch et al. 2002, Wu, Hong et al. 2002, Jakob, Schroeder et al. 2008, Takahashi, Tsutsumi et al. 2011). Furthermore, SHP2 was the first phosphatase found to be located in the mitochondria (Salvi, Stringaro et al. 2004).

In 2002, Wu et al. showed that nuclear SHP2 dephosphorylates the signal transducer and activator of transcription 1 (STAT1) thereby inhibiting its transcriptional activity (Wu, Hong et al. 2002). In the same year, Chughtai and colleagues found that prolactin stimulation of mouse mammary HC11 and human T47D breast cancer cells led to nuclear translocation of SHP2 in complex with signal transducer and activator of transcription 5a (STAT5a). This complex of SHP2 and STAT5a was found to bind to DNA and to regulate transcription of milk protein genes (Chughtai, Schimchowitsch et al. 2002). Nuclear SHP2 was further reported to dephosphorylate telomerase reverse transcriptase (TERT), the catalytic subunit of telomerase, at Tyr707, thus preventing nuclear oxidative stress-dependent nuclear export of TERT, and thus enhancing nuclear telomerase activity (Jakob, Schroeder et al. 2008). Takahashi and colleagues recently showed that nuclear SHP2 dephosphorylates parafibromin/Cdc73 which is a component of the nuclear RNA polymerase II-associated factor complex, transforming parafibromin from a tumor suppressor to an oncogenic activator. They argued, as parafibromin is a

strictly nuclear protein, dephosphorylation by SHP2 must occur in the nucleus. Based on their observation that SHP2 was abundant in the nuclei of proliferating cells but not of confluent cells, they proposed nuclear accumulation of SHP2 upon growth-stimulating signals (Takahashi, Tsutsumi et al. 2011). Whether nuclear SHP2 is important for its effects in breast cancer remains unknown.

Nuclear import.

The mechanism of SHP2 translocation into the nucleus is unknown. Access to the nucleus is limited by a double-membrane structure called the nuclear envelope. The only way to cross the membrane is through large pores, called nuclear pore complexes (NPC), which are embedded in the nuclear envelope (Poon and Jans 2005). While proteins with a size smaller than 40 kDa can diffuse through the NPCs, larger proteins need to be actively transported through the NPCs by the nuclear import machinery (Gasiorowski and Dean 2003). Usually proteins above 40 kDa contain a nuclear localization signal (NLS) that targets them into the nucleus through the NPC (**Figure 30**).
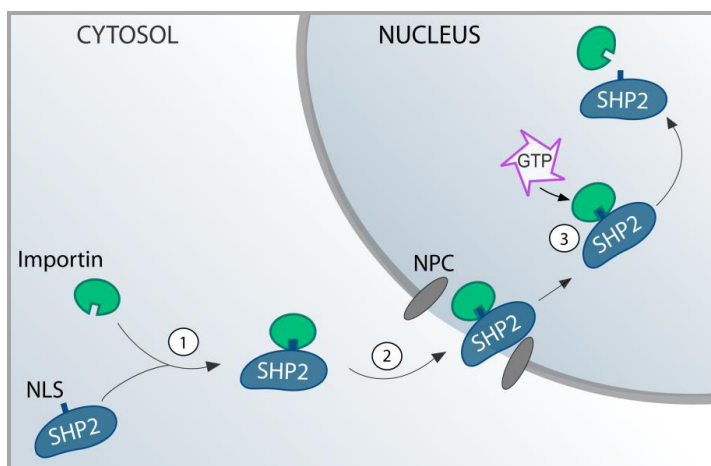
Figure 30. Simplified scheme for nuclear import
1) Nuclear localization sequence (NLS) on proteins above 40 kDa is recognized and bound by importin in the cytoplasm. 2) Then the importin/NLS protein complex translocates actively into the nucleus through the nuclear pore complex (NPC). 3) The release of the NLS containing protein requires the binding of RanGTP (GTP) to importin.

Although it is possible for proteins > 40 kDa without a NLS to enter the nucleus via co-transport with a protein that has a NLS, as suggested for SHP2 and STAT5a (Chughtai, Schimchowitsch et al. 2002), many nuclear proteins have their own NLS. NLS are short sequences of basic amino acids such as lysine (Lys) or arginine (Arg) that are exposed on the protein surface. These amino acids are recognized by importins that target the proteins through the NPCs. The most commonly found NLS are the pat4 and pat7 classical NLS and the bipartite NLS (Hicks and Raikhel 1995). The pat4 NLS consists of 4 basic amino acids (Lys or Arg) or of 3 basic amino acids and one histidine (His) or proline (Pro). The pat7 NLS starts with a Pro, followed by a basic segment within 3 residues from the starting Pro containing 3 out of 4 basic Lys or Arg residues. The bipartite NLS was first described in Xenopus nucleoplasmin (Robbins, Dilworth et al. 1991) and consists of 2 basic residues and a 10 residue spacer, followed by another basic segment containing at least 3 basic residues out of 5 residues. To date, no NLS has been described for SHP2. However, with a size of 72 kDa, it cannot simply diffuse through nuclear pores.

Therefore, we were interested to study the mechanism of nuclear import of SHP2 in our models. We further wanted to elucidate the roles of nuclear SHP2 in breast cancer.

6.2   RESULTS

SHP2 is present in the nucleus of breast cancer cell lines.

Nuclear SHP2 has been previously described in A431 and HEK293T cells (Wu, Hong et al. 2002), in fibroblasts (Jakob, Schroeder et al. 2008), and in AGS and lacC9 cells (Takahashi, Tsutsumi et al. 2011). In breast cancer, nuclear SHP2 has only been described in T47D cells (Chughtai, Schimchowitsch et al. 2002). Therefore, we first wanted to confirm the nuclear localization of SHP2 in other breast cancer cell lines.

Using nuclear and cytoplasmic fractionation followed by immunoblotting, we detected SHP2 in the cytosolic and nuclear fraction of all cell lines tested (BT474, SUM159, SUM1315, MDA-MB-231, and MCF10A HER2/3) (**Figure 31A**). To ensure the purity of the fractions, the nuclear enzyme Poly (ADP-ribose) polymerase (PARP) was used as a marker for the nuclear fraction and tubulin α was used as a cytoplasmic marker. The amount of nuclear SHP2 was found to be cell line-dependent between 21.5% and 43.5% (**Figure 31B**). Nuclear localization of SHP2 was further confirmed by immunofluorescence (**Figure 31C and D**) and mass spectrometry (**Figure 39D**) of nuclear and cytoplasmic fractions.
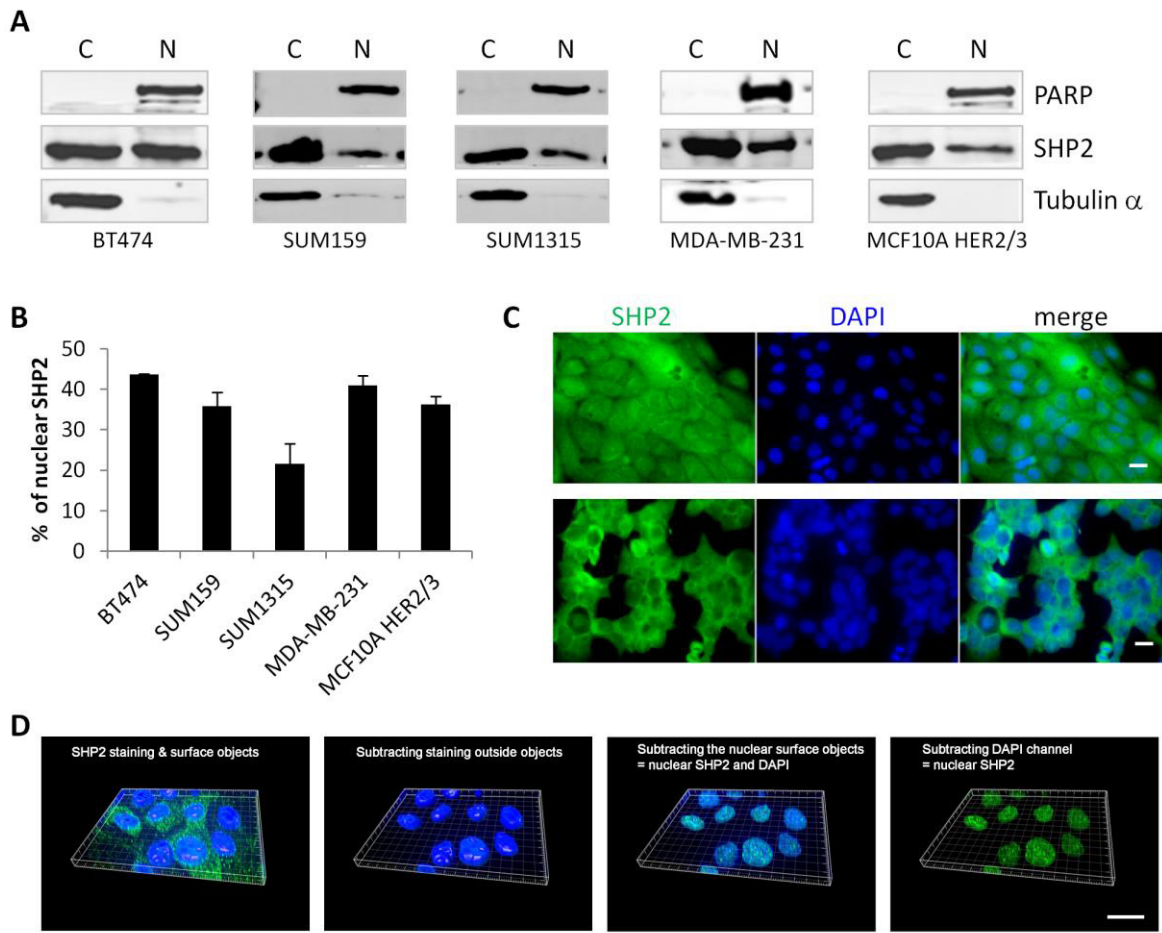
Figure 31. Nuclear and cytoplasmic localization of SHP2

(A) Representative immunoblots of subcellular fractionations of several breast cancer cell lines showing SHP2 in the cytoplasmic (C) and in the nuclear (N) fraction. To ensure the purity of the fractions, the enzyme PARP was used as a nuclear marker and tubulin α was used as a cytoplasmic marker.

(B) Bar graph showing the percentage of nuclear SHP2 in each cell line measured by densitometry of SHP2 immunoblots. Shown are means ± SEM (n=3).

(C) Representative pictures of SHP2 immunostaining in MCF10A HER2/3 (top) and BT474 cells (bottom). Cells were seeded on Poly-L-Lysine coated coverslips and stained with anti-SHP2 antibodies (green). Nuclei are visualized with DAPI staining (blue). Images were taken with a Zeiss Z1 widefield microscope. Scale bars represent 20 μm.

(D) Representative 3D images of deconvoluted z-stacks taken with a Zeiss Z1 widefield microscope showing that SHP2 staining (green) localizes inside the nucleus (DAPI staining, blue). After deconvolution, surface objects were defined around the nuclei using Imaris software. Next, the SHP2 signal outside these objects was removed. Then the surface object masks were removed, leaving the nuclei with DAPI and SHP2 staining. After switching off the DAPI channel, SHP2 staining could be observed in the nuclei. Scale bar represents 20 μm.

Nuclear import of SHP2 requires a pat4 NLS.

Although there are several reports on nuclear SHP2, it remains unclear how SHP2 is translocated into the nucleus. To elucidate the mechanism of its nuclear import, we analyzed the SHP2 amino acid sequence using a web based bioinformatics program for subcellular localization prediction based on amino acid sequence (PSORT II) (Nakai and Horton 1999).

We identified a potential pat4 NLS in the SHP2 sequence that could facilitate the nuclear import of SHP2. The pat4 NLS identified by PSORT II consists of Lys-Pro-Lys-Lys located at amino acid 322-325 in the phosphatase domain of SHP2. We then assessed whether the pat4 NLS was required for SHP2 nuclear translocation. The putative NLS found in the SHP2 sequence was deleted or mutated in a dox-inducible pLKO-TREX-SHP2-HA expression construct. To conserve the 3D structure, we did not alter the last Lys as it is important for the folding of SHP2. The other two basic residues were exchanged for serine (Ser), an uncharged amino acids of the same size, resulting in a change from Lys-Pro-Lys-Lys to Ser-Pro-Ser-Lys. In the NLS deleted mutant, the first three amino acids of the NLS and the four amino acids before the NLS were deleted (resulting in the deletion of amino acids 317-324) (**Figure 32A**). Direct DNA sequencing of the complete SHP2 sequence showed the correct insertion of the desired mutation or deletion without frame shifts or other errors (**Figure 32B**).
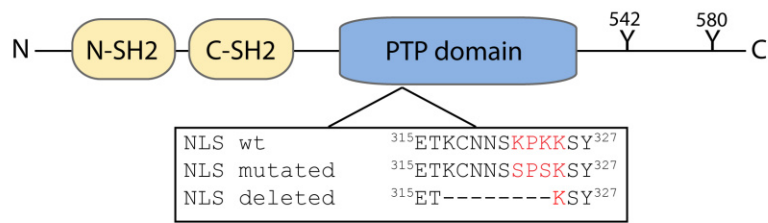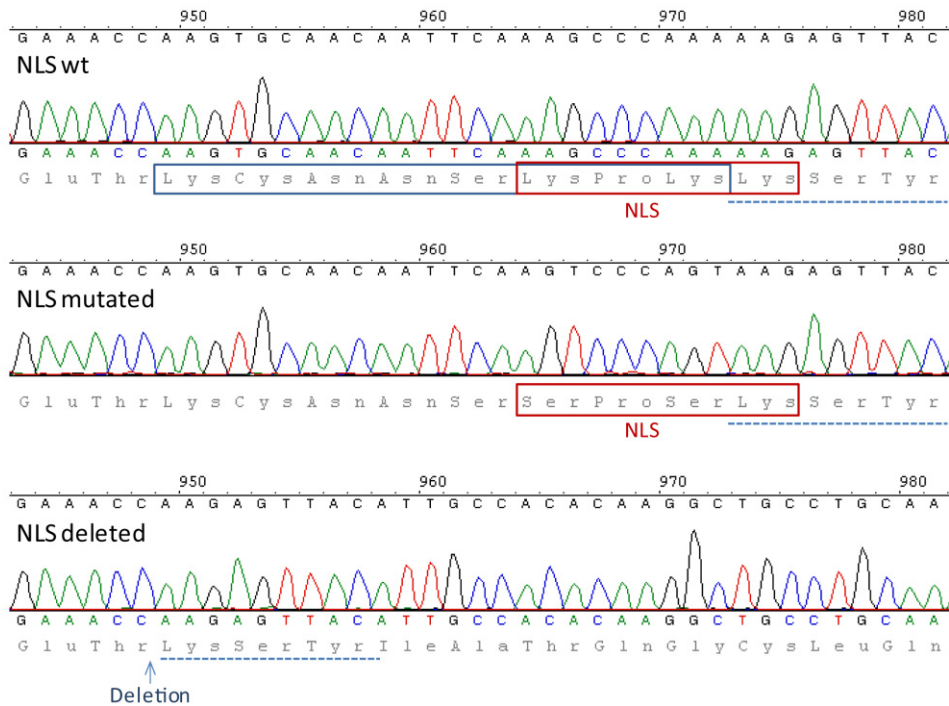
Figure 32. Mutation and deletion of the NLS in pLKO-TREX-SHP2-HA

(A) Schematic overview of the mutations introduced in the phosphatase domain of SHP2 by site directed mutagenesis.

(B) Pictures showing the chromatographic results of the direct sequencing of SHP2 around amino acids 322-325. Top: wild-type (wt) SHP2 sequence. Middle: SHP2 NLS mutated sequence. The nucleotide 965A was changed to G resulting in an amino acid change from Lys322 to Ser. In addition, the nucleotide 971A was changed to G altering the amino acid Lys324 to Ser. Bottom: SHP2 NLS deleted sequence. The 7 amino acids 317-324, indicated in blue in the wt sequence on top, were deleted shifting amino acid Lys325 of the original sequence to position 317 in the mutated sequence (blue dashed underlined).

To investigate the effect of this potential pat4 NLS, we attempted to rescue a dox inducible knockdown of endogenous SHP2 with constructs expressing either HA-tagged wild-type SHP2 with an intact NLS sequence (wt) or HA-tagged SHP2 NLS deleted (del) or SHP2 NLS mutated (mut), respectively (**Figure 33A**). First, cell lines were stably infected with a dox-inducible shRNA construct SHP2 miR2 targeting SHP2 or a control miR. Addition of dox to the cell cultures for 5-7 days led to the knockdown of endogenous SHP2 in the cells infected with SHP2 miR2 as shown for SUM159, SUM1315, and MCF10A HER2/3 cells (**Figure 33B**). These SHP2 miR2 expressing cells were then stably infected with dox inducible HA-tagged SHP2 NLS wt, mut or del and selected with Neomycin. Hence, upon addition of dox, endogenous SHP2 was knocked down and HA-tagged SHP2 NLS variants were expressed as shown by immunoblotting using anti-HA antibodies (**Figure 33C**). To test whether the NLS is indeed functional and required for SHP2 import into the nucleus, we performed subcellular fractionations of the dox induced cells expressing either SHP2 NLS wt, del or mut followed by immunoblotting using anti-HA antibodies. As before, tubulin α was used to ensure the purity of the cytoplasmic fraction and PARP was used as a nuclear marker. Whereas HA-tagged SHP2 was detectable in the cytoplasmic and nuclear fraction for cells infected with SHP2 NLS wt, deletion or mutation of the NLS prevented nuclear import of SHP2 as shown by the absence of SHP2 in the nuclear fraction (**Figure 33D**). We could therefore show that the identified NLS Lys-Pro-Lys-Lys at amino acid 322 of SHP2 targets SHP2 into the nucleus.
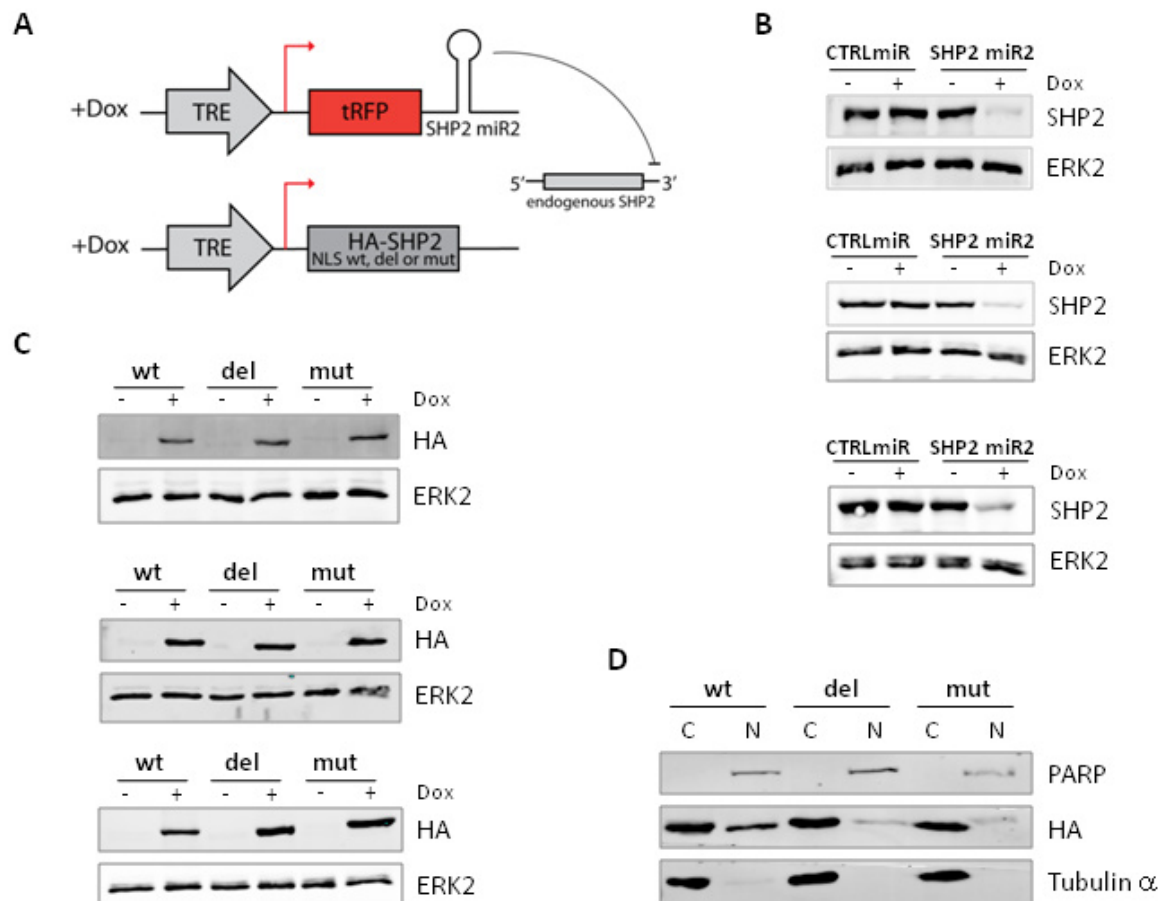
Figure 33. Nuclear import of SHP2 requires a pat4 NLS
(A) Schematic drawing of the constructs used to simultaneously knockdown endogenous SHP2 using a small hairpin RNA and to express HA-tagged SHP2 with either the wild-type NLS sequence (wt), a mutated NLS sequence (mut) or a deleted NLS sequence (del) upon addition of dox.
(B) Immunoblots of lysates from SUM159 (top), SUM1315 (middle), and MCF10A HER2/3 cells (bottom) infected with dox inducible CTRL miR or miR2 targeting SHP2. Addition of dox for 5-7 days induced knockdown of endogenous SHP2.
(C) Immunoblots of lysates from SUM159 (top), SUM1315 (middle), and MCF10A HER2/3 cells (bottom) expressing SHP2 miR2 and HA-tagged SHP2 NLS wt, SHP2 NLS del or SHP2 NLS mut upon addition of dox as shown by probing with anti-HA antibodies.
(D) Immunoblot of lysates from a subcellular fractionation of SUM159 cells showing that cells expressing HA-tagged SHP2 NLS del or NLS mut have no SHP2 in the nuclear fraction (N), whereas cells expressing HA-tagged SHP2 NLS wt have cytoplasmic (C) and nuclear (N) SHP2 as shown by anti-HA detection. PARP was used as a nuclear marker and tubulin α was used as a cytoplasmic marker.

Effects of nuclear SHP2 in vitro.

To address the function of nuclear SHP2, we tested the effects of depleting SHP2 from the nucleus on proliferation, colony formation and matrigel invasion in three-dimensional (3D) assays in vitro. We found that the absence of nuclear SHP2 had no effects the number of viable cells (**Figure 34A**). Next, the effect of the absence of nuclear SHP2 on colony formation was tested. We found that the absence of nuclear SHP2 increased the colony forming potential of SUM1315 cells expressing SHP2 NLS del or NLS mut significantly (**Figure 34B**).
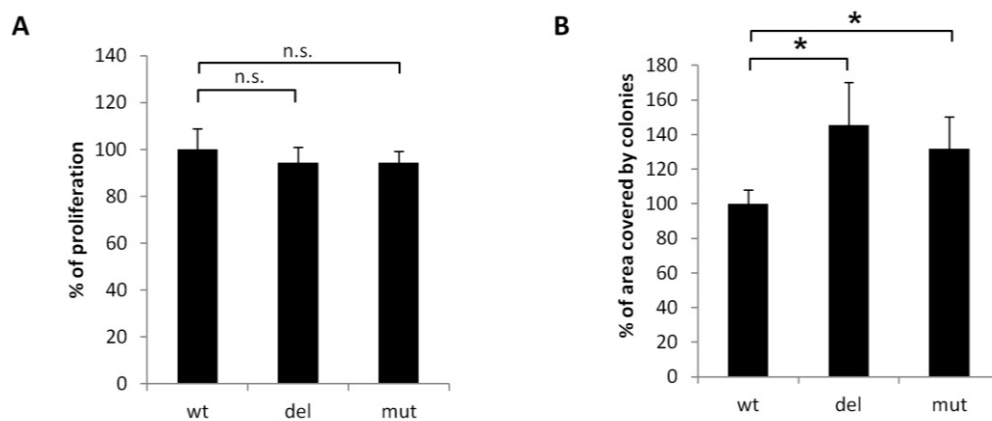
Figure 34. Effects of depletion of nuclear SHP2 in vitro
(A) Bar graphs showing that depletion of nuclear SHP2 did not affect cell numbers. 2,000 SUM1315 cells were plated in triplicates in 96-well plates and incubated for 5 days. Cell numbers were measured by WST-1 colorimetric assay. Results normalized to the NLS wt control are shown in means ± SEM (n=3). n.s. = not significant.
(B) Bar graphs showing the relative colony area. 2,000 SUM1315 cells were plated in 6-well plates for 14 days. Then, the colonies were fixed, stained with Crystal violet and the area covered by the colonies was analyzed using ImageJ software. Results are means ± SEM normalized to the wt control that was set to 100% (n=3). *P < 0.005 calculated by Student's t test.

Next, we assessed the invasive potential of cells lacking nuclear SHP2 using a 3D matrigel invasion assay. We first validated the morphological changes upon removal of SHP2 in the three cell lines. For MCF10A HER2/3 cells, we have previously shown that knockdown of SHP2 decreased the percentage of HER2/3-evoked invasive structures in MCF10A HER2/3 cells (Aceto, Sausgruber et al. 2012). A similar decrease in invasive

structures was observed in SUM1315 and, to a lesser extent, in SUM159 cells (**Figure 35A and B,** first 2 columns/bars). We then expressed pLKO-TREX-SHP2-HA NLS wt, NLS del or NLS mut in cells lacking SHP2. The reduction of invasive structures caused by SHP2 knockdown was rescued by all SHP2 constructs. These results showed that nuclear SHP2 is not required for the invasive phenotype of MCF10A HER2/3, SUM159 or SUM1315 cells in 3D cultures (**Figure 35A and B,** columns/bars 3-5).
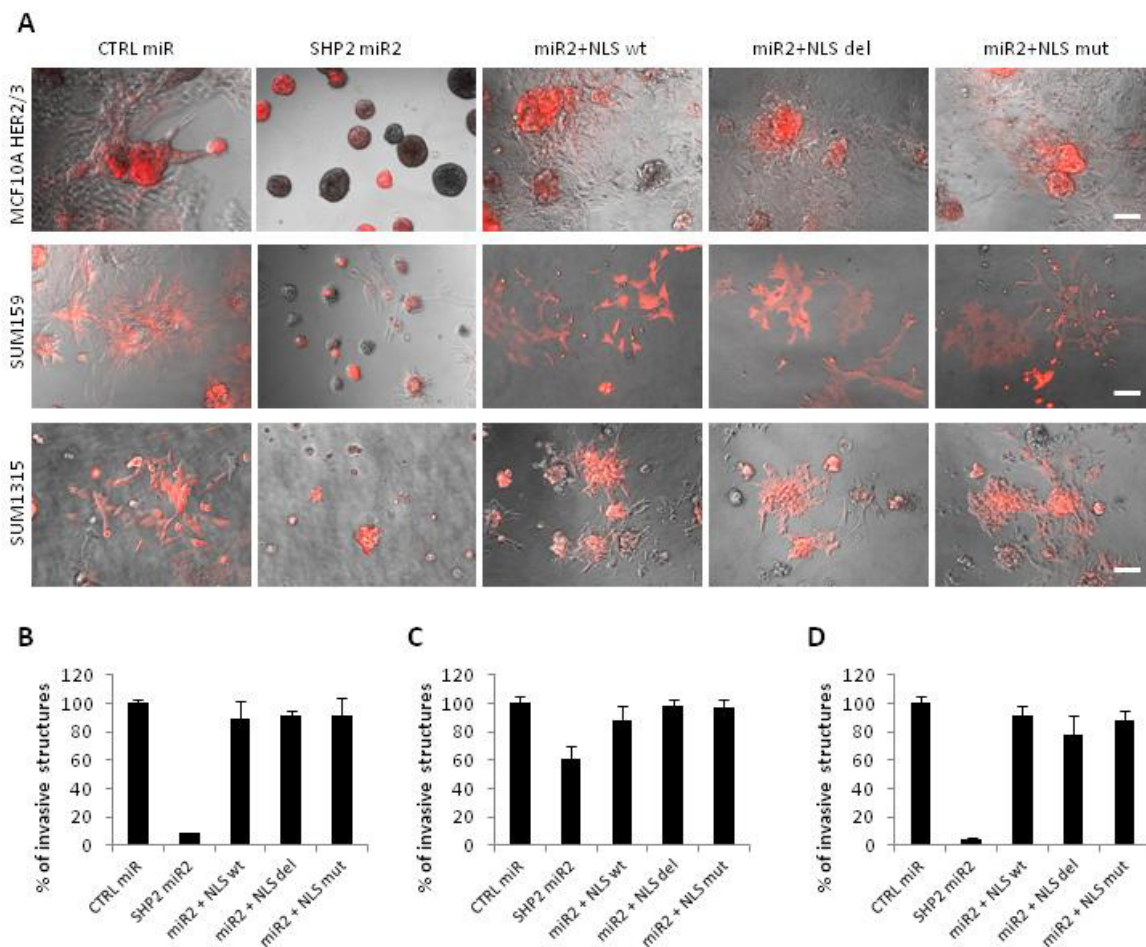
Figure 35 Nuclear SHP2 is not required for invasive behavior in 3D matrigel cultures
(A) Knockdown of endogenous SHP2 led to a decrease of invasive structures which could be rescued by all NLS constructs. Representative phase contrast images of MCF10A HER2/3 (top), SUM159 (middle), and SUM1315 cells (bottom) grown in 3D cultures expressing CTRL miR or SHP2 miR2, or SHP2 miR2 and SHP2 NLS wt, del or mut constructs as indicated. Scale bars represent 50 μm.
(B-D) Bar graphs showing the percentage of invasive structures. The invasive phenotype of MCF10A HER2/3 (B), SUM159 (C), and SUM1315 cells (D) lacking endogenous SHP2 could be rescued by expression of SHP2 NLS wt, del or mut. Results are shown in means ± SEM.

Effects of nuclear SHP2 in vivo.

To address the effects of nuclear SHP2 in vivo, we injected SUM1315 cells expressing dox-inducible SHP2 miR2 and dox-inducible HA-tagged SHP2 NLS wt, mut or del in the mammary fat pad of immunodeficient mice (**Figure 36A**). Inducing the knockdown of endogenous SHP2 and the expression of the different rescue constructs by dox food, we found that SUM1315 cells with only cytoplasmic SHP2 expressing the pLKO-TREX-SHP2-HA NLS mutated construct formed significantly bigger tumors than cells expressing SHP2 NLS wt (located in cytoplasm and nucleus). No significant increase of tumor volume was found for NLS deleted xenografts (**Figure 36B**). The increased tumor volume for mice with NLS mutated xenografts was not caused by a higher overall expression of the rescue construct as checked by immunoblotting for the HA-tag (**Figure 36C**).
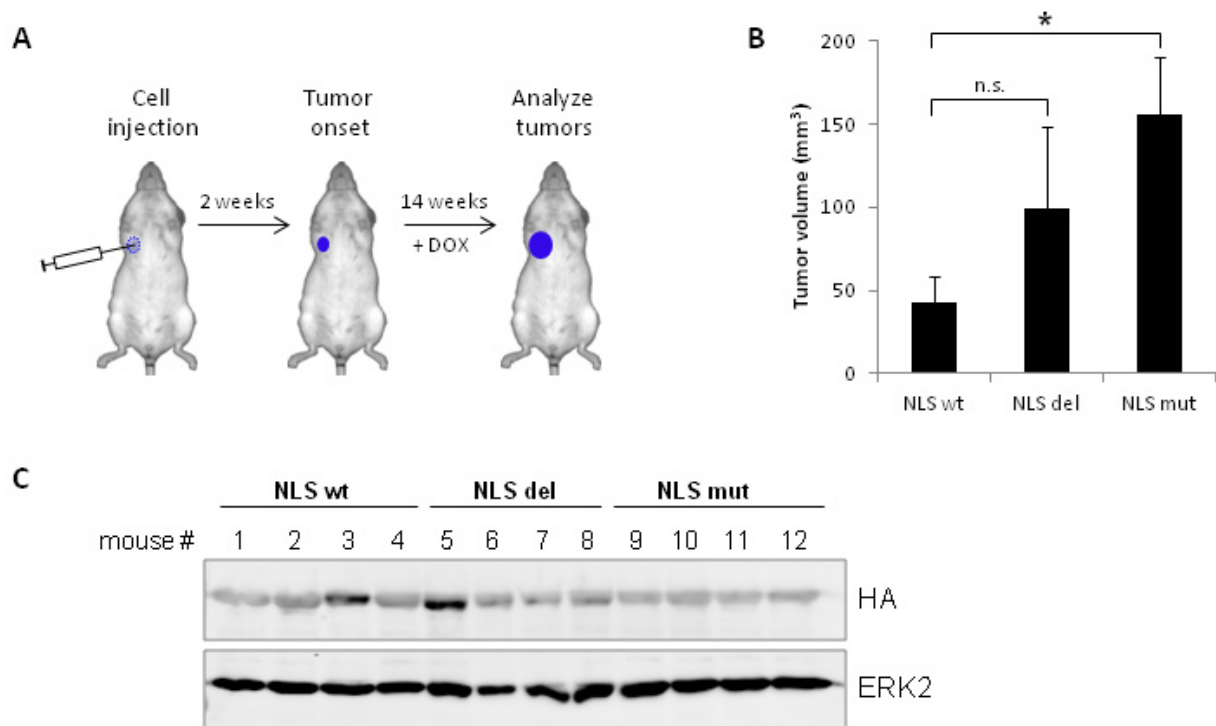
Figure 36. Effects of depletion of nuclear SHP2 in vivo
(A) Schematic overview of the in vivo experiment. 3×10^6 SUM1315 cells were injected in gland 2/3 of female NOD-SCID mice. Upon tumor onset, mice were fed with dox food to induce knockdown of endogenous SHP2 and expression of the different HA-tagged rescue constructs. 16 weeks after injection, the mice were sacrificed and tumors were dissected.

(B) Bar graph showing the tumor volumes. After dissection, the tumors were measured and the tumor volumes were calculated by the formula V = (a*b^2)/2 where a is the length and b is the width of the tumor. Means ± SEM are shown (n=6 per group). *P < 0.05 by Student`s t test. n.s. = significant.

(C) Representative immunoblot showing the expression level of the different rescue constructs in lysates from tumors. Equal expression of the HA-tagged rescue constructs among the different cohorts of mice was checked by immunoblotting of tumor lysates with anti-HA antibodies. ERK2 was used as a loading control.

Microarray analysis.

We then addressed the consequences of preventing nuclear import of SHP2 on gene expression by microarray analysis on these tumors. Gene expression in tumors from three animals per group was analyzed. The animals were selected on the basis of having the same level of rescue construct expression as checked by blotting against the HA-tag (**Figure 36C**). We found 15 genes that were commonly upregulated between tumors lacking nuclear SHP2 (NLS deleted and NLS mutated) when compared to tumors with nuclear and cytoplasmic SHP2 (NLS wt), while 44 genes were commonly downregulated between NLS mutated and NLS deleted when compared to NLS wt tumors (**Figure 37A and B**). Further in depth analysis will be required to understand the molecular effects of preventing nuclear import of SHP2.
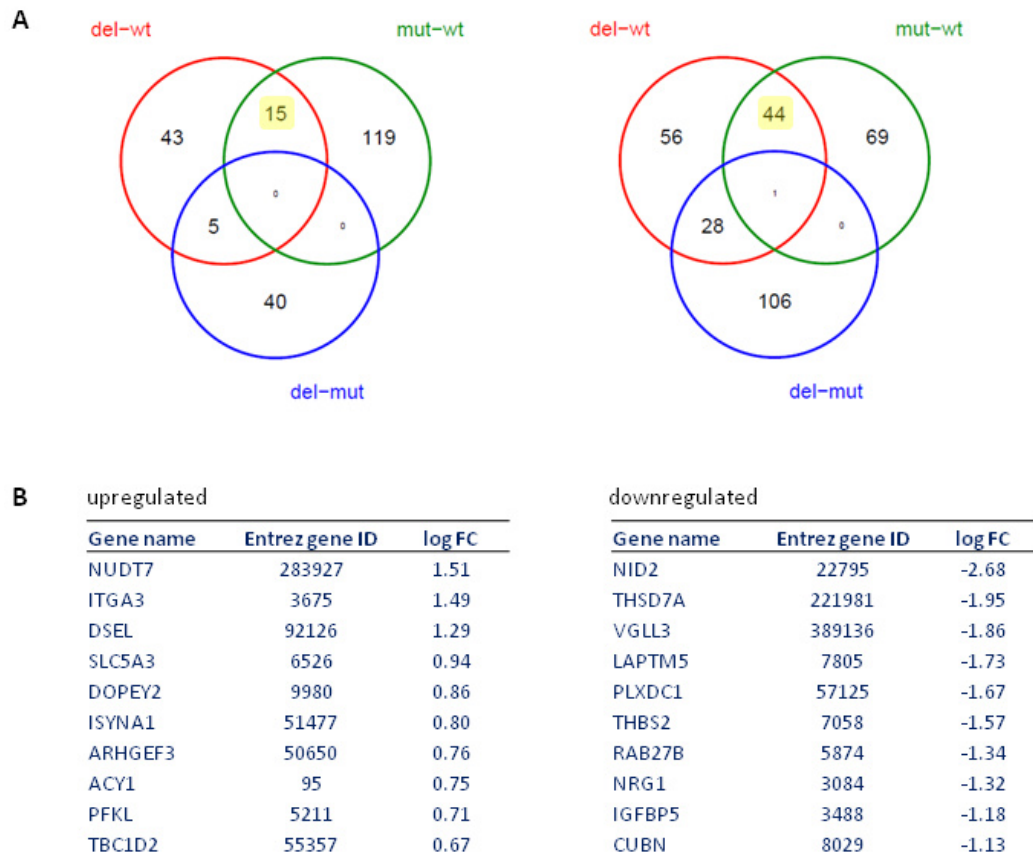
Figure 37. Microarray analysis of tumors from NLS wt, mut, and del animals
Gene expression of three SUM1315 xenografts per group (NLS wt mouse # 1, 2, and 4, NLS del mouse # 6, 7, and 8 and NLS mut mouse # 9, 10, and 11) was analyzed by microarray.
(A) Venn diagrams showing the number of genes that were differentially expressed between the different experimental groups. 15 genes were found to be commonly upregulated in tumors lacking nuclear SHP2 (NLS del and NLS mut) when compared to the control NLS wt (left) and 44 genes were found to be downregulated (right).
(B) List of the 20 most up- or downregulated genes between the NLS del and NLS mut tumors when compared to NLS wt tumors. The top 10 upregulated genes and their fold changes (FCs) are shown on the left and the top 10 downregulated genes their FCs are shown on the right.

Investigation of nuclear substrates of SHP2 by SILAC proteomics.

The physiological substrates of PTPs in the nucleus remain poorly defined, but they are important to understand the molecular mechanism of action of PTPs. Valuable tools to identify these substrates are substrate trapping mutants (Flint, Tiganis et al. 1997). These PTP mutants do not possess any catalytic activity and therefore bind tightly to their

tyrosine phosphorylated substrates. Hence, they can be used as tools to pull down their respective substrates from heterogeneous extracts. We used quantitative Stable Isotope Labeling by Amino acids in Cell culture (SILAC) proteomics in combination with substrate trapping mutants as an unbiased way to identify physiological substrates.

We used a dox inducible system to knockdown endogenous SHP2. At the same time, we stably expressed dox-inducible HA-tagged SHP2 rescue constructs, either expressing the wild-type SHP2 sequence (wt) or a SHP2 double trapping mutant (trap) (**Figure 38A-C**). The double trapping mutant we used was previously described by Agazie and colleagues (Agazie and Hayman 2003) and contains two mutations compared to the wt SHP2 sequence. The Aspartic acid at position 425 was changed to Alanine and the Cysteine 459 at the catalytic site was changed to Serine rendering the phosphatase catalytically dead.
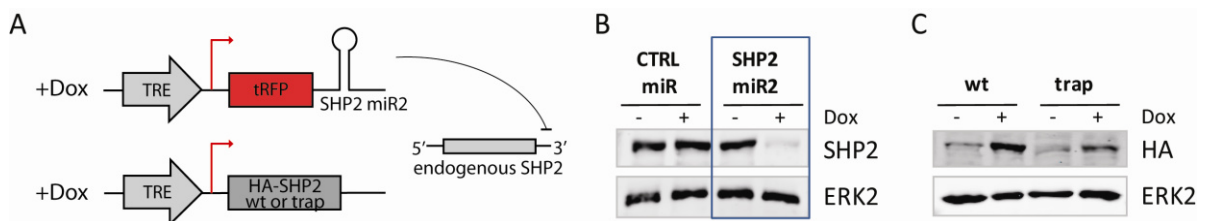
Figure 38. Cell lines used for SILAC experiments
(A) Schematic drawing of the constructs used. A small hairpin RNA SHP2 miR2 was used to knockdown endogenous SHP2 upon addition of dox. Dox also led to the expression of HA-tagged SHP2 with either the wild-type sequence (wt) or a double trapping mutant (trap) SHP2 with Asp425Ala+Cys459Ser mutations.
(B) Representative immunoblot of SUM159 cells expressing dox inducible CTRL miR or miR2 targeting SHP2. Addition of dox led to the knockdown of endogenous SHP2 as shown in the blue box. ERK2 was used as a loading control.
(C) Representative immunoblot of SUM159 cells expressing dox-inducible miR2 targeting endogenous SHP2 and dox-inducible HA-tagged SHP2 wt sequence or trapping mutant (trap). Expression of the rescue constructs is visualized by blotting with anti-HA antibodies and ERK2 was used as a loading control.

After ensuring the correct expression of all constructs, the cells were subjected to metabolic labeling by SILAC. A schematic overview of the quantitative SILAC MS procedure applied to detect differences in protein abundance between the SHP2 wt and SHP2 trapping mutant is given in **Figure 39A**.

SUM159 or MCF10A HER2/3 SHP2 knockdown cells expressing the HA-tagged wt SHP2 were cultured in normal (light) medium, whereas cells expressing the HA-tagged SHP2 trapping mutant construct were cultured in heavy SILAC medium (containing $^{13}C_6{}^{15}N_4$-Arginine and $^{13}C_6$-Lysine). Sufficient incorporation above 95% of the heavy amino acids was reached after 5-6 cell doublings as checked by mass spectrometry (data not shown). Upon successful labeling, the cells were either lysed as whole cell lysates (WCL) or separated into nuclear and cytosolic fractions, processed and the peptides were subjected to mass spectrometry analysis.

Validation of the IP efficiency in the cytosolic fraction, nuclear fraction and WCL showed good efficiency under the used conditions (**Figure 39B**). When separating the IP samples on 1D SDS gels, we detected many bands in each condition, each of them being one or more potential SHP2 substrates (**Figure 39C**). To verify the presence of SHP2 in each fraction, the bands around the molecular weight of SHP2 were excised and checked with mass spectrometry. This analysis confirmed the presence of SHP2 in the cytosolic and nuclear fraction of wt and trapping mutant cells (**Figure 39D**).
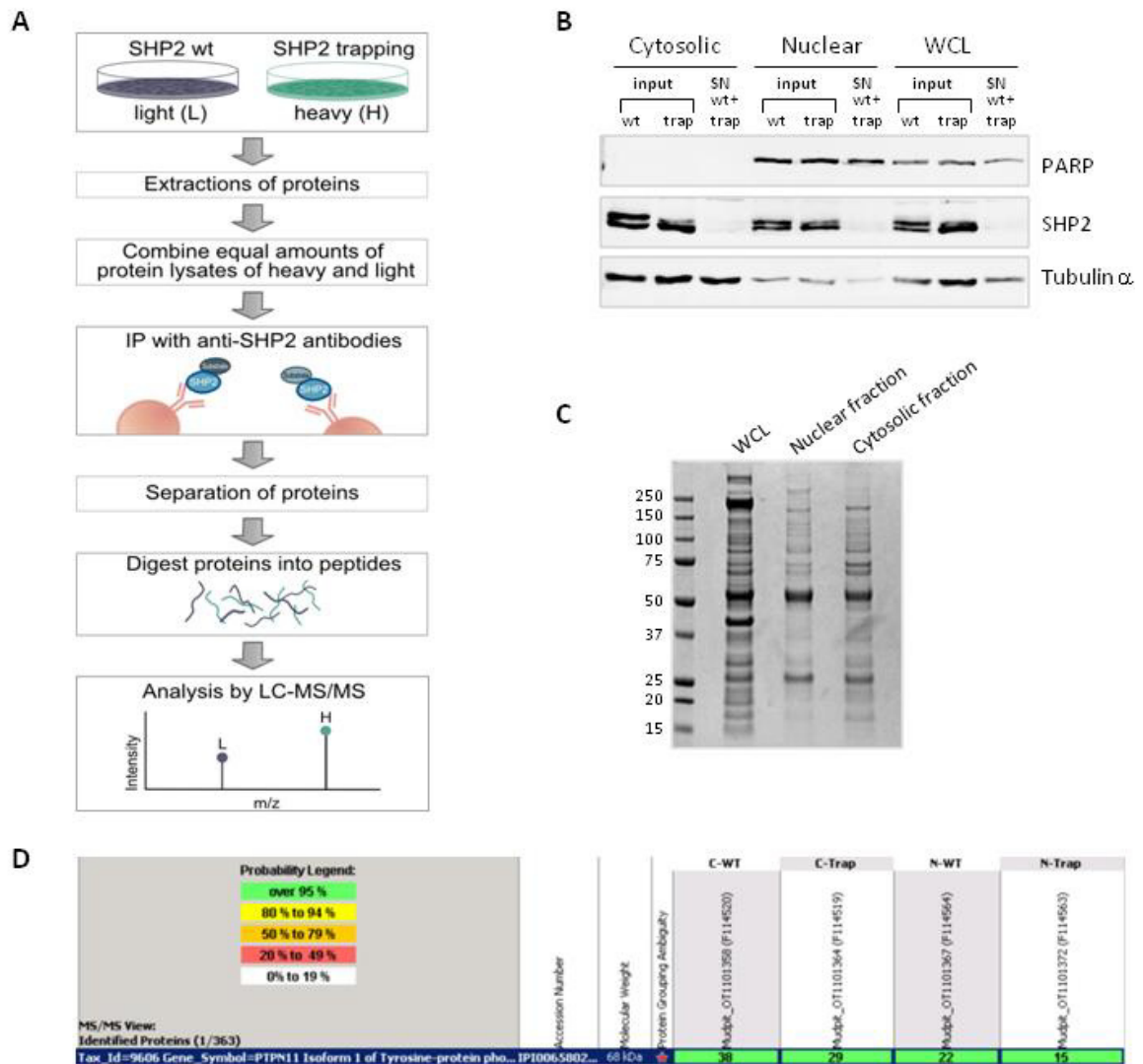
Figure 39. SILAC experiment with SUM159 cells

(A) Schematic overview of the SILAC workflow. Cells were grown for 12 days in heavy (H) $^{13}C_6{}^{15}N_4$-Arginine and $^{13}C_6$-Lysine containing or light normal medium (L) before being harvested as WCL or being fractionated into cytosolic and nuclear lysates. Equal amounts of protein of heavy and light fraction were mixed, immunoprecipitated with anti-SHP2 antibodies and loaded onto a 1D SDS PAGE gel followed by O/N in gel tryptic digest. Purified peptides were analyzed by mass spectrometry, and the log2 ratios between the abundance in the heavy labeled condition over the not labeled condition grown in light medium was calculated for each protein identified (log2 ratios H/L).

(B) Picture of a control immunoblot of the SUM159 samples before the anti-SHP2 IP (input) and after the IP (supernatants, SN). Shown are the cytosolic fraction, the nuclear fraction and the whole cell lysates (WCL) for wt SHP2 cells (wt) and cells expressing the trapping mutant (trap). While SHP2 is detected in all input fractions, no SHP2 signal is detected in the combined supernatant fractions (SN) showing a good efficiency of the IP. PARP is used as a nuclear marker and tubulin α is used as a cytoplasmic marker.

(C) Picture of a Coomassie blue stained 1D SDS PAGE gel showing the IP samples of cytoplasmic and nuclear fraction and WCL before trypsin digest. Each band denotes one or more potential SHP2 substrates.

(D) Identification of SHP2 by mass spectrometry in all fractions. Visualization of SHP2 peptides identified by Scaffold software analysis of the mass spectrometry data. Cytosolic and nuclear fractions of cells expressing wt SHP2 (C-WT and N-WT respectively) or trapping mutant SHP2 (C-Trap and N-Trap respectively) were analyzed. SHP2 was identified in all fractions and the number of peptides corresponding to SHP2 identified in each fraction is shown in green, indicating that the probability of correct identification is above 95%.

The quantitative mass spectrometry experiment led to the identification of several known (such as GAB1, EGFR, and HER2 in MCF10A HER2/3 cells, STAT1 in SUM159 cells and PZR and MVP in both cell lines) as well as several novel putative SHP2 substrates.

One interesting putative substrate that we found in the nuclear and WCL fraction is nucleolin. This multifunctional RNA-binding protein is mainly located in the nucleolus but also found in other nuclear regions as well as in the cytoplasm and at the plasma membrane (Borer, Lehner et al. 1989, Tuteja and Tuteja 1998, Ginisty, Sicard et al. 1999). Mammalian nucleolin has a predicted molecular mass of 77 kDa, however, because of highly phosphorylated residues in the N-terminal domain, the apparent mass is 100-110 kDa (Bicknell, Brooks et al. 2005). With several predicted phospho tyrosine sites, nucleolin could therefore well be a SHP2 substrate (www.phosphosite.org, **Figure 40A**). We validated the interaction between SHP2 and nucleolin by co-immunoprecipitation experiments. Using SUM159 cells expressing the SHP2 trapping mutant, we could show the interaction between SHP2 and nucleolin by co-IP with anti-nucleolin antibodies followed by immunoblotting for SHP2, as well as by co-IP with anti-SHP2 antibodies followed by immunoblotting for nucleolin (**Figure 40B**).
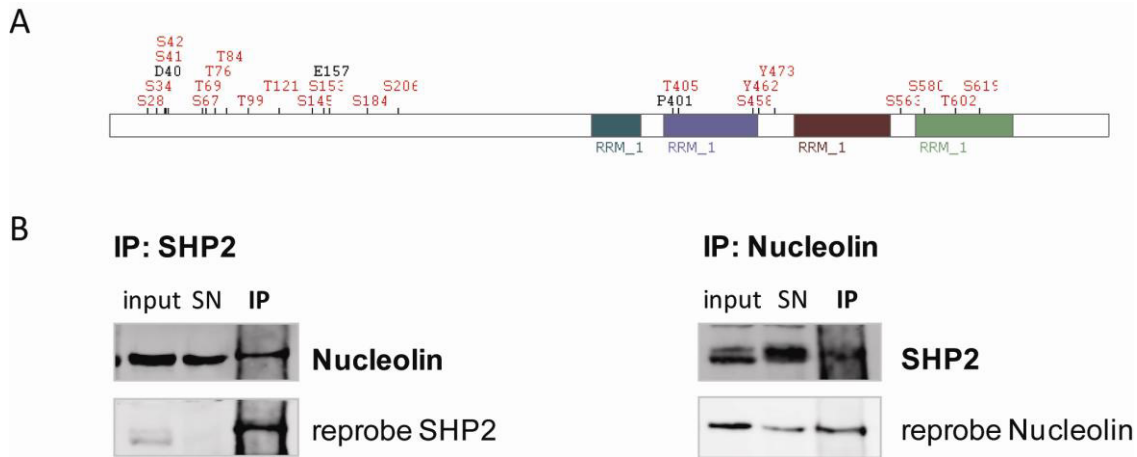
Figure 40. Nucleolin is a putative substrate of SHP2
(A) Schematic drawing of nucleolin sequence showing several tyrosine residues (www.phosphosite.org).
(B) Picture of co-immunoprecipitations between SHP2 and nucleolin. Co-IPs were carried out using lysates from SUM159 cells expressing the D425A+C459S SHP2 trapping mutant. Lysates were immunoprecipitated using polyclonal anti-SHP2 antibodies and then immunoblotted using anti-nucleolin antibodies (left) or vice versa using anti-nucleolin antibodies for IP followed by immunoblotting with anti-SHP2 antibodies (right). In addition to the IP fraction, input (before IP) and supernatant (SN, after IP) were loaded as controls. The SHP2 IP was reprobed with anti-SHP2 antibodies and the nucleolin IP was reprobed with anti-nucleolin antibodies to check the IP efficiencies.

Other putative substrates found in both cell lines included the Heat shock protein HSP90-beta encoded by the HSP90AB1 gene and the alpha2 subunit of the Guanine nucleotide-binding protein G(i) (Gαi2) encoded by the GNAI2 gene. We could, however, not confirm the interaction between SHP2 and HSP90 using co-immunoprecipitation. The IPs and antibodies worked, but SHP2 was not co-immunoprecipitated in the anti-HSP90 IP and vice versa HSP90 was not co-immunoprecipitated in the anti-SHP2 IP under the conditions used. Gαi2 belongs to the Gi family of α subunits that consists of the three members Gαi1-3 (Wiege, Ali et al. 2013). Despite several attempts trying different commercially available antibodies and IP conditions, we could not find an antibody

detecting a specific band for Gαi2. Therefore, we could not validate the interaction due to technical difficulties.

Chromatin immunoprecipitation.

We identified the silencing of several members of the HOX gene family in the absence of SHP2 as part of the "SHP2 signature" found by microarray analysis (Aceto, Sausgruber et al. 2012), suggesting a potential nuclear role of SHP2 in epigenetic regulation.

In eukaryotic cells, chromosomal DNA is wrapped into nucleosomes around histone octamers, containing two copies each of histone H2A, H2B, H3, and H4 (Kornberg 1977). Nucleosomes are then folded into chromatin fibers. Transcriptional regulation in eukaryotes is very complex and depends on RNA polymerases, transcription factors and co-regulators controlling their activity. Among these regulators, many proteins and enzymes modulating the chromatin by epigenetic mechanisms such as histone modifications or DNA methylation are found (Conaway 2012).

To explore a possible function of SHP2 in these regulatory processes, we used chromatin immunoprecipitation followed by high-throughput sequencing (ChIP-seq). Chromatin immunoprecipitation (ChIP) is a method used to study the interaction between a protein of interest and a specific region of genomic DNA (Carey, Peterson et al. 2009). ChIP-seq profiling was chosen because of its high signal-to-noise ratio, genome coverage and good spatial accuracy (Park 2009). To process the ChIP-seq data, the reads are aligned to the genome, followed by an evaluation of the read density pattern, which can be done by computational methods. Regions with statistically significant enrichment of reads aligned to the genome, indicate the binding of the protein of interest to this regions (Day, Luquette et al. 2010).

First, we tested whether SHP2 is found in the chromatin enriched fraction. During subcellular fractionations, the cells are divided into a cytoplasmic (C) and nuclear (N) fractions. The nuclear fraction can further be subdivided into a soluble part (N1) and a pellet, which is the chromatin enriched fraction N2 (Shiio, Eisenman et al. 2003, Liu and Fagotto 2011). We fractioned SUM159 and SUM1315 into cytoplasmic, nuclear and chromatin-enriched fractions and found SHP2 not only in the nuclear fraction N1, but also in the chromatin enriched fraction N2. SHP2 was further found in the chromatin-enriched fraction of MCF10A HER2/3, BT474 and MDA-MB-231 cells (**Figure 41A**). The histone mark H3K4me2 was used as a marker for the chromatin-enriched fraction.
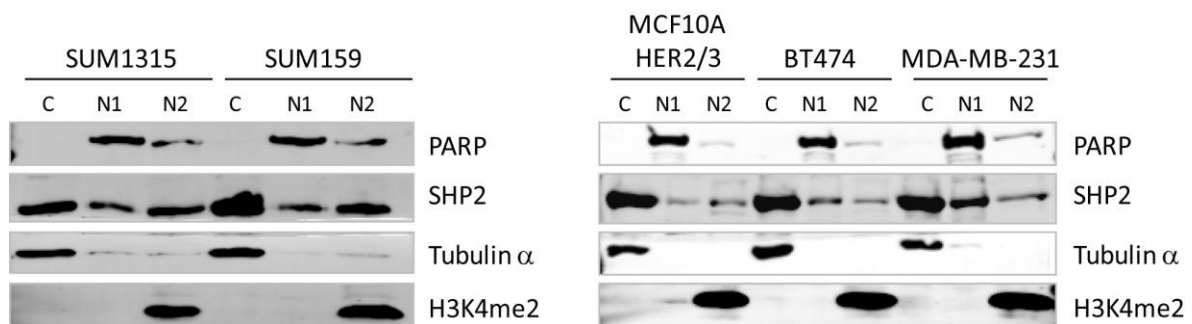
Figure 41. SHP2 is found in the chromatin enriched fraction N2
Immunoblots of lysates from subcellular fractionations of SUM1315, SUM159, MCF10A HER2/3, BT474, and MDA-MB-231 cells into cytoplasmic (C), nuclear (N1) and chromatin enriched fractions (N2). Tubulin α was used as a marker for the cytoplasmic fraction, PARP for the N1 fraction, and the chromatin mark H3K4me2 was used as a marker for the chromatin enriched fraction.

For the ChIP-seq experiment, the genomic DNA and interacting proteins were crosslinked. Afterwards, the DNA strands were fragmented by sonication followed by an IP of the target protein SHP2. Following the IP pulling down all DNA fragments linked to SHP2, the DNA was de-cross linked, purified, and sequenced by deep-sequencing and the reads were mapped against the genome (**Figure 42A**).

Due to a lack of a commercially available ChIP grade anti-SHP2 antibody, we first validated the specificity of the SHP2 antibody for ChIP application. We detected a specific band for SHP2 that markedly decreased in SHP2 knockdown cells (**Figure 42B and C**).
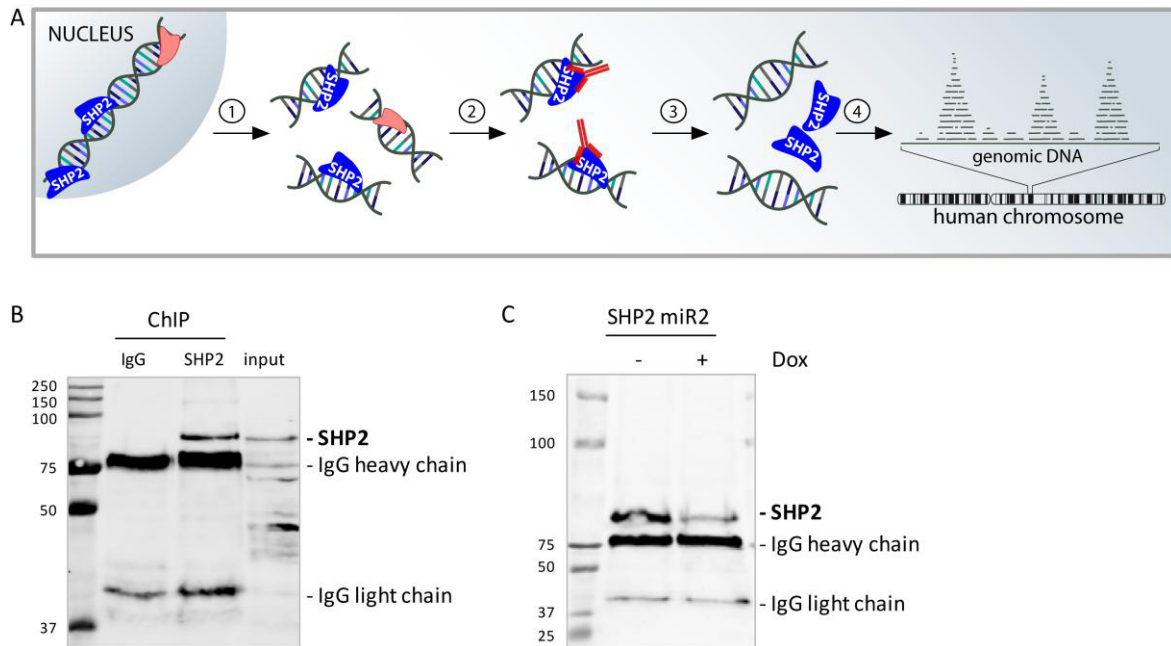
Figure 42. ChIP with anti-SHP2 antibodies
(A) Schematic overview of the ChIP-seq experiment. 1) After crosslinking DNA and proteins in the nucleus, the DNA was fragmented into 300 bp pieces by sonication. 2) Next, DNA fragments bound to the protein of interest (SHP2) were isolated by co-immunoprecipitation with SHP2. 3) De-crosslinking to remove the proteins from the DNA and DNA purification, 4) Sequencing of the isolated DNA fragments were sequenced and mapping of the reads to the genome.
(B) Immunoblot of lysates from a ChIP experiment of SUM159 cell lysate showing a specific band for SHP2 in the SHP2 ChIP that is absent in the IgG control. Whole cell lysate was used as a positive control (input).
(C) Immunoblot of lysates from a anti-SHP2 ChIP of SUM159 cells expressing the dox-inducible miR2 targeting SHP2 in absence (-) or presence (+) of dox. The decrease of the SHP2 band in the SHP2 knockdown cells (+ dox) confirmed the specificity of the SHP2 antibody under the experimental conditions used.

After establishing the ChIP conditions for cells grown in 2D, we performed a ChIP experiment in SUM159 and SUM1315 cells followed by deep sequencing. Preparation of the DNA libraries was successful, as indicated by single peaks at the expected size (**Figure**

43A), and the samples were sequenced. The high-throughput sequencing was also successful, however, a poor signal-to-noise ratio made computational analysis of the data impossible. Nevertheless, manual analysis revealed several promising peaks which could not be explained by abundant repetitive elements (**Figure 43B**).
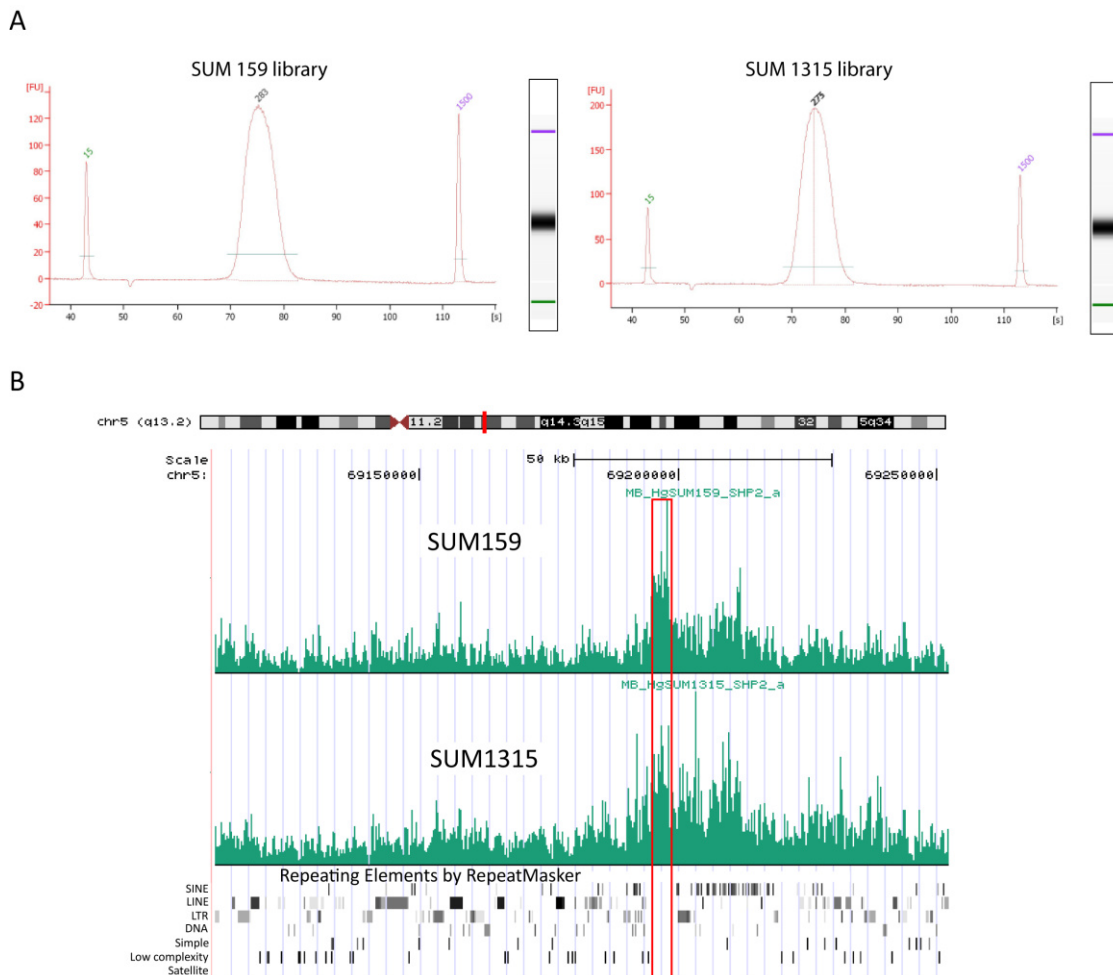
Figure 43. ChIP-seq analysis of DNA regions purified by SHP2 immunoprecipitation
(A) ChIP-seq library preparation. Snapshots of Agilent bioanalyzer quality control files are shown. After repairing the ends of the ChIP fragments, adding an A to the 3`ends and ligating the adapters, DNA fragments were selected for a size of 300 bp.
(B) Examples of University of California Santa Cruz (UCSC) genome browser snapshots with an example of a peak identified on chromosome 5 found in SUM159 (top) and SUM1315 cells (bottom) by anti-SHP2 IP mapped to the genome. The y-axis depicts the peak amplitude and the x-axis shows the position of each peak on the genome. The RepeatMasker function identifies repetitive DNA elements such as short interspersed nuclear elements (SINEs) and long interspersed nuclear elements (LINEs), which can cause accumulations of reads. The red box indicates a manually identified peak on chromosome 5 that was found in both cells lines at a position devoid of repetitive elements.

Therefore, the next step was to design real-time PCR primers to amplify the region under the manually identified peaks and also for areas with no peaks as negative controls. Quantitative real-time PCR using these primers on input chromatin and ChIP fraction would allow calculating the fold-enrichment after ChIP giving means to improve the IP conditions. However, the signal for the designed real-time PCR primers was below threshold level for input and ChIP samples.

6.3   DISCUSSION

Nuclear localization and nuclear import of SHP2.

An increasing number of non-cytoplasmic functions for the phosphatase SHP2 were reported over the recent years in several cell lines, but only in one HER2-positive breast cancer cell line (Chughtai, Schimchowitsch et al. 2002). For the first time, we could demonstrate the presence of nuclear SHP2 in a panel of breast cancer cell lines including other subtypes such as triple-negative breast cancer. We examined the nuclear localization with different methods. First, we used subcellular fractionations followed by immunoblotting, second we used immunofluorescence techniques, and third we detected SHP2 in the nuclear fraction by mass spectrometry. In summary, we showed that SHP2 is found in the nucleus in several breast cancer cell lines. The amount of nuclear SHP2 in breast cancer cell lines was similar to what was previously reported for fibroblasts (Yuan, Yu et al. 2003).

We further described a novel mechanism of nuclear import for SHP2 by a pat4 nuclear localization sequence (NLS). Most of the reports describing nuclear functions of SHP2, did not comment on the mechanism of nuclear import. One study identified a half-bipartite nuclear localization sequence within the carboxyl-terminal distal region of SHP1, but could not identify a NLS in the SHP2 sequence (Craggs and Kellie 2001). Chughtai and colleagues suggested STAT5a to act as a carrier to translocate SHP2 into the nucleus upon prolactin stimulation (Chughtai, Schimchowitsch et al. 2002). Other reports showing nuclear localization of the phosphatase did not comment on how SHP2 passes the nuclear pore complex to enter the nucleus (Jakob, Schroeder et al. 2008, Takahashi, Tsutsumi et al. 2011).

What is the function of nuclear SHP2 in breast cancer?

Using several in vitro assays, we tested the effects of cytoplasmic and nuclear versus only cytoplasmic SHP2. We did not find effects on the number of viable cells, but found increased colony formation capacity in absence of nuclear SHP2. We further found that nuclear SHP2 was dispensable for invasion in vitro. Testing the effects of depleting nuclear SHP2 in vivo, we found an increased tumor volume for xenografts of cells expressing the NLS mutated construct, but only a not significant trend for the NLS deleted construct. To assure that the bigger tumors in the NLS mutated and NLS deleted conditions were not the result of a higher overall SHP2 expression, we compared the expression levels in the tumors by anti-HA immunoblotting. This analysis revealed an even expression of SHP2 in all groups. Therefore, one could argue that the increased tumor growth is in fact the result of expression of only cytoplasmic SHP2. This would suggest, that a higher amount of SHP2 in the cytoplasm leads to more oncogenic signaling and hence more tumor growth. Following this line of thoughts, one can speculate that SHP2 translocation to the nucleus might have less of a functional role, but rather could be considered as a regulatory mechanism to stop from SHP2 signaling in the cytoplasm.

However, to test this hypothesis and confirm these results, we will repeat the in vivo experiment. It would also be advisable to test the effect of depletion of nuclear SHP2 in a second model to make sure the effects observed are not cell line specific. Repeating this experiment will also help to elucidate, if there are differences between deleting and mutating the NLS.

As three-dimensional modeling of the SHP2 protein showed the importance of the fourth Lysine residue of the NLS for the tertiary folding structure of the protein, we did not change this residue when mutating or deleting the NLS. However, it could still be possible

that the mutation or deletion caused structural changes that might explain the different results with the two constructs.

We also analyzed the gene expression profiles of tumors from each experimental group by microarray and found genes commonly up- or downregulated in absence of nuclear SHP2 when compared to NLS wt tumors. Understanding these changes upon depletion of nuclear SHP2 will require further in depth analysis of the microarray data. Repeating the in vivo experiment and microarray analysis in a second model would further be helpful, to unravel more general and not cell line specific changes.

What are nuclear substrates of SHP2?

We used an unbiased approach combining metabolic labeling proteomics and a phosphatase substrate trapping mutant to discover novel nuclear substrates of SHP2. Using quantitative SILAC proteomics, we identified several known and also novel putative substrates including nucleolin.

Nucleolin levels have been shown to be significantly elevated in many cancer cells (Tominaga, Srikantan et al. 2011) and more recently, cell-surface expressed nucleolin has been linked to tumor cell growth and angiogenesis (Destouches, El Khoury et al. 2008, Di Segni, Farin et al. 2008, Reyes-Reyes and Akiyama 2008). We confirmed the interaction between nucleolin and SHP2 by co-IP experiments. The next steps to validate nucleolin as a true SHP2 substrate will be: 1) To show increased phosphorylation of nucleolin in SHP2 depleted cells, 2) to identify the tyrosine sites dephosphorylated by SHP2, and 3) to show that a tyrosine to phenylalanine mutant of the substrate (that cannot be phosphorylated by a PTK) can mimic the effects of SHP2. This mutant should rescue the downstream functions of SHP2 in SHP2-deficient cells.

Other putative SHP2 substrates we attempted to validate were HSP90-beta and Gαi2. Although both were detected to be bound by the SHP2 trapping mutant by mass spectrometry, we did not succeed to validate the interaction by co-IP. This could be attributed to limitations of the antibodies used, or the co-IP conditions might need further optimization such as cross-linking to detect low affinity or transient interactions. Alternatively, one could try a pull-down assay in which, in contrast to the co-IP, not the antibody but a bait protein of the interacting pair is immobilized. Another advantage of the pull-down assay is that the amount of bait protein can be increased above native level.

However, both putative substrates are very interesting and worth future investigation. The chaperon protein HSP90 is often overexpressed in human tumors and mediates the folding and stabilization of many proteins playing important roles in a variety of signal transduction pathways including oncogenic proteins such as HER2, AKT and c-Raf (Pratt 1998, Maloney and Workman 2002). Further, there are some interesting parallels between Gαi2 and SHP2 functions. Enhanced signaling through Gαi2 produced a Noonan Syndrome (NS) like phenotype (Huang, Fu et al. 2009) and 50% of NS cases are caused by germline missense gain-of-function mutations of the PTPN11 gene encoding SHP2 (Tartaglia, Mehler et al. 2001). Another parallel placing SHP2 and Gαi2 in the same pathway, was the finding of a tumor suppressive function of Gαi2 in hepatocellular carcinoma (Yao, Liang et al. 2010), the one single cancer type in which SHP2 was found to be a tumor suppressor (Bard-Chapeau, Li et al. 2011) while acting as an proto-oncogene in many other cancers studied to date (Chan, Kalaitzidis et al. 2008).

Is SHP2 involved in epigenetic regulation?

We also explored a possible involvement of SHP2 in epigenetic regulation. This hypothesis was based on our finding that several HOX family members were silenced in absence of SHP2 (Aceto, Sausgruber et al. 2012). We therefore attempted to address a potential direct or indirect role for SHP2 in chromatin remodeling.

Indeed, we could show that SHP2 is found in the chromatin enriched fraction of several breast cancer cell lines. We validated our SHP2 antibody as being suitable for ChIP, but were unable to test the fold enrichment of the IP fraction over the input fraction (lysates before IP), as there are no known targets of SHP2 to test for. Therefore, after establishing the conditions, we performed a "blind" ChIP experiment not knowing the fold enrichment, followed by high-throughput sequencing. The fold enrichment was not sufficient and resulted in to a poor signal-to-noise ratio that made computational analysis of the data impossible. Therefore, we manually screened the genome browser tracks for peaks apparent in both cell lines and which could not be explained by known repetitive structures in the genome. Sequencing the input of both cell lines would help to exclude noise and repeats specific to the cell lines used. Based on the manual analysis, we identified several promising peaks and designed real-time PCR primers to amplify these regions; however the primers designed did not give any detectable product in either input or ChIP fraction making it impossible to calculate the fold enrichment. Being able to calculate the fold enrichment would enable us to directly observe consequences of altering the experimental conditions such as cross-linking, salt concentrations or the antibody used. This would allow optimization before repeating the ChIP under the newly found conditions followed by deep sequencing. Other options worth exploring could be to test other antibodies or to perform ChIP against a tagged protein.

7   OUTLOOK

We found that SHP2 knockdown eradicated tumor initiating cells (TICs), blocked primary tumor growth and reduced migration, invasion, and metastasis. These observations suggest SHP2 as a potential drug target in breast cancer, particularly in HER2-positive and triple-negative breast cancer, the two preclinical models that we studied.

Our findings suggest that inhibition of SHP2 blocks tumor growth and metastatic spread. The effect of SHP2 on the primary tumor growth can be explained by the effects of SHP2 on TICs, which are thought to drive and sustain the tumor and have been implicated in the relapse of disease after successful initial treatment (Clevers 2011). The effect of SHP2 on metastasis can be explained as a consequence of depleting TICs, which have been also implicated in metastatic spread (Li, Tiede et al. 2007). Alternatively, this effect could be explained by blocking the migration and invasion of all tumor cells.

Our studies focused only on the effects of SHP2 depletion on the primary tumor and early stages of metastasis. It remains to be determined whether inhibition of SHP2 in already established metastases will be effective.

Further, it remains unknown whether SHP2 inhibition would be effective as monotherapy or if combination therapies would be needed. Because TIC fate represents a dynamic equilibrium, inhibition of TICs alone might not be successful, as non-stem cancer cells can transform into TICs (Iliopoulos, Hirsch et al. 2011). Therefore, the combination between SHP2 inhibition and agents targeting the bulk of the (non-stem) tumor cells might increase and sustain efficacy.

Resistance to targeted therapies often occurs within a few months, especially when used as a single therapy (Sellers 2011). Studies addressing the effects of prolonged SHP2 inhibition will be needed to investigate the potential resistance mechanisms that might

arise. It is conceivable that upon inhibition of SHP2, tumor cells might mutate the target and/or activate SHP2 downstream or bypass pathways. Functional genetic screens are warranted to address this question. These studies should allow the design of rational combination therapies.

8   MATERIALS and METHODS

8.1   Materials

8.1.1   General laboratory reagents

General laboratory chemicals such as ethanol, methanol, isopropanol, glycerol, HCl, sodium hydroxide, Tris-HCl and Triton X-100 were obtained from Merck and Sigma. Bovine serum albumin (BSA) was purchased from Sigma. Purified water, phosphate buffered saline (PBS), 1 x LB-media and 1 x 2YT were prepared by the FMI media preparation facility according to standard protocols.

8.1.2   DNA manipulation reagents

DNA restriction enzymes, DNA markers and DNA modifying enzymes such as T4 ligase and CIP were obtained from New England Biolabs. DNA purification Miniprep and Midiprep system were obtained from GENOMED and PCR purification kits were from QIAGEN. Taq Polymerase and dNTPs were from ROCHE. Agarose and SYBR Safe DNA stain as well as 100 bp and 1 kb ladders were obtained from Invitrogen.

8.1.3   Tissue culture reagents

Dulbecco's Modified Eagle Medium (DMEM), Roswell Park Memorial Institute (RPMI) 1640 medium and anti-antibiotic cocktail (100 IU/ml of penicillin and 100 µg/ml of streptomycin) were obtained from the FMI media preparation facility. DMEM/F12 medium (Cat#31330-038), 0.05% Trypsin-EDTA (Cat#25300-054), and Horse serum (Cat#16050-122) were from Invitrogen. HAM's F12 medium (Cat#N6658), Fetal Bovine Serum (FBS; Cat#F7524), Hydrocortisone (Cat#H0888), Cholera Toxin (Cat#C8052), Doxycyclin (Cat#D9891) and human Insulin (Cat#I5500) were obtained from SIGMA. Human EGF (Cat#100-15) was from Peprotech. PD184352 (Cat#CI-1040) was purchased from Biovision.

8.1.4 Antibodies

Table 1 Primary and secondary antibodies

Antigen	species	Cat #	company	dilution
Akt	rabbit	9272	Cell Signaling	WB 1:1000
ERK2 (C-14)	rabbit	sc-154	Santa Cruz	WB 1:1000
ERK2 (D-2)	mouse	sc-1647	Santa Cruz	WB 1:1000
H3K4me2	rabbit	9725	Cell Signaling	WB 1:1000
HA	mouse	MMS-101P	Covance	WB 1:500
HER2	mouse	OP15	Calbiochem	WB 1:1000
HER3	rabbit	sc-285	Santa Cruz	WB 1:100
N-Cadherin	mouse	610920	BD Biosciences	WB 1:5000
p42/44 Erk	rabbit	9102	Cell Signaling	WB 1:1000
pAkt S473	rabbit	9271	Cell Signaling	WB 1:1000
PARP	rabbit	9542	Cell Signaling	WB 1:1000
pFAK Y577	rabbit	3281	Cell Signaling	WB 1:1000
pPaxillin Y118	rabbit	2541	Cell Signaling	IF 1:50
pSrc Y416	rabbit	2101	Cell Signaling	WB 1:1000
pSrc Y530	rabbit	2105	Cell Signaling	WB 1:1000, IF 1:50
pTyr 4G10	mouse	05-321	Millipore	WB 1:1000
SHP2 (B-1)	mouse	sc-7384	Santa Cruz	WB 1:1000, IF 1:500
SHP2 (C-18)	rabbit	sc-280	Santa Cruz	WB 1:1000, IP 1 µg / 1000 µg
Src	rabbit	2109	Cell Signaling	WB 1:1000
Src	mouse	05-184	Millipore	IP 4 µg /1000 µg protein
Tubulin α	mouse	MS-581-P1	Neomarker	WB 1:10000
Secondary antibodies				
Alexa Fluor 488	mouse	A11029	Invitrogen	IF 1:200
Alexa Fluor 488	rabbit	A11034	Invitrogen	IF 1:200
Alexa Fluor 568	mouse	A21202	Invitrogen	IF 1:200
Alexa Fluor 568	rabbit	A10042	Invitrogen	IF 1:200
Alexa Fluor 633	mouse	A21136	Invitrogen	IF 1:200
Alexa Fluor 633	rabbit	A21071	Invitrogen	IF 1:200
Alexa Fluor 647	mouse	A31571	Invitrogen	IF 1:200
Alexa Fluor 647	rabbit	A21245	Invitrogen	IF 1:200
Alexa Fluor 680	mouse	A21058	Invitrogen	WB 1:10000, IF 1:200
Alexa Fluor 680	rabbit	A21076	Invitrogen	WB 1:10000
IRDye800	mouse	610-632-002	Rockland	WB 1:10000

IF: Immunofluorescence; IP: immunoprecipitation; WB: Immunoblot

8.1.5 Vector information

For the inducible shRNA studies, 97-mer shRNAmiR (miR) were obtained from Sigma, PCR-amplified, sequence-confirmed and cloned into the dox inducible lentiviral vector pINDUCER (Meerbrey, Hu et al. 2011). We used 2 miRs targeting SHP2, SHP2 miR1 (5'-

TGCTGTTGACAGTGAGCGCGGGCACGAATATACAAATATTTAGTGAAGCCACA
GATGTAAATATTTGTATATTCGTGCCCTTGCCTACTGCCTCGGA-3') and SHP2
miR2 (5'-TGCTGTTGACAGTGAGCGACCACGTATATTATGTAGTCTATAGTGAA
GCCACAGATGTATAGACTACATAATATACGTGGGTGCCTACTGCCTCGGA-3')
and miR targeting ZEB1 (5'-TGCTGTTGACAGTGAGCGAGCGCAATAACGTTAC
AAATTATAGTGAAGCCACAGATGTATAATTTGTAACGTTATTGCGCCTGCCTA
CTGCCTCGGA-3'). As a control, we used a miR targeting firefly luciferase (CTRL miR).
Constitutive ERK5 shRNAs were obtained from Sigma. Rescue experiments were
performed with retroviral vector pMSCV-neo-SHP2-WT, the retroviral vector pBabe-
puro-LIN28B (Addgene), lentiviral vector pSD-94-c-Myc (Duss, Andre et al. 2007) and
the dox inducible lentiviral vector pLKO-TREX-HA (Wee, Wiederschain et al. 2008)
expressing SHP2 WT or the catalytically inactive SHP2 C/S or SHP2 D/A+C/S mutant or
SHP2 NLS deleted or mutated mutants. All SHP2 mutants were generated by site-directed
mutagenesis of SHP2 WT. For in vivo monitoring by fluorescence or bioluminescence, the
cells were infected with the lentiviral pFU-Luc2-eGFP vector expressing GFP-Luciferase
(Liu, Patel et al. 2010). For lentiviral production the following helper plasmids were used:
HDM-tat16, HDM-HgPM2, pRC-CMV-RaII and HDM-VSV-G. For retroviral production
retroviral constructs were co-transfected with VSV and gag-pol into the packaging cell line
293 EBNA.

8.2   Cell Culture & cell based functional assays

All cells were grown at 37°C in a humidified atmosphere with 5% CO_2 in presence of
100 IU/ml of penicillin and 100 µg/ml of streptomycin in their respective growth media.
Regular Mycoplasma tests were performed by PCR. All cells were frozen in their

respective growth medium with 10% DMSO except MCF10A cell lines, which were frozen in their growth medium with 20% horse serum and 8% DMSO.

Table 2 Culture condition of various cell lines

Cell line	medium	additives
BT474, HEK293T, MDA-MB-231	DMEM	10% FBS
SUM159	Ham`s/F12	5% FBS, 10 µg/ml Insulin, 500 ng/ml Hydrocortisone
SUM1315	Ham`s/F12	5% FBS, 10 µg/ml Insulin, 20 ng/ml EGF
SKBR3	RPMI 1640	10% FBS
MCF10A HER2/3	DMEM/F12	5% HS, 10 µg/ml Insulin, 20 ng/ml EGF, 100 ng/ml Cholera toxin, 500 ng/ml Hydrocortisone

8.2.1 Mammosphere assays

Single cells were seeded on Ultra Low Attachment Plates (ULA, Corning, Cat#734-1582) at a concentration of 100,000 cells/ml. For experiments with inducible miRs, dox was added at the beginning of the tumorsphere assay and refreshed every 2-3 days. Tumorspheres larger than 50 µm diameter were counted 7 days after seeding (1° tumorspheres). All the primary spheres were isolated from the rest of the cells, dissociated with HyQTase (Thermo Scientific) and filtered through a 40 µm cell strainer to obtain a single cell suspension. Equal numbers of single cells (20,000 cells/ml) were then seeded on new ULA plates in the presence of dox. The number of tumorspheres was counted after 7 days (2° tumorspheres).

8.2.2 Transwell migration assays

Migration assays were performed using transwell chambers (8 µm pore size, BD Biosciences, Cat#354778) according to the manufacturer's protocol. SUM159 or MDA-MB-231 cells expressing either the CTRL miR or SHP2 targeting miR1 or miR2 were starved for 16 h prior to seeding into the top well of the transwell insert. 15,000 cells were seeded in 500 µl medium containing 0.25% FBS (SUM159) or 0.5% FBS (MDA-MB-231)

and 750 µl of full growth medium including 5% FBS (SUM159) or 10% FBS (MDA-MB-231) was added to the lower well as the chemoattractant. Cells were allowed to migrate towards the FBS gradient for 24 h before the inserts were washed with PBS and non-migrated cells remaining on the upper surface of the membrane were removed using cotton swabs. The cells that had migrated through the membrane were fixed with 4% PFA and stained with 0.2% Crystal violet. The whole membranes were then imaged using a Leica MacroFluo widefield microscope with a 2 x objective and 0.9 x motor zoom. Migrated cells were counted on the whole membrane in 3 independent experiments. The number counted for cells expressing CTRL miR was set to 100%.

8.2.3 Invasion assay in vitro

In vitro invasion experiments were performed using BD BioCoat™ Matrigel invasion chambers (BD Bioscience, Cat#354480). 15,000 serum starved SUM159 or MDA-MB-231 cells were seeded into the upper well of the cell culture inserts containing an 8 µm pore size PET membrane with a thin layer of matrigel in 500 µl medium containing 0.25% or 0.5% FBS respectively. 750 µl full growth medium containing 5% FBS (SUM159) or 10% FBS (MDA-MB-231) was added to the lower well as a chemoattractant. The cells were allowed to migrate for 40 h at 37°C, after which the filter was washed 1 x with PBS. Then, the non-invading cells were removed from the upper surface of the membrane using a cotton swab. After this, the invading cells attached to the bottom of the membrane were fixed and stained with 0.2% Crystal violet 4% PFA in PBS solution for 30 min at RT. After 3 washes with PBS, the membranes were allowed to dry, then imaged with a MacroFluo widefield microscope using a 2 x objective and a 0.9 x zoom factor. Invasive cells were counted in 3 independent experiments. The average number of invasive cells counted for cells expressing the control construct was set to 100%.

8.2.4   3D cell culture assay

Growth factor reduced matrigel (BD Biosciences, Cat#354230) was thawed on ice O/N and 40 µl were spread evenly in each well of an 8-well glass chamber slide (BD Falcon, Cat#354108). The slide was put in the incubator (37°C) for 30 min to allow the matrigel to solidify. Then, MCF10A HER2/3 cells (4,500 cells per well) were seeded on the matrigel in a total volume of 400 µl in assay medium (DMEM/F12 medium supplemented with 2% matrigel, 2% HS, 5 ng/ml EGF, 0.5 µg/ml of hydrocortisone, 100 ng/ml of cholera toxin, 10 µg/ml of insulin, 100 IU/ml of penicillin and 100 µg/ml of streptomycin). The next day, 300 µl of assay medium containing 2% matrigel were added to the cells. On day 5, the medium was replaced with 400 µl fresh assay medium containing 2% matrigel. From this day on, the medium was replaced with 400 µl of assay medium every 4 days until the end of the experiment (14 days total). The same protocol was followed for the 3D culture of SUM159 and SUM1315 cells, only that these cells were cultured in their normal growth medium with reduced serum (2% FBS). After 2 weeks, the percentage of invasive structures was counted.

8.2.5   WST-1 proliferation assay

To compare the cell number of different cell lines, cell proliferation WST-1 reagent from ROCHE was used (Cat#05015944001). 2,000 SUM1315 cells in 200 µl were plated in triplicates in 96-well plates and incubated for 5 days. Then 10 µl WST-1 reagent was added to each well, incubated for 4 h at 37°C and read at 550 nm. The assay is based on the cleavage of the stable tetrazolium salt WST-1 into the dye formazan by metabolically active cells. The formazan dye formed is quantitated and the measured absorbance directly correlates to the number of viable cells.

8.2.6 Colony formation assay

2,000 SUM1315 cells were seeded per well in 6-well plates in 2 ml culture medium for 2 weeks. Then, the colonies were washed with PBS, fixed with 4% PFA and visualized by staining with 0.2% Crystal violet. The plates were scanned using an Epson Twain scanner and the area covered by colonies was analyzed and quantitated using ImageJ/Fiji software. Therefore, the images were converted to 8 bit format, followed by segmentation by adjusting the threshold, conversion to binary images and the number of colonies/area covered was obtained by using the analyze particles command.

8.3 Microscopy

8.3.1 Immunofluorescence

8-well glass chamber slides (BD Falcon, Cat#354108) were coated with 200 µl of 0.1 mg/ml Poly-L-Lysine (SIGMA, Cat#P6282) for 2 h at RT or 10 µg/ml Fibronectin (SIGMA, Cat#1141) for 1 h at 37°C. After the incubation, the slides were washed 2 x with dH$_2$O. Then, 5,000 cells were seeded per well in normal growth medium. The next day, the cells were washed 2 x with PBS and fixed with 4% PFA shaking at RT for 10 min. Before the staining, cells were permeabilized with 0.1% Triton-X in PBS for 10 min at RT. Afterwards the cells were washed 3 x 5 min with PBS and blocked with 2.5% normal goat serum (NGS) in PBS for 1 h at RT. Then, the samples were incubated with the primary antibody in 2.5% NGS in PBS O/N at 4°C in a humidified chamber. As a negative control, 1 well was left without primary antibody. The next day, the cells were washed 3 x 5 min shaking at RT with PBS+1% BSA, then incubated with the secondary antibody in 2.5% NGS in PBS for 1 h at RT in the dark. After 2 x 5 min washing with PBS, the nuclei were stained with DAPI (2 mg/ml; Invitrogen, Cat#1306) diluted 1:10,000 in PBS for 10 min at

RT. After 2 more washes for 5 min with PBS, the slides were dried and mounted with 1 drop Prolong Gold antifade mounting medium (Invitrogen, Cat# P36934). 24 h later, the slides were analyzed or stored at 4°C.

8.3.2 FRET acceptor photobleaching

Fluorescence resonance energy transfer (FRET) is based on the non-radioactive transfer of energy from one fluorescent protein (donor) to another fluorescent protein (acceptor), that needs to reside in close proximity (Snapp and Hegde 2006). Upon excitation, the donor transfers energy to the acceptor which then emits energy, although it was not excited. There are several different FRET methods and instrumental setups (Jares-Erijman and Jovin 2003). FRET acceptor photobleaching most widely used, as it is relatively simple to set up and interpret (Snapp and Hegde 2006).

FRET samples were always prepared fresh the day before conducting the experiment. Cells were grown in 8-well chambers coated with 10 µg/ml Fibronectin (Sigma, Cat#1141). SHP2 and total Src or pSrc Tyr530 were labeled with specific primary antibodies and with a donor (Alexa 568) or acceptor (Alexa 633) fluorophore-conjugated secondary antibody. As endogenous proteins (used in this setup) are rarely expressed at the same level, the decision which protein to use as donor or acceptor is crucial. Generally, the protein with lower abundance is used as the donor, as an excess of unpaired acceptor molecules does not interfere with the results, while an excess of unpaired donor molecules dilutes the detected FRET signal (Snapp and Hegde 2006). In this setup, SHP2 was visualized using secondary anti-mouse Alexa 633-conjugated antibody (acceptor). Src and pSrc Tyr530 were visualized using secondary anti-rabbit Alexa 568-conjugated antibody (donor). As a positive control for FRET, SHP2 (mouse primary antibody) was labeled with anti-mouse Alexa 568 and anti-mouse Alexa 633, ensuring that donor and acceptor are in close proximity. As a negative control, Src (rabbit primary antibody) was labeled with

anti-rabbit Alexa 568 and anti-mouse Alexa 633, resulting in no FRET signal. Slides were mounted in a mix of 90% glycerol and 10% Tris-HCl pH 8.5 without anti-fading additives. Acceptor photobleaching was used to assess FRET efficiency on a Zeiss LSM700 confocal microscope equipped with a 40 x/1.3 oil immersion objective. Alexa 568 was excited with a 555 nm laser line and the emission was measured with a LP560 filter. Alexa 633 was excited with a 640 nm laser line and the emission was measured with a LP640 filter. Several regions of interest (ROIs) were designated. ROI 1 was the region bleached, ROI 2 a region close by to control for unwanted bleaching and ROI 3 a region outside the cell to measure background fluorescence and serial images of the donor and acceptor intensities were taken before and after photobleaching. FRET efficiency (%E) was calculated by comparing the donor (D) intensities in the bleached ROI 1, before (D_{pre}) and after (D_{post}) photobleaching. Donor intensities were corrected for background fluorescence (subtraction of ROI 3) before E was calculated as $\%E = (D_{post}-D_{pre})/D_{post}$. This formula calculates the fluorescence that has been quenched from the donor in presence of the acceptor (Snapp and Hegde 2006). For each condition, 4 to 10 cells from 2-3 experiments were assessed.

8.3.3 Time-lapse microscopy

For live imaging studies, randomly growing SUM159 or MDA-MB-231 cells expressing dox-inducible CTRL miR or one of 2 miRs targeting SHP2 (miR1 or miR2) cultured in presence of 1 µg/µl dox were seeded on 6-well polystyrene dishes (Corning) and imaged the following day. For time-lapse analysis, cells were incubated on a heated stage at 37°C in a 5% CO_2 chamber. The imaging was carried out with a Zeiss Widefield Axiovert 200M enclosed in an incubator box with a CCD camera and 3-4 positions per well were imaged. Images were taken over a period of 12 h at 10 min intervals in the DIC channel using MetaMorph software. The acquired data was compiled to stacks, saved as movies and analyzed using ImageJ/Fiji software. Cell movement of 20 cells per movie was analyzed

using the ImageJ/Fiji plugin MTrackJ (Meijering, Dzyubachyk et al. 2012). Briefly, cells to be analyzed cells were randomly picked on the first frame of the movie. The position of one cell at a time was monitored manually by clicking on the nucleus of the cell in every second frame (20 min intervals) until the end of the movie, resulting in trajectories for each cell monitored. In the case of dividing cells, one of the daughter cells was randomly chosen and followed. Cells disappearing from the field of view were excluded from the analysis.

8.3.4 Multiphoton intravital microscopy

8.3.4.1 Microscope description

For intravital imaging experiments, we used our previously described custom built microscope. Signals from the microscope are acquired and converted to real-time images by a custom-made algorithm based on Matlab (MathWorks, Natick, Mass. USA), before being analyzed offline (Bonapace, Wyckoff et al. 2012).

8.3.4.2 Anesthesia and surgery of tumor-bearing animals

1×10^6 SUM159 cells or 5×10^5 MDA-MB-231 GFP-Luciferase positive breast cancer cells were injected into gland 4 of six week old female NOD-SCID immunodeficient mice. After two weeks, the injections were checked by Luciferase expression. The tumors of both groups were allowed to reach 6-8 mm diameter (6 weeks after injection for SUM159, 3 weeks for MDA-MB-231), before the knockdown of SHP2 was induced by feeding the mice with dox food. 10 days later, single cell movement in tumors was imaged by intravital microscopy using a custom built two-photon microscope (Bonapace, Wyckoff et al. 2012).

For the imaging, the mice were placed under anesthesia with 5% isoflurane and maintained for the course of the imaging session at 2.5% to 0.5% isoflurane to control constant breathing. Minimal surgery was performed to expose the tumor by removing a small skin flap. Then the mouse was put on the inverted microscope and imaged at 880 nm for GFP fluorescence. For visualizing the of the blood vessels and macrophages, 200 µl of 20 mg/ml 70,000 kDa Texas red-dextran (Molecular Probes, Cat#D1894) in PBS were injected into the tail vein of the mice before surgery.

8.3.4.3 Measurement of cell behavior

Cell motility, matrix density, macrophage density and vessel leakiness were visualized by time-lapse multiphoton microscopy by taking 100 µm Z-stacks collected at 2 min intervals for at least 30 min. Image analysis was carried out using Fiji/ImageJ software. Raw data was arranged into 4D hyperstacks for analysis. Velocity, directionality and path length were analyzed using the plugin ROI tracker (Entenberg, Wyckoff et al. 2011).

8.4 Molecular methods

8.4.1 Transformation

8.4.1.1 Preparation of chemically competent DH5α

A single colony of untransformed chemically competent DH5α cells was inoculated in 2 ml LB-only media and incubated O/N at 37°C shaking. The next morning, 1 ml of the culture was added to 150 ml LB media and incubated at 37°C shaking until an OD_{600} of 0.6 was reached (2.5-3 h). Then, the bacteria were pelleted by spinning for 15 min at 4,000 rpm at 4°C. The pellet was resuspended in 1/10 of the initial volume (i.e. 15 ml for 150 ml initial culture volume) TSB media (1 x LB medium, 5% DMSO, 10 mM $MgCl_2$, 10 mM

MgSO$_4$, 10% PEG4000; filter sterilize (0.2 µm) prior to use and store at 4°C) and kept on ice for 1 h. After the incubation, 1.5 ml Eppendorf tubes were placed on dry ice and the bacterial suspension was aliquoted into these tubes at 100 µl per tube and the aliquots were stored at -80°C.

8.4.1.2 Preparation of electrocompetent bacteria Stbl3

Electrocompetent Stbl3 from a previous batch were streaked out on a LB plate without antibiotics and incubated at 37°C O/N. The next evening, a 50 ml culture of one colony was started in 2YT medium (16 g/l Bactotryptone, 10 g/l yeast extract, 5 g/l NaCl) and incubated at 37°C O/N shaking. After 2 h incubation, 25 µg/ml Streptomycin was added in order to keep the bacteria stable. The next morning, 5 ml from this culture were diluted in 500 ml 2YT with 50 µg/ml Streptomycin and grown to an OD$_{600}$ of 0.6 to 0.8 (3-4 h) at 37°C shaking. Upon reaching the desired optical density, the bacterial suspension was chilled on ice for 15 min, then centrifuged for 20 min with 4,000 rpm at 4°C and the pellet was resuspended in 500 ml sterile dH$_2$O to remove the salt. After another 20 min of centrifugation with 4,000 rpm at 4°C, the pellet was resuspended in 40 ml sterile 10% glycerol. The bacteria were pelleted again by spinning them 10 min with 4,000 rpm at 4°C, before the pellet volume was estimated (about 500 µl from a 500 ml culture) and twice the volume of sterile 10% glycerol was added. Then, the cells were aliquoted on dry ice and stored at -80°C.

8.4.1.3 Chemical transformation of E. coli DH5α

100 µl of competent DH5α cells were thawed on ice. 20 µl of 5 x KCM buffer (500 mM KCL, 150 mM CaCl$_2$ and 250 mM MgCl$_2$) and 100 pg-10 ng circular plasmid or the entire volume of the ligation mix were mixed on ice, topped up to 100 µl with dH$_2$O and added to the cells. After addition of the DNA to the cells, the mixture was incubated on ice for 15

min before incubating the mix 5 min at 37°C and briefly placing it on ice afterwards. Then, 1 ml LB media was added, and the mixture was incubated at 37°C for at least 30 min shaking. After the recovery period, the bacteria were plated onto LB-agar plates containing the appropriate selection marker. For high-efficiency plasmids 10-100 µl were plated, whereas for low-efficiency plasmids and ligations, the cell suspension was centrifuged and the supernatant was discarded. The bacterial pellet was then resuspended in the remaining media, and plated onto pre-warmed agar plates containing the appropriate antibiotic. Then the plates were incubated (agar-side up) at 37°C O/N.

8.4.1.4 Electroporation of electrocompetent Stbl3

The Gene Pulser electroporation system and cuvette holder (Bio-Rad) was used and the conditions for transformation were set according to the bacterial strain used. For Stbl3 cells, the following settings were used: 25 µFD capacitance, 200 Ohms resistance and 1.8 kV. The time constant (tau value) should be 4.5-4.8 msec. Glass cuvettes and 2YT media without antibiotics were chilled on ice. Then, 1 µl of DNA was added to a 1.5 ml Eppendorf tube and mixed with electrocompetent bacteria before adding the mix to a cooled cuvette. Any moisture was dried off the outside of the cuvette before placing it in the holder of the power source. Then, the holder was brought into position and the cells were shocked. After hearing a constant tone, 1 ml of 2YT medium was added to the cells and the cells were transferred into a fresh 1.5 ml Eppendorf tube and kept on ice until all samples were done. The bacteria were allowed to recover for at least 30 min at 37°C shaking. After the recovery period, the bacteria suspension was added to 100 ml 2YT medium containing 33 µg/ml Streptomycin and 33 µg/ml of the resistance marker on the plasmid DNA transfected into the bacteria and incubated shaking at 37°C O/N.

8.4.2 Plasmid DNA preparation

8.4.2.1 Plasmid Miniprep

For the isolation of the plasmid DNA from the O/N cultures, the JETQUICK Plasmid Spin Miniprep Kit (GENOMED) was used and the isolation carried out as described by the manufacturer (i.e. volumes of buffers as stated by the manufacturer, speed of centrifugation adjusted). For each transformation, single colonies of transformed E. coli containing the required plasmid DNA were picked using a sterile pipette tip and transferred into bacterial tubes containing 2 ml LB medium and the appropriate antibiotic. The cultures were incubated at 37°C shaking for 16 h. The next morning, the cultures were transferred into a 2 ml Eppendorf tubes and centrifuged at 12,000 rpm for 1 min to pellet the bacteria. Then, each pellet was resuspended in 250 μl cell resuspension buffer G1 and mixed by vortexing. Then, 250 μl lysis buffer G2 was added and mixed by inverting the tube 4-6 times. 350 μl of neutralization buffer G3 were added to the clear lysate and mixed until a flocculent white precipitate formed and then centrifuged at 12,000 rpm for 10 min. To load and bind the plasmid DNA, the clear supernatant was transferred to a spin column in a 2 ml collection tube. The column was centrifuged for 1 min at 12,000 rpm at RT. The flow-through liquid was discarded, while the collection tube was kept for further steps. For the first washing step, the column was placed back in the collection tube and 500 μl GX buffer were added. For the second washing step 700 μl of wash buffer G4 were added to the column. Next, the column was centrifuged empty for 1 min to dry and remove all EtOH residues. To elute the bound plasmid DNA from the column, 30 μl dH$_2$O were pipetted directly onto the membrane and left on for 1 min before the column was placed into a fresh 1.5 ml microcentrifuge tube and centrifuged for 1 min. For a higher yield, the eluted DNA was pipetted again onto the membrane and centrifuged again.

8.4.2.2 Plasmid Midiprep

DNA constructs required for transfection were prepared using a JETQUICK Midi Kit (GENOMED) following the instructions by the manufacturer. Briefly, 100 ml LB medium cultures containing the appropriate selective marker and were grown at 37°C O/N shaking. Cells were harvested by centrifugation at 4,000 rpm for 20 min at 4°C in an Eppendorf 5810R centrifuge in 50 ml Falcon tubes. After removal of the supernatant, the bacterial pellet was resuspended in 4 ml buffer E1 by vortexing. The cell suspension was lysed with 4 ml of lysis buffer E2 and mixed thoroughly by inverting the tube 5 times. For the precipitation of genomic DNA, 4 ml of chilled buffer E3 were added and mixed immediately by gentle inversion followed by 15 min incubation on ice. The supernatant was separated from the precipitate by centrifugation in polypropylene tubes at 4,000 rpm for 30 min at 4°C. Meanwhile, a Lysate Filter Unit (LFU) was equilibrated by applying 10 ml buffer E4. After the centrifugation, the supernatant containing the plasmid DNA was filtered through medical gauze onto the LFU column and allowed to enter the resin by gravity flow. The LFU column was washed twice with 10 ml buffer E5. Afterwards, the DNA was eluted into a new centrifuge tube containing 3.5 ml isopropanol using 5 ml elution buffer E6 to precipitate the DNA. The solution was mixed and centrifuged at 4,000 rpm for 30 min at 4ºC. The supernatant was decanted carefully and the DNA pellet was washed with 2 ml of RT 70% EtOH and centrifuged at 4,000 rpm for 10 min at 4°C. The supernatant was discarded and the pellet was air-dried for 10 min. Then the pellet was dissolved in 200-300 µl dH_2O and transferred to a fresh 1.5 ml Eppendorf tube.

8.4.2.3 Quantification of DNA Concentrations

All DNA concentrations were directly measured with a NanoDrop ND-1000 spectrophotometer (NanoDrop Technologies). To do so, the spectrophotometer was first

calibrated, then 1.5 µl undiluted sample was pipetted onto the spectrophotometer and the sample concentration in ng/µl as well as the purity ratio was read of.

8.4.2.4 Gel electrophoresis of DNA

Linearized DNA was separated on agarose gels of the appropriate percentage. For example 1% agarose gels were cast by dissolving 1 g agarose in 100 ml of 1 x TAE (40 mM Tris pH 7.6, 20 mM acetic acid, 1 mM EDTA) buffer in a microwave. SYBR Safe DNA stain (Invitrogen, Cat#S33102) was added to the transparent agar solution, before the gel was poured into a gel tray and a Teflon comb was inserted to form the wells. Then, the gel was left to solidify at RT for 30-45 min before the gel was placed into an electrophoresis tank containing enough electrophoresis buffer (1 x TAE) to cover the surface of the gel. DNA samples were mixed with 1/5 volume of 6 x loading buffer (10 mM Tris-HCl pH 8, 60 mM EDTA, 60% glycerol, 0.1% orange G) and loaded into the wells. Either a 100 bp or 1 kb DNA marker (Invitrogen) was loaded in a separate well to determine the fragment sizes of the DNA sample. Agarose gels were run at 100 V for 45 min or until the dye front had run approximately 80% through the gel.

8.4.2.5 Visualization of DNA with SYBR Safe DNA stain

DNA fragments were visualized by placing the gel on a transilluminator and captured on Polaroid film.

8.4.2.6 Isolation of DNA fragments from agarose gels

DNA fragments required for cloning were purified in the appropriate percentage agarose gel, before the desired bands were visualized under UV light and quickly cut out with a clean scalpel. The exposure to the DNA damaging UV light was kept was short as possible. The gel pieces were then placed in individual 1.5 ml Eppendorf tubes and the weight of each piece was determined.

8.4.2.7 Gel Extraction clean up

The QIAquick Gel Extraction Kit (QIAGEN) was used to isolate of DNA fragments from gel pieces. All pieces had a weight of about 0.1 g and therefore an approximate volume of 0.1 ml. 300 µl solubilization buffer QG (i.e. 3 x the gel volume) was added per tube and the mixture was incubated at 50°C for 10 min and mixed by vortexing every 2-3 min until the gel pieces had melted. Then, 1 gel volume of isopropanol (100 µl) was added to each sample and mixed. Fresh QIAquick spin columns were placed in 2 ml collection tubes and a maximum of 800 µl of the DNA/agarose solution was added at a time. The assembly was centrifuged at 12,000 rpm for 1 min and the flow through was discarded. To remove all traces of agarose, 500 µl of buffer QG were added to each column and centrifuged at 12,000 rpm for 1 min. For a washing step, 750 µl PE DNA wash buffer was added to each column and centrifuged at 12,000 rpm for 1 min. To dry the column matrix, the column/tube assembly was centrifuged at 12,000 rpm for 1 min and after transferring the columns into fresh 1.5 ml Eppendorf tubes, the plasmid DNA was eluted with 30 µl dH$_2$O by centrifugation at 12,000 rpm for 1 min. After the agarose gel extraction, the concentration of the plasmid DNA was determined using the NanoDrop spectrophotometer.

8.4.3   Enzymatic modification of DNA

8.4.3.1 Digestion of DNA with restriction enzymes

Plasmids, vectors and fragments were digested with various endonucleases using the buffers provided with the enzymes. Preparative restriction digests were conducted during cloning in order to isolate the desired insert and to open the target vector. Analytical restriction digests on the other hand, were done to identify positive clones after transformation of bacterial cells and isolation of the plasmids from these cells by

Miniprep. Digests were carried out in 20 µl volumes. When preparing inserts or vectors, a double digests with 2 appropriate enzymes was carried out at 37°C for 2 h. The double digests were performed using the buffer with the lower salt concentration if a compatible buffer was not available. Restriction enzymes units were used according to the amount of DNA present in sample, ensuring that the enzyme concentration was not in excess to prevent star activity. In order to verify the correct insertion of the protein sequences into the target vector, analytical restriction digests were carried out using the respective restriction enzymes.

20 µl reactions were set up using 1 µg DNA, 0.5 µl per enzyme, 1 x of the suitable buffer (final concentration), 1 x BSA (final concentration) and water. The restriction digests were incubated at 37°C and the products visualized by gel electrophoresis using a 1% agarose gel containing SYBR Safe DNA stain.

8.4.3.2 Inactivation of enzymes

Before cleaning the opened target vector, it was treated with 1 µl calf intestine alkaline phosphatase (CIP) (NEB) and incubated for 1 h at 37°C to remove 5' phosphates to prevent self-ligation of the target vector.

8.4.3.3 Ligation

T4 DNA ligase (NEB) catalyses the formation of phosphodiester bonds between adjacent 5' phosphate and the 3' hydroxyl residues of adjacent nucleotides in either cohesive-ended or blunt-ended fragments. For all ligations an approximate molar insert:vector ratio of 3:1 was used. About 30-100 ng of the linearized target vector were used per ligation. The needed amount of insert to yield a molar insert:vector ratio of 3:1 was calculated using the following formula:

$$\frac{\text{ng Vector} \times \text{kb size Insert}}{\text{kb size Insert}} \times \text{Molar ratio} \frac{\text{Insert}}{\text{Vector}} = \text{ng Insert}$$

20 µl reactions were set up using the calculated amount of vector and insert, 1 µl T4 DNA ligase, 1 x T4 DNA ligase buffer (50 mM Tris-HCl, 10 mM MgCl$_2$, 10 mM DTT, 1 mM ATP; pH 7.5) and dH$_2$O. The ligation reaction was incubated at 4°C O/N. The following day, 10-20 µl of ligation mix were used to transform 100 µl of E. coli DH5α competent bacteria.

8.4.4   Site specific mutagenesis

Primers were designed according to the QuikChange Manual (Stratagene) and ordered HPLC-purified from microsynth (Balgach, Switzerland). The QuikChange site directed mutagenesis protocol can be applied in any plasmid vector for deletion, insertion of single or multiple amino acids. The QuikChange site-directed mutagenesis method is performed using high fidelity PfuTurbo DNA polymerase which replicates both plasmid strands.

Mutation was performed in 50 µl PCR reaction mix containing 5 µl 10 x PfuTurbo buffer, 40 ng template DNA in 5 µl, 1 µl forward primer 10 mM and 1 µl reverse primer 10 mM, 1 µl dNTP mix, 36 µl dH$_2$O and 1 µl PfuTurbo DNA polymerase. The PCR reaction was performed as follows: 95°C initial denaturation for 30 sec, 95°C denaturation for 30 sec, 55°C annealing for 1 min and 72°C extension for 7 min until 16 cycles. Then, 5 µl Dpn I buffer and 1 µl of Dpn I was added to the PCR mixture and incubated at 37°C for 2 h. The control reaction was prepared in the same way, but without PfuTurbo DNA polymerase. 10 µl of the PCR product were transformed into E. coli. Mutated sequences were verified by direct DNA sequencing.

Table 3 Primers used for site directed mutagenesis

name	sequence
SHP2 D425A fwd	5'-TTCGGACCTGGCCGGCCCACGGCGTGCCCAGCGACCCTGGGGGCG-3'
SHP2 D425A rev	5'-TGGGCACGCCGTGGGCCGGCCAGGTCCGAAAGTGGTATTGCCAGA-3'
SHP2 C459S fwd	5'-TTGCCACACAAGGCTCCCTGCAAAACACGGTGAATGACTTTTGGC-3'
SHP2 C459S rev	5'-CCGTGTTTTGCAGGGAGCCTTGTGTGGCAATGTAACTCTTTTTGG-3'
NLS mut fwd	5'-CCAAGTGCAACAATTCAAGTCCCAGTAAGAGTTACATTGCCACAC-3'
NLS mut rev	5'-GTGTGGCAATGTAACTCTTACTGGGACTTGAATTGTTGCACTTGG-3'
NLS del fwd	5'-TCATGCCTGAATTTGAAACCAAGAGTTACATTGCCACACAAGGCTGC-3'
NLS del rev	5'-TGTGGCAATGTAACTCTTGGTTTCAAATTCAGGCATGATGATATTTG-3'

8.4.5 Direct DNA sequencing

Sequencing was outsourced to the Novartis sequencing facility. Therefore, the DNA template (250-500 ng for PCR products or 0.5-1 µg for plasmids) dissolved in dH$_2$O was mixed with 1 µl of 10 mM sequencing primer and given to the Novartis facility for the readout.

8.4.6 Lentiviral production

Linear polyethylenimine (PEI; Polysciences Inc., Cat#23966-2) was used as a transfection reagent and a 1 µg/µl solution was made in dH$_2$O, neutralized with HCl to pH 7.2 and sterilized using a 0.2 µm filter (VWR international, Cat#28145-481). Aliquots were stored at -80°C or kept at 4°C for up to 4 months. 8 h before transfection, HEK293T cells were plated in T75 flasks at 80% confluency in normal growth medium. Before transfection, the medium was replaced with 7 ml of serum-free medium. In an Eppendorf tube, 10 µg DNA and helper plasmids (2 µg HDM-tat16, 2 µg HDM-HgPM2, 2 µg pRC-CMV-RaII, and 4 µg HDM-VSV-G) were mixed in 1 ml of serum free medium. PEI was added in a 4:1 PEI:DNA ratio (4 µg of PEI for every µg of DNA) to the diluted DNA, vortexed immediately and incubated for 15 min at RT. After the incubation, the mix was added to the cells in the T75 flask. 16 h after the transfection, the medium was changed to DMEM containing 10% FBS. 3 days later, the viral supernatant was harvested for the first time and

the cells were fed with 8 ml fresh DMEM 10% FBS medium. 2 days later, the second viral supernatant was harvested, filtered and combined with the first harvest (stored at 4°C in the meantime). The pooled virus supernatant was centrifuged at 1,000 rpm for 5 min and filtered through 0.45 µm filters (VWR international, Cat#28145-505) to remove cell debris. Then, the filtered virus was concentrated using Amicon Ultra-15 Centrifugal Filter Units with Ultracel-30 Membrane (Millipore, Cat#UFC903096), aliquoted and stored at -80°C.

8.4.7 Lentiviral infection of target cells

24 h before in infection, target cells were plated in 24-well plates (20,000 cells per well). Cells were infected at the desired Multiplicity of Infection (MOI) by incubation with the appropriate amount of virus supernatant in normal growth medium supplemented with 8 µg/ml Polybrene (Sigma, Cat#H9268) for 16 h at 37°C. The media was then changed and the cells were incubated another 24 h at 37°C before starting selection with the appropriate concentration of Puromycin (BD Bioscience, Cat#P7255), G418 (ROCHE, Cat# 04727878001) or Zeocin (Invitrogen, Cat# R25001).

8.5 Biochemistry

8.5.1 Protein extraction

8.5.1.1 SDS hot lysis

The cells were washed with PBS at RT and total proteins were extracted by lysis with SDS-Buffer (250 mM Tris HCl pH 7.4, 2.5% SDS) at 95°C. The lysates were sonicated for 10 sec to disrupt the genomic DNA and centrifuged for 5 min at 12,000 rpm before protein quantification.

8.5.1.2 Lysis in RIPA buffer

Cells were placed on ice and washed twice with cold PBS, before ice cold RIPA buffer (50 mM Tris, pH 8.0, 150 mM sodium chloride, 1% NP-40, 0.5% sodium deoxycholate, 0.1% SDS, 10 mM NaF, 2 mM PMSF, 2 mM Na_3VO_4, 1 x EDTA-free protease inhibitor cocktail (ROCHE, Cat#11873580001)) was added. Then, cells were scraped into an Eppendorf tube and kept on ice. Cells were incubated for 10 min, followed by centrifugation at maximum speed for 15 min at 4°C. The supernatant containing total cellular proteins was collected and stored at -80°C.

8.5.2   Immunoprecipitation

Cells were placed on ice, washed with ice cold PBS and lysed in IP buffer (20 mM Tris HCl pH 7.5, 100 mM NaCl, 1% NP-40, 10% glycerol, 5 mM idodoacetic acid, 1 x EDTA-free protease inhibitor cocktail (ROCHE, Cat#11873580001)). After protein measurement, lysates containing 0.5-1 mg of total protein were mixed with the recommended amount of antibody and incubated on a rotating wheel at 4°C O/N. The next morning, 50 µl of 50% Protein A or G coupled agarose bead slurry (Millipore) per samples were washed with IP buffer to remove all traces of EtOH and added to each IP sample. The samples were then incubated rotating at 4°C for 2 h. Following the incubation, the immuno-complexes were pelleted by centrifugation at 2,000 rpm at 4°C for 1 min and washed 5 x with ice-cold IP buffer. Each time, complexes were collected by centrifugation at 2,000 rpm at 4°C for 1 min. After the last wash, 5 x Laemmli loading buffer was mixed 1:1 with IP buffer and 60 µl were added to each IP sample and proteins were denatured by heating to 95°C for 5 min. Protein A or G agarose was pelleted by centrifugation at 12,000 rpm at RT for 10 min and supernatants, containing immunoprecipitated proteins were analyzed by SDS-PAGE electrophoresis.

8.5.3 Subcellular fractionation

Subcellular fraction is an enrichment method allowing the separation of cell organelles based on biological or physical properties. The fractionation is divided in two major steps: First, the cellular organization is disrupted by homogenization and then, the cell organelles are separated into fractions based on their physical and biological properties for example by centrifugation (Pasquali, Fialka et al. 1999).

Cells were grown on 10 cm dishes and washed 3 x with cold PBS. Then, 400 µl of ice-cold hypotonic buffer A (10 mM HEPES-KOH pH 7.9, 1.5 mM $MgCl_2$, 10 mM KCl, 0.2 mM PMSF, 1 mM DTT) was added directly onto the plates on ice for 10 min. Plates were swirled every 2 min to avoid drying of the cells. After the incubation time, cells were scraped off the plate using cell lifters (Corning, Cat#3008) and transferred to Eppendorf tubes. Each tube was then vortexed for 10 sec and centrifuged for 10 sec at full speed. The supernatant (cytoplasmic fraction) was transferred to a new tube without disturbing the pellet and kept on ice. The nuclear pellet was washed by resuspending it in 500 µl buffer A, pipetting gently up and down and vortexing for 10 sec followed by 10 sec centrifugation at full speed. The supernatant was discarded and the washing step was repeated 3 more times. Depending on the size, the nuclear pellet was then resuspended in 20-100 µl of cold buffer B (20 mM HEPES-KOH pH 7.9, 25% glycerol, 420 mM NaCl, 1.5 mM $MgCl_2$, 0.2 mM EDTA pH 8, 0.2 mM PMSF, 1 mM DTT), pipetted 3 x up and down and incubated on ice for 20 min. After the incubation, the mixture was centrifuged for 2 min at full speed and the supernatant (nuclear fraction N1) was transferred to a new tube. To also isolate the crude membrane and DNA (N2, chromatin enriched fraction), the pellet was resuspended in RIPA buffer. For checking the purity of each fraction by immunoblotting, α-tubulin was used as a marker for the cytoplasmic fraction and PARP

was used as a marker for the nuclear fraction. The histone mark H3K4me2 was used as a marker for the chromatin enriched fraction N2.

8.5.4 Immunoblotting

8.5.4.1 Quantification of protein concentration

To determine protein concentrations, a DC protein assay (Bio-Rad, Cat#500-0116) was used according to the manufacturer's instructions. Briefly, 5 µl of protein standards (10, 5, 2.5, 1.25, 0.625, 0.313 µg/ml BSA) and samples were pipetted in duplicates into a 96-well plate. 20 µl of reagent S were added to 1 ml of reagent A and 25 µl of this mix A' were added to each well. Then, 200 µl reagent B were added to each well and after mixing and incubating for 15 min at RT, the absorbance was measured at 750 nm using an ELISA plate reader.

8.5.4.2 Sample preparation

The desired amount of protein (10-50 µg) was mixed with 5 x loading buffer (62.5 mM Tris-HCl pH 6.8, 2% SDS, 10% glycerol, 5% β-mercaptoethanol, 0.01% bromophenol blue). Before loading, the samples were denatured by boiling them for 5 min at 95°C. Samples were loaded onto the prepared gel alongside with 8 µl of pre-stained protein marker Precision Plus Protein (Bio-Rad Laboratories).

8.5.4.3 SDS-polyacrylamide gel electrophoresis (PAGE)

For gel electrophoresis, a 8% resolving gel (8% acrylamide mix, 0.39 M Tris pH 8.8, 0.1% SDS, 0.1% APS, 0.06% TEMED) was prepared and poured into a mini Polyacrylamide Electrophoresis system (BioRad Laboratories, Hercules, CA) immediately. After allowing the resolving gel to solidify, a 5% stacking gel (5% acrylamide mix, 0.13 M Tris pH 6.8, 0.1% SDS, 0.1% APS, 0.01% TEMED) was prepared and pipetted on top of

the resolving gel and a comb was inserted. The electrophoresis was performed at 80 V until the samples began separating and then at 100 V at RT using a MINI-PROTEAN® II Electrophoresis Cell tank (Bio-Rad Laboratories, Hercules, CA) in 1 x SDS running buffer (250 mM Tris (unbuffered), 250 mM glycine, 0.1% SDS).

8.5.4.4 Semi-dry protein transfer

Proteins were transferred by electrophoresis from the polyacrylamide gel to a PVDF Immobilon-FL membrane (Millipore, Cat#IPFL00010) using a Trans-Blot SD Semi-Dry Transfer Cell (Bio-Rad Laboratories). The membrane was soaked in MetOH for 1 min, then in water for 1 min and subsequently in Transfer Buffer (250 mM Tris (unbuffered), 250 mM glycine, 0.1% SDS, 20% MetOH) for 10 min. In the meantime, the gels and Whatman papers were also soaked in Transfer Buffer. Then, the gel and the PVDF membrane were sandwiched between the Whatman papers and the transfer was performed at 15 V for 30 min for one gel in the chamber and at 20 V for 45 min for two gels.

8.5.4.5 Antigen detection

The nitrocellulose membrane was blocked in milk solution (5% skim milk powder in TBST (20 mM Tris HCl pH 7.5, 150 mM NaCl, 0.05% Tween20) for 1 h at RT. For immunodetection, blots were incubated with the primary antibodies in 10 ml blocking solution or TBST and 0.02% sodium azide O/N at 4°C shaking. The day after, blots were washed (3 x 15 min) in TBST and incubated with the fluorescent secondary antibodies in 10 ml blocking solution for 1 h at RT in the dark. After the incubation, membranes were washed (3 x 15 min) with TBST and the fluorescence signal was detected using the ODYSSEY Classic Infrared Imaging System (LI-COR) and analyzed with the Odyssey 2.1 software.

8.5.5 RNA extraction

The cells were lysed with TRIzol Reagent (Invitrogen, Cat#15596-018), vortexed and left for 15 min at RT. Subsequently the samples were centrifuged at 12,000 rpm for 15 min at 4°C and the highest phase, which contains the RNA, was transferred to a new 1.5 ml Eppendorf tube. The RNA was precipitated by adding 0.5 ml of isopropanol per 1 ml solution and centrifuging at 12,000 rpm for 10 min at 4°C. The RNA pellet was washed with 1 ml of 75% EtOH (diluted in DEPC-treated water) and the samples were centrifuged at 7,500 rpm for 5 min at 4°C. The RNA pellet was then air dried for 10-15 min and dissolved in 80 μl DEPC treated dH_2O at 55°C for 10 min to allow RNA solubilization. The RNA samples were stored at -80°C.

8.5.6 Quantitative real-time PCR

8.5.6.1 Reverse transcription PCR

The reverse transcription reaction was performed via the ThermoScript RT-PCR System (Invitrogen, Cat#11146-024) according to the manufacturer's protocol. Biefly, the primers (Oligo (dT)$_{20}$), RNA (1μg) and dNTPs were mixed and denatured by incubation at 65°C for 5 min. Subsequently the cDNA Synthesis Buffer, DTT, RNaseOUT and ThermoScript RT were added to the reaction and incubated at 50°C for 60 min. The retro-transcriptase reaction was terminated by incubating the samples at 85°C for 5 min. The residual RNA was then eliminated by incubating the samples with 1 μl of RNase H at 37°C for 20 min.

8.5.6.2 SYBR green quantitative real-time PCR

SYBR based quantitative real-time PCR was performed for quantification of the transcript levels. 25 μl reactions were set up using 12.5 μl Platinum SYBR Green qPCR SuperMix-UDG with ROX (Invitrogen, Cat#11744), 5 μl cDNA (of a 1:5 dilution of the reaction mix

from the RT-PCR per well), 1 µl 10 mM forward primer, 1 µl 10 mM reverse primer and 5.5 µl dH$_2$O in a Fast 96-well Reaction Plate (Applied Biosystems, Cat#4346907). The plate was then covered with an optical adhesive cover (Applied Biosystems, Cat#4360954) and centrifuged briefly. The real-time PCR was performed using the StepOnePlus Real-Time PCR System (Applied Biosystems) with the following settings: step1: 95°C for 15 min, step2: 95°C for 15 sec, 60°C for 30 sec, 72°C for 30 sec (40 cycles) and step3: 95°C for 15 sec and 60°C for 1 min (melting curve). The data was either analyzed using the standard curve method (absolute quantification) or the comparative CT method for relative quantification. All the primers were designed to specifically amplify human transcripts.

Table 4 SYBR green quantitative real-time PCR primers

gene	forward	reverse
HOXA5	5'-GCTGCAAAACGGGGGAAATAAAG-3'	5'-TTTCCCTCGCAGTTCCATTAGGA-3'
HOXA9	5'-GAGGGGAGGGGACAGAGAGGTAG-3'	5'-CTCCGCTGCTTTATGTTCCTGCT-3'
HOXA13	5'-GGCTCCAAGAAACACCCATTCTG-3'	5'-GCAGTGGGGACAGGTCAGGTAAT-3'
HOXB5	5'-AAAGCCCAACCCCTGCTCTAAAA-3'	5'-AGTCGCCGGGAGAGAAAGAAAC-3'
HOXB6	5'-CGACTGAGAAAAGGGTTGCTGGT-3'	5'-CAATCGCTGGATTCAACCACTCA-3'
HOXB9	5'-ACGCTTTATCAGGCAGTCGGAAA-3'	5'-CCTGCTCAACTTCTCAGCCAACA-3'
HOXD10	5'-TTCCAGTTTAGAGCCTGCCTTGC-3'	5'-GATGATATATGGGCGGGCACAG-3'
HOXD11	5'-CGGGTGGAAGAGAAATCTGGAAC-3'	5'-GTCTAAGGACAGTGGGGCAGTCG-3'
HOXD13	5'-TTTATAAACGTCCCGCGATGAGC-3'	5'-TAGCCCTCTCTCCCTCTGTGAGC-3'
ZEB1	5'-GCACCTGAAGAGGACCAGAG-3'	5'-TGCATCTGGTGTTCCATTTT-3'
Fibronectin1	5'-CAGTGGGAGACCTCGAGAAG-3'	5'-TCCCTCGGAACATCAGAAAC-3'
Vimentin	5'-GAGAACTTTGCCGTTGAAGC-3'	5'-GCTTCCTGTAGGTGGCAATC-3'
N-cadherin	5'-ACAGTGGCCACCTACAAAGG-3'	5'-CCGAGATGGGGGTTGATAATG-3'
LIN28B	5'-CTGTCAGAGCATCATGCACATG-3'	5'-GGGTGGCTGTGCAACATTTT-3'
GAPDH	5'-ACCCAGAAGACTGTGGATGG-3'	5'-TCTAGACGGCAGGTCAGGTC-3'
ACTIN	5'-TTGCCGACAGGATGCAGAA-3'	5'-GCCGATCCACACGGAGTACT-3'

8.5.7 Chromatin immunoprecipitation (ChIP)

For the crosslinking, 11 x formaldehyde solution was prepared by mixing 7.1 ml Paro Fix (50 mM Hepes pH 8.0 (NaOH), 1 mM EDTA pH 8.0, 0.5 mM EGTA pH 8.0, 100 mM NaCl) with 2.9 ml Formaldehyde (stock 37%). Then 1/10 of the 11 x formaldehyde solution was added into the cell into medium, e.g. 800 µl for 8 ml medium and the medium was redistributed to the cells and incubated at RT for 10 min. The crosslinking was stopped by adding 0.125 M glycine and incubation on ice for 10 min.

To prepare the chromatin, the cells were rinsed with 5 ml cold PBS, scraped off in 1 ml PBS + 1 x Complete Protease Inhibitor EDTA-free (PI, ROCHE), collected in a 15 ml Falcon tube and centrifuged for 5 min at 600 g at 4°C. Each pellet was then resuspended in 5 ml Paro Rinse 1 (10 mM Tris pH 8.0, 10 mM EDTA pH 8.0, 0.5 mM EGTA pH 8.0, 0.25% Triton X-100) + 1 x PI and incubated for 10 min on ice, followed by centrifugation for 5 min at 600 g at 4°C. Each pellet was then resuspended in 5 ml Paro Rinse 2 (10 mM Tris pH 8.0, 1 mM EDTA pH 8.0, 0.5 mM EGTA pH 8.0, 200 mM NaCl)+ 1 x PI and incubated for 15 min on ice, followed by centrifugation for 5 min at 600 g 4°C. Then, the pellets were resuspended in 300 µl Lysis buffer (50 mM HEPES/KOH pH 7.5, 500 mM NaCl, 1 mM EDTA, 1% Triton X-100, 0.1% DOC (10 mM Tris pH 8, 0.25 M LiCl, 0.5% NP-40, 0.5% DOC, 1 mM EDTA pH 8), 0.1% SDS) + 1 x PI and incubated on ice for at least 10 min up to O/N. Then, the chromatin concentration was measured with a Fluorometer and diluted to ~150 ng/µl with Lysis buffer + PI if necessary. 300 µl aliquots of 150 ng/µl chromatin were sonicated with 30 sec of ON & 45 sec OFF cycles at HIGH & 1C settings using a Diagenode sonicator to obtain fragments in range of 300 bp-1000 bp (11 cycles). Samples were spun for 10 min at 14,000 g at 4°C and the supernatant was taken. 20 µl were reverse crosslinked as indicated for the input and the sonication size was checked on a 1.2% agarose gel.

For the immunoprecipitation, the volume of all samples was adjusted to 600 µl with Lysis buffer + PI. To pre-clear the chromatin, 40 µl tRNA pre-blocked Protein G Agarose beads (Millipore, Cat#16-266) were added per sample with a cut tip and the samples were incubated on a rotating wheel for 1 h at 4°C. Then, the samples were centrifuged for 1 min at 4°C, kept on ice for 1 min and the supernatants were collected. 6 µl chromatin (1%) for input fraction were saved and stored at -20°C. Then 5 µl of SHP2 antibody (sc-280) was added and the samples were incubated O/N at 4°C rotating. The next morning, 40 µl pre-blocked Protein G Agarose beads were added and the samples were incubated for 3 h at 4°C rotating. After the incubation, the samples were centrifuged for 1 min at 10,000 rpm at 4°C and kept on ice for 2 min before the SN was discarded. Then the beads were resuspended in 1 ml lysis buffer + 20 µl PI using a 1ml tip. After 5 min incubation RT rotating, the samples were spun for 1 min at 10,000 rpm at 4°C, kept on ice for 2 min and the SN was discarded. The wash was repeated one more time with lysis buffer and 1 x with DOC buffer (10 mM Tris pH 8, 0.25 M LiCl, 0.5% NP-40, 0.5% DOC, 1 mM EDTA pH 8). Afterwards, the beads were transferred into a new Eppendorf tube in 1 ml TE pH 8.0 and spun for 2 min at 10,000 rpm at 4°C, kept on ice for 2 min before all SN was removed. For elution, the beads were resuspended in 150 µl elution buffer (0.1 M $NaHCO_3$, 1% SDS) and incubated for 20 min at RT with overhead shaking. Then, the samples were centrifuged for 1 min at RT and the SN was saved. The elution was repeated with 150 µl elution buffer and the elutes were pooled (300 µl final volume).

To reverse the crosslinking for the IP fraction, 0.2 mg/ml RNase A was added to the 300 µl elute, vortexed, and incubated for 30 min at 37°C. Then, 10 mM EDTA, 40 mM Tris pH 6.5, 50 µg/ml proteinase K were added and the mix was incubated at 55°C for 2.5 h followed by O/N incubation at 65°C at 550 rpm shaking.

For Input fraction (6µl) or to reverse crosslink to check sonication size, the volume of the samples was adjusted to 300 µl with TE pH 8.0. Then, 0.2 mg/ml RNase A was added to the 300 µl elute, vortexed and incubated for 30 min at 37°C. Afterwards 1% SDS, 100 mM NaCl, 200 µg/ml Proteinase K were added and the mix was incubated at 55°C for 2.5 h and then O/N at 65°C shaking at 550 rpm.

To extract the chromatin for Input and IP fraction, 350 µl Buffered Phenol was added to each sample. Samples were vortexed, spun for 10 min at RT at max speed and the upper layer was transferred to a new tube. Next, 350 µl chloroform/IAA were added, vortexed, spun for 10 min at RT at max speed and the upper layer was transferred to a new tube. To precipitate the chromatin, 700 µl 100% EtOH (-20°C), 35 µl 3M NaOAc pH 5.2 and 1 µl glycogen was added. The samples were centrifuged for 2 h at 4°C, before the SN was removed and a small white pellet was visible. The pellet was washed with 70% EtOH, vortexed and spun for 20 min at 4°C. The SN was removed and the pellet was air dried, before it was resuspended in 40 µl TE and heated to 50°C for 5 min to completely dissolve. 0.5 µl of IP or Input were used for real-time PCR.

Table 5 ChIP validation primers

name	forward	reverse
ChIP_Chr1	5'-TGCGGTTTTGACCTGCGGGCCT-3'	5'-ACGCAGGCGGGGGCTGTTCTT-3'
ChIP_Chr6	5'-ACGACCACTTACCGTCGCAGGCCA-3'	5'-AGGGGCGCACGATGGTCCCG-3'
ChIP_Chr11	5'-GCAGCCAAAGTGCCATTAAAGC-3'	5'-GAGGCGAATTGCGGAGTTCTTA-3'
ChIP_control	5'-GCACCAAAGTGCCATTAAAGC-3'	5'-GAGGCGAATTGCGGAGTTCTTA-3'

8.6   In vivo experiments

8.6.1   Orthotopic xenografts

Cells were injected orthotopically into female 6 weeks old non-obese diabetic severe combined immunodeficient (NOD-SCID) mice in mammary gland 2/3 (SUM1315 NLS experiment) or in gland 4 (intravital imaging and metastasis studies). For the injections 5 x 10^5 MDA-MB-231 cells, 1 x 10^6 SUM159 or 3 x 10^6 SUM1315 cells were counted and resuspended in 100 μl of a 50% phenolred-free matrigel 50% PBS mixture. Unless otherwise indicated, the mice were treated with 200 mg/kg doxycycline (PROMIVI KIBA SA, Kaiseraugst, Switzerland) in the food as soon as the tumors became palpable (tumor diameter 2-3 mm). Tumor dimensions were measured twice weekly with a caliper in two directions, and the volume of xenografts was calculated by the formula $V = (a*b^2)/2$ where a stands for the length and b the width of the tumor. At the end of the experiment, the mice were sacrificed, the tumor and the lungs were dissected and analyzed.

8.6.2   Bioluminescence imaging in vivo

Luciferase positive cell lines were used in order to monitor xenograft tumor growth and metastases formation in vivo. Therefore D-Luciferin (Biosynth, Cat#L-8220) solution was prepared at 15 mg/ml and sterilized through a 0.2 μm filter. Luciferin was injected at 10 μl/g bodyweight (e.g. 200 μl for a 20 g mouse) intra-peritoneally (i.p.) 10-15 min before imaging. The IVIS Lumina XL imaging system (Caliper LifeSciences) was used to detect the bioluminescent signal.

8.6.3   Powderizing xenografts for immunoblotting

Snap frozen tumor pieces stored at -80°C were cooled on dry ice and quickly dipped into liquid nitrogen, before the tissue was grinded using a liquid-nitrogen cooled mortar and a ceramic pestle (Scienceware). All equipment used was cooled on dry ice making sure that

the tumor pieces and powder stayed frozen during the entire procedure. The tumor powder was either directly lysed in RIPA buffer (50 mM Tris, pH 8.0, 150 mM sodium chloride, 1% NP-40, 0.5% sodium deoxycholate, 0.1% SDS, 10 mM NaF, 2 mM PMSF, 2 mM Na_3VO_4, 1 x protease inhibitor cocktail (ROCHE)) or stored at -80°C.

8.6.4   Fixation of tissue and embedding

The dissected tumors and lungs were fixed in 3.7% PFA O/N at 4°C and kept on 70% EtOH at 4°C until they were embedded in paraffin and cut with the Microm HM 355 S (Thermo Scientific) in 3 µm thick sections. The sections were dried for 24 h at 37°C and stained to analyze them.

8.6.5   FACS analysis of circulating tumor cells

50-100 µl blood was drawn from the jugular vein of anesthetized tumor bearing mice into EDTA coated tubes and placed on ice. Red blood cells were lysed using 4 ml of red blood cell lysis buffer (SIGMA, Cat#R7757) for 15 min, centrifuged and the pellet was resuspended in another 4 ml of red blood cell lysis buffer and incubated for 15 min. Then, the cells were washed in PBS and either stained for EpCAM (APC anti-human CD326, BioLegend, Cat#324207) and analyzed on the FACSCalibur based on GFP and EpCAM expression (MDA-MB-231 xenografts) or based RFP and GFP expression (SUM159 xenografts). For both cell lines, GFP-positive CTRL miR expressing cells were cultured in the presence of dox to induce RFP expression and used as a positive controls (RFP and GFP positive) and blood from non-tumor bearing mice was used as negative controls. The gates were set according to these controls.

8.7 Immunohistochemistry

8.7.1 Hematoxylin and Eosin (H&E) staining

Paraffin sections were deparaffinated and dehydrated by incubating them for 45 min at 60°C and placing them immediately after for 2 x 3 min into Ultraclear solution. Excess Ultraclear was removed before placing the slides 2 x 3 min in 100% EtOH, followed by 3 min in 95% EtOH, 3 min in 70% EtOH and 5 min in dH$_2$O. For the Hematoxylin staining, slides were placed 3 min into Hematoxylin, rinsed with dH$_2$O and placed 5 min into tap water for bluing. Subsequently, the slides were dipped eight times into acid EtOH to destain and rinsed 2 x in tap water and then 2 min in dH$_2$O. Excess water was removed before staining the slides for 30 sec in Eosin, followed by 2 x 2 sec in 95% EtOH and 2 x 2 sec in 100% EtOH. After removing excess EtOH, the slides were placed 2 x 5 min in Neo-clear solution for clearing. After blotting off excess Neo-clear, the slides were mounted with drop of Neo-mount and dried at least 30 min at 37°C. Sections were imaged with a Nikon DX1200 camera attached to a Nikon Eclipse 600 widefield microscope using a 10 x objective.

8.7.2 CD31 staining

Staining of tumor tissues for mouse CD31 was performed automatically in a DiscoveryXT instrument (Roche Diagnostics, Mannheim). The procedure "Research IHC BlueMap XT" was used, with a mild CC1 pre-treatment, incubation with the anti-mouse CD31 (PECAM-1) rat monoclonal antibody (Dianova, Cat#DIA310) at a dilution of 1:50 for 1 h at 37°C, followed by incubation for 32 min with the secondary biotinylated anti-rat secondary antibody (Jackson Lab, Cat#712-065-153) at a dilution of 1:100 and substrate incubation for 1 h. The counterstaining was done with Hematoxylin. Sections were imaged with a Nikon DX1200 camera attached to a Nikon Eclipse 600 widefield microscope using a 4 x objective.

8.8 Proteomics

8.8.1 Purification of tyrosine phosphorylated peptides

Cells were washed with cold PBS before 1 ml Lysis Buffer (8 M urea, 200 mM ammonium bicarbonate pH 7.5, 1 x PhosSTOP (Roche), 1 mM Na_3VO_4) was added per 15 cm plate. Cells were scraped off and transferred to a 15 ml Falcon tube and incubated on ice for 10 min. Then, the cell lysates were sonicated 3 x 30 sec (placed on ice 1 min between bursts) and spun 10 min at 12,000 rpm at RT. The supernatant was transferred to a new tube.

For in-solution reduction, 1/10 of the volume of the supernatant of reduction solution (110 mM DTT) was added to a final concentration of 10 mM and incubated 1 h at RT. Then 1/10 of the volume of alkylation solution (660 mM iodoacetamide) was added to a final concentration of 55 mM and incubated for 1 h at RT in the dark. Then, the urea concentration was diluted 4 x with 50 mM ammonium bicarbonate (e.g. 15 ml were added to 5 ml of lysate). An aliquot was taken to be checked by immunoblotting later on. Then 20 µg sequencing grade trypsin (Promega, Cat#V5111) were added per tube and incubated O/N at 37°C. The next morning, the samples from before and after digest were loaded on a SDS-PAGE gel to check the digestion. Then 1% Trifluoroacetic acid (TFA) was added and incubated 10 min at RT, before centrifugation at 4,500 rpm. The supernatant was kept.

The desalting was done using Sep-Pak C18 cartridges (Waters, Cat#WAT020515). Therefore the cartridges were pre-wet with ACN 0.1% TFA and washed 2 x with 10 ml 0.1% TFA. Then, the peptide mixture was loaded onto the cartridges and washed 2 x with 10 ml 0.1% TFA. The peptides were eluted into a 15 ml Falcon tube using 5 ml 60% ACN 0.1% TFA and 5 aliquots of 1 ml were prepared and cooled at -20°C for 30 min before O/N drying in the Speedvac.

For immunoprecipitation with anti-pTyr antibodies, 50 µl of anti-pTyr (Y99)-agarose (Santa Cruz, Cat#sc-7020AC) were pipetted into low-bind Eppendorf tubes (200 µl of slurry) and washed 4 x with IP buffer (50 mM Tris pH 7.4, 150 mM NaCl, 1% Octyl β-D-glucopyranoside, 1 mM PMSF, 1 x PhosSTOP) by centrifuging 1 min and discarding the supernatant. Then the dried peptides were dissolved in 1 ml IP buffer and incubated at RT for 5 min standing and 10 min shaking to dissolve the peptides. Then, the samples were centrifuge 5 min at 12,000 rpm to remove remaining insoluble material. Afterwards, the pH was checked and adjusted 7.4 if necessary using 1.5-2 µl 1 M NaOH and 1 ml was transferred to the anti-pTyr agarose for IP and incubated O/N at 4°C rotating. The following day, the samples were centrifuged at 2,000 g for 1 min at 4°C and the supernatants were collected and stored at -20°C to monitor the pSer/pThr enrichment. The agarose beads were washed 3 x with 1 ml cold IP buffer (without PMSF) and centrifuged for 1 min at 2,000 g in between and the supernatants were discarded. The wash steps were repeated 3 x with 1 ml H_2O. Then, 50 µl of 0.5% TFA was added to the beads and the tubes were tapped on the bench several times to disperse the agarose. After 10 min incubation at RT, the samples were centrifuged for 1 min at 2,000 g and the supernatants were transferred to fresh tubes before the step was repeated by adding another 50 µl of 0.5% TFA to the beads, incubating and spinning. The supernatants were pooled and centrifuged again for 1 min at 2,000 g to remove any remaining particles and the supernatant was transferred to new tube.

For further desalting, the peptides were filtered through POROS filled tips. To prepare the tips, a small piece of C-18 extraction disk was cut and inserted into a 20 µl gel loading tip. POROS oligo-R3 powder was mixed with ACN (5 mg in 200 µl) and 10 µl of the mix were added to the tip to fill the column with POROS powder. 1.5 ml Eppendorf tubes were closed and a hole, big enough to hold the tip columns, was poked into the lid.

These tubes were used as reservoirs for the columns during centrifugation steps. All centrifugation steps were done in mini centrifuges at 6,600 rpm until the all liquid passed through the columns. For humidification, the columns were washed with 40 µl ACN 0.1% TFA followed by 2 washes with 40 µl 0.1% TFA for equilibration. Then, the tubes containing the columns were replaced by fresh ones. Then 100 µl of the peptide mixture was loaded, the flow-through kept and reloaded. The 2nd flow-through was stored at -80°C. The columns were washed 2 x with 40 µl 0.1% TFA before the tubes containing the columns were exchanged for fresh ones. Then the peptides were eluted using 40 µL 80% ACN 0.1% TFA and 60 µl of 80% ACN 2.5% TFA and 1 M glycolic acid were added to the 40 µl elute to give a total volume of 100 µl.

For further enrichment of phosphopeptides, Titanium dioxide (TiO_2) columns were used. Therefore a small piece of C8 extraction disk was cut and inserted into a 20 µl gel loading tip. 2 µg TiO_2 beads were mixed with ACN and the mix was added to the tip. Then the TiO_2 beads were washed with 80 µl 80% ACN 2.5% TFA and centrifuged until everything went through the column. After this, the beads were washed with 80 µl 80% ACN 2.5% TFA 1 M glycolic acid and the reservoir tubes were changed afterwards. Then 100 µl of the peptide mixture was loaded, the flow-through kept and reloaded. The 2nd flow-through was stored at -80°C. The columns were washed with 80 µl 80% ACN 2.5% TFA 1 M glycolic acid followed by a wash with 100 µl 80% ACN 2.5% TFA. The tubes containing the columns were exchanged before eluting the peptides with 2 x 60 µl of ammonium hydroxide solution (20 µl NH_4OH, 300 µl ACN, 680 µl H_2O). 12 µl of 100% formic acid were added before the eluted peptides were placed at -80°C for 15 min followed by 15 min lyophilization.

8.8.2   Analysis of phosphoproteomics MS data

For LC-MS/MS, the purified phosphopeptides were resuspended in 10% formic acid and injected onto a 15 cm x 75 µm ProteoPep 2 PicoFrit column (New Objectives), connected to an LTQ-OrbiTrap Elite mass spectrometer (Thermo). Buffer A consisted of dH_2O with 0.1% FA and Buffer B of 100% ACN with 0.1% FA. Peptides were separated using a 120 min gradient from 2% B to 40% B. Data acquisition was done using a 'Top 15 method', where every full MS scan was followed by 15 data-dependent scans on the 15 most intense ions from the parent scan. Full scans were performed in the Orbitrap at 120,000 resolution with target values of 10^6 ions and 200 msec injection time, while MSMS scans were done in the ion trap with 10^4 ions and 200 msec. Database searches were performed with Mascot Server using the human IPI database (version 3.87). Mass tolerances were set at 10 ppm for the full MS scans and at 0.8 Da for MSMS. Search results were validated using Scaffold (Proteome Software) and peptide identifications accepted which exceeded the 95% confidence level. In case of ambiguous assignments, spectra were manually interpreted for confirmation of identity and localization of the phosphorylation site. Label free quantification was performed on duplicate LC-MS runs for each sample using Progenesis LC-MS (Nonlinear Dynamics Software).

8.8.3   SILAC proteomics

Cells were cultured in SILAC Advanced DMEM/F12-Flex medium (Invitrogen, Cat#06-0032DK) without arginine (Arg) and lysine (Lys), which was supplemented with $^{12}C_6$ (Arg) and $^{12}C_6^{14}N_2$ (Lys) for the light normal growth medium and with SILAC $[U-^{13}C_6]$-L-Lysine (Lys*) and SILAC $[U-^{13}C_6^{15}N_4]$-L-Arginine (Arg*) (Invitrogen) for the heavy growth medium. The medium was further supplemented with SILAC Glucose (Invitrogen, Cat#06-033SA), L-glutamine (Invitrogen, Cat#25030-149) and dialyzed FBS (Invitrogen,

Cat#26400) and cell line specific additives. Cells were cultured for at least 5 passages in SILAC medium and the level of incorporation was measured by mass spectrometry to be > 95%.

Cells were either harvested as whole cell lysates (WCL) or separated into nuclear and cytosolic fraction and immunoprecipitated using anti-SHP2 antibodies. 20 µl buffer with reducing agent was added to each sample and the beads were boiled for 10 min at 70°C. Then, the samples were mixed with loading dye and run on a 4-12% pre-cast gradient gel in MOPS SDS running buffer (50 mM MOPS, 50 mM Tris Base, 0.1% SDS, 1 mM EDTA, pH 7.7) for 10 min at 30 mA then 1 h at 60 mA. Afterwards, the gel was stained with Coomassie blue (0.1% Coomassie Brilliant Blue R-250, 50% MetOH and 10% glacial acetic acid) for 1 h at RT and destained (10% MetOH and 10% glacial acetic acid) O/N at 4°C.

The next day, the bands were cut in small pieces and each gel piece was placed in a separate well of a 96-well plate. To prepare the samples for MS analysis, the gel pieces were washed 3 x with 150 µl 50% ACN + 50% 50 mM NH_4CO_3, followed by 10 min incubation with 150 µl 100% ACN for dehydration. For reduction, 50 µl 10 mM DTT were added and the mix was incubated at 65°C for 45 min. Afterwards, 50 µl 55 mM iodoacetamide solution was added and the mix was incubated at RT in the dark for 30 min for alkylation. Then, the gel pieces were washed with 150 µl 50 mM NH_4CO_3 for 10 min at RT shaking followed by a dehydration step with 150 µl 100% ACN for 10 min at RT. Finally 20 µl Trypsin (Promega, Cat#V5280) was added to each well, followed by 50 µl NH_4CO_3 and the gel pieces were incubated at 37°C O/N.

The next morning, 5 µl of 50% formic acid was added to each well to stop the tryptic reaction and the first peptides were collected in the collection plate by centrifugation for 2 min at 1,500 rpm. 50 µl collection buffer (50% ACN, 1% formic acid)

was added to each well and incubated for 20 min at RT, before the plate was centrifuged for the 2nd collection of peptides. Then, the plate was put into the speedvac for 2-3 h to dry the mixed peptide collection. Samples were analyzed on the MS XL Orbitrap.

8.9 Computational analysis

8.9.1 Motif activity response analysis

We used motif activity response analysis (MARA) (Suzuki, Forrest et al. 2009) to model genome-wide gene expression patterns in terms of computationally predicted transcription factor binding sites. We calculated the means and standard errors of the activities of over 200 human regulatory motifs in the CTRL, SHP2 miR1 and SHP2 miR2 samples, identifying those motifs that were consistently downregulated in both SHP2 miR1 and SHP2 miR2 samples.

8.9.2 Analysis of let-7 target genes from microarray data

Contrasts between SHP2 miRs samples – CTRL miR were calculated for both MCF10A-HER2/3 cells grown in 3D cultures and BT474 tumors in the presence or absence of SHP2. Using the TargetScan 5.1 resource (www.targetscan.org), we defined three groups of expressed genes (average log2 expression level greater than 4.0): genes that are not targeted by let-7, genes that are predicted let-7 targets and genes that are the 100 most likely let-7 targets sorted by TargetScan scores. For each group of genes, we plotted the relative frequency (density) of log2-fold changes induced by SHP2 knockdown.

8.9.3 Microarray analysis

Total RNA was extracted with TRIzol reagent from BT474 tumors. RNA was processed, hybridized to GeneChip Human Gene 1.0 ST arrays (Affymetrix, Santa Clara, CA) and scanned according to the manufacturer's instructions. All gene arrays were processed in R (www.r-project.org) using bioconductor and the package oligo. Robust multi-array average (RMA) was performed using the following command: expr <- rma(read.celfiles (filenames, pkgname="pd.hugene.1.0.st.v1"), target="probeset"). Expressions for transcript clusters were calculated by averaging corresponding probeset values (using array annotation from Affymetrix). We plotted the contrast between SHP2 miR1–CTRL miR and SHP2 miR2–CTRL expressing tumors and found that 210 Affymetrix IDs were either upregulated or downregulated in both SHP2 miRs expressing tumors. Out of these 210 IDs, 182 had a human gene annotation. 180 genes were downregulated whereas only 2 were upregulated in SHP2 miR1/2 tumors. These 180 downregulated genes were considered as the "SHP2 signature".

For the transcriptome analysis of the SUM1315 xenografts expressing SHP2 NLS wt, SHP2 NLS deleted or NLS mutated constructs, RNA was extracted from three biological replicates per condition using TRIzol reagent and further purified using the RNeasy Plus Mini Kit (QIAGEN) according to the manufacturer's instructions. RNA concentration was measured using a NanoDrop ND-1000 and the quality of the RNA assessed using the Agilent 2100 bioanalyzer and RNA Nano Chip. Aliquots (100 ng) of extracted total RNA were amplified using the Ambion WT Expression Kit and the resulting sense-strand cDNA was fragmented and labeled using the Affymetrix GeneChip WT Terminal Labeling Kit. Affymetrix GeneChip Human Gene 1.0 ST arrays were hybridized following the GeneChip Whole Transcript (WT) Sense Target Labeling Assay Manual (Affymetrix) with a hybridization time of 16 h. The Affymetrix Fluidics protocol

FS450_0007 was used for washing. Scanning was performed with Affymetrix GCC Scan Control version 3.0.0.1214 on a GeneChip Scanner 3000 with autoloader. Probe sets were summarized and probeset level values normalized with the justRMA() function from the R (version 2.12.0)/Bioconductor (version 2.6) package affy using annotation as provided by Bioconductor. Differentially expressed genes were identified using the R package limma (Gentleman, Carey et al. 2004) and by selecting genes with a minimum absolute log2 fold change of at least 1.5 and a P-value of <= 0.05 and an average expression of at least 4. Venn diagrams were drawn using the overLapper() and vennPlot() functions of the limma package. Top 10 up- or downregulated gene lists were created sorted by logFC.

8.9.4 Analysis of public microarray data

CEL files were downloaded (http://www.ncbi.nlm.nih.gov/geo , accessions: GSE12276 for the Bos dataset, GSE2034 for the Wang dataset, GSE1456 for the Stockholm dataset and GSE2109 for the Bittner dataset) and normalized using gcrma from R/bioconductor. Probesets were linked to genes using Affymetrix annotation, and for genes represented by multiple probesets, the one with maximal variance across samples was selected. Genes not clearly detected (average log2 level below 4.0) were removed. For clustering and visualization, Z-scores were calculated from expression levels of each gene by subtracting the mean and dividing by the standard deviation. Patients were split into two groups by k-means clustering, and expression polarization was defined as the absolute difference between the mean expression levels over genes and patients in each group.

8.10 Statistical Analysis

All values represent mean ± SEM of at least 3 independent experiments unless otherwise indicated. Normally distributed data was analyzed by the Student's t-test or Fisher`s exact test, otherwise a Mann-Whitney test was used. P-values of < 0.05 were considered a statistically significant difference.

9 APPENDICES

9.1 Abbreviations

2D	Two-dimensional
3D	Three-dimensional
4D	Four-dimensional
ACN	Acetonitrile
AD	Anno Domini
ADH	Atypical ductal hyperplasia
Ala	Alanine (A)
AML	Acute myelogenous leukemia
APS	Ammonium persulfate
Arg	Arginine (R)
Asp	Aspartic acid (D)
BC	Before Christ
BCR	Breakpoint cluster region protein
BCR-ABL	ABL kinase-BCR protein fusion
bona fide	Latin: in good faith
bp	Base pair
BSA	Bovine serum albumin
CagA	Cytotoxin-associated gene A
CAS	Crk-associated substrate
Cat#	Catalogue number
CD	Cluster of differentiation
ChIP	Chromatin immunoprecipitation
CIP	Calf-intestinal alkaline phosphatase
CSC	Cancer stem cell
Csk	c-Src kinase
c-Src	Cellular Src
CTC	Circulating tumor cell
CTRL	Control
Cys	Cysteine (C)
D2S	Distance to start
DAPI	4′,6-diamidino-2-phenylindole
DCIS	Ductal Carcinoma in situ
de novo	Latin: from the beginning
del	NLS deleted
DEPC	Diethylpyrocarbonate
DMEM	Dulbecco's modified eagle's medium
DMSO	Dimethyl sulfoxide
DNA	Deoxyribonucleic acid
dNTPs	Deoxyribonucleotides
Dox	Doxycyline
DTT	Dithiothreitol
E. coli	Escherichia coli
ECM	Extracellular matrix
EGF(R)	Epidermal growth factor (receptor)
EMT	Epithelial-Mesenchymal Transition
EpCAM	Epithelial cell adhesion molecule
ER	Estrogen receptor
ERBB2	Epidermal growth factor receptor 2 (HER2)
ERK	Extracellular signal-regulated kinase
EtOH	Ethanol
FA	Formic acid
FACS	Fluorescence-activated cell sorting
FAK	Focal adhesion kinase
FBS	Fetal bovine serum
FEA	Flat epithelial atypia
FGF(R)	Fibroblast growth factor (receptor)
FRET	Fluorescence resonance energy transfer
GAB2	GRB2-associated binding protein 2
GAP	GTPase-activating proteins
GAPDH	Glyceraldehyde-3-phosphate dehydrogenase
GEF	Guanine-nucleotide exchange factors
GFP	Green fluorescent protein
GOF	Gain-of-function
GRB2	Growth factor receptor-bound protein 2
Gαi2	Guanine nucleotide-binding protein Gi, alpha 2 subunit
h	hour/s
H&E	Hematoxilin & Eosin
H. pylori	Helicobacter pylori
HCC	Hepatocellular carcinoma
HEK 293	Human embryonic kidney cells
HER2	Epidermal growth factor receptor 2
HGF	Hepatocyte growth factor
HR	Hormone receptor
HS	Horse serum
HSP90	Heat shock protein 90
i.p.	Intra-peritoneal
IDC	Infiltrating ductal carcinoma
IF	Immunofluorescence
IGF-I	Insulin-like growth factor I
IgG	Immunoglobulin G
IHC	Immunohistochemistry
IL6	Interleukin 6
in vitro	Latin: in glass
in vivo	Latin: in the living
IP	Immunoprecipitation
IVM	Intravital multiphoton
Jak	Janus kinase
JMML	Juvenile myelomonocytic leukemia

KCL	Potassium chloride		Rac	Ras-related C3 botulinum toxin substrate
kDa	kilo Dalton			
LB medium	Luria-Bertani		RET	Rearranged during transformation kinase
LC-MS/MS	Liquid chromatography-mass spectrometry		RhoA	Ras homolog gene family member A
LINE	Long interspersed nuclear elements		RISC	RNA-induced silencing complex
LOF	Loss-of-function		ROI	Region of interest
LS	LEOPARD syndrome		rpm	Rounds per minute
Lys	Lysine (K)		RPMI	Roswell Park Memorial Institute
mA	Milliampere			
MAPK	Mitogen-activated protein kinase		RT	Room temperature
			RTK	Receptor tyrosine kinases
MET	Mesenchymal-Epithelial Transition		SCID	Severe combined immunodeficient
MetOH	Methanol		SDS	Sodium dodecyl sulfate
min	Minute/s		sec	Second/s
ml	Milliliter/s		SEM	Standard error of the mean
MOI	Multiplicity of infection		Ser	Serine (S)
MOPS	3-(N-orpholino) propane sulfonic acid		SFK	Src family kinase
			SH2	Src homology 2
MPM	Multiphoton microscope		SHP1	Src-homology phosphotyrosyl phosphatase-1
MS	Mass spectrometry			
msec	Millisecond/s		SHP2	Src-homology phosphotyrosyl phosphatase-2
mTOR	Mammalian target of rapamycin			
mut	NLS mutated		SILAC	Stable isotope labeling by amino acids in cell culture
NaCl	Sodium chloride			
NGS	Normal goat serum		SINE	Short interspersed nuclear elements
NLS	Nuclear localization signal			
nm	Nanometer/s		SN	Supernatant
NOD	Non-obese diabetic		SRC	Gene encoding c-Src
NPC	Nuclear pore complexe		STAT	Signal transducer and activator of transcription
NRG	Neuregulin			
NS	Noonan syndrome		TBNC	Triple-negative breast cancers
NSCC	Non-stem cancer cell		TBS	Tris buffered saline
O/N	Overnight		TEMED	Tetramethylethylenediamine
OD_{600}	Optical density at 600 nm		TERT	Telomerase reverse transcriptase
PAGE	Polyacrylamide gel electrophoresis			
			TFA	Trifluoroacetic acid
PARP	Poly (ADP-ribose) polymerase		TGFα	Transforming growth factor alpha
PBS	Phosphate buffered saline			
PCR	Polymerase chain reaction		Thr	Threonine (T)
PDGF(R)	Platelet-derived growth factor (receptor)		TIC	tumor initiating cell
			TiO_2	Titanium dioxide
PEI	Polyethylenimine		TKI	Tyrosine kinase inhibitor
PFA	Paraformaldehyde		tRFP	Turbo red fluorescent protein
PI3K	Phosphatidylinositol 3-kinase		Tyr	Tyrosine (Y)
PMSF	Phenylmethylsulfonyl fluoride		ULA	Ultra low attachment
PR	Progesterone receptor		VEGF(R)	Vascular endothelial growth factor (receptor)
Pro	Proline (P)			
PTK	Protein tyrosine kinase		v-Src	Viral SRC
PTP	Protein tyrosine phosphatase		WCL	Whole cell lysates
PTPN11	Gene encoding SHP2		WHO	World Health Organization
PTPN6	Gene encoding SHP1		wt	Wild-type
$Puro_R$	Puromycin resistance cassette		μg	Microgram/s
PZR	Protein zero-related		μl	Microliter/s
qPCR	Quantitative real-time PCR		μm	Micrometer/s

9.2 SHP2 phosphoproteomics list

Description	Peptide sequence	Log2 ratios KD/wt
SRC	EERPTFEYLQAFLEDYFTSTEPQYQPGENL	3.61
YES1	DERPTFEYIQSFLEDYFTATEPQYQPGENL	3.48
FYN	ERPTFEYLQSFLEDYFTATEPQYQPGENL	3.27
PIK3R1	SREYDRLYEEYTR	3.05
CRIM1	QNHLQADNFYQTV	2.74
LYN	AEERPTFDYLQSVLDDFYTATEGQYQQQP	1.97
MAPK8	TAGTSFMMTPYVVTR	1.89
GAB1	HVSISYDIPPTPGNTYQIPR	1.73
PARVB	QLEEDLYDGQVLQK	1.70
PIK3R2	EYDQLYEEYTR	1.67
PKM2	EAEAAIYHLQLFEELRR	1.64
LIMD1	VFCEEDFLYSGFQQSADR	1.50
LCK	SVLEDFFTATEGQYQPQP	1.50
PRKCD	RSDSASSEPVGIYQGFEK	1.46
TMEM192	AKPEPDILEEEKIYAYPSNITSETGFR	1.44
GAB1	APSASVDSSLYNLPR	1.43
PTPRE	VVQDFIDIFSDYANFK	1.39
BCR	GHGQPGADAEKPFYVNVEFHHER	1.35
CTNND1	SYEDMIGEEVPSDQYYWAPLAQHER	1.30
DCBLD1	AHTFSAQSGYRVPGPQPGHK	1.28
FLNB	AIVHDNKDGTYAVTYIPDK	1.27
PIK3R1	EYDRLYEEYTR	1.25
DLG3	RDNEVDGQDYHFVVSR	1.23
TNS3	QQQMVVAHQYSFAPDGEAR	1.17
MYH9	ALELDSNLYR	1.17
EFNB1	VSGDYGHPVYIVQEMPPQSPANIYYKV	1.16
PIK3CB	ERVPFILTYDFIHVIQQGK	1.13
ACP1	QLIIEDPYYGNDSDFETVYQQCVR	1.05
CAV1	YVDSEGHLYTVPIR	0.98
TLN2	AVGSSMAQLLTCAAQGNEHYTGVAAR	0.97
DAB2IP	QLLAPLSFQNPVYQMAAGLPLSPR	0.96
PTPRA	VVQEYIDAFSDYANFK	0.96
TLN1	TMQFEPSTMVYDACR	0.92
CAV1	YVDSEGHLYTVPIR	0.92
CTNND1	HYEDGYPGGSDNYGSLSR	0.87
GDI2	TDDYLDQPCYETINR	0.86
SGK223	LNLSHSETNVHDESHFSYSLSPGNR	0.86
CLTC	ALEHFTDLYDIKR	0.83
PTK2	AAAYLDPNLNHTPNSSTK	0.82
TLN1	EAAAQAAYLVGVSDPNSQAGQQGLVEPT	0.81
PEAK1	NAIKVPIVINPNAYDNLAIYK	0.79

TENC1	GPLDGSPYAQVQRPPR	0.78
PKM2	TATESFASDPILYRPVAVALDTK	0.77
EEF1A2	STTTGHLIYK	0.76
NCK1	PDSASPADDSFVDPGERLYDLNMPAYVK	0.75
TLN1	TLAESALQLLYTAK	0.72
LPXN	STLQDSDEYSNPAPLPLDQHSR	0.72
PEAK1	NAIKVPIVINPNAYDNLAIYK	0.71
TKT	NMAEQIIQEIYSQIQSK	0.71
KIRREL	AIYSSFKDDVDLK	0.70
MAGI1	IEDPVYGIYYVDHINR	0.68
EEF1A1	EHALLAYTLGVK	0.67
CCDC50	PARPPPPIMTDGEDADYTHFTNQQSSTR	0.64
TXNRD1	KVVYENAYGQFIGPHR	0.63
EPHB4	FLEENSSDPTYTSSLGGK	0.61
CTNNA1	ATASDDASQHQGGGGGELAYALNNFDK	0.59
DCBLD1	TFRPMDTDAEEAGVSTDAGGHYDCPQR	0.57
PIK3R1	DQYLMWLTQK	0.56
FLNA	KTHIQDNHDGTYTVAYVPDVTGR	0.54
AFAP1L2	VAQQPLSLVGCEVVPDPSPDHLYSFR	0.53
DYRK1A	KVYNDGYDDDNYDYIVK	0.51
GIT1	LQPFHSTELEDDAIYSVHVPAGLYR	0.45
TLN1	AVSSAIAQLLGEVAQGNENYAGIAAR	0.45
STAT3	YCRPESQEHPEADPGAAPYLK	0.44
SET	IDFYFDENPYFENK	0.43
MSN	APDFVFYAPR	0.43
INPPL1	NSFNNPAYYVLEGVPHQLLPPEPPSPAR	0.42
CDCP1	GPAVGIYNGNINTEMPR	0.41
PXN	ECFTPFVNGSFFEHDGQPYCEVHYHER	0.41
KIRREL	EEYEMKDPTNGYYNVR	0.40
TJP1	RYEPIQATPPPPPLPSQYAQPSQPVTSASL	0.40
USP6NL	ASPAAEDASPSGYPYSGPPPPAYHYR	0.38
CTTN	LPSSPVYEDAASFK	0.38
PEAK1	ACSVEELYAIPPDADVAK	0.37
MYH9	YLYVDKNFINNPLAQADWAAK	0.34
PTK2	CIGEGQFGDVHQGIYMSPENPALAVAIK	0.32
PTK2	KPPRPGAPGHLGSLASLSSPADSYNEGVK	0.30
TYK2	LLAQAEGEPCYIR	0.28
KIAA1217	NEGFYADPYLYHEGR	0.26
INPPL1	NSFNNPAYYVLEGVPHQLLPPEPPSPAR	0.26
SEPT2	QQPTQFINPETPGYVGFANLPNQVHR	0.26
TWF1	KIEIDNGDELTADFLYEEVHPK	0.25
MAPK7	GLCTSPAEHQYFMTEYVATR	0.25
BCAR1	GLPPSNHHAVYDVPPSVSK	0.24
BCAR1	HLLAPGPQDIYDVPPVR	0.24
CARKD	IGVVGGCQEYTGAPYFAAISALK	0.23
RPLP0	IIQLLDDYPK	0.23
CDCP1	SPPESESEPYTFSHPNNGDVSSK	0.23
SHC1	ELFDDPSYVNVQNLDK	0.22

EPHA2	TYVDPHTYEDPNQAVLK	0.21
ACTN1	AIMTYVSSFYHAFSGAQK	0.19
STAT3	YCRPESQEHPEADPGSAAPYLK	0.19
FLNB	ESPLQFYVNYPNSGSVSAYGPGLVYGVA	0.19
SEPT9	APVDFGYVGIDSILEQMR	0.19
PEAK1	VPIVINPNAYDNLAIYK	0.17
YES1	LIEDNEYTAR	0.16
WDR1	AHDGGIYAISWSPDSTHLLSASGDK	0.16
ROS1	QVAYCPSGKPEGLNYACLTHSGYGDGSD	0.15
STARD13	VDDLYTLLPR	0.15
ANXA2P2	SLYYYIQQDTK	0.15
GIT1	LQPFHSTELEDDAIYSVHVPAGLYR	0.14
GAB1	HGMNGFFQQQMIYDSPPSR	0.14
PDLIM1	VITNQYNNPAGLYSSENISNFNNALESK	0.14
CTNND1	HQDHSHLLYSTIPR	0.13
TLN1	VSQMAQYFEPLTLAAVGAASK	0.13
LPP	GQIYGSGPQGYNTQPVPVSGQCPPPSTR	0.11
PKP4	SAVSPDLHITPIYEGR	0.09
MAPK1	VADPDHDHTGFLTEYVATR	0.07
ZDHHC5	LVPTGPTHREPSPVRYDNLSR	0.01
PRPF4B	LCDFGSASHVADNDITPYLVSR	0.00
LIMD1	SAFHQPGPCEDPSCLTHGDYYDNLSLA	0.00
TNS3	WDSYENLSADGEVLHTQGPVDGSLYAK	-0.01
HARS	LIYDLKDQGGELLSLR	-0.03
EGFR	GSHQISLDNPDYQQDFFPK	-0.03
MAPK3	IADPEHDHTGFLTEYVATR	-0.03
BCAR1	GPNGRDPLLEVYDVPPSVEK	-0.04
PTK2	THAVSVSETDDYAEIIDEEDTYTMPSTR	-0.05
ANKS1A	EEDEHPYELLLTAETK	-0.06
FCHSD2	SPKPHASLPPLPLYDQPPSSPYPSPDKR	-0.06
PKP4	TVHDMEQFGQQQYDIYER	-0.07
FERMT2	QSEDEALELEGPLITPGSGSIYSSPGLYSK	-0.08
FLNA	LQVEPAVDTSGVQCYGPGIEGQGVFR	-0.08
FXR1	VLKDPDSNPYSLLDNTESDQTADTDASE	-0.09
NEDD9	GPVFSVPVGEIKPQGVYDIPPTK	-0.09
NEDD9	DGVYDVPLHNPPDAK	-0.10
PKM2	EAEAAIYHLQLFEELR	-0.12
CTNND1	LNGPQDHSHLLYSTIPR	-0.14
ARHGAP35	SSPWLPQDGFDPSDYAEPMDAVVKPR	-0.15
RAB9A	EFIYYADVKEPESFPFVILGNK	-0.16
PFKP	NESCSENYTTDFIYQLYSEEGK	-0.16
LIMS1	VYKEFCDFYAK	-0.17
PHPT1	IHVYGYSMAYGPAQHAISTEK	-0.18
BCAR1	VLPPEVADGGVVDSGVYAVPPPAER	-0.19
TRIP6	VNFCPLPSEQCYQAPGGPEDR	-0.20
PIK3R2	NETEDQYALMEDEDDLPHHEER	-0.21
TNK2	KPTYDPVSEDQDPLSSDFKR	-0.22
ARHGAP12	ATTPPNQGRPDSPVYANLQELK	-0.22

ARRB2	DFVDHLDKVDPVDGVVLVDPDYLKDR	-0.22
SPTAN1	QVEELYHSLLELGEK	-0.22
TWF2	KIEIGDGAELTAEFLYDEVHPK	-0.23
CTTN	GPVSGTEPEPVYSMEAADYR	-0.23
EPHA2	SEQLKPLKTYVDPHTYEDPNQAVLK	-0.25
PEAK1	VPIVINPNAYDNLAIYK	-0.26
PLEKHN1	DPGYDHLWDETLSSSHQK	-0.27
SNORA6	ADHQPLTEASYVNLPTIALCNTDSPLR	-0.27
ENO2	AAVPSGASTGIYEALELR	-0.29
DDX3X	KGADSLEDFLYHEGYACTSIHGDR	-0.30
ACTB	TTGIVMDSGDGVTHTVPIYEGYALPHAILR	-0.32
EPHA2	SEQLKPLKTYVDPHTYEDPNQAVLK	-0.32
SLC38A2	FSISPDEDSSSYSSNSDFNYSYPTK	-0.33
PHLDB2	DLPHSVIDNDNYLNFSSLSSGALPYK	-0.33
NEDD9	DVYDIPPSHTTQGVYDIPPSSAK	-0.33
PTK2	EDGSLQGPIGNQHIYQPVGKPDPAAPPK	-0.35
CRKL	TLYDFPGNDAEDLPFK	-0.36
RASAL2	ALNQPGGLQPLSFQNPVYHLNNPIPAMPK	-0.36
LDHA	ATLKDQLIYNLLK	-0.37
ZDHHC8	DSLFGDSGVYDAPSSYSLQQASVLSEGPR	-0.39
LDHA	DQLIYNLLK	-0.39
BCAR1	GLLPSQYGQEVYDTPPMAVK	-0.39
NEDD9	QAGRPDLRPEGVYDIPPTCTKPAGK	-0.39
PIK3R1	EWLGNENTEDQYSLVEDDEDLPHHDEK	-0.40
SLC38A2	SHYADVDPENQNFLLESNLGK	-0.41
EPHA2	TYVDPHTYEDPNQAVLK	-0.41
ACLY	TTDGVYEGVAIGGDR	-0.42
LDLR	TTEDEVHICHNQDGYSYPSR	-0.42
EPHB4	VYIDPFTYEDPNEAVR	-0.43
PSMA2	LAQQYYLVYQEPIPTAQLVQR	-0.44
TNS3	LSLGQYDNDAGGQLPFSK	-0.45
BCAR1	AQQGLYQVPGPSPQFQSPPAK	-0.47
NAT10	EELEALFLPYDLKR	-0.48
NEDD9	HQSLSPNHPPPQLGQSVGSQNDAYDVPR	-0.49
DCBLD1	HEYALPLAPPEPEYATPIVER	-0.50
FER	GAQLHQNQYYDITLPLLLDSLQK	-0.51
PARD3	ISHSLYSGIEGLDESPSR	-0.53
NEDD9	YQKDVYDIPPSHTTQGVYDIPPSSAK	-0.53
CRK	GGPEGPYAQPSVNTPLPNLQNGPIYAR	-0.54
VIM	SLYASSPGGVYATR	-0.55
CTTN	LPSSPVYEDAASFK	-0.56
PTK2	THAVSVSETDDYAEIIDEEDTYTMPSTR	-0.57
TUBB2C	NSSYFVEWIPNNVK	-0.58
BCAR1	DPLLEVYDVPPSVEK	-0.59
NEDD9	SLSPNHPPPQLGQSVGSQNDAYDVPR	-0.59
RIN1	EKPAQDPLYDVPNASGGQAGGPQRPGR	-0.59
BCAR1	VGQGYVYEAAQPEQDEYDIPR	-0.60
NEDD9	DVYDIPPSHTTQGVYDIPPSSAK	-0.61

SIRPA	EYASIQTSPQPASEDTLTYADLDMVHLNR	-0.61
ERBB2IP	SATLLYDQPLQVFTGSSSSSDLISGTK	-0.61
ANKS1A	IIASLADRPYEEPPQKPPR	-0.62
PCBP2	IPYRPKPSSSPVIFAGGQAYTIQGQYAIPQP	-0.63
OSMR	PGPCICFENLTYNQAASDSGSCGHVPVSP	-0.63
ELMO2	EPSSYDFVYHYG	-0.63
PTK2	LSRGSIDREDGSLQGPIGNQHIYQPVGKPDPAAPPK	-0.63
TNK2	VSSTHYYLLPERPSYLER	-0.65
ARHGEF7	SLVDTVYALKDEVQELR	-0.69
GDI2	NPYYGGESASITPLEDLYK	-0.73
MPZL1	SLPSGSHQGPVIYAQLDHSGGHHSDK	-0.74
NCK1	LYDLNMPAYVK	-0.74
BCAR1	EETYDVPPAFAK	-0.76
IRS2	APYTCGGDSDQYVLMSSPVGR	-0.82
SDCBP	QTAFSANPANPAILSEASAPIPHDGNLYPR	-0.82
EPHA3	TYVDPHTYEDPTQAVHEFAK	-0.88
RFFL	MQAYSNPGYSSFPSPTGLEPSCK	-0.89
ARPC3	DTDIVDEAIYYFK	-0.92
DCBLD2	AGKPGLPAPDELVYQVPQSTQEVSGAGR	-0.95
CASP8	GIIYGTDGQEAPIYELTSQFTGLK	-0.95
NUDT3	VLQYHKPVQASYFETLR	-0.95
DCBLD1	AGRHEYALPLAPPEPEYATPIVER	-0.96
DCBLD1	GGFSPVAGVGAQDGDYQRPHSAQPADR	-1.02
TFRC	SAFSNLFGGEPLSYTR	-1.04
HSPA8	GPAVGIDLGTTYSCVGVFQHGK	-1.05
CRKL	YGIPEPAHAYAQPQTTTPLPAVSGSPGAAI	-1.06
FRK	HGHYFVALFDYQAR	-1.06
PXN	FIHQQPQSSSPVYGSSAK	-1.11
DCBLD1	HEYALPLAPPEPEYATPIVER	-1.11
ARHGAP12	ATTPPNQGRPDSPVYANLQELK	-1.13
PTPN11	IQNTGDYYDLYGGEK	-1.15
PKP4	NNYALNTTATYAEPYRPIQYR	-1.16
HMGB1	RPPSAFFLFCSEYRPK	-1.20
LASP1	PHHIPTSAPVYQQPQQQPVAQSYGGYK	-1.23
DCBLD1	AGVGAQDGDYQRPHSAQPADRGYDRPK	-1.35
TJP2	HPDIYAVPIK	-1.36
DNAJA1	NVVHQLSVTLEDLYNGATR	-1.42
PDLIM5	YTEFYHVPTHSDASK	-1.50
SIRPA	NNHTEYASIQTSPQPASEDTLTYADLDMVH	-1.54
SGK223	EATQPEPIYAESTKR	-1.71
HNRNPA2B1	GDGYNGYGGGPGGGNFGGSPGYGGGR	-1.74
BCAR3	VPSSPSAWLNSEANYCELNPAFATGCGR	-1.76
EPHA3	TYVDPHTYEDPTQAVHEFAK	-1.78
ITSN2	EEPEALYAAVNK	-1.83
ANXA2P2	LSLEGDHSTPPSAYGSVK	-1.87
CDK3	IGEGTYGVVYK	-2.06
EPHA2	VLEDDPEATYTTSGGK	-2.12
PKP4	NNYALNTTATYAEPYRPIQYR	-2.40

ARHGAP35	NEEENIYSVPHDSTQGK	-2.80
MPZL1	SESVVYADIR	-2.94
CDK3	IGEGTYGVVYK	-2.95
LPP	NDSDPTYGQQGHPNTWK	-3.01
PXN	VGEEEHVYSFPNK	-3.23
GSK3A	GEPNVSYICSR	-3.46

9.3 List of figures

9.4   List of tables

10 REFERENCES

Abercrombie, M., J. E. Heaysman and S. M. Pegrum (1971). "The locomotion of fibroblasts in culture. IV. Electron microscopy of the leading lamella." Exp Cell Res **67**(2): 359-367.

Aceto, N., N. Sausgruber, H. Brinkhaus, D. Gaidatzis, G. Martiny-Baron, G. Mazzarol, S. Confalonieri, M. Quarto, G. Hu, P. J. Balwierz, M. Pachkov, S. J. Elledge, E. van Nimwegen, M. B. Stadler and M. Bentires-Alj (2012). "Tyrosine phosphatase SHP2 promotes breast cancer progression and maintains tumor-initiating cells via activation of key transcription factors and a positive feedback signaling loop." Nat Med **18**(4): 529-537.

Aceto, N., N. Sausgruber, H. Brinkhaus, D. Gaidatzis, G. Martiny-Baron, G. Mazzarol, S. Confalonieri, M. Quarto, G. Hu, P. J. Balwierz, M. Pachkov, S. J. Elledge, E. van Nimwegen, M. B. Stadler and M. Bentires-Alj (2012). "Tyrosine phosphatase SHP2 promotes breast cancer progression and maintains tumor-initiating cells via activation of key transcription factors and a positive feedback signaling loop." Nature medicine **18**(4): 529-537.

Adachi, M., M. Sekiya, T. Miyachi, K. Matsuno, Y. Hinoda, K. Imai and A. Yachi (1992). "Molecular cloning of a novel protein-tyrosine phosphatase SH-PTP3 with sequence similarity to the src-homology region 2." FEBS Lett **314**(3): 335-339.

Agazie, Y. M. and M. J. Hayman (2003). "Development of an efficient "substrate-trapping" mutant of Src homology phosphotyrosine phosphatase 2 and identification of the epidermal growth factor receptor, Gab1, and three other proteins as target substrates." The Journal of biological chemistry **278**(16): 13952-13958.

Agazie, Y. M., N. Movilla, I. Ischenko and M. J. Hayman (2003). "The phosphotyrosine phosphatase SHP2 is a critical mediator of transformation induced by the oncogenic fibroblast growth factor receptor 3." Oncogene **22**(44): 6909-6918.

Aguilar, H., X. Sole, N. Bonifaci, J. Serra-Musach, A. Islam, N. Lopez-Bigas, M. Mendez-Pertuz, R. L. Beijersbergen, C. Lazaro, A. Urruticoechea and M. A. Pujana (2010). "Biological reprogramming in acquired resistance to endocrine therapy of breast cancer." Oncogene **29**(45): 6071-6083.

Aguirre-Ghiso, J. A. (2007). "Models, mechanisms and clinical evidence for cancer dormancy." Nat Rev Cancer **7**(11): 834-846.

Ahmad, S., D. Banville, Z. Zhao, E. H. Fischer and S. H. Shen (1993). "A widely expressed human protein-tyrosine phosphatase containing src homology 2 domains." Proc Natl Acad Sci U S A **90**(6): 2197-2201.

Al-Hajj, M., M. S. Wicha, A. Benito-Hernandez, S. J. Morrison and M. F. Clarke (2003). "Prospective identification of tumorigenic breast cancer cells." Proc Natl Acad Sci U S A **100**(7): 3983-3988.

Alonso, A., J. Sasin, N. Bottini, I. Friedberg, I. Friedberg, A. Osterman, A. Godzik, T. Hunter, J. Dixon and T. Mustelin (2004). "Protein tyrosine phosphatases in the human genome." Cell **117**(6): 699-711.

Andersen, J. N., O. H. Mortensen, G. H. Peters, P. G. Drake, L. F. Iversen, O. H. Olsen, P. G. Jansen, H. S. Andersen, N. K. Tonks and N. P. Moller (2001). "Structural and evolutionary relationships among protein tyrosine phosphatase domains." Mol Cell Biol **21**(21): 7117-7136.

Arpino, G., C. Gutierrez, H. Weiss, M. Rimawi, S. Massarweh, L. Bharwani, S. De Placido, C. K. Osborne and R. Schiff (2007). "Treatment of human epidermal growth factor receptor 2-

overexpressing breast cancer xenografts with multiagent HER-targeted therapy." <u>J Natl Cancer Inst</u> **99**(9): 694-705.

Arpino, G., L. Wiechmann, C. K. Osborne and R. Schiff (2008). "Crosstalk between the estrogen receptor and the HER tyrosine kinase receptor family: molecular mechanism and clinical implications for endocrine therapy resistance." <u>Endocr Rev</u> **29**(2): 217-233.

Arrandale, J. M., A. Gore-Willse, S. Rocks, J. M. Ren, J. Zhu, A. Davis, J. N. Livingston and D. U. Rabin (1996). "Insulin signaling in mice expressing reduced levels of Syp." <u>J Biol Chem</u> **271**(35): 21353-21358.

Arribas, J., J. Baselga, K. Pedersen and J. L. Parra-Palau (2011). "p95HER2 and breast cancer." <u>Cancer Res</u> **71**(5): 1515-1519.

Arthur, W. T. and K. Burridge (2001). "RhoA inactivation by p190RhoGAP regulates cell spreading and migration by promoting membrane protrusion and polarity." <u>Mol Biol Cell</u> **12**(9): 2711-2720.

Bard-Chapeau, E. A., S. Li, J. Ding, S. S. Zhang, H. H. Zhu, F. Princen, D. D. Fang, T. Han, B. Bailly-Maitre, V. Poli, N. M. Varki, H. Wang and G. S. Feng (2011). "Ptpn11/Shp2 acts as a tumor suppressor in hepatocellular carcinogenesis." <u>Cancer cell</u> **19**(5): 629-639.

Barford, D., A. J. Flint and N. K. Tonks (1994). "Crystal structure of human protein tyrosine phosphatase 1B." <u>Science</u> **263**(5152): 1397-1404.

Barnekow, A., E. Paul and M. Schartl (1987). "Expression of the c-src protooncogene in human skin tumors." <u>Cancer Res</u> **47**(1): 235-240.

Baselga, J., E. A. Perez, T. Pienkowski and R. Bell (2006). "Adjuvant trastuzumab: a milestone in the treatment of HER-2-positive early breast cancer." <u>Oncologist</u> **11 Suppl 1**: 4-12.

Beerling, E., L. Ritsma, N. Vrisekoop, P. W. Derksen and J. van Rheenen (2011). "Intravital microscopy: new insights into metastasis of tumors." <u>J Cell Sci</u> **124**(Pt 3): 299-310.

Behbod, F., F. S. Kittrell, H. LaMarca, D. Edwards, S. Kerbawy, J. C. Heestand, E. Young, P. Mukhopadhyay, H. W. Yeh, D. C. Allred, M. Hu, K. Polyak, J. M. Rosen and D. Medina (2009). "An intraductal human-in-mouse transplantation model mimics the subtypes of ductal carcinoma in situ." <u>Breast Cancer Res</u> **11**(5): R66.

Bennett, A. M., S. F. Hausdorff, A. M. O'Reilly, R. M. Freeman and B. G. Neel (1996). "Multiple requirements for SHPTP2 in epidermal growth factor-mediated cell cycle progression." <u>Mol Cell Biol</u> **16**(3): 1189-1202.

Bentires-Alj, M., S. G. Gil, R. Chan, Z. C. Wang, Y. Wang, N. Imanaka, L. N. Harris, A. Richardson, B. G. Neel and H. Gu (2006). "A role for the scaffolding adapter GAB2 in breast cancer." <u>Nature medicine</u> **12**(1): 114-121.

Bentires-Alj, M., S. G. Gil, R. Chan, Z. C. Wang, Y. Wang, N. Imanaka, L. N. Harris, A. Richardson, B. G. Neel and H. Gu (2006). "A role for the scaffolding adapter GAB2 in breast cancer." <u>Nat Med</u> **12**(1): 114-121.

Bentires-Alj, M., J. G. Paez, F. S. David, H. Keilhack, B. Halmos, K. Naoki, J. M. Maris, A. Richardson, A. Bardelli, D. J. Sugarbaker, W. G. Richards, J. Du, L. Girard, J. D. Minna, M. L. Loh, D. E. Fisher, V. E. Velculescu, B. Vogelstein, M. Meyerson, W. R. Sellers and B. G. Neel (2004). "Activating mutations of the noonan syndrome-associated SHP2/PTPN11 gene in human solid tumors and adult acute myelogenous leukemia." <u>Cancer research</u> **64**(24): 8816-8820.

Bentires-Alj, M., J. G. Paez, F. S. David, H. Keilhack, B. Halmos, K. Naoki, J. M. Maris, A. Richardson, A. Bardelli, D. J. Sugarbaker, W. G. Richards, J. Du, L. Girard, J. D. Minna, M. L. Loh, D. E. Fisher, V. E. Velculescu, B. Vogelstein, M. Meyerson, W. R. Sellers and B. G. Neel (2004). "Activating mutations of the noonan syndrome-associated SHP2/PTPN11 gene

in human solid tumors and adult acute myelogenous leukemia." <u>Cancer Res</u> **64**(24): 8816-8820.

Bicknell, K., G. Brooks, P. Kaiser, H. Chen, B. K. Dove and J. A. Hiscox (2005). "Nucleolin is regulated both at the level of transcription and translation." <u>Biochem Biophys Res Commun</u> **332**(3): 817-822.

Bissell, M. J., D. C. Radisky, A. Rizki, V. M. Weaver and O. W. Petersen (2002). "The organizing principle: microenvironmental influences in the normal and malignant breast." <u>Differentiation</u> **70**(9-10): 537-546.

Bjorge, J. D., A. Jakymiw and D. J. Fujita (2000). "Selected glimpses into the activation and function of Src kinase." <u>Oncogene</u> **19**(49): 5620-5635.

Bjorge, J. D., A. Pang and D. J. Fujita (2000). "Identification of protein-tyrosine phosphatase 1B as the major tyrosine phosphatase activity capable of dephosphorylating and activating c-Src in several human breast cancer cell lines." <u>J Biol Chem</u> **275**(52): 41439-41446.

Bocanegra, M., A. Bergamaschi, Y. H. Kim, M. A. Miller, A. B. Rajput, J. Kao, A. Langerod, W. Han, D. Y. Noh, S. S. Jeffrey, D. G. Huntsman, A. L. Borresen-Dale and J. R. Pollack (2010). "Focal amplification and oncogene dependency of GAB2 in breast cancer." <u>Oncogene</u> **29**(5): 774-779.

Bonapace, L., J. Wyckoff, T. Oertner, J. Van Rheenen, T. Junt and M. Bentires-Alj (2012). "If you don't look, you won't see: intravital multiphoton imaging of primary and metastatic breast cancer." <u>Journal of mammary gland biology and neoplasia</u> **17**(2): 125-129.

Bonnet, D. and J. E. Dick (1997). "Human acute myeloid leukemia is organized as a hierarchy that originates from a primitive hematopoietic cell." <u>Nat Med</u> **3**(7): 730-737.

Bonnomet, A., A. Brysse, A. Tachsidis, M. Waltham, E. W. Thompson, M. Polette and C. Gilles (2010). "Epithelial-to-mesenchymal transitions and circulating tumor cells." <u>J Mammary Gland Biol Neoplasia</u> **15**(2): 261-273.

Borer, R. A., C. F. Lehner, H. M. Eppenberger and E. A. Nigg (1989). "Major nucleolar proteins shuttle between nucleus and cytoplasm." <u>Cell</u> **56**(3): 379-390.

Bowman, T., M. A. Broome, D. Sinibaldi, W. Wharton, W. J. Pledger, J. M. Sedivy, R. Irby, T. Yeatman, S. A. Courtneidge and R. Jove (2001). "Stat3-mediated Myc expression is required for Src transformation and PDGF-induced mitogenesis." <u>Proc Natl Acad Sci U S A</u> **98**(13): 7319-7324.

Brown, M. T. and J. A. Cooper (1996). "Regulation, substrates and functions of src." <u>Biochim Biophys Acta</u> **1287**(2-3): 121-149.

Burnham, M. R., P. J. Bruce-Staskal, M. T. Harte, C. L. Weidow, A. Ma, S. A. Weed and A. H. Bouton (2000). "Regulation of c-SRC activity and function by the adapter protein CAS." <u>Mol Cell Biol</u> **20**(16): 5865-5878.

Burridge, K. and M. Chrzanowska-Wodnicka (1996). "Focal adhesions, contractility, and signaling." <u>Annu Rev Cell Dev Biol</u> **12**: 463-518.

Burridge, K., C. E. Turner and L. H. Romer (1992). "Tyrosine phosphorylation of paxillin and pp125FAK accompanies cell adhesion to extracellular matrix: a role in cytoskeletal assembly." <u>J Cell Biol</u> **119**(4): 893-903.

Burstein, H. J., Y. Sun, L. Y. Dirix, Z. Jiang, R. Paridaens, A. R. Tan, A. Awada, A. Ranade, S. Jiao, G. Schwartz, R. Abbas, C. Powell, K. Turnbull, J. Vermette, C. Zacharchuk and R. Badwe (2010). "Neratinib, an irreversible ErbB receptor tyrosine kinase inhibitor, in patients with advanced ErbB2-positive breast cancer." <u>J Clin Oncol</u> **28**(8): 1301-1307.

Cancer Genome Atlas, N. (2012). "Comprehensive molecular portraits of human breast tumours." <u>Nature</u> **490**(7418): 61-70.

Capelan, M., L. Pugliano, E. De Azambuja, I. Bozovic, K. S. Saini, C. Sotiriou, S. Loi and M. J. Piccart-Gebhart (2013). "Pertuzumab: new hope for patients with HER2-positive breast cancer." Ann Oncol **24**(2): 273-282.

Carey, L. A., E. C. Dees, L. Sawyer, L. Gatti, D. T. Moore, F. Collichio, D. W. Ollila, C. I. Sartor, M. L. Graham and C. M. Perou (2007). "The triple negative paradox: primary tumor chemosensitivity of breast cancer subtypes." Clin Cancer Res **13**(8): 2329-2334.

Carey, L. A., C. M. Perou, C. A. Livasy, L. G. Dressler, D. Cowan, K. Conway, G. Karaca, M. A. Troester, C. K. Tse, S. Edmiston, S. L. Deming, J. Geradts, M. C. Cheang, T. O. Nielsen, P. G. Moorman, H. S. Earp and R. C. Millikan (2006). "Race, breast cancer subtypes, and survival in the Carolina Breast Cancer Study." JAMA **295**(21): 2492-2502.

Carey, M. F., C. L. Peterson and S. T. Smale (2009). "Chromatin immunoprecipitation (ChIP)." Cold Spring Harb Protoc **2009**(9): pdb prot5279.

Chaffer, C. L., E. W. Thompson and E. D. Williams (2007). "Mesenchymal to epithelial transition in development and disease." Cells Tissues Organs **185**(1-3): 7-19.

Chan, G., D. Kalaitzidis and B. G. Neel (2008). "The tyrosine phosphatase Shp2 (PTPN11) in cancer." Cancer Metastasis Rev **27**(2): 179-192.

Chan, G., D. Kalaitzidis and B. G. Neel (2008). "The tyrosine phosphatase Shp2 (PTPN11) in cancer." Cancer metastasis reviews **27**(2): 179-192.

Chang, J. H., S. Gill, J. Settleman and S. J. Parsons (1995). "c-Src regulates the simultaneous rearrangement of actin cytoskeleton, p190RhoGAP, and p120RasGAP following epidermal growth factor stimulation." J Cell Biol **130**(2): 355-368.

Chang, J. H., L. K. Wilson, J. S. Moyers, K. Zhang and S. J. Parsons (1993). "Increased levels of p21ras-GTP and enhanced DNA synthesis accompany elevated tyrosyl phosphorylation of GAP-associated proteins, p190 and p62, in c-src overexpressors." Oncogene **8**(4): 959-967.

Chang, T. C., L. R. Zeitels, H. W. Hwang, R. R. Chivukula, E. A. Wentzel, M. Dews, J. Jung, P. Gao, C. V. Dang, M. A. Beer, A. Thomas-Tikhonenko and J. T. Mendell (2009). "Lin-28B transactivation is necessary for Myc-mediated let-7 repression and proliferation." Proc Natl Acad Sci U S A **106**(9): 3384-3389.

Charafe-Jauffret, E., C. Ginestier, F. Iovino, J. Wicinski, N. Cervera, P. Finetti, M. H. Hur, M. E. Diebel, F. Monville, J. Dutcher, M. Brown, P. Viens, L. Xerri, F. Bertucci, G. Stassi, G. Dontu, D. Birnbaum and M. S. Wicha (2009). "Breast cancer cell lines contain functional cancer stem cells with metastatic capacity and a distinct molecular signature." Cancer Res **69**(4): 1302-1313.

Chen, L., S. S. Sung, M. L. Yip, H. R. Lawrence, Y. Ren, W. C. Guida, S. M. Sebti, N. J. Lawrence and J. Wu (2006). "Discovery of a novel shp2 protein tyrosine phosphatase inhibitor." Molecular pharmacology **70**(2): 562-570.

Chou, M. T., J. Wang and D. J. Fujita (2002). "Src kinase becomes preferentially associated with the VEGFR, KDR/Flk-1, following VEGF stimulation of vascular endothelial cells." BMC Biochem **3**: 32.

Christofori, G. (2006). "New signals from the invasive front." Nature **441**(7092): 444-450.

Chughtai, N., S. Schimchowitsch, J. J. Lebrun and S. Ali (2002). "Prolactin induces SHP-2 association with Stat5, nuclear translocation, and binding to the beta-casein gene promoter in mammary cells." The Journal of biological chemistry **277**(34): 31107-31114.

Chughtai, N., S. Schimchowitsch, J. J. Lebrun and S. Ali (2002). "Prolactin induces SHP-2 association with Stat5, nuclear translocation, and binding to the beta-casein gene promoter in mammary cells." J Biol Chem **277**(34): 31107-31114.

Clarke, M. F., J. E. Dick, P. B. Dirks, C. J. Eaves, C. H. Jamieson, D. L. Jones, J. Visvader, I. L. Weissman and G. M. Wahl (2006). "Cancer stem cells--perspectives on current status and future directions: AACR Workshop on cancer stem cells." Cancer Res **66**(19): 9339-9344.

Clevers, H. (2011). "The cancer stem cell: premises, promises and challenges." Nat Med **17**(3): 313-319.

Conaway, J. W. (2012). "Introduction to theme "Chromatin, epigenetics, and transcription"." Annu Rev Biochem **81**: 61-64.

Condeelis, J. and R. Weissleder (2010). "In vivo imaging in cancer." Cold Spring Harb Perspect Biol **2**(12): a003848.

Conrads, T. P. and T. D. Veenstra (2005). "An enriched look at tyrosine phosphorylation." Nat Biotechnol **23**(1): 36-37.

Cooper, J. A. and B. Howell (1993). "The when and how of Src regulation." Cell **73**(6): 1051-1054.

Cooper, J. A. and T. Hunter (1981). "Changes in protein phosphorylation in Rous sarcoma virus-transformed chicken embryo cells." Mol Cell Biol **1**(2): 165-178.

Cordera, F. and V. C. Jordan (2006). "Steroid receptors and their role in the biology and control of breast cancer growth." Semin Oncol **33**(6): 631-641.

Cowan-Jacob, S. W., G. Fendrich, P. W. Manley, W. Jahnke, D. Fabbro, J. Liebetanz and T. Meyer (2005). "The crystal structure of a c-Src complex in an active conformation suggests possible steps in c-Src activation." Structure **13**(6): 861-871.

Craggs, G. and S. Kellie (2001). "A functional nuclear localization sequence in the C-terminal domain of SHP-1." J Biol Chem **276**(26): 23719-23725.

Creighton, C. J., X. Li, M. Landis, J. M. Dixon, V. M. Neumeister, A. Sjolund, D. L. Rimm, H. Wong, A. Rodriguez, J. I. Herschkowitz, C. Fan, X. Zhang, X. He, A. Pavlick, M. C. Gutierrez, L. Renshaw, A. A. Larionov, D. Faratian, S. G. Hilsenbeck, C. M. Perou, M. T. Lewis, J. M. Rosen and J. C. Chang (2009). "Residual breast cancers after conventional therapy display mesenchymal as well as tumor-initiating features." Proc Natl Acad Sci U S A **106**(33): 13820-13825.

Crown, J., J. O'Shaughnessy and G. Gullo (2012). "Emerging targeted therapies in triple-negative breast cancer." Ann Oncol **23 Suppl 6**: vi56-65.

Croxtall, J. D. and K. McKeage (2011). "Fulvestrant: a review of its use in the management of hormone receptor-positive metastatic breast cancer in postmenopausal women." Drugs **71**(3): 363-380.

Cunnick, J. M., L. Mei, C. A. Doupnik and J. Wu (2001). "Phosphotyrosines 627 and 659 of Gab1 constitute a bisphosphoryl tyrosine-based activation motif (BTAM) conferring binding and activation of SHP2." The Journal of biological chemistry **276**(26): 24380-24387.

D'Alessio, A., D. Califano, M. Incoronato, G. Santelli, T. Florio, G. Schettini, M. S. Carlomagno, L. Cerchia and V. de Franciscis (2003). "The tyrosine phosphatase Shp-2 mediates intracellular signaling initiated by Ret mutants." Endocrinology **144**(10): 4298-4305.

Day, D. S., L. J. Luquette, P. J. Park and P. V. Kharchenko (2010). "Estimating enrichment of repetitive elements from high-throughput sequence data." Genome Biol **11**(6): R69.

Deng, S., X. Yang, H. Lassus, S. Liang, S. Kaur, Q. Ye, C. Li, L. P. Wang, K. F. Roby, S. Orsulic, D. C. Connolly, Y. Zhang, K. Montone, R. Butzow, G. Coukos and L. Zhang (2010). "Distinct expression levels and patterns of stem cell marker, aldehyde dehydrogenase isoform 1 (ALDH1), in human epithelial cancers." PLoS One **5**(4): e10277.

Dent, R., M. Trudeau, K. I. Pritchard, W. M. Hanna, H. K. Kahn, C. A. Sawka, L. A. Lickley, E. Rawlinson, P. Sun and S. A. Narod (2007). "Triple-negative breast cancer: clinical features and patterns of recurrence." Clin Cancer Res **13**(15 Pt 1): 4429-4434.

Desgrosellier, J. S. and D. A. Cheresh (2010). "Integrins in cancer: biological implications and therapeutic opportunities." Nat Rev Cancer **10**(1): 9-22.

Desta, Z., B. A. Ward, N. V. Soukhova and D. A. Flockhart (2004). "Comprehensive evaluation of tamoxifen sequential biotransformation by the human cytochrome P450 system in vitro: prominent roles for CYP3A and CYP2D6." J Pharmacol Exp Ther **310**(3): 1062-1075.

Destouches, D., D. El Khoury, Y. Hamma-Kourbali, B. Krust, P. Albanese, P. Katsoris, G. Guichard, J. P. Briand, J. Courty and A. G. Hovanessian (2008). "Suppression of tumor growth and angiogenesis by a specific antagonist of the cell-surface expressed nucleolin." PLoS One **3**(6): e2518.

Di Segni, A., K. Farin and R. Pinkas-Kramarski (2008). "Identification of nucleolin as new ErbB receptors- interacting protein." PLoS One **3**(6): e2310.

Digilio, M. C., E. Conti, A. Sarkozy, R. Mingarelli, T. Dottorini, B. Marino, A. Pizzuti and B. Dallapiccola (2002). "Grouping of multiple-lentigines/LEOPARD and Noonan syndromes on the PTPN11 gene." Am J Hum Genet **71**(2): 389-394.

Dontu, G., M. Al-Hajj, W. M. Abdallah, M. F. Clarke and M. S. Wicha (2003). "Stem cells in normal breast development and breast cancer." Cell Prolif **36 Suppl 1**: 59-72.

dos Santos, P. B., J. S. Zanetti, A. Ribeiro-Silva and E. I. Beltrao (2012). "Beta 1 integrin predicts survival in breast cancer: a clinicopathological and immunohistochemical study." Diagn Pathol **7**: 104.

Duss, S., S. Andre, A. L. Nicoulaz, M. Fiche, H. Bonnefoi, C. Brisken and R. D. Iggo (2007). "An oestrogen-dependent model of breast cancer created by transformation of normal human mammary epithelial cells." Breast Cancer Res **9**(3): R38.

Eckhardt, B. L., P. A. Francis, B. S. Parker and R. L. Anderson (2012). "Strategies for the discovery and development of therapies for metastatic breast cancer." Nat Rev Drug Discov **11**(6): 479-497.

Egan, C., A. Pang, D. Durda, H. C. Cheng, J. H. Wang and D. J. Fujita (1999). "Activation of Src in human breast tumor cell lines: elevated levels of phosphotyrosine phosphatase activity that preferentially recognizes the Src carboxy terminal negative regulatory tyrosine 530." Oncogene **18**(5): 1227-1237.

Ekmektzoglou, K. A., T. Xanthos, V. German and G. C. Zografos (2009). "Breast cancer: from the earliest times through to the end of the 20th century." Eur J Obstet Gynecol Reprod Biol **145**(1): 3-8.

Elsawaf, Z. and H. P. Sinn (2011). "Triple-Negative Breast Cancer: Clinical and Histological Correlations." Breast Care (Basel) **6**(4): 273-278.

Eminaga, S. and A. M. Bennett (2008). "Noonan syndrome-associated SHP-2/Ptpn11 mutants enhance SIRPalpha and PZR tyrosyl phosphorylation and promote adhesion-mediated ERK activation." The Journal of biological chemistry **283**(22): 15328-15338.

Entenberg, D., J. Wyckoff, B. Gligorijevic, E. T. Roussos, V. V. Verkhusha, J. W. Pollard and J. Condeelis (2011). "Setup and use of a two-laser multiphoton microscope for multichannel intravital fluorescence imaging." Nat Protoc **6**(10): 1500-1520.

Etienne-Manneville, S. (2008). "Polarity proteins in migration and invasion." Oncogene **27**(55): 6970-6980.

Farrow, J. H. (1971). "Antiquity of breast cancer." Cancer **28**(6): 1369-1371.

Fedele, P., N. Calvani, A. Marino, L. Orlando, P. Schiavone, A. Quaranta and S. Cinieri (2012). "Targeted agents to reverse resistance to endocrine therapy in metastatic breast cancer: where are we now and where are we going?" Crit Rev Oncol Hematol **84**(2): 243-251.

Feng, G. S. (2007). "Shp2-mediated molecular signaling in control of embryonic stem cell self-renewal and differentiation." Cell research **17**(1): 37-41.

Feng, G. S., C. C. Hui and T. Pawson (1993). "SH2-containing phosphotyrosine phosphatase as a target of protein-tyrosine kinases." Science **259**(5101): 1607-1611.

Feng, G. S. and T. Pawson (1994). "Phosphotyrosine phosphatases with SH2 domains: regulators of signal transduction." Trends Genet **10**(2): 54-58.

Ferlay, J., D. Forman, C. D. Mathers and F. Bray (2012). "Breast and cervical cancer in 187 countries between 1980 and 2010." Lancet **379**(9824): 1390-1391.

Ferlay, J., H. R. Shin, F. Bray, D. Forman, C. Mathers and D. M. Parkin (2010). "Estimates of worldwide burden of cancer in 2008: GLOBOCAN 2008." Int J Cancer **127**(12): 2893-2917.

Fillmore, C. M. and C. Kuperwasser (2008). "Human breast cancer cell lines contain stem-like cells that self-renew, give rise to phenotypically diverse progeny and survive chemotherapy." Breast Cancer Res **10**(2): R25.

Fincham, V. J., V. G. Brunton and M. C. Frame (2000). "The SH3 domain directs acto-myosin-dependent targeting of v-Src to focal adhesions via phosphatidylinositol 3-kinase." Mol Cell Biol **20**(17): 6518-6536.

Fincham, V. J. and M. C. Frame (1998). "The catalytic activity of Src is dispensable for translocation to focal adhesions but controls the turnover of these structures during cell motility." EMBO J **17**(1): 81-92.

Finn, R. S., J. Dering, C. Ginther, C. A. Wilson, P. Glaspy, N. Tchekmedyian and D. J. Slamon (2007). "Dasatinib, an orally active small molecule inhibitor of both the src and abl kinases, selectively inhibits growth of basal-type/"triple-negative" breast cancer cell lines growing in vitro." Breast Cancer Res Treat **105**(3): 319-326.

Fisher, B., M. Bauer, R. Margolese, R. Poisson, Y. Pilch, C. Redmond, E. Fisher, N. Wolmark, M. Deutsch, E. Montague and et al. (1985). "Five-year results of a randomized clinical trial comparing total mastectomy and segmental mastectomy with or without radiation in the treatment of breast cancer." N Engl J Med **312**(11): 665-673.

Flint, A. J., T. Tiganis, D. Barford and N. K. Tonks (1997). "Development of "substrate-trapping" mutants to identify physiological substrates of protein tyrosine phosphatases." Proc Natl Acad Sci U S A **94**(5): 1680-1685.

Frame, M. C. (2002). "Src in cancer: deregulation and consequences for cell behaviour." Biochimica et biophysica acta **1602**(2): 114-130.

Frank, D. A. and A. C. Sartorelli (1986). "Regulation of protein phosphotyrosine content by changes in tyrosine kinase and protein phosphotyrosine phosphatase activities during induced granulocytic and monocytic differentiation of HL-60 leukemia cells." Biochem Biophys Res Commun **140**(1): 440-447.

Freeman, R. M., Jr., J. Plutzky and B. G. Neel (1992). "Identification of a human src homology 2-containing protein-tyrosine-phosphatase: a putative homolog of Drosophila corkscrew." Proc Natl Acad Sci U S A **89**(23): 11239-11243.

Freiss, G. and F. Vignon (2004). "Protein tyrosine phosphatases and breast cancer." Crit Rev Oncol Hematol **52**(1): 9-17.

Friedl, P. and D. Gilmour (2009). "Collective cell migration in morphogenesis, regeneration and cancer." Nat Rev Mol Cell Biol **10**(7): 445-457.

Garton, A. J., A. J. Flint and N. K. Tonks (1996). "Identification of p130(cas) as a substrate for the cytosolic protein tyrosine phosphatase PTP-PEST." Mol Cell Biol **16**(11): 6408-6418.

Gasiorowski, J. Z. and D. A. Dean (2003). "Mechanisms of nuclear transport and interventions." Adv Drug Deliv Rev **55**(6): 703-716.

Gentleman, R. C., V. J. Carey, D. M. Bates, B. Bolstad, M. Dettling, S. Dudoit, B. Ellis, L. Gautier, Y. Ge, J. Gentry, K. Hornik, T. Hothorn, W. Huber, S. Iacus, R. Irizarry, F. Leisch, C. Li, M. Maechler, A. J. Rossini, G. Sawitzki, C. Smith, G. Smyth, L. Tierney, J. Y. Yang and J. Zhang (2004). "Bioconductor: open software development for computational biology and bioinformatics." Genome Biol **5**(10): R80.

Ginisty, H., H. Sicard, B. Roger and P. Bouvet (1999). "Structure and functions of nucleolin." J Cell Sci **112 (Pt 6)**: 761-772.

Glenney, J. R., Jr. and L. Zokas (1989). "Novel tyrosine kinase substrates from Rous sarcoma virus-transformed cells are present in the membrane skeleton." J Cell Biol **108**(6): 2401-2408.

Gonzalez, L., M. T. Agullo-Ortuno, J. M. Garcia-Martinez, A. Calcabrini, C. Gamallo, J. Palacios, A. Aranda and J. Martin-Perez (2006). "Role of c-Src in human MCF7 breast cancer cell tumorigenesis." J Biol Chem **281**(30): 20851-20864.

Grossmann, K. S., M. Rosario, C. Birchmeier and W. Birchmeier (2010). "The tyrosine phosphatase Shp2 in development and cancer." Advances in cancer research **106**: 53-89.

Grubbe, E. H. (1947). "The origin and birth of x-ray therapy." Urol Cutaneous Rev **51**(7): 375-379.

Halsted, W. S. (1894). "I. The Results of Operations for the Cure of Cancer of the Breast Performed at the Johns Hopkins Hospital from June, 1889, to January, 1894." Ann Surg **20**(5): 497-555.

Handley, R. S. and A. C. Thackray (1969). "Conservative radial mastectomy (Patey's operation)." Ann Surg **170**(6): 880-882.

Hartman, Z. R., M. D. Schaller and Y. M. Agazie (2013). "The tyrosine phosphatase SHP2 regulates focal adhesion kinase to promote EGF-induced lamellipodia persistence and cell migration." Mol Cancer Res.

Hatakeyama, M. (2002). "Deregulation of SHP-2 tyrosine phosphatase by the Helicobacter pylori virulence factor CagA." Keio J Med **51 Suppl 2**: 26-32.

Hay, E. D. (1982). "Interaction of embryonic surface and cytoskeleton with extracellular matrix." Am J Anat **165**(1): 1-12.

Hicks, G. R. and N. V. Raikhel (1995). "Nuclear localization signal binding proteins in higher plant nuclei." Proc Natl Acad Sci U S A **92**(3): 734-738.

Higashi, H., R. Tsutsumi, S. Muto, T. Sugiyama, T. Azuma, M. Asaka and M. Hatakeyama (2002). "SHP-2 tyrosine phosphatase as an intracellular target of Helicobacter pylori CagA protein." Science **295**(5555): 683-686.

Hof, P., S. Pluskey, S. Dhe-Paganon, M. J. Eck and S. E. Shoelson (1998). "Crystal structure of the tyrosine phosphatase SHP-2." Cell **92**(4): 441-450.

Hood, J. D. and D. A. Cheresh (2002). "Role of integrins in cell invasion and migration." Nat Rev Cancer **2**(2): 91-100.

Hsia, D. A., S. K. Mitra, C. R. Hauck, D. N. Streblow, J. A. Nelson, D. Ilic, S. Huang, E. Li, G. R. Nemerow, J. Leng, K. S. Spencer, D. A. Cheresh and D. D. Schlaepfer (2003). "Differential regulation of cell motility and invasion by FAK." J Cell Biol **160**(5): 753-767.

Huang, X., Y. Fu, R. A. Charbeneau and R. R. Neubig (2009). "GNAI2 and regulators of G protein signaling as a potential Noonan syndrome mechanism." Med Hypotheses **73**(1): 56-59.

Hunter, T. (2009). "Tyrosine phosphorylation: thirty years and counting." Curr Opin Cell Biol **21**(2): 140-146.

Husemann, Y., J. B. Geigl, F. Schubert, P. Musiani, M. Meyer, E. Burghart, G. Forni, R. Eils, T. Fehm, G. Riethmuller and C. A. Klein (2008). "Systemic spread is an early step in breast cancer." Cancer Cell **13**(1): 58-68.

Huttenlocher, A. and A. R. Horwitz (2011). "Integrins in cell migration." Cold Spring Harb Perspect Biol **3**(9): a005074.

Hynes, N. E. and G. MacDonald (2009). "ErbB receptors and signaling pathways in cancer." Curr Opin Cell Biol **21**(2): 177-184.

Hynes, R. O. (2002). "Integrins: bidirectional, allosteric signaling machines." Cell **110**(6): 673-687.

Ilic, D., Y. Furuta, S. Kanazawa, N. Takeda, K. Sobue, N. Nakatsuji, S. Nomura, J. Fujimoto, M. Okada and T. Yamamoto (1995). "Reduced cell motility and enhanced focal adhesion contact formation in cells from FAK-deficient mice." Nature **377**(6549): 539-544.

Iliopoulos, D., H. A. Hirsch and K. Struhl (2009). "An epigenetic switch involving NF-kappaB, Lin28, Let-7 MicroRNA, and IL6 links inflammation to cell transformation." Cell **139**(4): 693-706.

Iliopoulos, D., H. A. Hirsch, G. Wang and K. Struhl (2011). "Inducible formation of breast cancer stem cells and their dynamic equilibrium with non-stem cancer cells via IL6 secretion." Proc Natl Acad Sci U S A **108**(4): 1397-1402.

Irby, R. B., W. Mao, D. Coppola, J. Kang, J. M. Loubeau, W. Trudeau, R. Karl, D. J. Fujita, R. Jove and T. J. Yeatman (1999). "Activating SRC mutation in a subset of advanced human colon cancers." Nat Genet **21**(2): 187-190.

Ishizawar, R. and S. J. Parsons (2004). "c-Src and cooperating partners in human cancer." Cancer cell **6**(3): 209-214.

Ishizawar, R. C., D. A. Tice, T. Karaoli and S. J. Parsons (2004). "The C terminus of c-Src inhibits breast tumor cell growth by a kinase-independent mechanism." J Biol Chem **279**(22): 23773-23781.

Iwasaki, T., A. Nakata, M. Mukai, K. Shinkai, H. Yano, H. Sabe, E. Schaefer, M. Tatsuta, T. Tsujimura, N. Terada, E. Kakishita and H. Akedo (2002). "Involvement of phosphorylation of Tyr-31 and Tyr-118 of paxillin in MM1 cancer cell migration." Int J Cancer **97**(3): 330-335.

Jacobs, C. and H. Rubsamen (1983). "Expression of pp60c-src protein kinase in adult and fetal human tissue: high activities in some sarcomas and mammary carcinomas." Cancer Res **43**(4): 1696-1702.

Jaffe, A. B. and A. Hall (2005). "Rho GTPases: biochemistry and biology." Annu Rev Cell Dev Biol **21**: 247-269.

Jakob, S., P. Schroeder, M. Lukosz, N. Buchner, I. Spyridopoulos, J. Altschmied and J. Haendeler (2008). "Nuclear protein tyrosine phosphatase Shp-2 is one important negative regulator of nuclear export of telomerase reverse transcriptase." The Journal of biological chemistry **283**(48): 33155-33161.

Jallal, H., M. L. Valentino, G. Chen, F. Boschelli, S. Ali and S. A. Rabbani (2007). "A Src/Abl kinase inhibitor, SKI-606, blocks breast cancer invasion, growth, and metastasis in vitro and in vivo." Cancer Res **67**(4): 1580-1588.

Jares-Erijman, E. A. and T. M. Jovin (2003). "FRET imaging." Nat Biotechnol **21**(11): 1387-1395.

Jia, Z., D. Barford, A. J. Flint and N. K. Tonks (1995). "Structural basis for phosphotyrosine peptide recognition by protein tyrosine phosphatase 1B." Science **268**(5218): 1754-1758.

Johnston, S. R. (2010). "New strategies in estrogen receptor-positive breast cancer." Clin Cancer Res **16**(7): 1979-1987.

Johnston, S. R. and M. Dowsett (2003). "Aromatase inhibitors for breast cancer: lessons from the laboratory." Nat Rev Cancer **3**(11): 821-831.

Jove, R. and H. Hanafusa (1987). "Cell transformation by the viral src oncogene." Annu Rev Cell Biol **3**: 31-56.

Jung, E. J. and C. W. Kim (2002). "Interaction between chicken protein tyrosine phosphatase 1 (CPTP1)-like rat protein phosphatase 1 (PTP1) and p60(v-src) in v-src-transformed Rat-1 fibroblasts." Exp Mol Med **34**(6): 476-480.

Kalluri, R. (2009). "EMT: when epithelial cells decide to become mesenchymal-like cells." J Clin Invest **119**(6): 1417-1419.

Kim, H., M. Laing and W. Muller (2005). "c-Src-null mice exhibit defects in normal mammary gland development and ERalpha signaling." Oncogene **24**(36): 5629-5636.

Klein, C. A. (2009). "Parallel progression of primary tumours and metastases." Nat Rev Cancer **9**(4): 302-312.

Kleinsmith, L. J. and G. B. Pierce, Jr. (1964). "Multipotentiality of Single Embryonal Carcinoma Cells." Cancer Res **24**: 1544-1551.

Klinghoffer, R. A., C. Sachsenmaier, J. A. Cooper and P. Soriano (1999). "Src family kinases are required for integrin but not PDGFR signal transduction." EMBO J **18**(9): 2459-2471.

Kontaridis, M. I., K. D. Swanson, F. S. David, D. Barford and B. G. Neel (2006). "PTPN11 (Shp2) mutations in LEOPARD syndrome have dominant negative, not activating, effects." The Journal of biological chemistry **281**(10): 6785-6792.

Kornberg, R. D. (1977). "Structure of chromatin." Annu Rev Biochem **46**: 931-954.

Kusano, K., T. N. Thomas and K. Fujiwara (2008). "Phosphorylation and localization of protein-zero related (PZR) in cultured endothelial cells." Endothelium : journal of endothelial cell research **15**(3): 127-136.

Landgren, E., P. Blume-Jensen, S. A. Courtneidge and L. Claesson-Welsh (1995). "Fibroblast growth factor receptor-1 regulation of Src family kinases." Oncogene **10**(10): 2027-2035.

Lawson, J. C., G. L. Blatch and A. L. Edkins (2009). "Cancer stem cells in breast cancer and metastasis." Breast Cancer Res Treat **118**(2): 241-254.

Lechleider, R. J., R. M. Freeman, Jr. and B. G. Neel (1993). "Tyrosyl phosphorylation and growth factor receptor association of the human corkscrew homologue, SH-PTP2." J Biol Chem **268**(18): 13434-13438.

Legius, E., C. Schrander-Stumpel, E. Schollen, C. Pulles-Heintzberger, M. Gewillig and J. P. Fryns (2002). "PTPN11 mutations in LEOPARD syndrome." J Med Genet **39**(8): 571-574.

Li, C., D. G. Heidt, P. Dalerba, C. F. Burant, L. Zhang, V. Adsay, M. Wicha, M. F. Clarke and D. M. Simeone (2007). "Identification of pancreatic cancer stem cells." Cancer Res **67**(3): 1030-1037.

Li, F., B. Tiede, J. Massague and Y. Kang (2007). "Beyond tumorigenesis: cancer stem cells in metastasis." Cell Res **17**(1): 3-14.

Li, X., M. T. Lewis, J. Huang, C. Gutierrez, C. K. Osborne, M. F. Wu, S. G. Hilsenbeck, A. Pavlick, X. Zhang, G. C. Chamness, H. Wong, J. Rosen and J. C. Chang (2008). "Intrinsic resistance of tumorigenic breast cancer cells to chemotherapy." J Natl Cancer Inst **100**(9): 672-679.

Liu, H., M. R. Patel, J. A. Prescher, A. Patsialou, D. Qian, J. Lin, S. Wen, Y. F. Chang, M. H. Bachmann, Y. Shimono, P. Dalerba, M. Adorno, N. Lobo, J. Bueno, F. M. Dirbas, S.

Goswami, G. Somlo, J. Condeelis, C. H. Contag, S. S. Gambhir and M. F. Clarke (2010). "Cancer stem cells from human breast tumors are involved in spontaneous metastases in orthotopic mouse models." Proc Natl Acad Sci U S A **107**(42): 18115-18120.

Liu, X. and F. Fagotto (2011). "A method to separate nuclear, cytosolic, and membrane-associated signaling molecules in cultured cells." Sci Signal **4**(203): pl2.

Loh, M. L., M. G. Reynolds, S. Vattikuti, R. B. Gerbing, T. A. Alonzo, E. Carlson, J. W. Cheng, C. M. Lee, B. J. Lange, S. Meshinchi and G. Children's Cancer (2004). "PTPN11 mutations in pediatric patients with acute myeloid leukemia: results from the Children's Cancer Group." Leukemia **18**(11): 1831-1834.

Lopez-Novoa, J. M. and M. A. Nieto (2009). "Inflammation and EMT: an alliance towards organ fibrosis and cancer progression." EMBO Mol Med **1**(6-7): 303-314.

Lowe, C., T. Yoneda, B. F. Boyce, H. Chen, G. R. Mundy and P. Soriano (1993). "Osteopetrosis in Src-deficient mice is due to an autonomous defect of osteoclasts." Proc Natl Acad Sci U S A **90**(10): 4485-4489.

Lutz, M. P., I. B. Esser, B. B. Flossmann-Kast, R. Vogelmann, H. Luhrs, H. Friess, M. W. Buchler and G. Adler (1998). "Overexpression and activation of the tyrosine kinase Src in human pancreatic carcinoma." Biochemical and biophysical research communications **243**(2): 503-508.

Maloney, A. and P. Workman (2002). "HSP90 as a new therapeutic target for cancer therapy: the story unfolds." Expert Opin Biol Ther **2**(1): 3-24.

Malvezzi, M., P. Bertuccio, F. Levi, C. La Vecchia and E. Negri (2012). "European cancer mortality predictions for the year 2012." Ann Oncol **23**(4): 1044-1052.

Manes, S., E. Mira, C. Gomez-Mouton, Z. J. Zhao, R. A. Lacalle and A. C. Martinez (1999). "Concerted activity of tyrosine phosphatase SHP-2 and focal adhesion kinase in regulation of cell motility." Molecular and cellular biology **19**(4): 3125-3135.

Martin, G. S. (1970). "Rous sarcoma virus: a function required for the maintenance of the transformed state." Nature **227**(5262): 1021-1023.

Masaki, T., M. Okada, M. Tokuda, Y. Shiratori, O. Hatase, M. Shirai, M. Nishioka and M. Omata (1999). "Reduced C-terminal Src kinase (Csk) activities in hepatocellular carcinoma." Hepatology **29**(2): 379-384.

May, C. D., N. Sphyris, K. W. Evans, S. J. Werden, W. Guo and S. A. Mani (2011). "Epithelial-mesenchymal transition and cancer stem cells: a dangerously dynamic duo in breast cancer progression." Breast Cancer Res **13**(1): 202.

Meerbrey, K. L., G. Hu, J. D. Kessler, K. Roarty, M. Z. Li, J. E. Fang, J. I. Herschkowitz, A. E. Burrows, A. Ciccia, T. Sun, E. M. Schmitt, R. J. Bernardi, X. Fu, C. S. Bland, T. A. Cooper, R. Schiff, J. M. Rosen, T. F. Westbrook and S. J. Elledge (2011). "The pINDUCER lentiviral toolkit for inducible RNA interference in vitro and in vivo." Proceedings of the National Academy of Sciences of the United States of America **108**(9): 3665-3670.

Meijering, E., O. Dzyubachyk and I. Smal (2012). "Methods for cell and particle tracking." Methods Enzymol **504**: 183-200.

Meyer, M. J., J. M. Fleming, M. A. Ali, M. W. Pesesky, E. Ginsburg and B. K. Vonderhaar (2009). "Dynamic regulation of CD24 and the invasive, CD44posCD24neg phenotype in breast cancer cell lines." Breast Cancer Res **11**(6): R82.

Micalizzi, D. S., S. M. Farabaugh and H. L. Ford (2010). "Epithelial-mesenchymal transition in cancer: parallels between normal development and tumor progression." J Mammary Gland Biol Neoplasia **15**(2): 117-134.

Mody, N., J. Leitch, C. Armstrong, J. Dixon and P. Cohen (2001). "Effects of MAP kinase cascade inhibitors on the MKK5/ERK5 pathway." FEBS Lett **502**(1-2): 21-24.

Morris, G. J., S. Naidu, A. K. Topham, F. Guiles, Y. Xu, P. McCue, G. F. Schwartz, P. K. Park, A. L. Rosenberg, K. Brill and E. P. Mitchell (2007). "Differences in breast carcinoma characteristics in newly diagnosed African-American and Caucasian patients: a single-institution compilation compared with the National Cancer Institute's Surveillance, Epidemiology, and End Results database." Cancer **110**(4): 876-884.

Morrison, R., S. M. Schleicher, Y. Sun, K. J. Niermann, S. Kim, D. E. Spratt, C. H. Chung and B. Lu (2011). "Targeting the mechanisms of resistance to chemotherapy and radiotherapy with the cancer stem cell hypothesis." J Oncol **2011**: 941876.

Musgrove, E. A. and R. L. Sutherland (2009). "Biological determinants of endocrine resistance in breast cancer." Nat Rev Cancer **9**(9): 631-643.

Nakai, K. and P. Horton (1999). "PSORT: a program for detecting sorting signals in proteins and predicting their subcellular localization." Trends Biochem Sci **24**(1): 34-36.

Nakamura, K., H. Yano, H. Uchida, S. Hashimoto, E. Schaefer and H. Sabe (2000). "Tyrosine phosphorylation of paxillin alpha is involved in temporospatial regulation of paxillin-containing focal adhesion formation and F-actin organization in motile cells." J Biol Chem **275**(35): 27155-27164.

Naruke, T., R. Tsuchiya, H. Kondo, H. Nakayama and H. Asamura (1999). "Lymph node sampling in lung cancer: how should it be done?" Eur J Cardiothorac Surg **16 Suppl 1**: S17-24.

Neel, B. G. (1993). "Structure and function of SH2-domain containing tyrosine phosphatases." Semin Cell Biol **4**(6): 419-432.

Nguyen, D. X., P. D. Bos and J. Massague (2009). "Metastasis: from dissemination to organ-specific colonization." Nat Rev Cancer **9**(4): 274-284.

Nieman, M. T., J. B. Kim, K. R. Johnson and M. J. Wheelock (1999). "Mechanism of extracellular domain-deleted dominant negative cadherins." J Cell Sci **112 (Pt 10)**: 1621-1632.

Nieman, M. T., R. S. Prudoff, K. R. Johnson and M. J. Wheelock (1999). "N-cadherin promotes motility in human breast cancer cells regardless of their E-cadherin expression." J Cell Biol **147**(3): 631-644.

Nigg, E. A., B. M. Sefton, T. Hunter, G. Walter and S. J. Singer (1982). "Immunofluorescent localization of the transforming protein of Rous sarcoma virus with antibodies against a synthetic src peptide." Proc Natl Acad Sci U S A **79**(17): 5322-5326.

Noonan, J. and W. O'Connor (1996). "Noonan syndrome: a clinical description emphasizing the cardiac findings." Acta Paediatr Jpn **38**(1): 76-83.

O'Brien, C. A., A. Pollett, S. Gallinger and J. E. Dick (2007). "A human colon cancer cell capable of initiating tumour growth in immunodeficient mice." Nature **445**(7123): 106-110.

O'Reilly, A. M. and B. G. Neel (1998). "Structural determinants of SHP-2 function and specificity in Xenopus mesoderm induction." Mol Cell Biol **18**(1): 161-177.

Oh, E. S., H. Gu, T. M. Saxton, J. F. Timms, S. Hausdorff, E. U. Frevert, B. B. Kahn, T. Pawson, B. G. Neel and S. M. Thomas (1999). "Regulation of early events in integrin signaling by protein tyrosine phosphatase SHP-2." Molecular and cellular biology **19**(4): 3205-3215.

Ostman, A., C. Hellberg and F. D. Bohmer (2006). "Protein-tyrosine phosphatases and cancer." Nature reviews. Cancer **6**(4): 307-320.

Ottenhoff-Kalff, A. E., G. Rijksen, E. A. van Beurden, A. Hennipman, A. A. Michels and G. E. Staal (1992). "Characterization of protein tyrosine kinases from human breast cancer: involvement of the c-src oncogene product." Cancer Res **52**(17): 4773-4778.

Park, P. J. (2009). "ChIP-seq: advantages and challenges of a maturing technology." Nat Rev Genet **10**(10): 669-680.

Parri, M. and P. Chiarugi (2010). "Rac and Rho GTPases in cancer cell motility control." Cell Commun Signal **8**: 23.

Parsons, J. T. and M. J. Weber (1989). "Genetics of src: structure and functional organization of a protein tyrosine kinase." Curr Top Microbiol Immunol **147**: 79-127.

Pasquali, C., I. Fialka and L. A. Huber (1999). "Subcellular fractionation, electromigration analysis and mapping of organelles." J Chromatogr B Biomed Sci Appl **722**(1-2): 89-102.

Patsialou, A., Y. Wang, J. Lin, K. Whitney, S. Goswami, P. A. Kenny and J. S. Condeelis (2012). "Selective gene-expression profiling of migratory tumor cells in vivo predicts clinical outcome in breast cancer patients." Breast Cancer Res **14**(5): R139.

Pawson, T. (1995). "Protein modules and signalling networks." Nature **373**(6515): 573-580.

Pawson, T. and M. Kofler (2009). "Kinome signaling through regulated protein-protein interactions in normal and cancer cells." Curr Opin Cell Biol **21**(2): 147-153.

Peddi, P. F. and S. A. Hurvitz (2013). "Trastuzumab emtansine: the first targeted chemotherapy for treatment of breast cancer." Future Oncol **9**(3): 319-326.

Peinado, H., F. Portillo and A. Cano (2004). "Transcriptional regulation of cadherins during development and carcinogenesis." Int J Dev Biol **48**(5-6): 365-375.

Peng, Z. Y. and C. A. Cartwright (1995). "Regulation of the Src tyrosine kinase and Syp tyrosine phosphatase by their cellular association." Oncogene **11**(10): 1955-1962.

Perou, C. M. (2010). "Molecular stratification of triple-negative breast cancers." Oncologist **15 Suppl 5**: 39-48.

Perou, C. M. (2011). "Molecular stratification of triple-negative breast cancers." Oncologist **16 Suppl 1**: 61-70.

Perou, C. M., T. Sorlie, M. B. Eisen, M. van de Rijn, S. S. Jeffrey, C. A. Rees, J. R. Pollack, D. T. Ross, H. Johnsen, L. A. Akslen, O. Fluge, A. Pergamenschikov, C. Williams, S. X. Zhu, P. E. Lonning, A. L. Borresen-Dale, P. O. Brown and D. Botstein (2000). "Molecular portraits of human breast tumours." Nature **406**(6797): 747-752.

Pierce, G. B. and W. C. Speers (1988). "Tumors as caricatures of the process of tissue renewal: prospects for therapy by directing differentiation." Cancer Res **48**(8): 1996-2004.

Pierce, G. B. and C. Wallace (1971). "Differentiation of malignant to benign cells." Cancer Res **31**(2): 127-134.

Pollard, T. D. and G. G. Borisy (2003). "Cellular motility driven by assembly and disassembly of actin filaments." Cell **112**(4): 453-465.

Poon, I. K. and D. A. Jans (2005). "Regulation of nuclear transport: central role in development and transformation?" Traffic **6**(3): 173-186.

Prat, A., J. S. Parker, O. Karginova, C. Fan, C. Livasy, J. I. Herschkowitz, X. He and C. M. Perou (2010). "Phenotypic and molecular characterization of the claudin-low intrinsic subtype of breast cancer." Breast Cancer Res **12**(5): R68.

Pratt, W. B. (1998). "The hsp90-based chaperone system: involvement in signal transduction from a variety of hormone and growth factor receptors." Proc Soc Exp Biol Med **217**(4): 420-434.

Puls, L. N., M. Eadens and W. Messersmith (2011). "Current status of SRC inhibitors in solid tumor malignancies." Oncologist **16**(5): 566-578.

Rao, R. D. and M. A. Cobleigh (2012). "Adjuvant endocrine therapy for breast cancer." Oncology (Williston Park) **26**(6): 541-547, 550, 552 passim.

Ren, Y., S. Meng, L. Mei, Z. J. Zhao, R. Jove and J. Wu (2004). "Roles of Gab1 and SHP2 in paxillin tyrosine dephosphorylation and Src activation in response to epidermal growth factor." The Journal of biological chemistry **279**(9): 8497-8505.

Reyes-Reyes, E. M. and S. K. Akiyama (2008). "Cell-surface nucleolin is a signal transducing P-selectin binding protein for human colon carcinoma cells." Exp Cell Res **314**(11-12): 2212-2223.

Ricci-Vitiani, L., D. G. Lombardi, E. Pilozzi, M. Biffoni, M. Todaro, C. Peschle and R. De Maria (2007). "Identification and expansion of human colon-cancer-initiating cells." Nature **445**(7123): 111-115.

Ridley, A. J., M. A. Schwartz, K. Burridge, R. A. Firtel, M. H. Ginsberg, G. Borisy, J. T. Parsons and A. R. Horwitz (2003). "Cell migration: integrating signals from front to back." Science **302**(5651): 1704-1709.

Robbins, J., S. M. Dilworth, R. A. Laskey and C. Dingwall (1991). "Two interdependent basic domains in nucleoplasmin nuclear targeting sequence: identification of a class of bipartite nuclear targeting sequence." Cell **64**(3): 615-623.

Romond, E. H., E. A. Perez, J. Bryant, V. J. Suman, C. E. Geyer, Jr., N. E. Davidson, E. Tan-Chiu, S. Martino, S. Paik, P. A. Kaufman, S. M. Swain, T. M. Pisansky, L. Fehrenbacher, L. A. Kutteh, V. G. Vogel, D. W. Visscher, G. Yothers, R. B. Jenkins, A. M. Brown, S. R. Dakhil, E. P. Mamounas, W. L. Lingle, P. M. Klein, J. N. Ingle and N. Wolmark (2005). "Trastuzumab plus adjuvant chemotherapy for operable HER2-positive breast cancer." N Engl J Med **353**(16): 1673-1684.

Roof, R. W., M. D. Haskell, B. D. Dukes, N. Sherman, M. Kinter and S. J. Parsons (1998). "Phosphotyrosine (p-Tyr)-dependent and -independent mechanisms of p190 RhoGAP-p120 RasGAP interaction: Tyr 1105 of p190, a substrate for c-Src, is the sole p-Tyr mediator of complex formation." Mol Cell Biol **18**(12): 7052-7063.

Rosen, J. M. and C. T. Jordan (2009). "The increasing complexity of the cancer stem cell paradigm." Science **324**(5935): 1670-1673.

Roskoski, R., Jr. (2004). "Src protein-tyrosine kinase structure and regulation." Biochem Biophys Res Commun **324**(4): 1155-1164.

Roskoski, R., Jr. (2005). "Src kinase regulation by phosphorylation and dephosphorylation." Biochemical and biophysical research communications **331**(1): 1-14.

Rous, P. (1910). "A Transmissible Avian Neoplasm. (Sarcoma of the Common Fowl.)." J Exp Med **12**(5): 696-705.

Rous, P. (1911). "A Sarcoma of the Fowl Transmissible by an Agent Separable from the Tumor Cells." J Exp Med **13**(4): 397-411.

Roush, S. and F. J. Slack (2008). "The let-7 family of microRNAs." Trends Cell Biol **18**(10): 505-516.

Sachdev, S., Y. Bu and I. H. Gelman (2009). "Paxillin-Y118 phosphorylation contributes to the control of Src-induced anchorage-independent growth by FAK and adhesion." BMC Cancer **9**: 12.

Sakorafas, G. H. and M. Safioleas (2009). "Breast cancer surgery: an historical narrative. Part I. From prehistoric times to Renaissance." Eur J Cancer Care (Engl) **18**(6): 530-544.

Sakorafas, G. H. and M. Safioleas (2010). "Breast cancer surgery: an historical narrative. Part III. From the sunset of the 19th to the dawn of the 21st century." Eur J Cancer Care (Engl) **19**(2): 145-166.

Salvi, M., A. Stringaro, A. M. Brunati, E. Agostinelli, G. Arancia, G. Clari and A. Toninello (2004). "Tyrosine phosphatase activity in mitochondria: presence of Shp-2 phosphatase in mitochondria." Cell Mol Life Sci **61**(18): 2393-2404.

Sattler, M., M. G. Mohi, Y. B. Pride, L. R. Quinnan, N. A. Malouf, K. Podar, F. Gesbert, H. Iwasaki, S. Li, R. A. Van Etten, H. Gu, J. D. Griffin and B. G. Neel (2002). "Critical role for Gab2 in transformation by BCR/ABL." Cancer cell **1**(5): 479-492.

Saxton, T. M., M. Henkemeyer, S. Gasca, R. Shen, D. J. Rossi, F. Shalaby, G. S. Feng and T. Pawson (1997). "Abnormal mesoderm patterning in mouse embryos mutant for the SH2 tyrosine phosphatase Shp-2." EMBO J **16**(9): 2352-2364.

Saxton, T. M. and T. Pawson (1999). "Morphogenetic movements at gastrulation require the SH2 tyrosine phosphatase Shp2." Proceedings of the National Academy of Sciences of the United States of America **96**(7): 3790-3795.

Schaller, M. D. (2001). "Paxillin: a focal adhesion-associated adaptor protein." Oncogene **20**(44): 6459-6472.

Schatton, T., G. F. Murphy, N. Y. Frank, K. Yamaura, A. M. Waaga-Gasser, M. Gasser, Q. Zhan, S. Jordan, L. M. Duncan, C. Weishaupt, R. C. Fuhlbrigge, T. S. Kupper, M. H. Sayegh and M. H. Frank (2008). "Identification of cells initiating human melanomas." Nature **451**(7176): 345-349.

Schmidt-Kittler, O., T. Ragg, A. Daskalakis, M. Granzow, A. Ahr, T. J. Blankenstein, M. Kaufmann, J. Diebold, H. Arnholdt, P. Muller, J. Bischoff, D. Harich, G. Schlimok, G. Riethmuller, R. Eils and C. A. Klein (2003). "From latent disseminated cells to overt metastasis: genetic analysis of systemic breast cancer progression." Proc Natl Acad Sci U S A **100**(13): 7737-7742.

Schober, M., S. Raghavan, M. Nikolova, L. Polak, H. A. Pasolli, H. E. Beggs, L. F. Reichardt and E. Fuchs (2007). "Focal adhesion kinase modulates tension signaling to control actin and focal adhesion dynamics." J Cell Biol **176**(5): 667-680.

Scott, L. M., H. R. Lawrence, S. M. Sebti, N. J. Lawrence and J. Wu (2010). "Targeting protein tyrosine phosphatases for anticancer drug discovery." Curr Pharm Des **16**(16): 1843-1862.

Sellers, W. R. (2011). "A blueprint for advancing genetics-based cancer therapy." Cell **147**(1): 26-31.

Sen, B. and F. M. Johnson (2011). "Regulation of SRC family kinases in human cancers." Journal of signal transduction **2011**: 865819.

Sen, B. and F. M. Johnson (2011). "Regulation of SRC family kinases in human cancers." J Signal Transduct **2011**: 865819.

Shi, Z. Q., D. H. Yu, M. Park, M. Marshall and G. S. Feng (2000). "Molecular mechanism for the Shp-2 tyrosine phosphatase function in promoting growth factor stimulation of Erk activity." Mol Cell Biol **20**(5): 1526-1536.

Shiio, Y., R. N. Eisenman, E. C. Yi, S. Donohoe, D. R. Goodlett and R. Aebersold (2003). "Quantitative proteomic analysis of chromatin-associated factors." J Am Soc Mass Spectrom **14**(7): 696-703.

Shoji, S., T. Kurosawa, H. Inoue, T. Funakoshi and Y. Kubota (1990). "Human cellular src gene product: identification of the myristoylated pp60c-src and blockage of its myristoyl acylation with N-fatty acyl compounds resulted in the suppression of colony formation." Biochem Biophys Res Commun **173**(3): 894-901.

Sidani, M., J. Wyckoff, C. Xue, J. E. Segall and J. Condeelis (2006). "Probing the microenvironment of mammary tumors using multiphoton microscopy." J Mammary Gland Biol Neoplasia **11**(2): 151-163.

Sieg, D. J., C. R. Hauck, D. Ilic, C. K. Klingbeil, E. Schaefer, C. H. Damsky and D. D. Schlaepfer (2000). "FAK integrates growth-factor and integrin signals to promote cell migration." Nat Cell Biol **2**(5): 249-256.

Siemann, D. W., M. Dong, C. Pampo and W. Shi (2012). "Src-signaling interference impairs the dissemination of blood-borne tumor cells." Cell Tissue Res **349**(2): 541-550.

Sims, A. H., A. Howell, S. J. Howell and R. B. Clarke (2007). "Origins of breast cancer subtypes and therapeutic implications." Nat Clin Pract Oncol **4**(9): 516-525.

Singh, S. K., C. Hawkins, I. D. Clarke, J. A. Squire, J. Bayani, T. Hide, R. M. Henkelman, M. D. Cusimano and P. B. Dirks (2004). "Identification of human brain tumour initiating cells." Nature **432**(7015): 396-401.

Slamon, D. J., G. M. Clark, S. G. Wong, W. J. Levin, A. Ullrich and W. L. McGuire (1987). "Human breast cancer: correlation of relapse and survival with amplification of the HER-2/neu oncogene." Science **235**(4785): 177-182.

Slamon, D. J., B. Leyland-Jones, S. Shak, H. Fuchs, V. Paton, A. Bajamonde, T. Fleming, W. Eiermann, J. Wolter, M. Pegram, J. Baselga and L. Norton (2001). "Use of chemotherapy plus a monoclonal antibody against HER2 for metastatic breast cancer that overexpresses HER2." N Engl J Med **344**(11): 783-792.

Snapp, E. L. and R. S. Hegde (2006). "Rational design and evaluation of FRET experiments to measure protein proximities in cells." Curr Protoc Cell Biol **Chapter 17**: Unit 17 19.

Sommers, C. L., E. P. Gelmann, R. Kemler, P. Cowin and S. W. Byers (1994). "Alterations in beta-catenin phosphorylation and plakoglobin expression in human breast cancer cells." Cancer Res **54**(13): 3544-3552.

Sommers, C. L., E. W. Thompson, J. A. Torri, R. Kemler, E. P. Gelmann and S. W. Byers (1991). "Cell adhesion molecule uvomorulin expression in human breast cancer cell lines: relationship to morphology and invasive capacities." Cell Growth Differ **2**(8): 365-372.

Songyang, Z., S. E. Shoelson, M. Chaudhuri, G. Gish, T. Pawson, W. G. Haser, F. King, T. Roberts, S. Ratnofsky, R. J. Lechleider and et al. (1993). "SH2 domains recognize specific phosphopeptide sequences." Cell **72**(5): 767-778.

Soriano, P., C. Montgomery, R. Geske and A. Bradley (1991). "Targeted disruption of the c-src proto-oncogene leads to osteopetrosis in mice." Cell **64**(4): 693-702.

Sorlie, T., C. M. Perou, R. Tibshirani, T. Aas, S. Geisler, H. Johnsen, T. Hastie, M. B. Eisen, M. van de Rijn, S. S. Jeffrey, T. Thorsen, H. Quist, J. C. Matese, P. O. Brown, D. Botstein, P. E. Lonning and A. L. Borresen-Dale (2001). "Gene expression patterns of breast carcinomas distinguish tumor subclasses with clinical implications." Proc Natl Acad Sci U S A **98**(19): 10869-10874.

Sottoriva, A., L. Vermeulen and S. Tavare (2011). "Modeling evolutionary dynamics of epigenetic mutations in hierarchically organized tumors." PLoS Comput Biol **7**(5): e1001132.

Stehelin, D., R. V. Guntaka, H. E. Varmus and J. M. Bishop (1976). "Purification of DNA complementary to nucleotide sequences required for neoplastic transformation of fibroblasts by avian sarcoma viruses." J Mol Biol **101**(3): 349-365.

Stehelin, D., H. E. Varmus, J. M. Bishop and P. K. Vogt (1976). "DNA related to the transforming gene(s) of avian sarcoma viruses is present in normal avian DNA." Nature **260**(5547): 170-173.

Stein, P. L., H. Vogel and P. Soriano (1994). "Combined deficiencies of Src, Fyn, and Yes tyrosine kinases in mutant mice." Genes Dev **8**(17): 1999-2007.

Stingl, J. and C. Caldas (2007). "Molecular heterogeneity of breast carcinomas and the cancer stem cell hypothesis." Nat Rev Cancer **7**(10): 791-799.

Stoker, A. W. (2005). "Protein tyrosine phosphatases and signalling." J Endocrinol **185**(1): 19-33.

Summy, J. M. and G. E. Gallick (2003). "Src family kinases in tumor progression and metastasis." Cancer Metastasis Rev **22**(4): 337-358.

Sun, T., N. Aceto, K. L. Meerbrey, J. D. Kessler, C. Zhou, I. Migliaccio, D. X. Nguyen, N. N. Pavlova, M. Botero, J. Huang, R. J. Bernardi, E. Schmitt, G. Hu, M. Z. Li, N. Dephoure, S. P. Gygi, M. Rao, C. J. Creighton, S. G. Hilsenbeck, C. A. Shaw, D. Muzny, R. A. Gibbs, D. A. Wheeler, C. K. Osborne, R. Schiff, M. Bentires-Alj, S. J. Elledge and T. F. Westbrook (2011). "Activation of multiple proto-oncogenic tyrosine kinases in breast cancer via loss of the PTPN12 phosphatase." Cell **144**(5): 703-718.

Suzuki, H., A. R. Forrest, E. van Nimwegen, C. O. Daub, P. J. Balwierz, K. M. Irvine, T. Lassmann, T. Ravasi, Y. Hasegawa, M. J. de Hoon, S. Katayama, K. Schroder, P. Carninci, Y. Tomaru, M. Kanamori-Katayama, A. Kubosaki, A. Akalin, Y. Ando, E. Arner, M. Asada, H. Asahara, T. Bailey, V. B. Bajic, D. Bauer, A. G. Beckhouse, N. Bertin, J. Bjorkegren, F. Brombacher, E. Bulger, A. M. Chalk, J. Chiba, N. Cloonan, A. Dawe, J. Dostie, P. G. Engstrom, M. Essack, G. J. Faulkner, J. L. Fink, D. Fredman, K. Fujimori, M. Furuno, T. Gojobori, J. Gough, S. M. Grimmond, M. Gustafsson, M. Hashimoto, T. Hashimoto, M. Hatakeyama, S. Heinzel, W. Hide, O. Hofmann, M. Hornquist, L. Huminiecki, K. Ikeo, N. Imamoto, S. Inoue, Y. Inoue, R. Ishihara, T. Iwayanagi, A. Jacobsen, M. Kaur, H. Kawaji, M. C. Kerr, R. Kimura, S. Kimura, Y. Kimura, H. Kitano, H. Koga, T. Kojima, S. Kondo, T. Konno, A. Krogh, A. Kruger, A. Kumar, B. Lenhard, A. Lennartsson, M. Lindow, M. Lizio, C. Macpherson, N. Maeda, C. A. Maher, M. Maqungo, J. Mar, N. A. Matigian, H. Matsuda, J. S. Mattick, S. Meier, S. Miyamoto, E. Miyamoto-Sato, K. Nakabayashi, Y. Nakachi, M. Nakano, S. Nygaard, T. Okayama, Y. Okazaki, H. Okuda-Yabukami, V. Orlando, J. Otomo, M. Pachkov, N. Petrovsky, C. Plessy, J. Quackenbush, A. Radovanovic, M. Rehli, R. Saito, A. Sandelin, S. Schmeier, C. Schonbach, A. S. Schwartz, C. A. Semple, M. Sera, J. Severin, K. Shirahige, C. Simons, G. St Laurent, M. Suzuki, T. Suzuki, M. J. Sweet, R. J. Taft, S. Takeda, Y. Takenaka, K. Tan, M. S. Taylor, R. D. Teasdale, J. Tegner, S. Teichmann, E. Valen, C. Wahlestedt, K. Waki, A. Waterhouse, C. A. Wells, O. Winther, L. Wu, K. Yamaguchi, H. Yanagawa, J. Yasuda, M. Zavolan, D. A. Hume, T. Arakawa, S. Fukuda, K. Imamura, C. Kai, A. Kaiho, T. Kawashima, C. Kawazu, Y. Kitazume, M. Kojima, H. Miura, K. Murakami, M. Murata, N. Ninomiya, H. Nishiyori, S. Noma, C. Ogawa, T. Sano, C. Simon, M. Tagami, Y. Takahashi, J. Kawai and Y. Hayashizaki (2009). "The transcriptional network that controls growth arrest and differentiation in a human myeloid leukemia cell line." Nature genetics **41**(5): 553-562.

Svitkina, T. M., A. B. Verkhovsky and G. G. Borisy (1996). "Plectin sidearms mediate interaction of intermediate filaments with microtubules and other components of the cytoskeleton." J Cell Biol **135**(4): 991-1007.

Takahashi, A., R. Tsutsumi, I. Kikuchi, C. Obuse, Y. Saito, A. Seidi, R. Karisch, M. Fernandez, T. Cho, N. Ohnishi, O. Rozenblatt-Rosen, M. Meyerson, B. G. Neel and M. Hatakeyama (2011). "SHP2 tyrosine phosphatase converts parafibromin/Cdc73 from a tumor suppressor to an oncogenic driver." Mol Cell **43**(1): 45-56.

Takahashi, A., R. Tsutsumi, I. Kikuchi, C. Obuse, Y. Saito, A. Seidi, R. Karisch, M. Fernandez, T. Cho, N. Ohnishi, O. Rozenblatt-Rosen, M. Meyerson, B. G. Neel and M. Hatakeyama (2011). "SHP2 tyrosine phosphatase converts parafibromin/Cdc73 from a tumor suppressor to an oncogenic driver." Molecular cell **43**(1): 45-56.

Tartaglia, M., S. Martinelli, G. Cazzaniga, V. Cordeddu, I. Iavarone, M. Spinelli, C. Palmi, C. Carta, A. Pession, M. Arico, G. Masera, G. Basso, M. Sorcini, B. D. Gelb and A. Biondi (2004). "Genetic evidence for lineage-related and differentiation stage-related contribution of somatic PTPN11 mutations to leukemogenesis in childhood acute leukemia." Blood **104**(2): 307-313.

Tartaglia, M., E. L. Mehler, R. Goldberg, G. Zampino, H. G. Brunner, H. Kremer, I. van der Burgt, A. H. Crosby, A. Ion, S. Jeffery, K. Kalidas, M. A. Patton, R. S. Kucherlapati and B. D. Gelb (2001). "Mutations in PTPN11, encoding the protein tyrosine phosphatase SHP-2, cause Noonan syndrome." Nat Genet **29**(4): 465-468.

Tartaglia, M., C. M. Niemeyer, A. Fragale, X. Song, J. Buechner, A. Jung, K. Hahlen, H. Hasle, J. D. Licht and B. D. Gelb (2003). "Somatic mutations in PTPN11 in juvenile myelomonocytic leukemia, myelodysplastic syndromes and acute myeloid leukemia." Nat Genet **34**(2): 148-150.

Tatosyan, A. G. and O. A. Mizenina (2000). "Kinases of the Src family: structure and functions." Biochemistry (Mosc) **65**(1): 49-58.

Tautz, L. and T. Mustelin (2007). "Strategies for developing protein tyrosine phosphatase inhibitors." Methods **42**(3): 250-260.

Thiery, J. P. (2002). "Epithelial-mesenchymal transitions in tumour progression." Nat Rev Cancer **2**(6): 442-454.

Thomas, S. M. and J. S. Brugge (1997). "Cellular functions regulated by Src family kinases." Annu Rev Cell Dev Biol **13**: 513-609.

Tice, D. A., J. S. Biscardi, A. L. Nickles and S. J. Parsons (1999). "Mechanism of biological synergy between cellular Src and epidermal growth factor receptor." Proceedings of the National Academy of Sciences of the United States of America **96**(4): 1415-1420.

Tiganis, T. and A. M. Bennett (2007). "Protein tyrosine phosphatase function: the substrate perspective." Biochem J **402**(1): 1-15.

Tiganis, T., A. M. Bennett, K. S. Ravichandran and N. K. Tonks (1998). "Epidermal growth factor receptor and the adaptor protein p52Shc are specific substrates of T-cell protein tyrosine phosphatase." Mol Cell Biol **18**(3): 1622-1634.

Tominaga, K., S. Srikantan, E. K. Lee, S. S. Subaran, J. L. Martindale, K. Abdelmohsen and M. Gorospe (2011). "Competitive regulation of nucleolin expression by HuR and miR-494." Mol Cell Biol **31**(20): 4219-4231.

Tonks, N. K. (2006). "Protein tyrosine phosphatases: from genes, to function, to disease." Nat Rev Mol Cell Biol **7**(11): 833-846.

Turner, C. E., J. R. Glenney, Jr. and K. Burridge (1990). "Paxillin: a new vinculin-binding protein present in focal adhesions." J Cell Biol **111**(3): 1059-1068.

Tuteja, R. and N. Tuteja (1998). "Nucleolin: a multifunctional major nucleolar phosphoprotein." Crit Rev Biochem Mol Biol **33**(6): 407-436.

Tutt, A., M. Robson, J. E. Garber, S. M. Domchek, M. W. Audeh, J. N. Weitzel, M. Friedlander, B. Arun, N. Loman, R. K. Schmutzler, A. Wardley, G. Mitchell, H. Earl, M. Wickens and J. Carmichael (2010). "Oral poly(ADP-ribose) polymerase inhibitor olaparib in patients with BRCA1 or BRCA2 mutations and advanced breast cancer: a proof-of-concept trial." Lancet **376**(9737): 235-244.

van der Burgt, I. (2007). "Noonan syndrome." Orphanet J Rare Dis **2**: 4.

van Oijen, M. G., G. Rijksen, F. W. ten Broek and P. J. Slootweg (1998). "Overexpression of c-Src in areas of hyperproliferation in head and neck cancer, premalignant lesions and benign mucosal disorders." Journal of oral pathology & medicine : official publication of the International Association of Oral Pathologists and the American Academy of Oral Pathology **27**(4): 147-152.

Vargo-Gogola, T. and J. M. Rosen (2007). "Modelling breast cancer: one size does not fit all." Nat Rev Cancer **7**(9): 659-672.

Verbeek, B. S., T. M. Vroom, S. S. Adriaansen-Slot, A. E. Ottenhoff-Kalff, J. G. Geertzema, A. Hennipman and G. Rijksen (1996). "c-Src protein expression is increased in human breast cancer. An immunohistochemical and biochemical analysis." The Journal of pathology **180**(4): 383-388.

Vermeulen, L., F. de Sousa e Melo, D. J. Richel and J. P. Medema (2012). "The developing cancer stem-cell model: clinical challenges and opportunities." Lancet Oncol **13**(2): e83-89.

Vicente-Manzanares, M., D. J. Webb and A. R. Horwitz (2005). "Cell migration at a glance." J Cell Sci **118**(Pt 21): 4917-4919.

Visvader, J. E. (2009). "Keeping abreast of the mammary epithelial hierarchy and breast tumorigenesis." Genes Dev **23**(22): 2563-2577.

Viswanathan, S. R., G. Q. Daley and R. I. Gregory (2008). "Selective blockade of microRNA processing by Lin28." Science **320**(5872): 97-100.

Voena, C., C. Conte, C. Ambrogio, E. Boeri Erba, F. Boccalatte, S. Mohammed, O. N. Jensen, G. Palestro, G. Inghirami and R. Chiarle (2007). "The tyrosine phosphatase Shp2 interacts with NPM-ALK and regulates anaplastic lymphoma cell growth and migration." Cancer Res **67**(9): 4278-4286.

Voena, C., C. Conte, C. Ambrogio, E. Boeri Erba, F. Boccalatte, S. Mohammed, O. N. Jensen, G. Palestro, G. Inghirami and R. Chiarle (2007). "The tyrosine phosphatase Shp2 interacts with NPM-ALK and regulates anaplastic lymphoma cell growth and migration." Cancer research **67**(9): 4278-4286.

Vogel, W., R. Lammers, J. Huang and A. Ullrich (1993). "Activation of a phosphotyrosine phosphatase by tyrosine phosphorylation." Science **259**(5101): 1611-1614.

Vogelstein, B. and K. W. Kinzler (2004). "Cancer genes and the pathways they control." Nat Med **10**(8): 789-799.

Walter, A. O., Z. Y. Peng and C. A. Cartwright (1999). "The Shp-2 tyrosine phosphatase activates the Src tyrosine kinase by a non-enzymatic mechanism." Oncogene **18**(11): 1911-1920.

Wang, F. M., H. Q. Liu, S. R. Liu, S. P. Tang, L. Yang and G. S. Feng (2005). "SHP-2 promoting migration and metastasis of MCF-7 with loss of E-cadherin, dephosphorylation of FAK and secretion of MMP-9 induced by IL-1beta in vivo and in vitro." Breast cancer research and treatment **89**(1): 5-14.

Wang, F. M., H. Q. Liu, S. R. Liu, S. P. Tang, L. Yang and G. S. Feng (2005). "SHP-2 promoting migration and metastasis of MCF-7 with loss of E-cadherin, dephosphorylation of FAK and secretion of MMP-9 induced by IL-1beta in vivo and in vitro." Breast Cancer Res Treat **89**(1): 5-14.

Weaver, A. M. (2006). "Invadopodia: specialized cell structures for cancer invasion." Clin Exp Metastasis **23**(2): 97-105.

Wee, S., D. Wiederschain, S. M. Maira, A. Loo, C. Miller, R. deBeaumont, F. Stegmeier, Y. M. Yao and C. Lengauer (2008). "PTEN-deficient cancers depend on PIK3CB." Proc Natl Acad Sci U S A **105**(35): 13057-13062.

Wellner, U., J. Schubert, U. C. Burk, O. Schmalhofer, F. Zhu, A. Sonntag, B. Waldvogel, C. Vannier, D. Darling, A. zur Hausen, V. G. Brunton, J. Morton, O. Sansom, J. Schuler, M. P. Stemmler, C. Herzberger, U. Hopt, T. Keck, S. Brabletz and T. Brabletz (2009). "The EMT-activator ZEB1 promotes tumorigenicity by repressing stemness-inhibiting microRNAs." Nat Cell Biol **11**(12): 1487-1495.

Wiege, K., S. R. Ali, B. Gewecke, A. Novakovic, F. M. Konrad, K. Pexa, S. Beer-Hammer, J. Reutershan, R. P. Piekorz, R. E. Schmidt, B. Nurnberg and J. E. Gessner (2013). "Galphai2 is the essential galphai protein in immune complex-induced lung disease." J Immunol **190**(1): 324-333.

Wiener, J. R., K. Nakano, R. P. Kruzelock, C. D. Bucana, R. C. Bast, Jr. and G. E. Gallick (1999). "Decreased Src tyrosine kinase activity inhibits malignant human ovarian cancer tumor growth in a nude mouse model." Clinical cancer research : an official journal of the American Association for Cancer Research **5**(8): 2164-2170.

Williams, I. G., R. S. Murley and M. P. Curwen (1953). "Carcinoma of the female breast: conservative and radical surgery." Br Med J **2**(4840): 787-796.

Wong, A. L. and S. C. Lee (2012). "Mechanisms of Resistance to Trastuzumab and Novel Therapeutic Strategies in HER2-Positive Breast Cancer." Int J Breast Cancer **2012**: 415170.

Wu, T. R., Y. K. Hong, X. D. Wang, M. Y. Ling, A. M. Dragoi, A. S. Chung, A. G. Campbell, Z. Y. Han, G. S. Feng and Y. E. Chin (2002). "SHP-2 is a dual-specificity phosphatase involved in Stat1 dephosphorylation at both tyrosine and serine residues in nuclei." J Biol Chem **277**(49): 47572-47580.

Xing, L., C. Ge, R. Zeltser, G. Maskevitch, B. J. Mayer and K. Alexandropoulos (2000). "c-Src signaling induced by the adapters Sin and Cas is mediated by Rap1 GTPase." Mol Cell Biol **20**(19): 7363-7377.

Yamada, K. M. and B. Geiger (1997). "Molecular interactions in cell adhesion complexes." Curr Opin Cell Biol **9**(1): 76-85.

Yamaguchi, H., M. Lorenz, S. Kempiak, C. Sarmiento, S. Coniglio, M. Symons, J. Segall, R. Eddy, H. Miki, T. Takenawa and J. Condeelis (2005). "Molecular mechanisms of invadopodium formation: the role of the N-WASP-Arp2/3 complex pathway and cofilin." J Cell Biol **168**(3): 441-452.

Yamaguchi, H., Y. Takeo, S. Yoshida, Z. Kouchi, Y. Nakamura and K. Fukami (2009). "Lipid rafts and caveolin-1 are required for invadopodia formation and extracellular matrix degradation by human breast cancer cells." Cancer Res **69**(22): 8594-8602.

Yamaguchi, H., J. Wyckoff and J. Condeelis (2005). "Cell migration in tumors." Curr Opin Cell Biol **17**(5): 559-564.

Yang, J. and R. A. Weinberg (2008). "Epithelial-mesenchymal transition: at the crossroads of development and tumor metastasis." Dev Cell **14**(6): 818-829.

Yang, W., L. D. Klaman, B. Chen, T. Araki, H. Harada, S. M. Thomas, E. L. George and B. G. Neel (2006). "An Shp2/SFK/Ras/Erk signaling pathway controls trophoblast stem cell survival." Developmental cell **10**(3): 317-327.

Yang, Z. F., D. W. Ho, M. N. Ng, C. K. Lau, W. C. Yu, P. Ngai, P. W. Chu, C. T. Lam, R. T. Poon and S. T. Fan (2008). "Significance of CD90+ cancer stem cells in human liver cancer." Cancer Cell **13**(2): 153-166.

Yao, J., L. Liang, S. Huang, J. Ding, N. Tan, Y. Zhao, M. Yan, C. Ge, Z. Zhang, T. Chen, D. Wan, M. Yao, J. Li, J. Gu and X. He (2010). "MicroRNA-30d promotes tumor invasion and metastasis by targeting Galphai2 in hepatocellular carcinoma." Hepatology **51**(3): 846-856.

Yeatman, T. J. (2004). "A renaissance for SRC." Nature reviews. Cancer **4**(6): 470-480.

Yilmaz, M. and G. Christofori (2009). "EMT, the cytoskeleton, and cancer cell invasion." Cancer Metastasis Rev **28**(1-2): 15-33.

Yoneda, T., M. Niewolna, C. Lowe, E. Izbicka and G. R. Mundy (1993). "Hormonal regulation of pp60c-src expression during osteoclast formation in vitro." Mol Endocrinol **7**(10): 1313-1318.

Yu, D. H., C. K. Qu, O. Henegariu, X. Lu and G. S. Feng (1998). "Protein-tyrosine phosphatase Shp-2 regulates cell spreading, migration, and focal adhesion." The Journal of biological chemistry **273**(33): 21125-21131.

Yu, D. H., C. K. Qu, O. Henegariu, X. Lu and G. S. Feng (1998). "Protein-tyrosine phosphatase Shp-2 regulates cell spreading, migration, and focal adhesion." J Biol Chem **273**(33): 21125-21131.

Yu, Z. H., J. Wu, C. D. Walls, L. Chen, S. Zhang, R. Zhang, L. Wu, L. Wang, S. Liu and Z. Y. Zhang (2013). "Structural and Mechanistic Insights into LEOPARD Syndrome-Associated SHP2 Mutations." J Biol Chem.

Yuan, L., W. M. Yu, Z. Yuan, C. C. Haudenschild and C. K. Qu (2003). "Role of SHP-2 tyrosine phosphatase in the DNA damage-induced cell death response." The Journal of biological chemistry **278**(17): 15208-15216.

Zhan, L., A. Rosenberg, K. C. Bergami, M. Yu, Z. Xuan, A. B. Jaffe, C. Allred and S. K. Muthuswamy (2008). "Deregulation of scribble promotes mammary tumorigenesis and reveals a role for cell polarity in carcinoma." Cell **135**(5): 865-878.

Zhan, Y., G. J. Counelis and D. M. O'Rourke (2009). "The protein tyrosine phosphatase SHP-2 is required for EGFRvIII oncogenic transformation in human glioblastoma cells." Exp Cell Res **315**(14): 2343-2357.

Zhan, Y. and D. M. O'Rourke (2004). "SHP-2-dependent mitogen-activated protein kinase activation regulates EGFRvIII but not wild-type epidermal growth factor receptor phosphorylation and glioblastoma cell survival." Cancer Res **64**(22): 8292-8298.

Zhang, S. Q., W. Yang, M. I. Kontaridis, T. G. Bivona, G. Wen, T. Araki, J. Luo, J. A. Thompson, B. L. Schraven, M. R. Philips and B. G. Neel (2004). "Shp2 regulates SRC family kinase activity and Ras/Erk activation by controlling Csk recruitment." Mol Cell **13**(3): 341-355.

Zhang, S. Q., W. Yang, M. I. Kontaridis, T. G. Bivona, G. Wen, T. Araki, J. Luo, J. A. Thompson, B. L. Schraven, M. R. Philips and B. G. Neel (2004). "Shp2 regulates SRC family kinase activity and Ras/Erk activation by controlling Csk recruitment." Molecular cell **13**(3): 341-355.

Zhang, Z. Y., Y. Wang and J. E. Dixon (1994). "Dissecting the catalytic mechanism of protein-tyrosine phosphatases." Proc Natl Acad Sci U S A **91**(5): 1624-1627.

Zhao, R., A. Guerrah, H. Tang and Z. J. Zhao (2002). "Cell surface glycoprotein PZR is a major mediator of concanavalin A-induced cell signaling." The Journal of biological chemistry **277**(10): 7882-7888.

Zhao, R. and Z. J. Zhao (2000). "Dissecting the interaction of SHP-2 with PZR, an immunoglobulin family protein containing immunoreceptor tyrosine-based inhibitory motifs." J Biol Chem **275**(8): 5453-5459.

Zhao, R. and Z. J. Zhao (2003). "Identification of a variant form of PZR lacking immunoreceptor tyrosine-based inhibitory motifs." Biochem Biophys Res Commun **303**(4): 1028-1033.

Zhao, R. and Z. J. Zhao (2003). "Identification of a variant form of PZR lacking immunoreceptor tyrosine-based inhibitory motifs." Biochemical and biophysical research communications **303**(4): 1028-1033.

Zhao, Z. J. and R. Zhao (1998). "Purification and cloning of PZR, a binding protein and putative physiological substrate of tyrosine phosphatase SHP-2." J Biol Chem **273**(45): 29367-29372.

Zheng, H., S. Alter and C. K. Qu (2009). "SHP-2 tyrosine phosphatase in human diseases." Int J Clin Exp Med **2**(1): 17-25.

Zheng, X. M., Y. Wang and C. J. Pallen (1992). "Cell transformation and activation of pp60c-src by overexpression of a protein tyrosine phosphatase." Nature **359**(6393): 336-339.

Zhou, G., J. M. Denu, L. Wu and J. E. Dixon (1994). "The catalytic role of Cys124 in the dual specificity phosphatase VHR." J Biol Chem **269**(45): 28084-28090.

Zhou, X., J. Coad, B. Ducatman and Y. M. Agazie (2008). "SHP2 is up-regulated in breast cancer cells and in infiltrating ductal carcinoma of the breast, implying its involvement in breast oncogenesis." Histopathology **53**(4): 389-402.

Zomer, A., E. Beerling, E. J. Vlug and J. van Rheenen (2011). "Real-time intravital imaging of cancer models." Clin Transl Oncol **13**(12): 848-854.

11   ACKNOWLEDGMENTS

First, I would like to thank Momo for giving me the opportunity to do my PhD in his group. In addition to providing me with this interesting project, he offered me guidance and support throughout my time in his laboratory. I further want to thank Nancy Hynes and Gerhard Christofori for being in my thesis committee and supporting me during the last four years.

I would like to acknowledge the present and former members of the Bentires lab, who have offered me invaluable practical advice at the beginning of my PhD and for interesting discussions and input later on. We had good times and I hope we will keep in touch.

A special thanks to the FMI facilities without whom doing cutting-edge research would be much harder. I enjoyed the great friendly working atmosphere and the readiness of everybody to help in times of need.

Big thanks to my collaborators at the FMI and at Novartis Basel and Cambridge. I very much enjoyed the experience of working in an industrial setting and learned a lot during this time.

Last but not least, I would like to thank my friends, at the FMI and outside, and my family for their support during the last years, and especially during the last months. Last but not least, I want to express my deepest gratitude to Adrian and Steve for critical reading of the thesis and everything else, and to Ira, for drawing the figures in the introduction by hand and for constant support.